

**INTERNATIONAL CONFERENCE
OF THE POLISH SOCIETY OF
BIOMECHANICS**

BIOMECHANICS
2023

Acta of Biomechanics and Bioengineering
Vol. 25, Supplement 1, 2023

EDITORS

Marta Kozuń, Anna Nikodem, Ewelina Świątek-Najwer

Wrocław, Poland
13-16.09.2023

ISBN: 978-83-967265-0-6

ISSN 1509-409X



ISBN 978-83-967265-0-6



9 788396 726506

Copyright © 2023, by Department of Mechanics, Materials and
Biomedical Engineering, Faculty of Mechanical Engineering,
Wrocław University of Science and Technology,
Wrocław, Poland

All right reserved

Editorial office

Wrocław University of Science and Technology,
Department of Mechanics, Materials and Biomedical Engineering,
Faculty of Mechanical Engineering
Łukasiewicza 7/9, 50-371 Wrocław, Poland

Technical editor

Anna Nikodem

Proofreading

Ewelina Świątek - Najwer

Cover design

Marcin Zawadzki

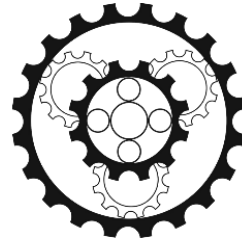
CONFERENCE ORGANIZERS

WROCLAW UNIVERSITY OF SCIENCE AND TECHNOLOGY,
FACULTY OF MECHANICAL ENGINEERING,
WROCLAW, POLAND



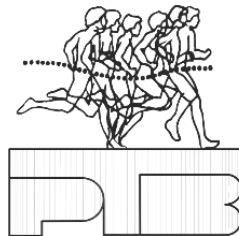
Wrocław
University
of Science
and Technology

*Rector of the Wrocław University of Science
and Technology,
Prof. Arkadiusz Wójs, DSc, PhD, Eng.*



*Dean of the Faculty of Mechanical
Engineering
Prof. Celina Pezowicz, DSc, PhD, Eng.*

THE POLISH SOCIETY OF BIOMECHANICS



SCIENTIFIC PATRONAGE



*European Society of
Biomechanics*



*Association of Polish
Engineers and Technicians,
Wrocław Branch*



*Biomechanics Section of the
Committee on Mechanics of the
Polish Academy of Sciences*



Ministry of Education and Science Republic of Poland

Project co-financed by the state budget, granted by the Ministry of Education and Science Republic of Poland under the Programme “Excellent Science II” – project No. KONF/SN/0491/2023/012.

ORGANISING COMMITTEE

Conference Chairperson

Anna Nikodem

Deputy Conference Chairperson

Małgorzata Żak

Members

Urszula Czajkowska

Adrianna Filipiak – Kaczmarek

Karolina Jasiurkowska

Marta Kozuń

Justyna Lichosik

Karol Marcula

Bartosz Martyniuk

Jakub Słowiński

Klaudia Szkoda-Poliszuk

Sylwia Szotek

Ewelina Świątek-Najwer

Justyna Wolicka

Magdalena Żuk

SCIENTIFIC COMMITTEE

Chairperson of the Scientific Committee

Celina Pezowicz, Poland

Co-Chairperson of the Scientific Committee

Jarosław Filipiak, Poland

Honorary Chairpersons of the Scientific Committee, *The President of the Polish Society of Biomechanics*

Małgorzata Syczewska, Poland

Members

- | | |
|--------------------------------------|---|
| <i>Taiji ADACHI, Japan</i> | <i>Daniel MATEJ, Czech Republic</i> |
| <i>Katarzyna ARKUSZ, Poland</i> | <i>Adam MAZURKIEWICZ, Poland</i> |
| <i>Wojciech BLAJER, Poland</i> | <i>Grzegorz MILEWSKI, Poland</i> |
| <i>Michalina BŁAŻKIEWICZ, Poland</i> | <i>Andrzej MŁYNIEC, Poland</i> |
| <i>Tadeusz BURCZYŃSKI, Poland</i> | <i>Karol MILLER, Australia</i> |
| <i>Krzysztof BUŚKO, Poland</i> | <i>Zbigniew NAWRAT, Poland</i> |
| <i>Luca CRISTOFOLINI, Italy</i> | <i>Grace O'CONNELL, USA</i> |
| <i>Adam CZAPLICKI, Poland</i> | <i>Elżbieta PAMUŁA, Poland</i> |
| <i>Manuel DOBLARÉ, Spain</i> | <i>Jolanta PAUK, Poland</i> |
| <i>Thomas DREHER, Switzerland</i> | <i>Marek PAWLKOWSKI, Poland</i> |
| <i>Jan GAJEWSKI, Poland</i> | <i>Szczepan PISZCZATOWSKI, Poland</i> |
| <i>Joanna GORWA, Poland</i> | <i>Maria Ángeles PÉREZ ANSÓN, Spain</i> |
| <i>Marek GZIK, Poland</i> | <i>Gwendolen REILLY, United Kingdom</i> |
| <i>Christian HELLMICH, Austria</i> | <i>Danuta ROMAN-LIU, Poland</i> |
| <i>Daoud Robert ISKANDER, Poland</i> | <i>Alicja RUTKOWSKA-KUCHARSKA, Poland</i> |
| <i>Sona JANDOVA, Czech Republic</i> | <i>Eugeniusz SAJEWICZ, Poland</i> |
| <i>Antoni JOHN, Poland</i> | <i>Małgorzata SOBERA, Poland</i> |
| <i>Ilse JONKERS, Belgium</i> | <i>Małgorzata SYCZEWSKA, Poland</i> |
| <i>Grzegorz JURAS, Poland</i> | <i>Arkadiusz SZAREK, Poland</i> |
| <i>Jacek JURKOJC, Poland</i> | <i>Wojciech ŚWIĘSZKOWSKI, Poland</i> |
| <i>Michał KUCZYŃSKI, Poland</i> | <i>Bert van RIETBERGEN, The Netherlands</i> |
| <i>Izabela LUBOWIECKA, Poland</i> | <i>Giuseppe VANNOZZI, Italy</i> |
| <i>Tomasz ŁODYGOWSKI, Poland</i> | <i>Wiktoria WOJNICZ, Poland</i> |
| <i>Ewa MAJCHRZAK, Poland</i> | <i>Wojciech WOLAŃSKI, Poland</i> |
| <i>Jerzy MAŁACHOWSKI, Poland</i> | <i>Michał WYCHOWAŃSKI, Poland</i> |
| <i>Andrzej MASTALERZ, Poland</i> | |

CONFERENCE SPONSORS

Golden sponsor



Silver sponsors



Bronze sponsors



Supporting sponsors



Preface

We warmly welcome you to the **International Conference Biomechanics 2023**, bi-annual Conference of the Polish Society of Biomechanics. This prestigious event marks a milestone in our long tradition of over 36 year.

The conference has its roots dating back to 1959 when the inaugural Biomechanics Symposium took place, organized by the Higher School of Physical Education in Poznań. In 1987, the National Conference on Biomechanics commenced under the leadership of Professor Włodzimierz Erdman from the Academy of Physical Education in Gdańsk, shaping the landscape of our field.

This tradition has cultivated a network of universities engaged in comprehensive biomechanical research, resulting in interdisciplinary projects across Medicine, Engineering, Rehabilitation, and Sports. The evolution of Biomechanics, coupled with technological advancements, has contributed to related sciences like sports biomechanics, clinical biomechanics, biocybernetics, and biomaterials. Numerous scientific conferences, both nationally and internationally, have showcased the extensive and interdisciplinary nature of our work. These efforts have also educated generations of researchers attuned to cutting-edge technologies and innovative solutions, with a primary focus on the human condition.

This year, the conference will be hosted in Wrocław University of Science and Technology – Wrocław is a city renowned for its centuries-old history of cultural amalgamation, characterized by an atmosphere of openness and hospitality.

Wrocław's vitality is further enriched by its vibrant student population. Founded in 1945, **Wrocław University of Science and Technology** plays a pivotal role in the city's academic landscape. We are pleased to announce the inauguration of our 14th faculty, the Faculty of Medicine, which will empower future doctors with advanced skills and knowledge, leveraging the latest technological advancements.

As we proudly host the **International Biomechanics Conference 2023**, we present a book of abstracts as a supplement to **Acta of Biomechanics and Bioengineering**, a journal published by the Wrocław University of Science and Technology Publishing House since 1999 (<https://actabio.pwr.edu.pl>, an official journal of Polish Society of Biomechanics). This compilation comprises over 85 contributions from researchers across Poland and the world, a proof of our collaborative interdisciplinary endeavours.

We extend our gratitude to the authors and anticipate insightful discussions during the 9 oral sessions and poster session. Additionally, we offer workshops organized by the Faculty of Mechanical Engineering and acknowledge our sponsors for their invaluable support.

We trust that your time in **Wrocław** will enrich your professional network and deepen your understanding of biomechanics. Welcome to our city and university, where you will experience a unique and enriching atmosphere.

Celina Pezowicz
Anna Nikodem
Małgorzata Syczewska

List of Contents

| | |
|--|----|
| Sponsors | 6 |
| Preface | 7 |
| List of contents | 8 |
| Book of abstracts: | |
| K. Arkusz, K. Pasik, A. Haliński <i>Comprehensive evaluation of urological Double-J stent encrustation: patient age, stent material, and implantation duration.....</i> | 12 |
| P. Aschenbrenner, R. Urbański, W. Erdmann <i>Mathematical model of a turn in alpine skiing.....</i> | 14 |
| B. Bacik, G. Sobota, K.A. Bacik, T. Rogers <i>Velocity distribution in a pedestrian contraflow experiment</i> | 16 |
| M. Błażkiewicz, R. Borkowski, K. Kaczmarczyk, A. Zdrodowska, M. Jarocka <i>Gait kinetics during induced perturbations in the pre-swing phase of the gait cycle</i> | 18 |
| M. Bobrowska, Z. Kosobucka, P. Tabor, E. Olszewska, J. Pniewski <i>Visual disorders and selected features of body posture - a pilot study</i> | 20 |
| A. Bonik, L.F. Ciupik, A. Kierzkowska, E. Słoński <i>Ilio-sacral stabilization supported with bone cement</i> | 22 |
| P. Borkowski <i>Temporal bone support in a finite element analysis of bone conduction stimulation on the otic capsule</i> | 24 |
| A.Brachman, B.Bacik, G.Sobota <i>Gait stability evaluation after tripping simulated perturbation – assumptions of the project</i> | 26 |
| G.P. Carmo, A. Silva, M. Dymek, M. Ptak, F.A.O. Fernandes, R.J. Alves de Sousa <i>Development, Validation and a Case Study: The Female Finite Element Head Model</i> | 28 |
| M. Chmura, P.Wodarski, M. Szlęzak, G. Gruszka, J.Romanek, J. Jurkojć <i>Influence of postural adjustment in response to anterior-posterior ground perturbation</i> | 30 |
| A. Cichański, K. Nowicki <i>Numerical analysis of trabecular bone microstructure for different voxel modelling methods</i> | 32 |
| A. Cieślak, M. Łabowska, A. Krakos (Podwin), J. Kulbacka, J. Detyna <i>Development of biocompatible hydrogel matrices for 3D cell cultures in lab-on-chip applications.....</i> | 34 |
| A. Ciszkiewicz <i>Optimization and random sampling in selected aspects of modeling body joints with a multibody system method</i> | 36 |
| L.F. Ciupik, A. Kierzkowska, G. Pająk, P. Powchowicz, F. Andruszkiewicz <i>Innovative 3D-Ti-Truss procedure in biomechanical spinal stabilisation</i> | 38 |
| U.Czajkowska, M. Żuk, K. Smerd, C. Pezowicz, M. Popek, M. Łopusiewicz, K. Bulińska <i>Application of joint kinematics analysis to evaluate the correctness of users' exercise performance in a virtual reality environment.....</i> | 40 |
| A. Czaplicki, M. Jarocka, T. Sacewicz, J. Walawski <i>Spectral analysis of ground reactions evoked by patients after medial patellofemoral ligament (MPFL) reconstruction</i> | 42 |
| N. Daniel, K. Sybilski, J. Małachowski <i>Technical aspects and limitations of signal acquisition during dynamic movement on the rowing ergometer</i> | 44 |
| O. Denisov, N. Kizilova <i>Biomechanics and efficiency of n-link extremities of insects</i> | 46 |
| A. Ferreira, M. Górski, P. Tabor, J. Gajewski <i>Gender differences in kinematic determinants of shuttlecock velocity and flight angle in the badminton forehand smash</i> | 48 |
| A. Filipiak-Kaczmarek, A. Nikodem, K.Naplocha <i>Mechanical and structural properties of AZ91-based Ti reinforcement composite</i> | 50 |

| | |
|---|----|
| D. Fryc, K. Wojciechowski <i>Gait kinematics asymmetry change induced by multijoint hip flexion resistance training – a preliminary research</i> | 52 |
| M. Głowacki, A. Mazurkiewicz <i>Methods to increase the strength of 3D printed PLA samples, a mini review</i> | 54 |
| D. Grygier, P. Kowalewski, M. Dziubek, R. Jastrzębek, M. Opałka, J. Słowiński <i>The possibility of using the OrthoNail hybrid intramedullary nail in the human body without risk of decohesion</i> | 56 |
| A. Gryko, P. Prochor <i>Finite element analysis of the influence of porosity and pore geometry on mechanical properties of orthopaedic scaffolds</i> | 58 |
| A. Hadamus, B. Osuch, K. Wiaderna, T. Jankowski, A. Ferenc, D. Białoszewski <i>Influence of a single session of occlusion training on time parameters in isokinetic knee flexion - extension strength measurements</i> | 60 |
| A. Handke, S. Wudarczyk <i>Simulation Research on Kinematic and Dynamic Requirements of Prosthetic Hand During Grasping</i> | 62 |
| D. Iwan, P. Prochor <i>Numerical evaluation of the influence of selected parameters of orthopaedic scaffolds on load transfer within long bone</i> | 64 |
| B. Jasiński, P. Krowicki <i>Development of a simulator of surgical procedures supported by a vision system</i> | 66 |
| M. Jasiński, M. Zadoń <i>Mathematical modelling of coupled thermal and chemical effects in biological tissue during laser irradiation</i> | 68 |
| K. Jasiurkowska, J. Filipiak <i>Analysis of the influence of the bone fracture stabilization system on the biomechanics of the bone healing process</i> | 70 |
| K. Kaczmarczyk, P. Bobowik, I. Wiszomirska, J. Gajewski, M. Błażkiewicz, M. Czuba, A. Maciejewska- Skrendo, Y. Matharu, K. Kulig <i>Developing a Literature-informed Intervention Protocol to Address post-COVID-19 Balance Disorders, Weakness and Muscle Fatigue in Individuals Aged 65+</i> | 72 |
| S. Kalinowski, K. Szepietowska, E. Florentin, I. Lubowiecka <i>Optimisation of thickness of surgical implant used in abdominal hernia repair</i> | 74 |
| E. Kawlewska, P. Czarnecki, A. Mol, T. Koszutski, M. Gzik, W. Wolański <i>Quantitative evaluation of the surgical treatment of cleft palate in infants</i> | 76 |
| M. Kazalski, E. Świątek-Najwer <i>Electromyographic-based hand prosthesis movements control in Virtual Reality application for patient adaptation</i> | 78 |
| N. Kizilova, L. Batyuk <i>Comparative analysis of rheological models for human blood</i> | 80 |
| S. Klimas, A. Nikodem, M. Dobrzyński <i>An in-vitro evaluation of mechanical properties and thermographic investigation of selected dental materials used in primary dentition - glass-ionomer cement (Fuji IX) and composite (Charisma)</i> | 82 |
| M. Kobielarz. A. Chwilkowska <i>Hyperelastic models comparison for abdominal aortic aneurysms</i> | 84 |
| P. Kowalewski, D. Grygier, P. Krowicki, R. Jastrzębek, M. Opałka, M. Kielb <i>Evaluation of the possibility of using a hybrid magneto-mechanical drive in dynamic implants for lengthening long bones</i> | 86 |
| M. Kozuń, M. Kobielarz <i>The effect of atherosclerosis on the susceptibility of the human aorta to delamination</i> | 88 |
| K.H. Krawiec, D. Pyka, K. Jamroziak, A. Noszczyk - Nowak <i>Experimental and numerical tests of piercing the head of a pig subjected to a shock load</i> | 90 |
| S. Kuliś, J. Gajewski <i>Kinematic analysis of sway motions of elite dance sport competitors</i> | 92 |

| | |
|--|-----|
| J. Kurowiak | |
| <i>Analysis of material and mechanical properties of stents to increase the effectiveness of urethral stenosis treatment</i> | 94 |
| A. Mackiewicz, W. Dylewicz, J. Gach, I. Janus, T. Klekiel, A. Noszczyk - Nowak | |
| <i>Numerical analysis of damages chordae tendineae caused by myxomatous mitral valve disease in dogs</i> | 96 |
| E. Majchrzak, B. Mochnicki | |
| <i>Sensitivity of biological tissue heating process described by Cattaneo–Vernotte equation with respect to perturbation of lag time</i> | 98 |
| J. Małachowski, Ł. Mazurkiewicz, K. Pietroń, K. Sybilski | |
| <i>Determination of bone stiffness using multi-model optimisation</i> | 100 |
| K. Marcula, M. Kozuń, J. Filipiak | |
| <i>Mechanical characteristics determination of elastomer elements intended for the long gap esophageal atresia treatment</i> | 102 |
| A. Nikodem | |
| <i>Investigation of 24-month biodegradation of PCL scaffolds with the addition of bioglass and Zn using computer microtomography</i> | 104 |
| A. Nikodem, M. Kozuń | |
| <i>The influence of cyclic loads on the structural properties of the femur bone tissue with osteoarthritis</i> | 106 |
| G. Ostrowski, M. Pawlikowski, P. Garbacz | |
| <i>Application of Transformer-Based Neural Networks in the Cells Segmentation Task in Fluorescent Microscopic Images</i> | 108 |
| R. Perz | |
| <i>Investigating Pediatric Head Trauma in Unmanned Aerial Vehicle Accidents</i> | 110 |
| A. Piszko, A. Nikodem, P. Piszko, M. Dobrzyński | |
| <i>Fluoride release and selected chemo mechanical characteristics of three different commercially available dental materials for sealing</i> | 112 |
| P. Prochor, A. Szczerba, S. Piszczatowski | |
| <i>Concept of mechatronic device for supporting balance during locomotion with the function of recording kinematic parameters</i> | 114 |
| A. Ptak, A. Tomczak | |
| <i>Analysis of tribological properties of prosthetic materials under different conditions of use</i> | 116 |
| D. Pyka, A. Nowicki, Ł. Pałka, A. Kurzawa, K.H. Krawiec, K. Jamroziak | |
| <i>Analysis of implant-bone junction fracture induced by force impulse in traffic collision</i> | 118 |
| M. Roszak, M. Mamys, D. Pyka, M. Bocian, K. Jamroziak | |
| <i>Analytical and numerical analysis of soft tissue penetration on the example of a pistol ammunition shot</i> | 120 |
| S. Sikora, M. Pawlikowski, K. Jankowski | |
| <i>Preliminary 3D simulations of osteoarthritis in the knee joint</i> | 122 |
| M. Skrodzka, M. Nowicka, M. Łabowska, J. Detyna, K. Matczyszyn | |
| <i>Mechanistic evaluation of the sodium alginate/chitosan hydrogel matrices for the release of a photosensitizing substance</i> | 124 |
| M. Sobera, P. Proskura | |
| <i>Trunk rotation and posture control asymmetry in children and young adults</i> | 126 |
| P. Stróżyk | |
| <i>Determination of intrinsic strength for the mandibular elevator muscles during unilateral mastication of different foodstuffs</i> | 128 |
| A. Struzik | |
| <i>Relationships between leg stiffness and displacement of centre of mass during countermovement jumps to specific and various height</i> | 130 |
| M. Syczewska, J. Michoński, M. Kalinowska, E. Szczerbik, R. Sitnik | |
| <i>Proper identification of body mass distribution modifies the outcome of the simulation. Preliminary results</i> | 132 |
| K. Szepietowska, M. Staat, M. Rykaczewski, I. Lubowiecka | |
| <i>Personalised finite element models of the human abdominal wall under material model uncertainties</i> | 134 |
| K. Szkoda-Poliszuk, M. Żak, A. Brończyk, C. Pezowicz | |
| <i>Analysis of the degree of mechanical wear in the transpedicular stabilization of the spine</i> | 136 |
| S. Szotek, J. Dawidowicz, A. Czogalla, K. Maksymowicz | |
| <i>Mechanical properties and microscopic characterization of human fascia lata</i> | 138 |

| | |
|---|-----|
| A. Szpala, M. Kołodziej, M. Kaźmierczak, Z. Bańkosz <i>Electromyographic activity of selected muscles of the lower limbs and the type of lunge in badminton</i> | 140 |
| A. Szust, A. Wybraniec, D. Nasulicz, M. Maj <i>Analysis of ways to mount prosthetic dental bridge on implants</i> | 142 |
| P. Szymczyk-Ziółkowska, G. Ziółkowski, D. Kęszczycki, K. Kobiela, M. Rusińska, K. Sekuła <i>Advancements in Maxillofacial Reconstruction: Design and Manufacturing of Patient-Specific Implants</i> | 144 |
| A. Tomaszewska, S. Piszczatowski <i>Analysis of bone remodelling in the mandible with the implant reconstruction of bone defect</i> | 146 |
| M. Tomaszewski, M. Kucewicz, R. Rzepliński, J. Małachowski, B.M. Ciszek <i>Research on the flow characteristics in artificial vessels: an experimental investigation using the PIV method</i> | 148 |
| M. Troka, K. Szepietowska, I. Lubowiecka <i>Clustering of Strains Datasets of Human Abdominal Wall with Self-Organising Maps</i> | 150 |
| I. Ważydrąg, S. Łagan <i>The development process of the tissue's direct piezoelectric effect measurement device</i> | 152 |
| P. Wądołowski <i>Numerical simulations of mandible angle fracture stabilization by means of mini-plate stabilization</i> | 153 |
| D. Wdowicz, M. Ptak <i>Multitechnique analysis of dynamics of numerical pedestrian model for forensic applications</i> | 155 |
| K. Wilińska, A. Nikodem, M. Kozuń <i>Mechanical properties of lattice structures fabricated using incremental technology</i> | 157 |
| P. Wodarski, J. Jurkojć, J. Michalska, A. Kamieniarz, G. Juras, M. Gzik <i>Stock market indexes in assessing balance of patients with Parkinson's disease</i> | 159 |
| W. Wojnicz, B. Zagrodny, M. Ludwicki, A. Sobierajska-Rek, J. Jabłońska-Brudło, K. Forysiak <i>Assessment of type of control in chosen ADL performances of wheelchair patient with DMD and healthy adolescent: case study</i> | 161 |
| J. Wolicka, J. Filipiak, A. Nikodem <i>Long-term observation of porous structure PLGA scaffold degradation in an incubation environment</i> | 163 |
| A. Wybraniec, A. Szust <i>A comparative study of mandibular bone implants using commercial reconstructive and personalized implants</i> | 165 |
| R. Zabłotni, R. Rusinek <i>Influence of double excitation in Lumped Parameter Model of Implanted Human Middle Ear</i> | 167 |
| Z. Zając, A. Liber-Kneć, S. Łagan <i>Comparison of the surface and mechanical properties of low viscosity acrylic bone cements</i> | 169 |
| P. Zalewska, T. Guszczyn, S. Piszczatowski <i>Comparison of knee joint kinematics in patients after ACL reconstruction and ACL repair using Internal Bracing method.</i> | 171 |
| X. Zhao, J. Awrejcewicz, D. Grzelczyk, Y. Gu <i>A three-link model of a fetal lower limb for simulating the fetal kicking movement</i> | 173 |
| M. Żak, A. Nikodem, C. Pezowicz <i>Methods of evaluating mechanical parameters and the stability of the cervical interbody fusion cage</i> | 175 |
| M. Żak, S. Szotek, K. Szkoda-Poliszuk, J. Filipiak, M. Wrzosek, K. Kołtowski, P. Menartowicz, C. Pezowicz <i>Effect of DLC coating of growth-guidance system implants on changes in mechanical and kinematic properties of the spine</i> | 177 |
| K. Żerdzicki, W. Korbut, A. Kondrusik <i>Compressive properties of polyurethane foam mimicking trabecular tissue in femoral head of synthetic bones</i> | 179 |
| M. Żuk, U. Czajkowska, K. Bulińska, M. Popek, M. Łopusiewicz <i>eMotion - system for computer aided rehabilitation- first usability tests on patients</i> | 181 |
| Index of authors | 183 |

Comprehensive evaluation of urological Double-J stent encrustation: patient age, stent material, and implantation duration

K. ARKUSZ^{1*}, K. PASIK¹, A. HALIŃSKI²

¹Department of Biomedical Engineering, Faculty of Mechanical Engineering, University of Zielona Góra, Zielona Góra, Poland

²Department of Clinical Genetics and Pathomorphology, University of Zielona Góra, Zielona Góra, Poland

Key words: *Double-J stent, encrustation, biofilm formation, mechanical strength, kidney stone*

1. Introduction

Urolithiasis, defined as the process of forming kidney stones localized within the tubular lumen and lower urinary tract or primary bladder stones, is a common problem affecting 20% of the population worldwide, which will grow significantly over the coming years [1]. Ureteral stenting is a standard procedure used in 60% of patients after treatment for ureteral stones and 80% of patients after treatment for renal stones [2]. The colonization of bacteria and encrustation on the surface of stents are two of the most common complications: stent-related and blockage, which can lead to the device's inability to function [3]. How serious this problem is evidenced by the statistics developed by Tomer et al., showing as many as 41,369 complications on 50,000 procedures of implantation of a ureteral stent [4]. Solving this problem first requires understanding the clinical significance of encrustation and bacterial colonization on ureteral stents - there is no consensus on which specific pathogens, if any, increase the risk of encrustation. Additionally, it is unclear how biofilm formation on the surface of the stent may precipitate minerals and trigger encrustation.

2. Materials and Methods

In total, 240 double-J ureteral stents (DJ stents) were removed from renal stone patients and recruited to the study between January 2019 and May 2023. First, the most susceptible material for biofilm formation was indicated. The first kind of DJ stent was built with a proprietary silicone-modified styrene/ethylene/butylene block copolymer (copolymer DJ stents); the second was a classic polyurethane stent. Second, the influence of patient age (1.5 - 55 years) and implantation time (from 7 to 124 days) on encrustation and biofilm formation was examined. Microscopic analysis was performed on the ureteral stents implanted after the URS-L. The microscopic observation was performed by the scanning electron field emission microscope JEOL JSM 7600F (SEM). Representative polyurethane and copolymer DJ stents before and after implantation for 31 days were characterized by Fourier transform infrared spectroscopy (FTIR) (Thermo Scientific™ Nicolet™ iS50 FTIR Spectrometer, Thermo Scientific™, USA). Data were collected in the absorption mode between 4000 cm⁻¹ and 400 cm⁻¹ with a resolution of 4 cm⁻¹. Tensile strength and stiffness were tested for all DJ stents before and after urinary exposure. The tensile strength was measured using a Zwick Testing System, using a 5 N load cell. DJ stents were tested in uniaxial tension at 1 mm/s for 1 second. Unpaired Student's t-test was used to compare each DJ-stent group. A value of $p < 0.05$ was considered statistically significant.

*Corresponding author: Katarzyna Arkusz, e-mail: k.arkusz@iimb.uz.zgora.pl

3. Results

Performed research has shown that polyurethane DJ stents have a much higher affinity for the encrustation of calculi than silicone-based copolymers. Residues deposited on the surface of the DJ stent form a homogeneous multi-layer, mainly composed of weddellite and uric acid crystals. Encrustation of silicone DJ stents during 31 days reduces Young's modulus by 27-30%, which confirms the loss of DJ stent elasticity and increased probability of cracks or interruption. Moreover, crystalline and calculi deposition on DJ stent was observed even 7 days after implantation in children's patients. Microscopic analysis indicated that the distal and proximal parts of the stent (the part located in the renal pelvis) are the most susceptible to post-URS-L fragments and urea salt deposition. DJ stent diameter (1.00, 1.33, 1.66 mm) impacts the encrustation phenomenon: the most extensive aggregation of crushed stones and crystals was observed for the DJ stents with a diameter of 1.00 mm, and the least encrustation was observed for 1.66 mm. Implantation affects the surface by increasing its roughness, thus increasing the affinity for biofilm formation.

Further research indicated that the spectrum of bacterial pathogens is significantly different in patients with struvite stones compared to patients with other stones. For microbial isolates in patients with struvite stones, the most common ones were *Escherichia coli* (27.7%) and *Proteus spp.* (27.7%) followed by *Klebsiella spp.* (16.7%), Gram-positive bacteria (5.5%), and *Pseudomonas aeruginosa* (5.5%). These bacteria accounted for 83.3% of the total flora tested. In other types of stone, *Escherichia coli* was the most frequent isolate (47.6%), followed by Gram-positive bacteria (14.0%) and *Klebsiella spp.* (7.8%). *Proteus spp.* and *Pseudomonas aeruginosa* accounted for only 4.6% and 2.3%, respectively. The uropathogens in the Gram-positive group were *Enterococcus faecalis*, *Enterococcus faecium*, *Staphylococcus aureus*, *Staphylococcus cepreae*, *Streptococcus agalactiae*.

Acknowledgments: K.A, K.P, A.H. acknowledge the financial support from the program of the Polish Minister of Science and Higher Education under the name "Regional Initiative of Excellence" in 2019 - 2022, project no. 003/RID/2018/19, funding amount 11 936 596.10 PLN.

References

- [1] ZHANG L., ZHANG X., PU Y., ZHANG Y., FAN J. *Global, regional, and national burden of Urolithiasis from 1990 to 2019: A systematic analysis for the global burden of disease study 2019*, J Clin Epidemiol, 2022, 14, 971–983. doi:10.2147/clep.s370591
- [2] ORDONEZ M., HWANG E.C., BOROFKY M., BAKKER C.J., GANDHI S., DAHM P. *Ureteral stent versus no ureteral stent for ureteroscopy in the management of renal and ureteral calculi*, The Cochrane Database of Systematic Reviews, 2019, 2. doi:10.1002/14651858.CD012703.pub2
- [3] GEAVLETE P., GEORGESCU D., MULȚESCU R., STANESCU F., COZMA C., GEAVLETE B. *Ureteral stent complications - experience on 50,000 procedures*, J Med Life Sci, 2021, 14(6), 769–775. doi: 10.25122/jml-2021-0352
- [4] TOMER N., GARDEN E., SMALL A., PALESE M. *Ureteral Stent Encrustation: Epidemiology, Pathophysiology, Management and Current Technology*, J Urol, 2021, 205(1), 68–77. doi:10.1097/JU.0000000000001343

Mathematical model of a turn in alpine skiing

P. ASCHENBRENNER*, R. URBAŃSKI, W. ERDMANN

Gdańsk University of Physical Education and Sport, Gdańsk, Poland

Key words: simulation, speed distribution, optimization, trajectory

Abstract

The objective of professional alpine skiers is to attain the minimal time possible on a slalom course delineated by gates. In recent years, a plethora of scientific research has been carried out to examine this sport, seeking optimal solutions concerning technique, equipment, athlete preparation, and course trajectories, among other factors. Mathematical models describing alpine skiers' movements can be employed to analyze these topics [1]. This study aims to create a model that considers crucial elements associated with athletes' slalom courses.

Existing alpine skiing models were analyzed, including: biomechanical models [2][3], aerodynamic models [4][5], trajectory optimization models [6][7]. Based on the literature review, the mathematical model of the alpine skier's run should take into account the following elements: forces acting on the skier (gravity, air resistance, friction force), biomechanical variables (angle of the ski relative to the horizontal plane, angle of the ski edge, position of the skier's body), aerodynamic parameters (skier's body shape, skis, helmet and clothing), route-related variables (terrain profile, slope, type of snow) and individual characteristics of the competitor (weight, height, skill level) and the specificity of the alpine skiing discipline (SL, G, SG, DH). Based on such a model, strategies for optimizing the alpine skier's ride can be developed.

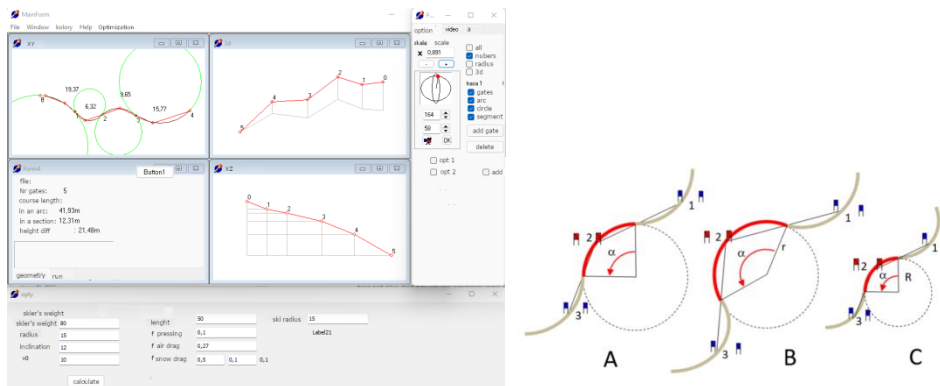


Fig. 1. Simulation application. and segments with different lengths and the same radius - A, B and with different radius C

The first stage of the simulation includes determining the parameters describing the run with simplified assumptions: The path is enforced by passing the gate on the given side; The geometry of the goals (XYZ) is known; The path is described by the sum of arcs with the given radius and angle (in the next step with polynomials); A segment is one arc in a plane with a constant slope angle; The skier can change the radius of the turn and the friction forces in the range from min to max values for a given

*Corresponding author: Piotr Aschenbrenner, e-mail: piotr.aschenbrenner@awf.gda.pl

section at the beginning of the section (at any point in the next stage); Forces taken into account: gravity, air resistance, friction and ski-ground resistance, centrifugal (in the next stage of elasticity, damping, etc.); The skier's model is a point (in the next step, a model with body parts and equipment); Skier's parameters: weight, frontal area (in the next stage, energy resources, power, muscle strength, etc.)

Numerical simulations were performed in a computer application created in the Delphi Borland environment. (Fig. 1) The preliminary results allow to calculate the travel time of the marked section with variable parameters such as arc length and radius, slope inclination, skier's weight, initial speed (Fig. 2).

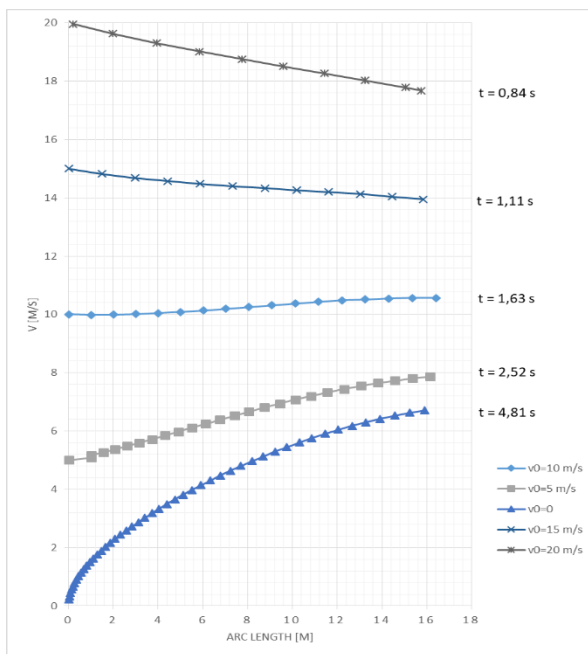


Fig. 2. Speed distribution on a turn with a radius of 14,5 m and a length of 16 m depending on the initial speed (skier's weight 80 kg)

References

- [1] MAROŃSKI R.. *Minimum-time running and swimming: an optimal control approach*. J Biomech, 1996, 29, 245–249
- [2] REID, R., GILGIEN, M., & HAUGEN, P. *Aerodynamic drag is not the major determinant of performance during giant slalom skiing at the elite level*. Scand J Med Sci Sports, 2010, 20(1), 34–42
- [3] MÜLLER E., SCHWAMEDER H., KORNEXL E., RASCHNER C. *The effects of alpine skiing on leg-pulling force, balance and coordination*. J Sports Sci, 2013, 31(8), 819–827
- [4] HOLMÉR I., GAVHED D., NIELSEN R. *Aerodynamic testing of speed ski racing suits*. Appl. Ergon, 2005, 36(2), 185–190
- [5] SUPEJ M., HOLMBERG H. C., ŠARABON N. *Aerodynamic drag in alpine skiing: validation of CFD simulations with wind tunnel experiments*. Comput Methods Biomech Biomed Eng, 2008, 11(6), 617–624
- [6] FEDEROLF P., ROOS M., LÜTHI A. *The effect of skier speed on the kinematics of the ski–snow interaction*. Sports Eng, 2012, 15(3), 129–137
- [7] SPÖRRI J., KRÖLL J., AMESBERGER G., BLAKE O. M., MÜLLER E. *Perceived key injury risk factors in World Cup alpine ski racing—an explorative qualitative study with expert stakeholders*. Br J Sports Med, 2012, 46(15), 1059–1064

Velocity distribution in a pedestrian contraflow experiment

B. BACIK^{1*}, G. SOBOTA¹, K.A. BACIK², T. ROGERS²

¹Department of Human Motor Behavior, Institute of Sport Sciences,
Academy of Physical Education in Katowice, Katowice, Poland

²Centre for Networks and Collective Behaviour, Department of Life Sciences,
Department of Mathematical Sciences, University of Bath, UK

Key words: crowd motion, lane formation, walking speed

1. Introduction

Crowd motion is a complex phenomenon which can be of interest to a range of disciplines from psychology, through biomechanics, to physical and mathematical sciences [1,3,4]. Understanding crowd dynamics can also contribute to efficient and safe design of buildings and pedestrian concourses. In our recent experiment, which served to validate the kinetic model in complex active flow [1], we analysed the motion of two groups with opposing walking targets, such as the contraflow of two groups moving across a zebra crossing. In such scenarios one often observes spontaneous spontaneous formation of lanes parallel to the direction of differential velocity.

Here we present more detailed, secondary analysis of our previously published data, where we analyse the relative velocities of pedestrians within one walking group. Specifically, we focus on the differences in behaviour between the 'leading' (L), 'middle' (M), and 'trailing' (T) members of the group, as well as the differences in velocity between the exterior (EX) and middle lanes (MID). The key quantity of interest is the average gait speed, which can be notably different before the encounter with the other group (V_{before}), during collision-like dodging manoeuvres ($V_{\text{collisions}}$), and after passing all the members of the other group (V_{after}). We interpret the results in terms of local crowd density, and global structure of the flow.

2. Material and Methods

We present here new, more extensive analysis the dataset published in Ref. [2], which comprises pedestrian trajectories from a suite of experiments conducted across two sessions with 60 and 73 participants, respectively. Here we focus exclusively on the archetypal lane formation scenario, with two groups of parallel, but opposite moving directions. The experiments were conducted in a relatively dilute, freely flowing regime, with average crowd densities at the order of 2 persons/m². Detailed description of the data collection methodology can be found in Materials and Methods of Ref. [1].

We employ an automated interaction detection algorithm to divide the motion of an individual into three epochs: before, during, and after the interaction with the opposing group. To test the influence of the contraflow on the movement, we analyse the average velocity in each of these periods. As we are primarily interested in relative differences between members of the same walking group, we normalise the velocity for each trial.

3. Results

The first finding of our analysis is that in the side (exterior) lanes the values are much higher than in the middle (interior) lanes (Fig. 1). Secondly, we find notable differences between the individuals positioned in front, and at the back of a given group. Whilst the post-interaction velocities are uniform across the group, in the middle period the leaders (L) move significantly faster than the middle group

*Corresponding author: Bogdan Bacik, e-mail: b.bacik@awf.katowice.pl

(M), which is in turn faster than the trailing group (T). This trend points to an interaction-induced rarefaction of a group. Towards, the end of the experiment, however, the elongation is compensated by the acceleration of the trailing group (middle panel of Fig. 1).

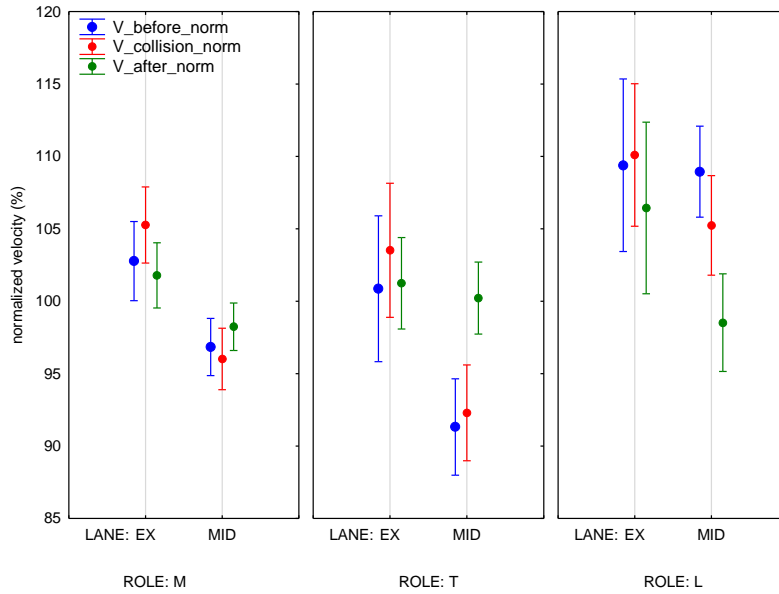


Fig. 1. Speeds distribution

References

- [1] BACIK K. A., BACIK B. S., ROGERS T. *Lane nucleation in complex active flows*. Science (New York, N.Y.), 2023, 379(6635), 923–928, doi.org/10.1126/science.add8091
- [2] BACIK K., BACIK B., ROGERS T. *Dataset for "Lane nucleation in complex active flows"*. Bath: University of Bath Research Data Archive. 2023, Available from: <https://doi.org/10.15125/BATH-01242>.
- [3] MURAKAMI H., FELICIANI C., NISHIYAMA Y., NISHINARI K. *Mutual anticipation can contribute to self-organization in human crowds*. Sci Adv, 2021, 7(12), 1–9, doi.org/10.1126/sciadv.abe7758
- [4] THOMPSON P., NILSSON D., BOYCE K., MOLLOY M., MCGRATH D. *Exploring the biomechanics of walking and crowd "flow"*. Fire and Mater, 2020, 44(6), 879–893, doi.org/10.1002/fam.2889

Gait kinetics during induced perturbations in the pre-swing phase of the gait cycle

M. BŁAŻKIEWICZ^{1*}, R. BORKOWSKI¹, K. KACZMARCZYK¹, A. ZDRODOWSKA¹, M. JAROCKA²

¹Department of Rehabilitation, Józef Piłsudski University of Physical Education in Warsaw, Warsaw, Poland

²Józef Piłsudski University of Physical Education in Warsaw, Biała Podlaska Branch, Poland

Key words: gait, perturbations, treadmill, provoked trips

1. Introduction

Post-perturbation falls are frequent in daily life, posing a significant issue for various age groups. Mechanical, neurological, or psychological constraints can hinder post-perturbation balance. The aim of this study was to analyse the impact of perturbations occurring during the pre-swing phase on gait kinetics in young and older people.

2. Material and Methods

Twenty-one young ($a = 21.38 \pm 1.32$ y.o., $m = 61.38 \pm 6.48$ kg, $h = 165.9 \pm 4.53$ cm) and twenty-one older ($a = 67.75 \pm 4.7$ y.o., $m = 73.36 \pm 11.06$ kg, $h = 161.5 \pm 5.18$ cm) women participated in this study. Subjects walked on a dual split-belt instrumented treadmill (GRAIL, Motek Medical B.V., NL), which was synchronized with a motion capture system operating at 100 Hz. Lower limb kinematics and kinetics were recorded using the HBM model and 26 markers. Perturbations were applied at toe-off every 10 seconds on the left treadmill belt, generating left belt accelerations. While walking, five perturbations at the toe-off were generated every 10 seconds on the left belt of the treadmill. The perturbations consisted of left belt accelerations. The shapes of the vertical components of the ground reaction forces (GRF) classified three perturbation impact Strategies, analysed for dominance in both groups. Extreme values of kinetic parameters during perturbed and unperturbed gait were calculated for the left lower limb. Friedman Anova, with a Dunn-Bonferroni post-hoc test, determined inter-Strategies differences within each age group.

3. Results

3.1. Extracting Strategies based on vertical component of GRF

The first Strategy in the group of young people was adopted in 42.17% of gait cycles, II – in 39.76%, and III – in 18.07%. In the elderly group, the distribution looks different: I – 28.79%, II – 45.45%, and III – 25.76% of gait cycles recorded for the left lower limb (Fig.1).

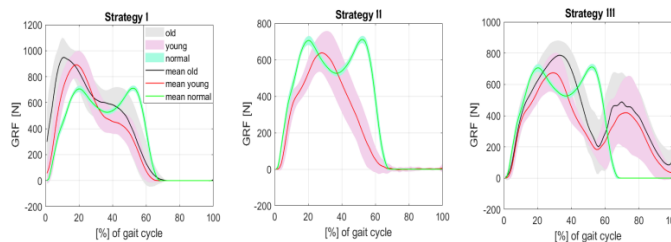


Fig. 1. Three types of shapes of the vertical component of the ground reaction force in adaptation to perturbation under the left lower limb

*Corresponding author: Michalina Błażkiewicz, e-mail: michalina.blazkiewicz@awf.edu.pl

3.2 Differences between Strategies within young and elderly groups

For both young and elderly groups, there are no significant hip torque differences in maximum values. However, statistically significant differences exist in minimum hip torque values across all Strategies, with Strategy I displaying the greatest minimal extension. In the knee joint of young participants, Strategy I exhibited the highest mean maximum values, while Strategy III had the lowest. Significant differences were observed between Strategies I and II, as well as I and III. Among the elderly, no significant differences appeared in maximal knee torque values, and minimum knee torque values did not significantly vary between Strategies in either group.

Regarding ankle torque, Strategy III yielded the highest maximum values in both groups, significantly surpassing Strategy I. In the young group, minimal values of ankle torque exhibited no statistically significant differences among Strategies. However, in the elderly group, Strategy I's values significantly exceeded those of Strategy III.

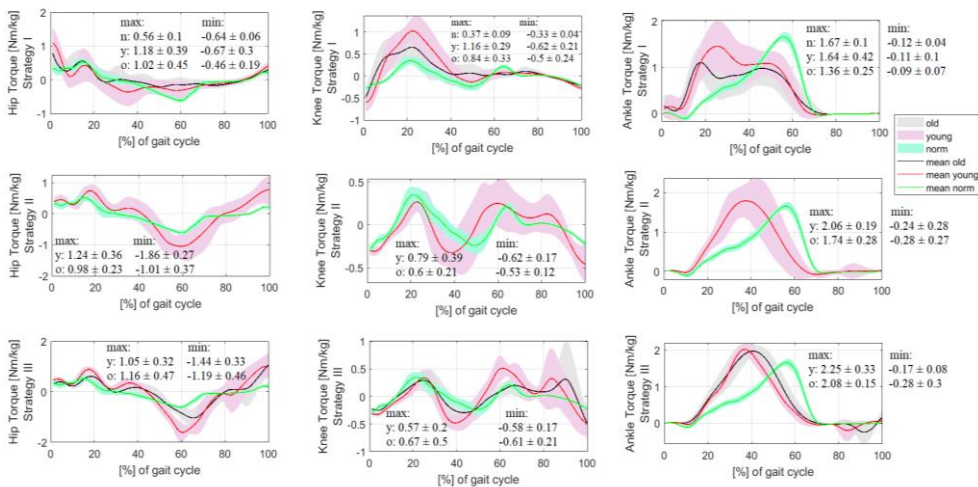


Fig. 2. Torque curves for each Strategy's lower limb joints. Mean and standard deviation of max/min values for each group: n - unperturbed gait, y - young, o - elderly. Unperturbed gait values are shown in the first line

4. Discussion

Notably, both young and elderly individuals exhibit similar responses to the studied perturbations. However, Strategy III poses heightened risk for the elderly across all joints. This Strategy involves elevated hip flexor torques, both flexor and extensor engagement at the knee joint, and pronounced dorsiflexor activity at the ankle joint.

Acknowledgments: This research was funded by the Józef Piłsudski University of Physical Education in Warsaw, UPB no. 2 (114/12/PRO/2023) – Evaluation of postural control in response to induced perturbations in different age groups. Thanks to Karol Kowieski for collecting the data.

Visual disorders and selected features of body posture - a pilot study

M. BOBROWSKA¹, Z. KOSOBUCKA¹, P. TABOR^{2*}, E. OLSZEWSKA², J. PNIEWSKI¹

¹University of Warsaw/ACKO, Warsaw, Poland

²Józef Piłsudski University of Physical Education in Warsaw, Warsaw, Poland

Key words: *astigmatism, foria, body posture, Diers scanner*

1. Introduction

Relationships of various types of vision disorders with body posture have been noticed for a long time [1]. Muscles that are controlled like other skeletal muscles are responsible for setting the eyeballs. Hence, an increase in the tension of some muscle groups may have a compensatory effect (through the control system) on other muscle groups [2]. In studies on the body posture of children with amblyopia, disturbances in the size of the physiological curvature of the spine were found [3], as well as disorders in the position of the head, shoulders, chest, and abdomen [4]. Therefore, the aim of the study is to search for relationships between visual impairment and selected features of body posture.

2. Material and Method

2.1. Material

The subjects were 21 students of the University of Warsaw and the University of Physical Education in Warsaw, of both sexes (6 men and 15 women), aged 24.9 ± 2.09 years. They were people with different levels of physical activity and time spent working at the computer.

2.2. Methods

Information about the level of physical activity and the time spent working at the computer was collected. Those who work more than 5 hours at the computer were considered people with a long working time of close vision. Body posture was assessed using the Diers posture scanner according to the procedure proposed by Schroder [5]. The following parameters were used for the analysis: thoracic kyphosis angle, lumbar lordosis angle, trunk deviation, pelvic obliqueness and averaged trunk rotation.

Visual disturbances were determined by standard optometric examination. Visual acuity, accommodation and convergence as well as phoria and fusion ranges of the eyes were assessed.

Absolute values were used in the body posture analysis for trunk deviation, pelvic obliqueness and rotation. Relationships between visual parameters and values characterizing body posture were determined by Spearman's rank correlation coefficients. The Man-Whitney U test was used to assess differences between active and close-workers.

3. Results

Among the analyzed indices of vision and body posture, a significant negative correlation was observed between the size of the phoria horizontal to distance and the size of the lumbar lordosis. There was also a significant positive relationship between the amount of astigmatism in at least one eye and the absolute value of the lateral deviation (Table.1).

Table 1. Values of Spearman's rank correlation coefficients and probability levels of selected features of vision and body posture

*Corresponding author: Piotr Tabor, e-mail: piotr.tabor@awf.edu.pl

| Correlated indicators | Spearman's R | p |
|---|--------------|-------|
| Angle of lordosis - Horizontal phoria | -0.56 | 0.008 |
| Lateral deviation - the amount of astigmatism | 0.64 | 0.002 |

Taking into account the normal tilt of the trunk ($\pm 5\text{mm}$), it was noticed that among people outside the norm, astigmatism in at least one eye is much more common (6 people compared to 1). Among people with normal trunk deflection, 5 people had astigmatism compared to 9 without it. In addition, in people with astigmatism, abnormal pelvic obliqueness and average trunk rotation were noticed significantly more often.

In people with reduced lumbar lordosis, a more frequent occurrence of distant esophoria was observed, and in those with increased lordosis, far exophoria was observed.

Significantly less fusion rupture towards BS was also found in people working at the computer for a long time (Fig1.).

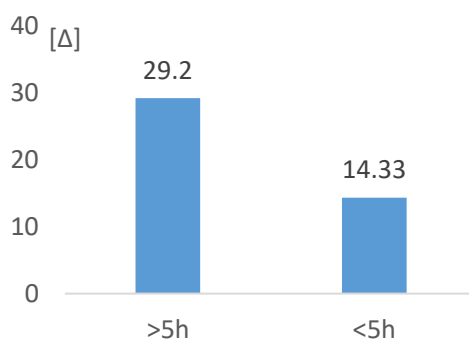


Fig. 1. Mean magnitudes of fusion rupture in the direction of BS measured near in persons divided according to the number of hours spent at the computer per day

4. Discussion and Conclusion

The relationships between visual disturbances and body posture characteristics are generally consistent with those observed in the literature. However, the observed statistical associations should be interpreted with caution due to the small study sample. Research should be continue on a more homogeneous one and larger group.

References

- [1] KUTZNER-KOZIŃSKA M. *Proces korygowania wad postawy (in Polish)*. Warszawa 2008.
- [2] SILVESTRINI-BIAVATI A., MIGLIORATI M., DEMARZIANI E., TECCO S., SILVESTRINI-BIAVATI P., POLIMENI A., SACCUCCI M. *Clinical association between teeth malocclusions, wrong posture and ocular convergence disorders: an epidemiological investigation on primary school children*, BMC Pediatr, 2013, 13, 12, doi.org/10.1186/1471-2431-13-12
- [3] BARCZYK K., SKOLIMOWSKI T. POSTAWA CIAŁA OSÓB NIEDOWIDZĄCYCH, „FIZJOTERAPIA”, 1999. ŻYCHOWICZ P. *Postawa ciała dzieci i młodzieży z uszkodzeniem narządu wzroku (in Polish)*. Problemy higieny epidemiologicznej, 2008/89 (1), 67-70. Schröder J. Stiller T. Mattes K., Referenzdaten in der Wirbelsäulenformanalyse, Manuelle Medizin, 2011, 49:161–166

Ilio-sacral stabilization supported with bone cement

A. BONIK, L.F. CIUPIK*, A. KIERZKOWSKA, E. SŁOŃSKI

LfC Sp. z o.o., ul Koźuchowska 41, 65-364 Zielona Góra, Poland

Key words: *ilio-sacral joint, implant stabilisation, autogenous fusion, cement reinforcement*

1. Introduction

The reliability of bio-stabilization is influenced by a number of factors related to the type of dysfunction, the implantation technique, the implant, the anatomical conditions of the assisted area or the physiological conditions of the patient, among others. One of the aspects is the quality of the implant-bone interface.

LfC's 33 years of experience in spondyloimplantology and in developing functional surgical procedures with implants indicate that bone quality plays a key role. Osteoporotic changes and reduced bone quality can lead to implant loosening and post-operative complications. One way to enhance stabilization is the use of intraosseous agents, which can affect bone fusion [1][2] or provide an additional bond to fix the implant in osteoporotic bone [3]-[5]. Due to the aging of the population and the increase in the average age of surgically treated patients, this problem is being highlighted more and more by the medical community.

Determination of the distribution/dispersion of the reinforcing intraosseous agent, used with innovative ilio-sacral-autogenous-fusion (ISaF) stabilization procedure, in the treatment of the ilio-sacral joint with a multifunctional multi-threaded implant for reduced bone density to improve the effectiveness of bio-stabilization; a model.

2. Materials and Methods

Engineering software n-Topology and DICOM data were used to design anatomical models, corresponding to morphometric parameters of healthy and osteoporotic bones with bone densities defined on the basis of literature data [6]-[9]. 3D prints of physical models were made on a Form2 printer (Formlabs) using stereolithography technology.

Tests on anatomical models were preceded by tests on 3D models of bone in the form of a cylinder with a regular grid pattern using a model medium (Fig.1). In the final stage of the study, PMMA-type cement dedicated to the spine was used, which was prepared according to the manufacturer's instructions/procedure before injection.

The distribution was carried out on a laboratory station equipped with a pressure transducer and a force sensor to evaluate the pressure and force of the medium delivery over time. The entire research set up was submerged in a fluid with a pressure of 12 cm H₂O corresponding to the conditions of the body fluid environment.

The distribution of a specific dose of cement in the model bone was parameterized using industrial computed tomography (GE, CTt). The geometry of the cement distribution was analysed in two perpendicular planes identified with the sagittal and transverse planes in relation to the anatomy and position of the implant. CT data was also used to control the porosity of the prepared models.

*Corresponding author: Lechosław F. Ciupik, e-mail: lf@lfc.com.pl



Fig. 1. An example shot of model medium injection

3. Results

The conditions for delivering the medium to the bone strongly depend on its quality. Injection of 3cm^3 of cement in healthy bone model required 20-30% higher pressure/force. In osteoporotic bone, cement reinforces mainly the frontal part of the implant, and the distribution is more irregular oriented to fill the lower-density spaces. For higher-density bone, the distribution is evenly through the central channel and side channels. Cement along the implant distributes more elliptically due to the changing bone density towards the cortical bone, which limits cement distribution, in this case the cement seeks the easiest distribution paths which can result in single directional outflow paths.

4. Conclusions

Through controlled cement distribution, the quality of the implant-bone interface can be influenced, increasing the biomechanical certainty of stabilization. Pre-operatively defined bone integrity, anatomy and density, as well as the design of transport channels and intra-operative management tactics, make it possible to predict the areas and extent of cement distribution in bone tissue. This translates into improvements in the surgical treatment of "difficult" patients with reduced bone quality/density.

Acknowledgments: In the paper results of studies subsidized by the European Regional Development Found within the framework of the Intelligent Development Operational Program, 2014-2020 (No.POIR.01.01.01-00-0377/16) were used.

References

- [1] YUANLIANG X., ET AL., *Engineered bone cement trigger bone defect regeneration*. Front Mater, 2022 9:929618
- [2] LIU X., ET AL., *A promising material for bone repair: PMMA bone cement modified by dopamine-coated strontium-doped calcium phosphate particles*. R Soc Open Sci, 2019, 6:191028
- [3] SCHMOELZ W., ET AL., *Timing of PMMA cement application for pedicle screw augmentation affects screw anchorage*. Eur Spine J, 2017, 26:2883-2890
- [4] LIH-HUEI C., ET AL., *Pullout strength of pedicle screws with cement augmentation in severe osteoporosis: A comparative study between cannulated screws with cement injection and solid screws with cement pre-filling*. BMC Musculoskeletal Disorders 2011, 12:33
- [5] COSTA F., ET AL., *Pedicle screw cement augmentation. A mechanical pullout study on different cement augmentation techniques*. Med Eng Phys, 2016, 38, 2016, 181-186
- [6] RICHARDS A.M., COLEMAN N.W., KNIGHT T.A., BELKOFF S.M., MEARS S.C. *Bone density and cortical thickness in normal osteopenic, and osteoporotic sacra*. J Osteoporos, 2010, ID 504078
- [7] HOEL R.J., LEDONIO CH.G.T., TAKAHASHI T., POLLY D.W. *Sacral bone mineral density (BMD) Assessment using opportunistic CT scans*. J Orthop Res, 2017;35(1):160-166
- [8] BERGER-GROCH J., ET AL., *Determination of bone density in patients with sacral fractures via CT scan*. Orthop Traumatol Surg Res, 2018, 104(7):1037-1041.
- [9] EASTMAN J.G., SHELTON T.J., ROUIT M.L.CH., ADAMS M.R. *Posterior pelvic ring bone density with implications for percutaneous screw fixation*. J Orthop Surg Res, 2021, 31:383-389

Temporal bone support in a finite element analysis of bone conduction stimulation on the otic capsule

P. BORKOWSKI*

The Faculty of Power and Aeronautical Engineering, Warsaw University of Technology, Warsaw, Poland

Key words: *FE analysis, temporal bone, cochlea, inner ear, bone conduction*

1. Introduction

Sound transmission to the human ear by the bone conduction pathway causes vibration of the bone itself and soft tissues [1]. Numerical modeling of bone conduction in the case of an implant placed on the skull surface requires considering the entire head [2]. The finite element model published in [3] included the skull bone, brain, cerebrospinal fluid, and skin, but the inner ear was simplified because of the model's complexity. If the implant position is close to the inner ear, the skull vibrations are smaller than the vibrations of the petrous temporal bone due to damping and synchondroses between the skull bones [4]. In this case, the numerical model of the entire head can be replaced with the model of the temporal bone only, but appropriate boundary conditions must be defined [5]. The fixed support of the temporal bone boundary is a significant simplification, but since the motion of the entire head is unknown, neglecting its vibrations in the case of the bone conduction stimulation applied on the otic capsule is justified. Supporting the model is unnecessary in harmonic analysis; therefore, the mass elements imitating the mass of the head can be used instead of the fixed support applied on the temporal bone boundary. This study aimed to check the effect of the temporal bone support on the displacement of the promontory bone and the volume displacement of the fluid under the round window membrane for selected directions of the harmonic force and as a function of frequency.

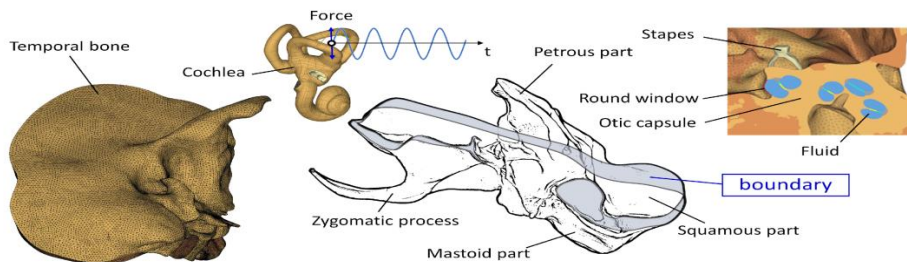


Fig. 1. Finite element model of the temporal bone with the inner ear: mesh, bone conduction stimulation on the otic capsule as a force in the primary direction, the bone boundary, a cross-section through the cochlea

2. Material and Methods

2.1. FE model of the temporal bone with the inner ear

The subject of numerical simulation was a 3D finite element model of the temporal bone with the inner ear (Fig. 1) previously published in [5]. Harmonic analysis of bone conduction stimulation applied on the otic capsule was performed in ANSYSv17 (ANSYS Inc., Canonsburg, Pennsylvania, US). The case of stapes otosclerosis was considered, for which the annular ligament was modeled as ossified, and the middle and outer ear structures were not included. The implant was modeled as a concentrated

*Corresponding author: Paweł Borkowski, email: pawel.borkowski@pw.edu.pl

mass of 0.16 g, connected to nodes lying on the surface of the otic capsule inside a circle with a radius of 1.5 mm. The constant force magnitude applied to the mass was 0.1 N and 17 frequencies from the hearing range were considered (0.2, 0.3, 0.4, 0.5, 0.63, 0.8, 1.0, 1.25, 1.6, 2.0, 2.5, 3.15, 4.0, 5.0, 6.3, 8 and 10 kHz). Two support types on the temporal bone boundary (shaded area in Fig. 1) included: a) fixed support and b) free boundary with an applied mass of the human head.

3. Results

Discrepancies between the two types of support depended on the direction of stimulation. Differences occurred mainly at low frequencies, for which rigid body motion of the human head was observed in experimental cadaver research [3]. The results of the promontory bone vibrations (Fig. 2) and the volume displacement on the round window membrane differed significantly at low frequencies if the force direction was perpendicular to the stapes footplate. The differences obtained for other excitation directions, such as the force in the primary direction (Fig. 1), were slight in the entire frequency range.

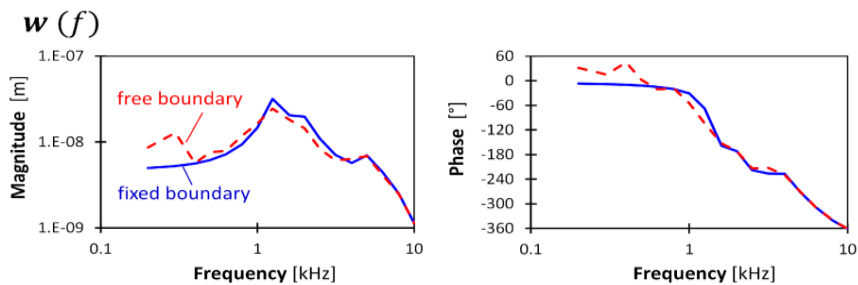


Fig. 2. The promontory displacement in the direction perpendicular to the round window membrane versus frequency for two types of support imposed on the temporal bone boundary. The force direction was perpendicular to the stapes footplate

4. Conclusions

The influence of support imposed in a finite element model on the temporal bone boundary was decreasing with frequency due to damping and more complex vibration modes for higher frequencies, and also depended on the direction of the excitation force due to nonuniform distributions of mass and stiffness in the petrous temporal bone, and was affected by the position of the gravity center.

Acknowledgments: This research was partially supported by the National Centre for Research and Development: PBS3/B7/25/2015.

References

- [1] DOBREV I., SIM J.H., PFIFFNER F., HUBER A.M., STENFELT S., RÖÖSLI C. *Experimental investigation of promontory motion and intracranial pressure following bone conduction: Stimulation site and coupling type dependence.* Hear Res, 2019; 378, 108-125
- [2] DOBREV I., SIM J.H., STENFELT S., IHRLE S., GERIG R., PFIFFNER F., EIBER A., HUBER A.M., RÖÖSLI C. *Sound wave propagation on the human skull surface with bone conduction stimulation.* Hear Res, 2017, 355, 1-13
- [3] CHANG Y., STENFELT S. *Characteristics of Bone-Conduction Devices Simulated in a Finite-Element Model of a Whole Human Head.* Trends Hear, 2019, 23, 1-20
- [4] STENFELT S., HAKANSSON B., TJELLSTRÖM A. *Vibration characteristics of bone conducted sound in vitro.* J Acoust Soc Am, 2000, 107(1), 422-31
- [5] BORKOWSKI P., MAREK P., NIEMCZYK K., LACHOWSKA M., KWACZ M., WYSOCKI J. *Bone conduction stimulation of the otic capsule: a finite element model of the temporal bone.* Acta Bioeng Biomech 2019, 21(3),75-86

Gait stability evaluation after tripping simulated perturbation- assumptions of the project

A. BRACHMAN*, B. BACIK, G. SOBOTA

The Jerzy Kukuczka Academy of Physical Education in Katowice, Department of Biomechanics,
Katowice, Poland

Key words: tripping device, gait stability, treadmill, gait perturbation

1. Introduction

The literature indicates that locomotor adaptability in general, and anticipatory and reactive adaptation in particular, remain largely intact in the elderly [1]. Therefore, experiencing near-fall situations in a safe environment (known as perturbation training) can facilitate reactive balance control in everyday life situations [1], and thus increase fall prevention. Various methods have been used to generate perturbations in the laboratory, including a low-friction plate [2], sudden acceleration/deceleration of the treadmill belt [3],[4], stopping a rope attached to the ankle of the swing leg [5]. Although terrestrial systems can have a high ecological value (i.e. similarity to real-world conditions), induced perturbations tend to occur in a fixed location and may result in a loss of 'unpredictability' [1],[6]. Moreover, knowledge of the location of perturbations may cause anticipatory postural adjustments, which may interfere with the reassessment of "reactive balance" as well as reduce the effectiveness of training [2],[6]. The solution to this problem is the examination and training on the treadmill, which allows to study many gait cycles and the application of multiple perturbations in an unpredictable way for the subject.

Therefore, our aim is to create a protocol that allows the assessment of gait stability after perturbation, which as much as possible resembles a trip in natural conditions (resistance applied to the area of the toes, reminiscent of contact with an obstacle). This need to be done in few steps: 1- creating device; 2 - applying measure which can evaluate gait stability a) obtaining baseline values b) values after perturbation; 3 - creating protocol with different values of starting and lasting perturbation time.

2. Methods

The proposed prototype of a perturbation device allows to work during walking on a mechanical treadmill. It consists of a braking element (electromagnetic brake), it's task is to block the movement of a rigid tie-rod attached to a handle which transfers resistance to the forefoot. The handle attached to the foot is connected to the tie-rod in a movable manner and allows free plantar and dorsal flexion of the foot as well as external and internal foot rotation (Fig.1). The braking module is synchronized with the moment of taking the foot off the ground (beginning of the swing phase) by footswitch (contact sensors of foot pressure on the ground, patent application: Folic tactile sensor, patent no. PL.222119.B1), which allows for wireless signal transmission to the perturbation triggering system. The perturbation delay time and duration are controlled by a microcomputer which steers the electromagnetic cramp. The microcontroller program also prevents the activation of the braking module when the foot is in contact with the walking belt, which could damage the device or the treadmill belt.

To measure gait stability we decided to use margin of stability (MoS) in anteroposterior (ap) direction calculated as the difference between the anterior boundary of the base of support (projection of the toe from the leading limb to the ground) and the extrapolated XCoM (1), by using a reduced

*Corresponding author: Anna Brachman, email: a.brachman@awf.katowice.pl

kinematic model (Süptitz 2013). Kinematic data during walking was recorded with a 3D motion capture system (Innovision Motion Systems, Columbiaville, USA) using six cameras ($f=120$ Hz).

$$XCoM = P_{Tro} + \frac{1/2(V_{Tro} + V_{C7}) + V_{BS}}{\sqrt{\frac{L}{g}}} \quad (1)$$

P_{Tro} is the projection of the trochanter marker to the ground, V_{Tro} is the ap velocity of the trochanter marker, V_{C7} is the ap velocity of the C7 marker, V_{BS} is the ap velocity of the marker of the leading foot during stance phase, L is the distance between the trochanter and the ankle joint center in the sagittal plane. The results for the four consecutive baseline right steps (during touch down) are presented in Table 1.

Table 1. Results for the Margin of Stability for the four steps during unperturbed gait

| P_{Tro} (m) | V_{Tro} (m/s) | V_{C7} (m/s) | V_{BS} (m/s) | XCoM (m) | toe projection (m) | MoS (m) |
|---------------|-----------------|----------------|----------------|----------|--------------------|---------|
| 0.177 | 0.006 | 0.078 | 0.417 | 0.2520 | 0.34 | 0.088 |
| 0.176 | 0.06 | -0.042 | 0.417 | 0.2411 | 0.337 | 0.096 |
| 0.168 | 0.042 | 0.024 | 0.417 | 0.2403 | 0.332 | 0.092 |
| 0.17 | 0.048 | 0.006 | 0.417 | 0.2405 | 0.324 | 0.084 |

Results of the MoS during unperturbed gait are similar for these reported in previous research [7]. Next step will be to verify whether Innovision system will be capable to register all kinematic data after perturbation and then to adopt various selection of perturbation parameters (duration and time of occurrence during the swing phase).

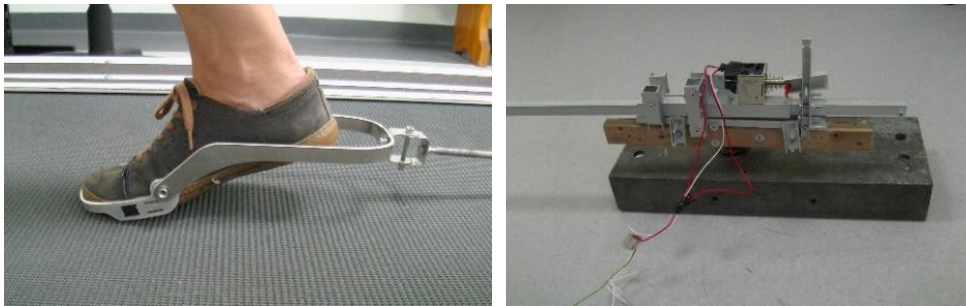


Fig.1. The braking module (right) and the foot handle (left)

References

- [1] BOHM S., MADEMLI L., MERSMANN F., ARAMPATZIS A. *Predictive and Reactive Locomotor Adaptability in Healthy Elderly: A Systematic Review and Meta-Analysis*. Sports Med. 2015; 45(12):1759-77
- [2] OKUBO Y., STURNIKES D.L., BRODIE M.A., DURAN L., LORD S.R., NEWMAN A. *Effect of Reactive Balance Training Involving Repeated Slips and Trips on Balance Recovery among Older Adults: A Blinded Randomized Controlled Trial*. J Gerontol A Biol Sci Med Sci. 2019, 16;74(9):1489-1496
- [3] FOUCHER K.C., ET AL., *Task - Specific Perturbation Training Improves the Recovery Stepping Responses by Women With Knee Osteoarthritis Following Laboratory - Induced Trips*. J Orthop Res. 2020, 38(3):663-669
- [4] RIEGER M.M., PAPEGAAL S., STEENBRINK F., VAN DIEËN J.H., PIJNAPPELS M. *Perturbation-based gait training to improve daily life gait stability in older adults at risk of falling : protocol for the REACT randomized controlled trial*. BMC Geriatr. 2020, 7;20(1):167
- [5] KÖNIG M., EPRO G., SEELEY J., CATALÁ-LEHNEN P., POTTHAST W., KARAMANIDIS K. *Retention of improvement in gait stability over 14 weeks due to trip-perturbation training is dependent on perturbation dose*. J Biomech. 2019, 14;84:243-246
- [6] MCCRUM C., GERARDS M.H.G., KARAMANIDIS K., ZIJLSTRA W., MEIJER K. *A systematic review of gait perturbation paradigms for improving reactive stepping responses and falls risk among healthy older adults*. Eur Rev Aging Phys Act. 2017, 2;14:3
- [7] SÜPTITZ F., CATALÁ M.M., ET AL., *Dynamic stability control during perturbed walking can be assessed by a reduced kinematic model across the adult female lifespan*. Hum Mov Sci. 2013, 32(6):1404-14

Development, Validation and a Case Study: The Female Finite Element Head Model

G. P. CARMO^{1*}, A. SILVA¹, M. DYMEK², M. PTAK², F. A.O. FERNANDES¹,
R. J. ALVES DE SOUSA¹

¹Mechanical Technology and Automation (TEMA), University of Aveiro, Portugal

²Mechanical Department, Wrocław University of Science and Technology, Wrocław, Poland

Key words: *Finite element model, Head model, Brain injury, Female, Validation*

1. Introduction

Traumatic brain injuries (TBI) are one of the leading causes of death in the world. Several finite element head models have been developed throughout the years, offering an excellent cost-effective and ethical approach compared to experimental tests. However, these models are usually of male or unspecified-sex subjects, even though multiple studies indicate different outcomes of injury for men and women under similar conditions [1]. Once validated, the female finite element head model (FeFEHM) will allow a better understanding of sex-specific injury mechanisms resulting in neuronal damage, which can later evolve into neurodegenerative diseases.

2. Methods

The methodology starts from medical images and finite element modelling until the validation process, using novel experimental data of brain displacements conducted on human cadavers [2]. The model created, based on the medical images of a 65-year-old female patient, is the first of a set of three, representing three different age spans (young adult, middle-aged and elderly female subjects). This validation allows the model to accurately mimic brain motion during a certain acceleration scenario, enabling correlation between injury and outcome.

2.1. Computational Modelling

The material modelling of the brain is performed using an age-specific characterization of the brain using microindentation at dynamic rates and under large deformation [3], with a similar age to the patient used to model the FeFEHM. This experiment was selected for being one of the few experiments suitable for traumatic brain injury studies [4]. The material model was validated by numerically replicating the experimental conditions, using similar parameters to the ones used in the FeFEHM. The computational model developed, presented in Fig. 1, is comprised of both brain hemispheres with detailed geometry (comprised of white and grey matter), cerebellum, corpus callosum, pituitary gland and cerebrospinal fluid (CSF).

After validation, a case study was also performed using recorded accelerations using instrumented mouthguards on an American football player that resulted in a mild TBI [5], also comparing stress and strain fields between FeFEHM and another model.

*Corresponding author: Gustavo P. Carmo, e-mail: gustavopcarmo@ua.pt

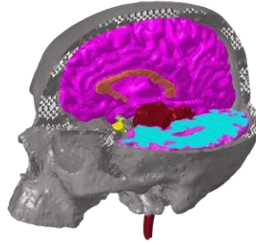


Fig. 1. The Female Finite Element Head Model (FeFEHM). The CSF is not visible to display the main brain components and overall detail of the model

3. Results

After performing the numerical simulation with the boundary conditions for validation, the numerical displacement curves were in good accordance with the experimental validation data, displaying similar peak times and values in all three anatomical planes. Fig. 2 displays an example of curve similarity for one of the points tracked in the simulation. The case study performed afterwards shows a similarity between the pressure fields of the FeFEHM compared to another model.

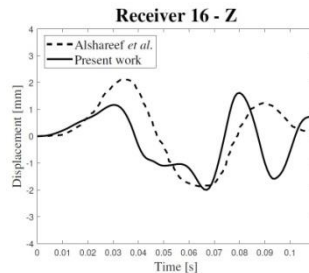


Fig. 2. Example of curve similarity in the validation experiment

4. Discussion

The successful validation of the model using one of the few material characterizations suitable to study TBI demonstrates the future possibilities of this model for trauma studies focused on female subjects. After the creation of the three aforementioned models, future comparison studies when subjecting the models to the same boundary conditions will allow to establish age-dependent thresholds in terms of measurable parameters in a numerical simulation (e.g., stress, strain, intracranial pressure). The case study performed comparing two different models also ensures the potential of the FeFEHM for future studies of sex-specific sequelae resultant from TBI.

References

- [1] KOERTE I.K., ET AL., *Sex-related differences in the effects of sports related concussion: A review.* J Neuroimaging, 2020, 30(4), 387-409
- [2] ALSHAREEF A., GIUDICE J.S., FORMAN J., SALZAR R.S., PANZER M.B. *A novel method for quantifying human in situ whole brain deformation under rotational loading using sonomicrometry.* J Neurotrauma, 2018, 35(5), 780-789
- [3] MENICHETTI ET AL., *A novel regional characterization of the dynamic mechanical properties of human brain tissue by microindentation.* Int J Eng Sci, 2020, 155
- [4] MACMANUS D.B., GHAJARI M. *A Material properties of human brain tissue suitable for modelling traumatic brain injury.* Brain Multiphysics, 2020, 100059
- [5] HERNANDEZ F., ET AL., *A Six degree-of-freedom measurements of human mild traumatic brain injury.* Ann Biomed Eng, 2015, 43(8):1918-1934

Influence of postural adjustment in response to anterior-posterior ground perturbation

M. CHMURA^{1*}, P. WODARSKI¹, M. SZŁĘZAK², G. GRUSZKA¹, J. ROMANEK¹, J. JURKOJC¹

¹Department of Biomechanics, Faculty of Biomedical Engineering, Silesian University of Technology,
Gliwice, Poland

²Silesian Fizjosport Medical Center, Association of Neurophysiological-Orthopedic,
Maniulative Physical Therapists, Gliwice, Poland

Key words: *muscle activation, disturbance response, anticipatory postural control, stabilography*

1. Introduction

Preparing the body to react to a disorder can take various forms, such as anticipatory postural preparation (APA) and early postural preparation (EPA) [1], [2]. APA and EPA are most often assessed by measuring muscle activity [3] or displacement of individual body parts, the center of mass and the center of pressure [1]. Basing on the APA and EPA measurements, we can distinguish two types of stimuli: internally initiated movements and external stimuli destabilizing posture [1], [3].

The aim of the research is to determine whether the appearance of an increase in muscle tone in response to information about the upcoming postural destabilization caused by an external stimulus brings a beneficial result in preventing this destabilization.

2. Materials and Methods

A group of 38 people (27 women and 11 men) with an average age of 23 ± 2.6 years and a weight of 70 ± 17 kg took part in the study. All participants reported that they are healthy.

The research procedure consisted of two stages: rest and perturbation. In the first part - rest (ERx), the subject was asked to sit down on a chair, place his feet flat on the floor, and relax his leg muscles. The test lasted 15 s, during which the resting activity of the leg muscles was recorded. In the second part of the research, the participant participated in three trials: without any information about time and character of the perturbation (1), with information about character but without information about time of the perturbation (2), and with information about time and character of the perturbation (3). Every trial lasted 60 s. The study used EMG system, a set of IMU sensors and force plate.

3. Analysis of results

Absolute values of EMG were calculated and filtered with a moving average filter with a 50 ms window. In the first step of the analysis, mean resting muscle activity values (ERx) were calculated for each muscle. Then, the activity of each muscle was divided by the ERx value, which allowed the measured values to be standardized in relation to the resting values.

Then, based on the data from the IMU sensor placed on the running belt, the beginning of the forward and backward movement was identified. The next step was to examine the activity of leg muscles under APA and EPA in three trials (1, 2 and 3) in order to determine whether the information about the time and direction of perturbation affects the increase in muscle tone.

Graphs of muscle activity has been divided into three periods: period P0 - muscle activity during free standing (1100 ms to 900 ms before perturbation), period P1 - increase in muscle activity as a result

*Corresponding author: Marta Chmura, e-mail: marta.chmura@polsl.pl

of EPA (600 ms to 400 ms before perturbation), period P2 - increase in muscle activity as a result of APA (150 ms before to 50 ms after perturbation).

In the next step, it was investigated whether the increase in muscle activity associated with APA affects the displacement and velocity of the center of pressure (COP) after loss of balance. COP velocity was analyzed as the change in displacement within 150 ms after the disturbance, and COP displacement was analyzed as the maximum displacement of the COP after the disturbance, regardless of when it occurred, but no later than two seconds after the disturbance. Statistical analysis was performed for the calculated values - Friedman test followed by pairwise Wilcoxon post-hoc test with Holm correction.

4. Results

Examples of activity results of selected muscles for the forward movement of the treadmill and related to the occurrence of APA are shown in Fig. 1.

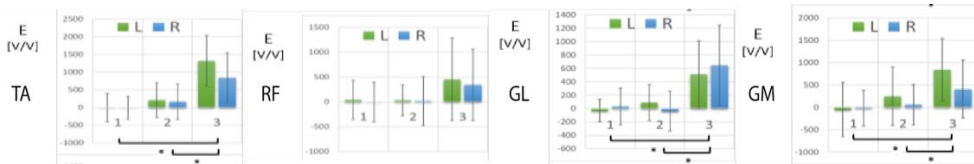


Fig. 1. EMG_{APA} for selected muscles RF (rectus femoris), TA (tibialis anterior), GL (gastrocnemius lateralis) and GM (gastrocnemius medialis) for subsequent Tr1, Tr2 and Tr3 tests. Statistically significant values are marked

Table 1 presents the results of the correlation between the APA value and the COP velocity in the initial phase of movement, and between the APA and the maximum COP displacement due to the perturbation - for muscles in which an increase in load was observed in the APA search phase

Table 1. Results of the correlations. Only statistically significant values are included in the table

| APA – V | TA L | TA R | GL L | GL R | GM L | GM R |
|------------------------|------|------|------|------|------|------|
| Shift forward | 0.72 | 0.70 | | | | |
| Shift backward | | | 0.54 | 0.56 | | |
| APA – COP displacement | TA L | TA R | GL L | GL R | GM L | GM R |
| Shift forward | 0.73 | 0.6 | | | | |
| Shift backward | | | 0.52 | 0.53 | | |

5. Conclusions

The conducted research clearly shows that information about the time of occurrence of the disorder is an important factor influencing postural preparation and readiness to react to this disorder.

It was shown that greater muscle tension led to greater stiffening of the lower limbs, which in turn caused a greater displacement of the center of pressure after the onset of the disorder.

References

- [1] WODARSKI P., JURKOJC J., GZIK M. *Wavelet Decomposition in Analysis of Impact of Virtual Reality Head Mounted Display Systems on Postural Stability*. Sensors 2020, 20(24):7138
- [2] HORAK F.B., DIENER H.C., NASHNER L.M. *Influence of central set on human postural responses*. J Neurophysiol, 1989, 62(4):841-53
- [3] LAPRADE R.F., MORGAN P. M, FRED A. *The Anatomy of the Posterior Aspect of the Knee. An Anatomic Study*. J Bone Jt Surg, 2007, 89:758-764

Numerical analysis of trabecular bone microstructure for different voxel modelling methods

A. CICHANŃSKI*, K. NOWICKI

Bydgoszcz University of Science and Technology, Faculty of Mechanical Engineering, Bydgoszcz, Poland

Key words: *trabecular bone structure, apparent stiffness, μ FEM*

1. Introduction

Predicting cancellous bone strength is interesting because of its ability to diagnose bone fracture risk and to better understand the mechanisms that affect their strength. Experimental studies in this area confirm the existence of a relationship between bone strength and its stiffness. To numerically determine the stiffness of such structures a voxel approach is often used. For voxel models, the value of the calculated stiffness is significantly influenced by the definition and size of voxel [1]. In order to improve the accuracy of numerical calculations without increasing the scanning resolution, the used voxels are extended evenly [1] or unevenly [2] in the direction of scanning. The aim of the study was to assess the impact of geometric modelling on the accuracy of determining the stiffness of the trabecular structure.

2. Material and Methods

The tests were conducted on samples of the structure of the femur. Samples were obtained from 17 patients by excising them from the head of the femur obtained after surgery hip arthroplasty [1]. From such obtained slices, for further testing, cylinders with a diameter of $\varnothing 9.8$ mm and a height of 7.7 mm were cut out. Cylindrical samples were scanned at base resolution $36\mu\text{m}$ on microtomograph $\mu\text{CT}80$. Verification of the proposed method was carried out on the basis of 6 samples selected from the set of $n=17$ based on the value of the BV/TV.

In previous work, the effectiveness of the method of reconstruction of the structure called 3D method was proposed and assessed [2]. It was assumed then that the 3D method was to reflect the changing of the resolution of the μCT scanning. The voxel increased homogeneously in all three directions while keeping the cube form. In this method, as the voxel size increased, the sample stiffness decreased. In the presented work it was assumed that it is possible to reconstruct the trabecular structure in a way that its stiffness will be similar to the reference, but the number of used scans will be smaller than for reference models. A new approach called the FS method was formulated (Fig. 1).

In the FS method, the voxel grows only in sample axis direction, which caused it to have the shape of a cuboid. In this method voxel was created by comparing adjacent pixels lying in two consecutive scans. If both pixels represented the mineral fraction, a voxel was created whose base size was constant $36\mu\text{m}$ what resulted from the scanning resolution. Voxel length, treated as the characteristic size, changed from 72 to 288 μm in 36 μm increment, which allowed to skip several consecutive scans. Reference values were determined with application of models with cubic voxel 36 μm side. The presented work showed the influence of such approach on the apparent stiffness of the analyzed bone structures.

*Corresponding author: Artur Cichanski, e-mail: artur.cichanski@pbs.edu.pl

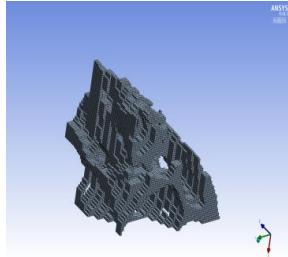


Fig. 1. Part of the model obtained by the FS method

Numerical analyses were performed in ANSYS APDL. Isotropic material properties $E=10$ GPa and $\nu=0.3$ were assumed for the analysis [2]. The boundary conditions reflected the compression of the cylindrical sample $\varepsilon=0.8\%$ in the axial direction.

3. Results

The results obtained for both considered methods were related to reference values obtained for $36\ \mu\text{m}$ voxels. The relative error of determining the volume is shown in Fig. 2a, and the relative error of determining Young apparent modules in Fig. 2b.

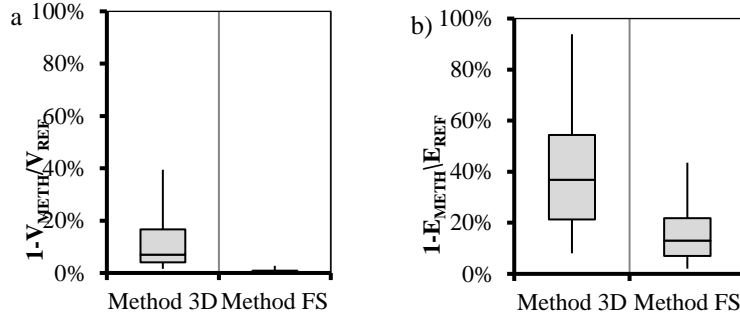


Fig. 2. Comparison of relative error for 3D and FS methods: a) volume, b) apparent stiffness

The assumed goal was achieved in the work, obtaining the median of apparent stiffness error determination for the FS method of 13.0%, compared to 36.8% for the 3D method. Also the interquartile range of apparent stiffness error determination for FS method $IQR=14.7\%$ is smaller than $IQR=33.1\%$ for 3D method. The value of the median of volume error is an order of magnitude lower for the FS method compared to the 3D method.

4. Conclusions

The proposed methods of modelling trabecular bone structures allow to reduce the number of scans necessary for structure reconstruction. This allows for such a reduction in the amount of radiation absorbed by the patient during computed tomography, which does not result in the loss of important information about the mechanical properties of the bone structure.

References

- [1] TOPOLIŃSKI T., ET AL., *The relationship between trabecular bone structure modeling methods and the elastic modulus as calculated by FEM*. ScientificWorldJournal, 2012, 827196
- [2] CICHANŃSKI A., NOWICKI K. *Trabecular bone microstructural FEM analysis for out-of plane resolution change*, in *Biomechanics in Medicine and Biology*. K. Arkusz, et al., Editors. 2019, Springer International Publishing Ag: Cham, 210-218

Development of biocompatible hydrogel matrices for 3D cell cultures in lab-on-chip applications

A. CIEŚLAK^{1*}, M. ŁABOWSKA¹, A. KRAKOS (PODWIN)², J. KULBACKA³, J. DETYNA¹

¹Department of Mechanics, Materials and Biomedical Engineering, Faculty of Mechanical Engineering, Wrocław University of Science and Technology, Wrocław, Poland

²Department of Microsystems, Faculty of Electronics, Photonics and Microsystems, Wrocław University of Science and Technology, Wrocław, Poland

³Department of Molecular and Cellular Biology, Faculty of Pharmacy, Wrocław Medical University, Wrocław, Poland

Keywords: hydrogel, lab-on-chip, LOC, cancer cell, natural polymer

1. Introduction

Due to the rapidly evolving epidemiological situation of cancers, the scientific community is focused on developing increasingly innovative cancer research methods. A combination of knowledge and skills in biomedicine and engineering is key to achieving this development. In this context, the fabrication of a hydrogel matrix on glass and polymer substrates is presented as a lab-on-chip (LOC) platform for biomedical applications. The prepared chip was biologically and mechanically validated. A general schematic of this study is shown in Fig. 1. To emphasize its innovation, the research activity is interdisciplinary, combining theoretical and practical knowledge from biomedical engineering, mechanics, molecular and cellular biology, and microsystems.

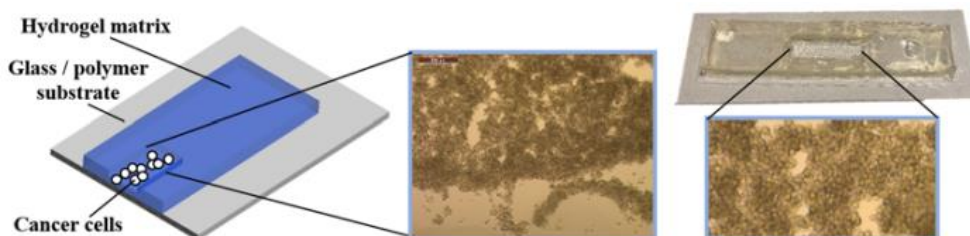


Fig. 1. Graphical abstract of the designed lab-on-chip (cross-section) and the fabricated LOC platform with the culture of the H69AR cancer cell line

2. Experiments

2.1. Materials

Different hydrogel matrices with a unique composition were fabricated using natural polymer powders such as sodium alginate (Sigma Aldrich, Norway), chitosan (Sigma Aldrich, USA), agar (Agnex, Poland), methylcellulose (Sigma Aldrich, China), and gelatin (Warchem, Poland). The solvents were deionized water (DI) and saline solution (NaCl). As a result, six types of hydrogels and twelve lab-on-chip configurations were obtained, and subsequently evaluated. The prepared polymer solutions were applied to the substrates (biocompatible borosilicate glass or polymer material VisiJet M3 Crystal) using the molding method. Then the mentioned polymeric solutions were cross-linked with (0.1 M) calcium chloride solution for 18 minutes to obtain hydrogel matrices. The deposited layers

*Corresponding author: Adrianna Cieślak, e-mail: adrianna.cieslak@pwr.edu.pl

possessed defined geometry, allowing the implantation and cultivation of biological cells, as shown in Fig. 1.

2.2. Mechanical research – methods and results

The hydrogels were exposed to degradation tests by incubation in a liquid (saline solution) providing a temperature of 37°C, and 5% CO₂ to mimic the *in vitro* environment. Subsequently, a compression test was performed, and the results (modulus of elasticity) of the incubated (test group) and nonincubated (control group) hydrogel samples were compared. Moreover, the obtained values of the modulus of elasticity (range of 0.062 - 0.619 MPa) are quite similar to the modulus of elasticity of biological tissues, such as skin (0.060 - 0.850 MPa) [1], heart muscles (0.008 - 0.150 MPa) and skeletal muscles (0.005 - 0.170 MPa) [2]. Therefore, the possibility of using the prepared hydrogel matrices in biomedicine and cell engineering is justified.

2.3. Biological validation – methods and results

The *in vitro* model was created using H69AR lung cancer cells resistant to chemotherapeutics (e.g., doxorubicin). The culture was carried out to evaluate the biological activity of the cells (viability, proliferation, morphology) placed on the LOC platform. The biological effects were studied qualitatively (Trypan Blue staining and microscopy) and quantitatively (incubation in Presto Blue reagent and fluorescence intensity measurements). The tested samples showed the biocompatibility of the hydrogels, as evidenced by the observed cell growth and proliferation under these specific conditions. Cells in a growth medium were used as the control sample, and their viability was 100%. In addition, the biological activity of cell cultures in hydrogels was also the subject of extensive research. We can see this, among other things, in the work of Li Q. *et al.* [3], and Cavo M. *et al.* [4].

3. Conclusion and future perspectives

To conclude, hydrogel-based LOC platforms signify a groundbreaking approach with immense prospects for advancing bioengineering. The subsequent phase of the investigation will involve improving the LOC platform through additive manufacturing of microfluidic lab-on-chip devices equipped with microchannels i.a. specifically designed for the controlled flow of cell medium. In addition, research will focus on the advancement and implementation of on-chip anticancer therapies, such as photodynamic therapy. Although there have been limited studies in this field, supported by scientific publications, including research conducted by Polish scientists from Warsaw [5], as well as by foreign scientists - Marzioch J. *et al.* [6]. Nevertheless, the subject matter in this area is developing rapidly, offering opportunities to optimize existing techniques or create new ones.

References

- [1] CONSTANTINIDES G., KALCIOGLU Z.I., MCFARLAND M., ET. AL., *Probing Mechanical properties of fully hydrated gels and biological tissues*. J Biomech. 2008, 14;41(15):3285-9
- [2] DOMIAN I.J., YU H., MITTAL N. *On materials for cardiac tissue engineering*. Adv Healthc Mater. 2017, 6(2): 27774763
- [3] LI Q., LIN H., WANG O., QIU X., KIDAMBI S., DELEYROLLE L.P., ET. AL., *Scalable production of glioblastoma tumor-initiating cells in 3 dimension thermoreversible hydrogels*. Sci Rep, 2016, 6(1), 31915.
- [4] CAVO M., FATO M., PEÑUELA L., BELTRAME F., RAITERI R., SCAGLIONE S. *Microenvironment complexity and matrix stiffness regulate breast cancer cell activity in a 3D in vitro model*. Sci Rep, 2016, 6(1), 35367.
- [5] ZUCHOWSKA A., JASTRZEBSKA E., ET. AL., *3D lung spheroid cultures for evaluation of photodynamic therapy (PDT) procedures in microfluidic Lab-on-a-Chip system*. Anal Chim Acta, 2017, 990, 110-120
- [6] MARZIOCH J., KIENINGER J., SANDVIK, PETTERSEN E., PENG Q., URBAN G. *Photodynamic therapy – in vitro investigation using an electrochemical microsensor system*. Procedia Eng, 2015, 120, 468-471

Optimization and random sampling in selected aspects of modeling body joints with a multibody system method

A. CISZKIEWICZ*

Faculty of Mechanical Engineering, Cracow University of Technology, Cracow, Poland

Key words: *Genetic Algorithm, Monte Carlo, prestrain, 2D projection, uncertainty*

1. Introduction

This abstract is sent for consideration in Morecki & Fidelus Award and encapsulates the main findings published in [1-4], in accordance with the rules of the contest.

Modeling body joints is a complex issue and with the increasing power of computers, more physical features can be incorporated into the models. Nevertheless, including more features can be problematic, as the models are still much simpler than their real-life counterparts. This study summarizes the finding on the following three issues:

- adjusting planar models of joints so that they mimic the behavior of three-dimensional joints [1],
- analyzing uncertainty of biomechanical models [2],
- including physical prestrain in the ligaments of the models [3],[4].

These problems can be partially solved by employing modern optimizational approaches, such evolutionary approaches and Monte Carlo sampling-based methods. The findings were based on the simulations performed using a planar model of an ankle joint, presented in [1], with six nonlinear cables representing the ligaments and two Hertzian contact pairs, sphere-to-sphere type. The model was studied in statics using equilibrium equations under external moment loads.

2. Converting three-dimensional multibody models into planar models

Due to their numerical simplicity, two-dimensional (2D) models of body joints are an attractive choice. While many 2D models of synovial joints were presented in the literature, the relation between them and their three-dimensional (3D) counterparts is rarely fully explored. Nevertheless, representing 3D ligaments with 2D cables can have significant impact on the results, as seen in [1]. This issue can be mitigated by sampling the displacements of the 3D model and optimizing the material parameters of the corresponding 2D model, which was presented in [1]. This method allows 2D links to respond in the same way 3D would. Furthermore, only the material parameter modification is required, which means that the geometry can still be obtained from regular medical scans. The method offers a simple to transition complex 3D models to simple 2D ones.

3. Analyzing uncertainty in biomechanical models

As seen in [1] multibody models of the ankle can be very sensitive to parameter changes. Nevertheless, a simple sensitivity analysis, in which the parameters are changed in a one-by-one fashion, does not fully capture the behavior of the model. In fact, in most cases checking all of the combinations of multiple parameters is infeasible. In the literature many methods to analyze uncertainty in biomechanical models were presented. An interesting choice comes from electrical circuit analysis, in which a popular method to account for uncertainties is referred to as the worst-case analysis [5]. The method is a numerical search for a combination of parameters for which the output of the model is the highest (or lowest). This approach can be transferred to biomechanical models, as seen in [2]. In [2],

*Corresponding author: Adam Ciszkiwicz, e-mail: adam.ciszkiwicz@pk.edu.pl

the search is performed with genetic algorithm. Defining the worst-case is difficult in this case, as the output of the models is usually a function. In order to incorporate that, in [2] the optimization is carried out on two models at the same time with the objective being to maximize the difference between their outputs. It was shown that approach can provide results up to 9 times better than a regular sensitivity analysis. Moreover, with the changes to the material and geometrical parameters capped at 5% and 0.5mm respectively, the obtained structures offered drastically different angular displacement curves differing by nearly 10 deg, while the changes in the forces generated by the ligaments could be as high as 68%.

4. Including physical prestrain in the ligaments of the models

A typical body joint often functions in a state of prestrain, this means that some or all of its elements are under strain even when no external load is present [6]. Including prestrain in a model usually revolves around computing the slack lengths of the ligaments. This is often done by shortening their lengths at the rest configuration of the joint by an arbitrary amount, such as 2%. This simple approach can cause numerical issues, such as a shift of the rest configuration and changes in both the load system and the output of the model, as shown in [3]. The other to compute the slack lengths is to assume a strain-free configuration. While the two approaches differ significantly in the results they provide, it is unclear which one provides the results closer to reality. This is also difficult to measure, as measuring prestrain is an invasive test. Therefore, in [4], a numerical method based on sampling was proposed to address this issue. The idea was to generate variants of the original model [1], while perturbing its geometrical and material parameters. Then, the slack lengths were also perturbed, creating a prestrained ankle-joint pseudo-model. Finally, the models were subjected to the two aforementioned prestrain approaches. Interestingly, in 19 out of 30 cases, the strain-free approach offered better results than the 2% prestrain. This result meant that in some cases, it is better not to include prestrain in the model. Nevertheless, these findings should be interpreted with caution as they may not hold every model.

5. Conclusion

As aforementioned, the abstract contains a summary of the most important findings presented in [1]-[4]. It was shown that the problem of converting a 3D joint into a 2D model can be solved with optimization of material parameters. Furthermore, the sensitivity of the planar ankle model is very high and can be analyzed with evolutionary optimization. Also, prestrain in multibody models is difficult to include and can cause numerical problems, but it can be studied in a numerical way by generating pseudo joint models. Interestingly, in case of the proposed planar model of the ankle, omitting prestrain provides better results than applying arbitrary prestrain of 2%.

References

- [1] BORUCKA A., CISZKIEWICZ A. *A planar model of an ankle joint with optimized material parameters and Hertzian contact pairs*. *Materials*, 2019, 12(16), 2621
- [2] CISZKIEWICZ A. *Analyzing uncertainty of an ankle joint model with genetic algorithm*. *Materials*, 2020, 13(5), 1175
- [3] CISZKIEWICZ A. *Arbitrary Prestrain Values for Ligaments Cause Numerical Issues in a Multibody Model of an Ankle Joint*. *Symmetry*, 2022, 14(2), 261
- [4] CISZKIEWICZ A. *Comparison of Common Methods for Ligament Prestrain in a Multibody Model of an Ankle Joint Using a Generative Approach*. *ECCOMAS Thematic Conference on Multibody Dynamics*, July 24- 28, 2023, Lisbon, Portugal
- [5] SLELBOE S. *True Worst-Case Analysis of Linear Electrical Circuits by Interval Arithmetic*. *IEEE Trans. Circuits Syst.* 1979, 26, 874–879.
- [6] MAAS S.A. ET AL., *A general framework for application of prestrain to computational models of biological materials*. *J Mech Behav Biomed Mater.* 2016, 61, 499–510

Innovative 3D-Ti-Truss procedure in biomechanical spinal stabilisation

L.F. CIUPIK*, A. KIERZKOWSKA, G. PAJAŁ, P. POWCHOWICZ, F. ANDRUSZKIEWICZ

LfC Sp. z o.o., ul Koźuchowska 41, 65-364 Zielona Góra, Poland

Key words: *spinal implant, 3D-print, Ti-alloy, organic truss, osseointegration*

1. Introduction

There are two main 3D printing technologies used in the manufacture of titanium implants, offering great opportunities for building complex structures. The first is laser-based (SLM - Selective Laser Melting), while the second uses an electron beam to melt titanium powders (EBM - Electron Beam Melting). The EBM process does not require additional heat treatment and produces robust $\alpha+\beta$ structures [1,2,3], which are free of biomechanically undesirable residual stress [2,3,4], oxides [5], do not exhibit anisotropy and are free of pores [3], and do not have tendency to hydrogen embrittlement, as is the case with 3D-SLM [2,6]. The geometry of the surface roughness has been shown to have a strong influence on osseointegration [7]. The above aspects have a direct bearing on the safety and functionality of the medical device and the therapeutic effects.

2. Aim

The objective of this study is to demonstrate the feasibility of 3D-EBM printing technology for 3D-Ti-Truss titanium spinal implants with TrabeQcell® (3D printed Ti6Al4V organic lattice) on the basis of 12 years of follow-up in cooperation between R&D Dept-LfC and hospitals.

3. Materials and Methods

The subject of this study was the pioneering CarRLIF®-patented spinal implant [8], made by incremental sintering of Ti6Al4V powder by 3D-EBM, as the most clinically tested representative of the 3D-Ti-Truss implant family (Fig.1). The therapeutic efficacy related to the geometry of the implant and the bio-mechanical principles of the surgical procedure were evaluated. Osseointegration and tissue safety of 3D structures directly after printing and after the manufacturer's technological processing were studied on the basis of alkaline phosphatase activity (ALP), surface energy (SEP-surface free energy) and contact angle. The results were compared to polymeric biomaterials.

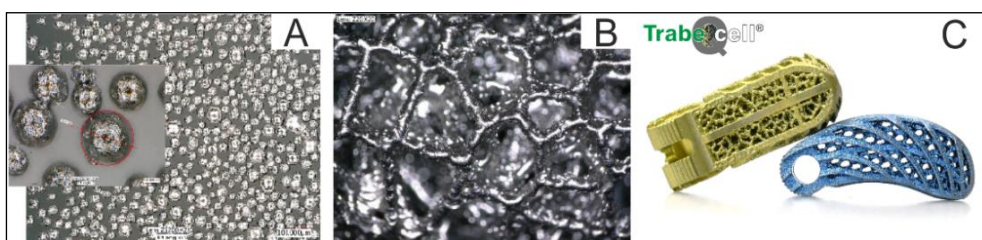


Fig. 1. 3D-EBM printing: A-Ti6Al4V powder with 45-106 μm grains (optical microscopy), B-porous titanium organic geometry (optical microscopy), C-pioneering in the world, 3D printed spinal implant, EBM (2011)

* Corresponding author: Lechosław F. Ciupik, e-mail: lfc@lfc.com.pl

4. Results

The implant structure obtained in the 3D-EBM process has low contact angle ($50\div 60$ [deg] mean 55.32 and SD 2.95 for unmodified surfaces and $20\div 30$ [deg] mean 24.82 and SD 2.86 after technological process), indicating favourable hydrophilicity. The surface energy SEP/L is in the range of $50\div 70$ [mJ/m²] mean 59.55 and SD 5.43 for all 3D-EBM surfaces tested. ALP activity for 3D-modified surfaces is $0.020\div 0.025$ [nmol/min/mL] mean 0.013 and SD 0.002, for unmodified surfaces $0.010\div 0.015$ [nmol/min/mL] mean 0.023 and SD 0.002 and is higher than for polymeric biomaterials. Long-standing clinical practice (2011–2022) confirms the increased efficacy and safety of 3D-Ti-Truss implants made with 3D-EBM technology, which, in independent follow-up observations, fulfil therapeutic expectations (accelerated osseointegration, minimised possibility of migration and subsidence) [9].

5. Conclusions

3D-EBM-printed titanium alloy, when used in the 3D-Ti-Truss implant load-bearing lattice structure and with technological processing and obtaining so-called "volcanic surfaces", is a favourable biomaterial for implants. The roughness and the organic lattice (TrabeQcell®) favour osseointegration according to the "Ivy-like mimetic bone overgrowth mechanism" (hypothesis described by L.Ciupik, 2013), which is confirmed by biological studies (Fig.2) and the results of in vivo animal studies with fusion after 3-4M [10]. The 3D-EBM technology and the printed Ti6Al4V biomaterial accelerate osseointegration by approximately 35–40% and are the best means currently available to produce therapeutically effective implants.

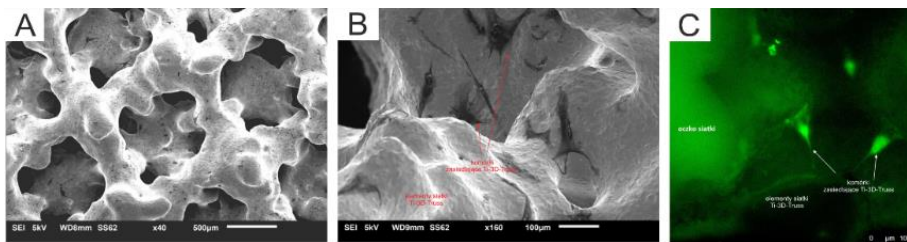


Fig. 2. Viable bone cells on Ti-3D-Truss on the surface and inside the porous structures in the initial contact phase; A and B - SEM electron microscopy and C - fluorescence microscopy with green-labelled cells; in cooperation with BioNanoPark, (Lodz) and NIGRiR (Warsaw)

Acknowledgments: In the paper results of studies subsidized by the European Regional Development Fund within the framework of the Intelligent Development Operational Program, 2014-2020 (No. POIR.01.01.01-00-0377/16) were used.

References

- [1] FOUISOVÁ M., ET AL., *Influence of Inherent Surface and Internal Defects*. Materials, 2018, 11: 537
- [2] METALNIKOV P., ET AL., *Hydrogen trapping*. Mater Sci Eng, 2021, 811 (1): 141050
- [3] WYSOCKI B., ET AL., *Laser and Electron Beam Additive Manufacturing Methods*. Appl. Sci. 2017, 7, 657.X.
- [4] ZHAO, S. LI, ET AL., *Comparison of the microstructures and mechanical*, Materials and Design, 2016. 95
- [5] KOLAMROUDI, ET AL., *Developments on EBM*. Trans Indian Inst. Met, 2021, 74(4):783–790
- [6] METALNIKOV P, ET AL., *Hydrogen embrittlement*. J Mater Res Technol, 2020, 9 (6): 16126-16134
- [7] CALLENS S.J.P., ET AL., *Emergent collective organization of bone cells*. Nat Commun, 14 (1), 2023 14:885
- [8] Patent no. EP 2768435, US 8900311, PL 218461
- [9] WEHNER D. *Pilotstudie zur Evaluation der Anwendbarkeit eines DICOM basierten Datenanalyseprogrammes*, Doctoral dissertation, Frankfurt am Main, 2020
- [10] CIUPIK L.F., ET AL., *The use of incremental technology to produce 3D-Truss Ti6Al4V implants which improves the spinal treatment effectiveness*, Key. Eng Mater, 2016, 687: 179-184

Application of joint kinematics analysis to evaluate the correctness of users' exercise performance in a virtual reality environment

U. CZAJKOWSKA^{1*}, M. ŻUK¹, K. SMERD¹, C. PEZOWICZ¹,
M. POPEK¹, M. ŁOPUSIEWICZ¹, K. BULIŃSKA²

¹Faculty of Mechanical Engineering, Wrocław University of Science and Technology, Wrocław, Poland

²Department of Physiotherapy, Wrocław University of Health and Sport Sciences, Wrocław, Poland

Key words: *virtual reality, motion tracking, Vive Trackers, eMotion*

1. Introduction

In biomechanical research and clinical practice, the quantitative analysis of human movement plays a vital role. Motion analysis, which involves tracking joint angles, segment velocity, and body position, is employed to assess sports performance and technique [1],[2].

The literature contains descriptions of joint kinematics during various exercises, including walking, running and squatting [3]-[5]. The experiments revealed that the Vive HTC Pro system with Vive Trackers exhibited a high level of position reproducibility within a few millimeters [6]. When evaluating the exercise performance of virtual reality (VR) users using motion tracking, conducting a thorough analysis of the kinematics of individual joints and body segments serves as a foundation for drawing additional conclusions.

2. Purpose

The purpose of this study was to evaluating the usefulness of using HTC virtual reality accessories for motion capture and quantitative analysis of performed motion tasks.

3. Material and Methods

The study included 15 healthy participants. HTC Vive Pro system was used during the measurement, including two base stations, two controllers, VR goggles and seven trackers placed on the participants' bodies, according to instructions described in the literature [7]. The study focused on analyzing the kinematics of the exercises in the prepared game. The eMotion Data Acquisition Module was used to collect data from the Vive Tracker and the HTC Vive VR system during three stages of the study: initial gameplay recording the performance of correctly performed exercises, and replaying the gameplay.

4. Results

Achieved results are presented in Fig. 1 and Fig. 2. The graphs show kinematic variables of the knee joint during the backward step averaged for single person repetitions performed correctly and incorrectly. A blue line represents average value, and the gray line \pm standard deviation. Graph on the right side shows correct execution of the exercise and the one on the left side represent case of not lowering the body

*Corresponding author: Urszula Czajkowska, e-mail: urszula.czajkowska@pwr.edu.pl

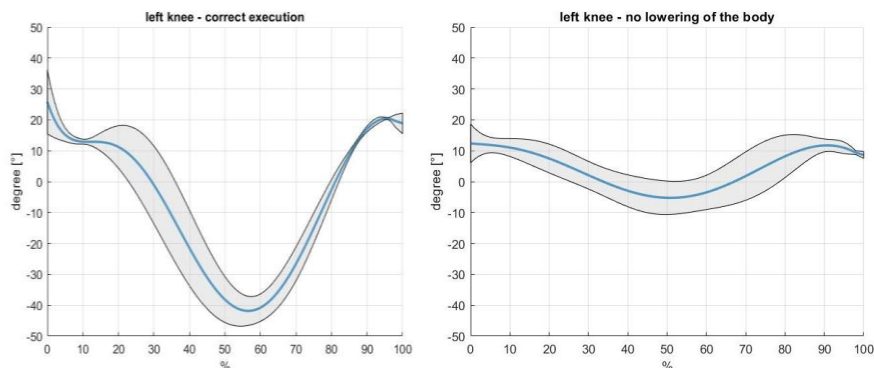


Fig. 2. Kinematic variables of the knee joint during the backward step averaged for single person repetitions performed correctly and incorrectly. Blue line = average value, gray line \pm SD.
Right side: correct execution of the exercise, left side: error of not lowering the body

5. Discussion and Conclusion

The objective of this study was to analyze the kinematics of human movement during virtual reality sports game and propose a method for analyzing the obtained data. Furthermore, the study aimed to identify indicators that could effectively characterize specific movements and assess their quality in comparison to the ideal execution of the exercise. The ability to analyze multiple parameters simultaneously is a significant advantage of motion tracking methods, giving them an edge over traditional approaches based on visual assessment, which face challenges in simultaneously observing numerous body segments. The position and orientation coordinate values over time of trackers placed on the body allow for a wide range of analyses that can be used to quantitatively describe a given movement. Proper preparation data for analysis and developing a way to use this information to create guidelines for assessing the correctness of a given movement is an essential task.

Acknowledgments: This work was supported by the The National Centre for Research and Development in Poland, in frames of the project: “eMotion-system for computer aided workout and rehabilitation using motion capture technology and virtual reality”, LIDER/37/0200/L-10/18/NCBR/2019.

References

- [1] GOURGOULIS V., NIKODELIS T. *Comparison of the arm-stroke kinematics between maximal and sub-maximal breaststroke swimming using discrete data and time series analysis*. J Biomech. 2022, 142:111255. doi: 10.1016/j.jbiomech.2022.111255. PMID: 35973308
- [2] GATTI A.A., KEIR P.J., NOSEWORTHY M.D., BEAUCHAMP M.K., MALY M.R. *Hip and ankle kinematics are the most important predictors of knee joint loading during bicycling*. J Sci Med Sport. 2021, 24(1):98-104
- [3] FERNANDEZ-GONZALES P., KOUTSOU A., CUESTA-GOMEZ A., CARRATALA-TEJADA M., MIANGOLLARA-PAGE J.C., MOLINARUEDA F. *Reliability of Kinovea® Software and Agreement with a Three-Dimensional Motion System for Gait Analysis in Healthy Subjects*. Sensors 2020, 20, 3154
- [4] SCHOENFIELD B.J. *Squatting kinematics and kinetics and their application to exercise performance*. J Strength Cond Res. 2010, 24(12), doi: 10.1519/JSC.0b013e3181bac2d7
- [5] BISCHOFJ E., ABBEY A.N., CHUCKPAINWONG B., NUNLEY J.A., QUEEN R.M. *Three-dimensional ankle kinematics and kinetics during running in women*. Gait Posture, 2010, 31(4):502-5
- [6] BAUER P., LIENHART W., JOST S. *Accuracy Investigation of the Pose Determination of a VR System*. Sensors (Basel), 202, 21(5):1622. doi: 10.3390/s21051622.
- [7] ŽUK M., WOJTKÓW M., POPEK M., MAZUR J., BULIŃSKA K. *Three-dimensional gait analysis using a virtual reality tracking system*. Measurement, 2022, 188: 110627

Spectral analysis of ground reactions evoked by patients after medial patellofemoral ligament (MPFL) reconstruction

A. CZAPLIICKI^{1*}, M. JAROCKA², T. SACEWICZ¹, J. WALAWSKI³

¹Faculty of Physical Education and Health in Białą Podlaska, Department of Biomechanics and Anatomy, Józef Piłsudski University of Physical Education in Warsaw, Warsaw, Poland

²Faculty of Physical Education and Health in Białą Podlaska, Department of Physiotherapy Fundamentals, Józef Piłsudski University of Physical Education in Warsaw, Warsaw, Poland

³ŻagielMed Hospital, Lublin, Poland

Key words: MPFL, reconstruction, spectral analysis

1. Introduction

Dislocation of the patella is responsible for rupture of the MPFL in 90 % of cases. The primary orthopaedic treatment in such situations is reconstruction of the MPFL. This procedure is generally followed by a satisfactory clinical assessment of the knee joint. Despite the development of effective surgical techniques, the timing of return to full physical activity for people after MPFL reconstruction remains an open question. With this in mind, the primary aim of the present study was to investigate, using spectral analysis, the postural stability of patients before MPFL reconstruction and 6 months after surgery. An additional objective was to check the quality of the signal from a baroresistive platform, as this signal was subjected to spectral analysis.

2. Material and Methods

The study involved a group of 14 female subjects (age: 22.9 ± 6.9 years; weight: 57.3 ± 5.8 kg) after MPFL reconstruction and a control group of 26 healthy females (23.2 ± 2.8 years; 61.1 ± 7.7 kg). The subjects were provided with information on the research process and profits related to participating in the study. The research was completed in accordance with the ethical standards of the Helsinki Declaration and was approved by the University Research Ethics Committee.

The subjects performed a 30-second classic Romberg test on a treadmill (Noraxon FDN-T) equipped with a matrix of baroresistive sensors to measure ground reaction forces. The sampling frequency of the matrix was 100 [Hz]. The time courses of these reactions for the front and back of the foot were pre-processed by smoothing with a low-pass filter with a cut-off frequency of 5 [Hz], and de-meaning. Welch's method was then used to obtain averaged power spectral density (PSD) estimate. The input signal was broken into eight 2048 point overlapping segments. Such a signal was multiplied by a Hamming window and run through a fast Fourier transform (FFT) with a frequency resolution of 0.0488 [Hz] between 0 and 50 [Hz]. After estimating the PSD of the signal, we calculated for each subject the energy contained in the three frequency bands $0 < f \leq 0.1$, $0.1 < f \leq 0.5$ and $f > 0.5$ [1] as well as the ratio of this energy to the total energy of the signal. The significance of the differences between these ratios for the two research groups was checked with Student's or Mann-Whitney tests.

3. Results

The results show (Fig. 1) that the spectral analysis can only be carried out for one time course (Fig. 2). Statistically significant differences were found in the first and third frequency bands between the control group and the patients before MPFL reconstruction.

*Corresponding author: Adam Czaplicki, e-mail: adam.czaplicki@awf.edu.pl

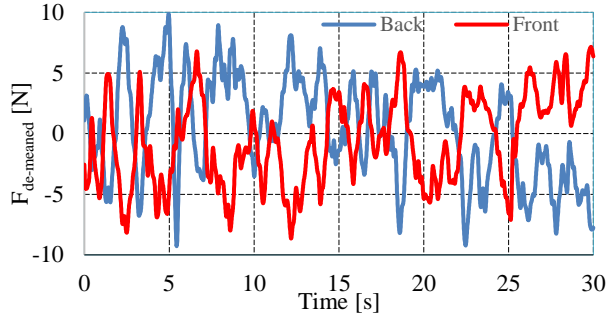


Fig. 1. Pre-processed time courses of ground reactions evoked by the right foot of one of the MPFL patient

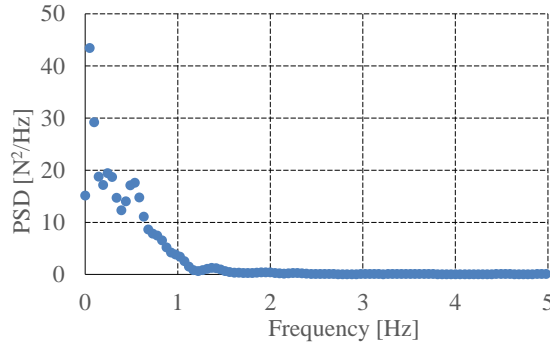


Fig. 2. Welch power spectral density estimate for the time course in Fig. 1 (the back of the right foot)

Table 1. Percentage ratio of energy contained in three frequency bands to total energy, asterisks indicate statistically significant differences ($p < 0.05$)

| | Control | Before reconstruction | | | 6 months after reconstruction | | | | |
|--|------------|-----------------------|------------|-----------|-------------------------------|----------|-----------|-----------|----------|
| | 44.8±15.5* | 40.0±9.0 | 14.8±10.2* | 57.7±6.3* | 35.0±7.6 | 7.6±3.3* | 47.6±18.3 | 40.3±12.2 | 12.1±7.9 |

4. Discussion

It is believed in the traditional analysis of body sway that the first frequency band can be associated with visual control, the second band is linked to vestibular control and the third band is related to somatosensory activity [1]. Our results showed statistically significant differences in postural control in the first and third bands before and after MPFL reconstruction.

The spectral analysis of the time series of ground reactions measured with the baroresistive platform may give discriminating results for the groups studied. However, a precise numerical pre-processing of the empirical data is necessary. Our results appear to be a contribution to further research in this area.

Acknowledgments: This research was funded by the Józef Piłsudski University of Physical Education in Warsaw, UPB no. 2 (114/12/PRO/2023) - Evaluation of postural control in response to induced perturbations in different age groups.

References

- [1] SALSABILI H., BAHRPEYMA F., ESTEKI A., KARIMZADEH M., GHOMASHCHI H. *Spectral characteristics of postural sway in diabetic neuropathy patients participating in balance training.* J Diabetes Metab Disord. 2013, 19;12:29

Technical aspects and limitations of signal acquisition during dynamic movement on the rowing ergometer

B. N. DANIEL^{1*}, K. SYBILSKI², J. MAŁACHOWSKI²

¹Faculty of Mechatronics, Armament and Aviation, Institute of Rocket Technology and Mechatronics, Military University of Technology, Warsaw, Poland

²Faculty of Mechanical Engineering, Institute of Mechanics and Computational Engineering, Military University of Technology, Warsaw, Poland

Keywords: *measurement limitation, EMG, fNIRS, dynamic movement*

1. Introduction

This study aimed to identify the selected limitations of signal acquisition during dynamic movement on a rowing ergometer. Functional near-infrared spectroscopy (fNIRS) techniques were employed on the head and muscles, along with electromyography (EMG). These techniques aimed to provide information on the level of brain and muscle involvement during movement. Several significant limitations were encountered during the study. The findings of this study highlight selected limitations in signal acquisition from many sensors during dynamic rowing ergometer exercises. Future research is recommended to develop and employ more advanced measurement techniques that are less susceptible to motion-related disturbances and artifacts. This would allow for a more accurate analysis of brain and muscle activity during such movements.

Data acquisition during dynamic movement presents a challenge for both EMG and fNIRS measurements. The fNIRS technique on the head was susceptible to motion-related disturbances and skin artifacts, resulting in signal distortions and impeding accurate data analysis regarding brain activity [1]. fNIRS technique on muscles also had limitations [2]. Precise measurements on smaller muscle groups were challenging due to the limited spatial resolution of this technique. Both brain and muscle fNIRS have a limitation connected with colour of the skin and colour and thickness of hair [3]. Additionally, muscle motion artifacts could cause signal disturbances and hinder the interpretation of results. The application of EMG to measure muscle activity had its limitations. Although EMG is commonly used, it is susceptible to electrical interferences and signals from other muscles, potentially leading to misinterpretation of results and impeding precise analysis of muscle activity [4]–[6].

The measurement conducted in this study involved the utilization of multiple techniques, which brings about complications that have been previously described in the literature. However, additional challenges were also observed, particularly related to the synchronization of the equipment during movement on the ergometer and its performance during the actual motion.

2. Research description

The study was conducted on eight participants from an academic rowing sports section using a Concept II rowing ergometer. Measurements were made at a rate of 30 strokes per minute, with the principle of adjusting to the maximum (subjective) fatigue level of the participants. During the measurement, signals were recorded from the following devices: fNIRS (OctaMon M system, Artinis, LLC, New York, NY, USA), fNIRS (OctaMon + system, Artinis, LLC, New York, NY, USA), as well as EMG for muscle activity, heart rate, and motion recordings (Noraxon, DTS, Desktop Direct Transmission System, Scottsdale, AZ, USA). Sensors used in the study are presented in Fig. 1.

*Corresponding author: Natalia Daniel, e-mail: natalia.daniel@wat.edu.pl

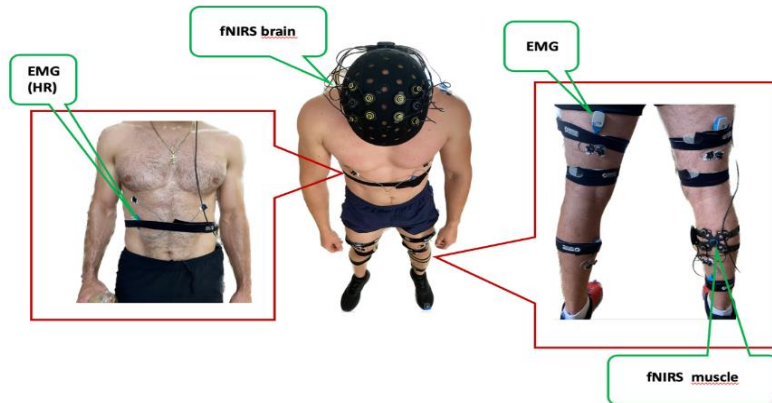


Fig. 1. Devices used in measurement (HR, EMG, fNIRS (brain and muscle))

During such a long duration of the measurement (up to the time participants reported fatigue), several issues were encountered. Some of them were related to those described in the literature, such as hair thickness, length, and color in the case of fNIRS or electrode detachment in the case of EMG. It was also found that the installation of equipment on the participants' bodies was problematic due to the possibility of overlap between two devices and the selection of appropriate muscles. For example, the fNIRS device was placed on the calf, where the EMG sensor was also placed. Furthermore, bending the limb in a manner determined by the ergometer caused displacement of the sensors placed on the calf's gastrocnemius muscle. Therefore, it was necessary to precisely position the sensor cables to eliminate electrode displacement issues. Similarly, the medial and lateral quadriceps muscles were excluded from the study due to additional arm movements and varying dimensions of the participants' limbs, resulting in electrode detachment in almost every case. In the case of fNIRS, anatomical differences, such as head geometry, posed challenges. Therefore, activating all the sensors on the head required the use of different cap configurations (strap adjustments, the application of pads). In addition, the simultaneous activation of all measurement devices required precision and commitment. This presentation is part of ongoing research, and the described aspects will be further discussed during the conference.

References

- [1] HUO C., XU G., LI W., XIE H., ZHANG T., LIU Y., LI Z. *A Review on Functional Near-Infrared Spectroscopy and Application in Stroke Rehabilitation*. Med Nov Technol Devices. 2021, 11, 100064, doi:10.1016/J.MEDNTD.2021.100064
- [2] DANIEL N., SYBILSKI K., KACZMAREK W., SIEMIASZKO D., MAŁACHOWSKI J. *Relationship between EMG and FNIRS during Dynamic Movements*. Sensors, 2023, 23:5004, doi:10.3390/s23115004.
- [3] DOHERTY E.J., SPENCER C.A., BURNISON J., ČEKO M., CHIN J., ELOY L., HARING K., KIM P., PITTMAN D., POWERS S., ET AL., *Interdisciplinary Views of FNIRS: Current Advancements, Equity Challenges, and an Agenda for Future Needs of a Diverse FNIRS Research Community*. Front Integr Neurosci 2023, 17, doi:10.3389/FNINT.2023.1059679
- [4] FELICI F., DEL VECCHIO A. *Surface Electromyography: What Limits Its Use in Exercise and Sport Physiology?* Front Neurol, 2020, 11: 578504, doi:10.3389/FNEUR.2020.578504
- [5] DEJNEKA A., MAŁACHOWSKI J., MAZURKIEWICZ L. *Identification of Muscle Movements and Activity by Experimental Methods for Selected Cases - Stage#1*. 2022, Acta Bioeng Biomech, 2022,24(3):69-82
- [6] DEJNEKA A., MAŁACHOWSKI J., MAZURKIEWICZ L. *Identification of Muscle Movements and Activity by Experimental Methods for Selected Cases - Stage#2*. Acta Bioeng Biomech, 2022,24(4):3-11.

Biomechanics and efficiency of n-link extremities of insects

O. DENISOV^{1*}, N. KIZILOVA²

¹Biological Faculty, Karazin Kharkiv National University, Kharkiv, Ukraine

²Institute of Aeronautics and Applied Mechanics, Warsaw University of Technology, Warsaw, Poland

Key words: locomotion, extremity, kinematics, mechanical efficiency, biomimetic robotic arm

1. Introduction

Upper and low extremities in animals can be considered as n-link chains with the number of segments from n=3 in humans and mammals to n=4-8 in insects [1]. Different types of extremities are designed by the nature for walking, running, crawling, jumping, grasping, digging, swimming, collecting pollen and other functions [2]. Biomechanics of any type of extremity is based on mechanical principles [3] and is frequently satisfies the principle of least action [1]-[3]. Better understanding the locomotion biomechanics of extremities is important either for theoretical biology or for robotic technologies with robotic arms of different design for manipulations at any scales from macro (industrial robots) to micro/nano scales (medical microrobots) [2]. In this study the results of kinematic analysis of known types of insect legs is given and their optimal design is analysed.

2. Materials and method

High resolution images of insects with their extremities elongated have been selected from open access virtual collections of the Natural History and zoological institutions. The segments of each extremity (Fig.1) have been digitized as n-link chains, and the lengths $\{l_j\}_{j=1}^n$, widths $\{w_j\}_{j=1}^n$ and surface areas $\{S_j^\perp\}_{j=1}^n$, $\{S_j^\parallel\}_{j=1}^n$ in two orthogonal directions (bottom view, Fig.1a, and side view \perp , Fig.1b) have been measured (Fig.1c) and collected in the database for further statistical processing. All the lengths have been normalized by the total length of the extremity. Important statistical regularities between the normalized lengths $\{l_j\}_{j=1}^n$ are presented in Table 1 for the Mantis (*Mantodea*) with n=5 and the ladybird (*Coccinellidae*) with n=3.

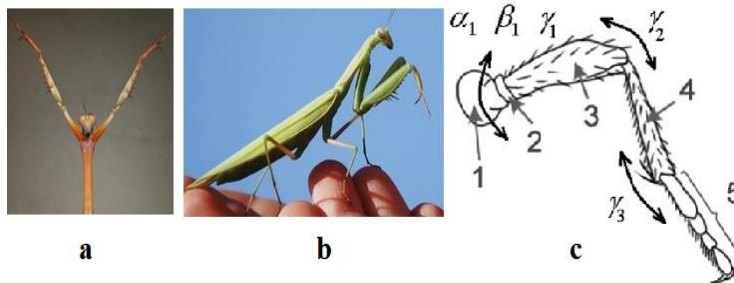


Fig. 1. Bottom view (a) and side view (b) of the first pair of legs, and their segments n=1-5 (c)

Table 1. The fractions of the length of each segment in the upper pair of legs in mantis and ladybirds

| Name | $l_1(\%)$ | $l_2(\%)$ | $l_3(\%)$ | $l_4(\%)$ | $l_5(\%)$ |
|----------|-----------|-----------|-----------|-----------|-----------|
| Mantis | 23,6±6,5 | 30,9±7,2 | 16,9±4,6 | 13,5±5,6 | 4,5±2,1 |
| Ladybird | 39,2±6,8 | 46,4±7,7 | 14,3±5,9 | - | - |

*Corresponding author: Natalia Kizilova, e-mail: n.kizilova@gmail.com

The linear regression dependencies and their coefficients of determination (R^2) for the pairs of have been computed, and strong correlations between the adjacent segments $\{l_1, l_2\}$ ($l_2 = 0,9174l_1 + 0,0921$; $R^2 = 0,675$) and $\{l_2, l_3\}$ ($l_3 = 0,5175l_2 + 0,0086$; $R^2 = 0,664$) compared to the remote segments have been found.

Kinematics of the chain movement towards a target (prey) has been studied based on minimum of following optimization functions: work (W), kinetic energy (K), time of the movement performance (T), jerk (J), torque (Q), torque change during the movement (Q^*), and total rotation in the joints (R). The values $\{l_j^o, w_j^o, I_j^o, m_j^o\}_{j=1}^n$ for the segments have been taken from the database. The movement optimization problem $K = 0,5 \sum (m_j \bar{v}_{Cj}^2 + I_j \bar{\omega}_j^2) \rightarrow \min$; $T \rightarrow \min$, where $\bar{v}_{Cj}, \bar{\omega}_j$ are velocities of the centre of mass and angular frequency of the j-th segment, have been considered for all the pairs of the criteria from the list {W,K,T,J,Q,Q*,R}. The movement was subjected for the Lagrangian dynamic equation with the relative angles $\{\gamma\}_{j=1}^{n-1}$ (Fig.1c) between the adjacent segments as general coordinated in the space. The drag in the joints was neglected.

3. Results and Discussion

It was shown, the purpose of the extremity (for movement, catching or digging) influences its design and the functions minimized by the fastest ($T \rightarrow \min$) movement. Some pairs of the criteria were contradictory while others produced similar optimal trajectories of motion. The Pareto frontiers approach revealed the best representation of the optimal trajectories for given geometry of the n-link chains described by the pair (K,T). Based on this multicriteria approach, different extremities can be classified by their function (Fig.2a) and some differences between the families of insects (Fig.2b).

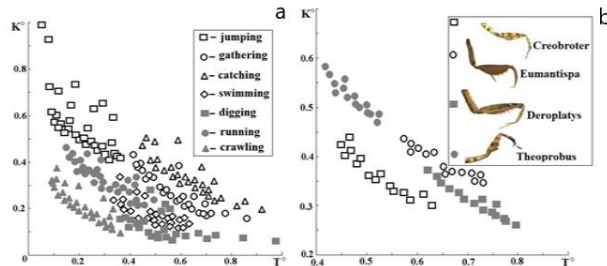


Fig.2. The Pareto frontiers for the legs of different types (a) and families of Mantis (b)

4. Conclusions

Based on the measurement results, different relationships between the adjacent segments are proper to different purpose extremities (to walk, catch, dig, etc.) of insects. Their geometry provides trajectory optimization for some pair of functions like total kinetic energy and performance time (K,T). For optimal grasping and catching purposes some 4-6 link extremities can be more efficient compared to human arm, that is important for the robotic arm design especially for micromanipulation of small medical robots with sensors, cells and large molecules.

References

- [1] DENISOV O., KIZILOVA N. *Geometry and mechanical function of multijoint extremities from mammals to insects: towards biomimetic design of robotic arm*. Proceedings of 11th International Conference BIOMDLORE, VGTU Press Technika, 2016, 69-72.
- [2] PUSHENKO V., KIZILOVA N., USTIMENKO E. *Kinematics of catching arms in insects: towards optimal design of robotic manipulators*. *Engineering for a Changing World*, Ilmenau Technische Universität Press, 2017, 75
- [3] MCNEIL A.R. *Principles of Animal Locomotion*. Princeton University Press, 2006

Gender differences in kinematic determinants of shuttlecock velocity and flight angle in the badminton forehand smash

A. FERREIRA^{1*}, M. GÓRSKI², P. TABOR¹, J. GAJEWSKI¹

¹Faculty of Physical Education, Józef Piłsudski University of Physical Education in Warsaw, Poland

²Institute of Sport – National Research Institute, Department of Kinesiology, Warsaw, Poland

Key words: *biomechanics, technique, racket sport, speed, motion capture*

1. Introduction

Badminton is a very popular Olympic sport worldwide, however, scientific reports on the technique of movement and biomechanical analysis of badminton strokes are rare. The most lacking in this area are studies involving female players. The aim of this study was to demonstrate any differences in the smash technique between male and female professional badminton players.

2. Materials and Methods

Twenty-one elite professional badminton players (12 males and 9 females) – members of the Polish National Badminton Team participated in the study (Table 1). The study received Ethical approval from the Senate Research Ethics Committee of Józef Piłsudski University of Physical Education in Warsaw, Poland.

Table 1. Basic characteristics of studied groups

| | Age (years) | Training practice (years) | Body mass (kg) | Body height (m) | BMI | % FAT (%) |
|---------------------|-------------|---------------------------|----------------|-----------------|------------|-----------|
| Male players (n=12) | 22.8 ± 4.7 | 14.2 ± 3.7 | 77.3 ± 5.6 | 1.83 ± 0.07 | 23.0 ± 2.0 | 13 ± 3 |
| Female players (9) | 21.8 ± 4.1 | 12.2 ± 4.7 | 60.3 ± 7.0 | 1.64 ± 0.07 | 22.3 ± 1.8 | 23 ± 5 |

In order to measure kinematic variables during the forehand smash, the Vicon 3D motion capture system with 10 cameras (MX T40S, 200 Hz) was used. Thirty-nine reflective markers were placed on the participant's body, and reflective tape was placed on the shuttlecock's cork base. Each player's task was to perform five forehand smashes, giving the shuttlecock the highest possible velocity. The shuttlecock had to pass above the badminton net (155 cm) and under a colourful string visible for the athlete, placed 30 cm over the net. The shuttlecock was released by the Leopard Smart shuttlecock's feeding machine. Kinematics variables (angles, angular velocities, and displacement of the centre of player's body mass) were calculated for the fastest smash of each participant. Relationships between the variables were assessed by calculating Spearman's rank correlation coefficient. Computations were performed with STATISTICA software (v. 13.3, StatSoft, USA) and MS Excel.

3. Results

Both in mean shuttlecock velocity (V_{sh}) and in mean shuttlecock flight angle (shuttlecock velocity vector inclination to the horizontal plane) (α_{sh}) male players obtained mean values significantly higher than female players ($V_{sh}= 81.4 \pm 5.2$ vs 68.3 ± 3.9 m/s, $\alpha_{sh}= 14.6 \pm 2.5^\circ$ vs $8.2 \pm 1^\circ$).

*Corresponding author: Anna Ferreira, e-mail: anna.glebocka@interia.pl

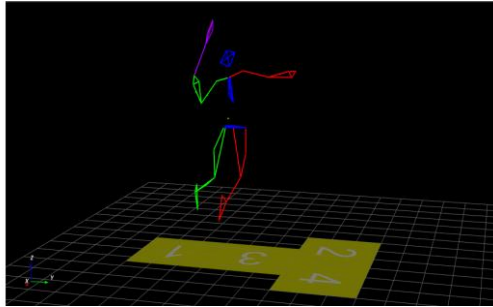


Fig. 1. Three-dimensional model of one of the players created with the use of the Vicon Motion Capture System

The differences between male and female players in joints angles were noted in the trunk position in the sagittal plane. During the moment of the racket's and shuttlecock's contact, women kept the torso straight (-4.1 deg), while men, after trunk extension, moved to its flexion (11.7 deg). Greater forearm rotation has been reported in women than in men. Significant differences in the angular positions and angular velocities of individual joints were recorded between male and female players. Among men, a positive correlation was found between the height of the shuttlecock's position at the moment of the contact with the racket and α_{sh} ($r=0.746$). This relationship was not confirmed in women. It was found that female players use two different smashing techniques (jump or semi jump), neither of these techniques guaranteed to achieve higher V_{sh} or α_{sh} values. The lack of benefits recorded from performing a jump before the smash execution in women results in common resignation from the forehand jump smash observed in female's elite matches. A positive correlation was found for both female ($r=0.667$) and male ($r=0.748$) players between the quality of smash and the angular velocity of the elbow flexion during the impact. In the case of women, it was found that during the moment of the racket's and shuttlecock's contact, greater radial abduction of the radiocarpal joint increases in the values of V_{sh} and α_{sh} . Numerous correlations of trunk movement in sagittal plane prove the importance of a correct movement in this axis on smash quality in men.

4. Conclusion

The jump before a smash recorded in men is intended to create appropriate conditions for players to hit the shuttlecock at the greatest possible angle downwards, which, from a tactical point of view, opens up the possibility of playing the shuttle in various parts of the court. Demonstrated differences in the studied variables between men and women and the different correlations of smash quality and biomechanical variables in female and male players indicate the need to diversify the training aiming to improve smashing techniques in both genders.

Acknowledgments: Financial support: Scientific School No. 5 and Project DM-61 implemented at the Józef Piłsudski University of Physical Education in Warsaw, Poland. DSN Scientific project implemented under contract No. 18/07/104.06/2019/WIN at the Institute of Sport – National Research Institute, Warsaw, Poland.

References

- [1] KING M., TOWLER H., DILLON R., MCERLAIN-NAYLOR S. *A correlation analysis of shuttlecock speed kinematic determinants in the badminton jump smash*. Appl Sci, 2020, 10(4), 1248.
- [2] RAMASAMY Y., USMAN J., SUNDAR V., TOWLER H., KING M. *Kinetic and kinematic determinants of shuttlecock speed in the forehand jump smash performed by elite male Malaysian badminton players*. Sports Biomech, 2021, 4:1-16

Mechanical and structural properties of AZ91-based Ti reinforcement composite

A. FILIPIAK-KACZMAREK^{1*}, A. NIKODEM², K. NAPLOCHA¹

¹Department of Lightweight Elements Engineering, Foundry and Automation, Faculty of Mechanical Engineering
Wrocław University of Science and Technology, Wrocław, Poland

²Department of Mechanics, Materials and Biomedical Engineering, Faculty of Mechanical Engineering,
Wrocław University of Science and Technology, Wrocław, Poland

Key words: AZ91, composite, SBF, Ti reinforcement

1. Introduction

Lightweight metals are increasingly used in biomedical engineering, and can be found in orthopedics (screws, implants), stomatology, cardiology (stents) and as scaffolds. Magnesium alloys have a low density (1.74 g/cm³), which is very close to that of bone (1.75 g/cm³), as well as high biocompatibility and are biodegradable. Unfortunately, their disadvantage is their low resistance to corrosion in the human body, which further causes deterioration of mechanical and physical properties. Improvement of this properties can be achieved by making the composite on magnesium matrix - depending on the reinforcement added, the required properties can be obtained.

2. Materials and Methods

In this study AZ91 magnesium alloy and AZ91 magnesium-based composite reinforced with titanium mesh (Titanium Gaze 100 mesh) were used. All samples were in the form of beams with 5,07x3,02 mm dimensions and were made by squeeze casting. In this investigation were made three types of specimens: AZ91 magnesium alloy and AZ91 magnesium-based composite reinforced with two and three mesh layers.

The tree-point bending test was conducted using a Tinius Olsen H25KT machine with a total load capacity of 25 kN. The test was carried out at a speed of 500 mm/min with the force that was applied 50 N.

The AZ91 composite with reinforced with titanium mesh samples were immersed in SBF by maintaining the temperature constant at 36°C to determine the degradation behaviour. Two types of measurements were made during the incubation: measuring the pH value of SBF and measuring the weight of the specimens after 1, 2, 4, 8, 12 and 24 hours.

The structural studies included SEM microscopy, EDS analysis and microstructure analysis using computer microtomography (1172 SkyScan Bruker).

3. Results

All types of samples were used for mechanical testing: AZ91 magnesium alloy and AZ91 magnesium-based composite reinforced with two or three titanium mesh layers. A three – point bending test showed that specimens reinforced with three layers of titanium mesh have higher strain compared to specimens with two layers of titanium mesh or without. However, it can be seen that for Young's modulus values, two layers cause an increase. On the other hand, for more reinforcement, the Young's modulus value is comparable to pure AZ91 (Table 1).

*Corresponding author: Adrianna Filipiak – Kaczmarek, e-mail: adrianna.filipiak@pwr.edu.pl

Table 1. Three-point bending results for AZ91 specimens and AZ91-Ti composite

| Material | Flexural strength [MPa] | E [GPa] | Break strain [%] |
|---------------|-------------------------|---------|------------------|
| AZ91 | 235-250 | 23-27 | 2.5-2.9 |
| AZ91 + 2 mats | 257-283 | 27-28 | 3.1-3.8 |
| AZ91 + 3 mats | 285-305 | 23-24 | 4.4-5.5 |

For the aging tests were used specimens reinforced with two layers of titanium mesh after strength testes. Aging tests showed that the weight of the samples decreased with longer immersion time. Equally, the pH value of the SBF solution increased. However, the SEM pictures of composite surface showed that a layer of oxides forms on the surface of the samples, which further prevents the identification of titanium reinforcement (Fig. 1).

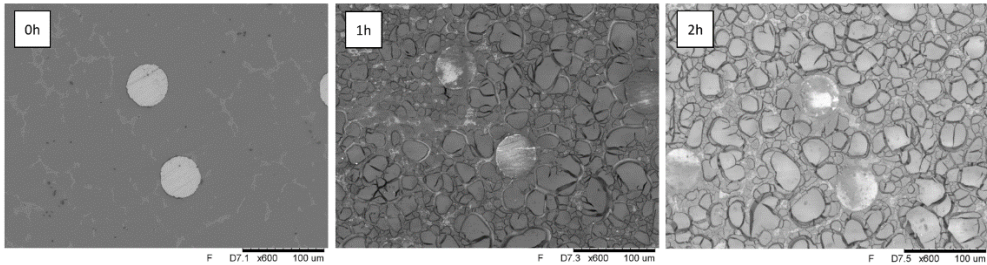


Fig. 1. SEM images of a sample with visible titanium fibers before and after 2 hours in SBF solution

4. Conclusion

The use of a titanium mesh as a reinforcement in composite allows for better strength properties compared to the AZ91 alloy. However, after the test was observed separation of the titanium fibers from the magnesium matrix, which resulted in the formation of free space around the fibers. On the other hand, the corrosion resistance of such composites should be corrected. The aging tests carried out prove that the AZ91 alloy degrades rapidly in the SBF solution.

References

- [1] ESEN Z., OCAL E.B., AKKAYA A., GURCAY B., OZCAN C., OZGUMUS B.A., DUYGULU O., DERICIOGLU A.F. *Corrosion behaviour of Ti6Al4V-Mg/Mg-Alloy composites*. Corrosion Science, 2020, 166: 108470
- [2] OCAL E.B., ESEN Z., AYDINOL K., DERICIOGLU A.F. *Comparasion of the short and long-term degradation behaviors of as-cast pure Mg, AZ91 and WE43 alloys*. Mater Chem Phys, 2020: 241
- [3] KOKUBO T., TAKADAMA H. *Fabric dependence of bone ultrasoundHow useful is SBF in predicting in vivo bone bioactivity?* Biomaterials. 2006, 27(15):2907-15
- [4] OUYANG S., LIU Y., HUANG Q., GAN Z., TANG H. *Effect of composition on in vitro degradability of Ti – Mg metal-metal composites*. Mater Sci Eng C Mater Biol Appl. 2020, 107:110327

Gait kinematics asymmetry change induced by multijoint hip flexion resistance training – a preliminary research

D. FRYC^{1*}, K. WOJCIECHOWSKI²

¹Department of Biomechanics, Faculty of Biomedical Engineering, Silesian University of Technology, Zabrze, Poland

²Research and Development Centre, Polish-Japanese Academy of Information Technology, Bytom, Poland

Key words: *asymmetry, gait analysis, human biomechanics, resistance training, hip flexion*

1. Introduction

The topic of gait symmetry is usually considered when studying amputees or injured patients. However, gait studies of healthy subjects may also bring some value to the understanding of human physiology and biomechanics. It was already found that ground reaction forces present high level of symmetry [1]. Spatio-temporal and kinematic parameters [2] as well as EMG [3] tend to differ laterally. The asymmetry level differ in population and can have several causes but the primal cause lays in the natural process of lateralization that occur in the early ontogenesis [4],[5]. Morphological symmetry is usually considered a physical development correctness indicator. Studies also confirm, that increased gait asymmetry correlates with poorer performance in professional runners [6] and higher injury risk in professional athletes [7],[8].

2. Aim

The aim of this preliminary study was to verify the influence of multijoint hip flexion resistance training with the use of a machine according to the patent PL 242345 B1 on the gait kinematics symmetry of the lower extremity.

3. Materials and Methods

The subject of this preliminary study was a healthy woman aged 29, weight 49kg with no severe posture defects. The gait of the subject was recorded with optical motion capture system (Vicon, Oxford Metrics plc, UK) before and after the training intervention.

The exercise of multi-joint resistance hip flexion was applied. Training was conducted with the use of a machine with free weights load and foot bindings attached to the platforms that allows for the application of downward directed force to the foot. Subject was standing on the platforms with her foot fastened in bindings and lifting legs alternately. Each training was preceded with a proper warm-up. Subject performed 120 trainings with the volume of 100 repetitions for each leg, divided into 10 sets of 10 repetitions and 30 sec rest periods. Training was performed every other day with the load equal to 60% 1RM. The load was adjusted to the progress in 1RM that was tested after every 10 sessions and changed gradually from 15 to 25 kg. The patient did not engage in any other regular training for the entire duration of the study.

The joint angles' asymmetry was calculated as an absolute difference between both sides at corresponding times of the interpolated gait cycles. The method was chosen in order to preserve information about angular value of asymmetry for joints angles' comparison.

*Corresponding author: Dobrochna Fryc, e-mail: dobrochna.fryc@polsl.pl

4. Results

Almost all joints angles asymmetries were significantly reduced after the training intervention (Fig. 1). Asymmetry reduction was proportional to mean asymmetry (correlation: $R=-0.88$, $p<0.001$)(Fig. 1). Among all studied angles only hip flex-extension and foot progression in sagittal plane presented asymmetry increase. Angles demonstrating the most asymmetry reduction were ankle inter-external rotation (19.26 deg.) and hip inter-external rotation (18.53 deg.). Both parameters indicate a radical change in right extremity joints ROM. Asymmetry reduction exciding 5 degrees was also observed in ankle in-eversion and knee in-external rotation.

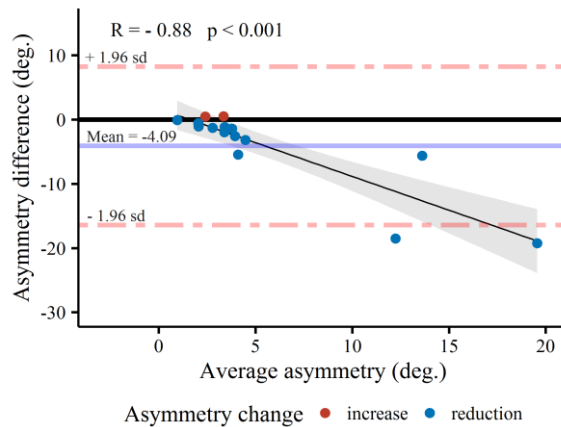


Fig. 1. Bland-Altman plot of difference between asymmetries to average asymmetry before and after training intervention ratio in gait

5. Conclusions

The preliminary study shows that the use of hip flexion resistance training and a machine according to patent PL 242345 B1 has a potential to reduce gait asymmetry in healthy subjects. The exercise is planned to be further validated in a proper study with healthy subjects.

Acknowledgments: I wish to show my appreciation to Tomasz Pytel and Amanda Frey for their work and support in the collecting data process. I wish also to extend my special thanks to Michał Rossa for his work in the training equipment construction.

References

- [1] HAMILL J., BATES B.T., KNUTZEN K.M. *Ground reaction forces symmetry during walking and running*. Res Q Exerc Sport, 1984, 55, 288-93
- [2] CIMOLIN V., CAU N., SARTORIO A., ET AL., *Symmetry of gait in underweight, normal and overweight children and adolescents*. Sensors, 2019, 19(9), 2054
- [3] ARSENAULT A.B., WINTER D.A., MARTENIUK R.G. *Is there a 'normal' profile of EMG activity in gait?* Med Biol Eng Comput. 1986, 24(4):337-43
- [4] COREN S., BISHOP D.V.M. *Handedness and developmental disorder*. Am J Psychol, 1993, 106(2), 294
- [5] GÜNTÜRKÜN O., STRÖCKENS F., OCKLENBURG S. *Brain lateralization: a comparative perspective*. Physiol Rev. 2020, 1,100(3):1019-1063
- [6] TRIVERS R., FINK B., RUSSELL M., ET AL., *Lower body symmetry and running performance in elite Jamaican track and field athletes*. Plos one, 2014, 9(11):e113106
- [7] HELME M., TEE J., EMMONDS S., LOW C. *Does lower-limb asymmetry increase injury risk in sport? A systematic review*. Phys Ther Sport. 2021 May;49:204-213
- [8] PLUMMER H.A., CAI Z., DOVE H., ET AL., *Hip abductor strength asymmetry: relationship to upper extremity injury in professional baseball players*. Sports Health. 2023, 15(2):295-302

Methods to increase the strength of 3D printed PLA samples, a mini review

M. GŁOWACKI, A. MAZURKIEWICZ*

Bydgoszcz University of Science and Technology, Faculty of Mechanical Engineering, Bydgoszcz, Poland

Key words: 3D print, PLA, mechanical properties

1. Introduction

3D printing has become a versatile tool in many fields, enabling the creation of elements in a wide variety of shapes and applications. Polylactide (PLA) is one of the most popular materials used in 3D printing due to its ease of use, availability, biodegradability and low toxicity. However, strength of elements printed from PLA sometimes is lower than require. Therefore, various methods are develop to improve of mechanical properties of PLA printed parts. In this paper, we present some methods to improve the properties of PLA made by 3D printing. We show some techniques and modification methods which increase the strength, resistance to external factors and adaptability of PLA printed elements.

2. Material and Methods

Heat and chemical treatment

One of the most common methods for improving the mechanical properties of prints is to expose to higher temperatures for a certain period of time. Jayanth and co-authors, the process in question is referred to as quenching [1]. Printed samples were exposed to 90 °C for 60 minutes, what affected in a significant increase in strength. Strength was assessed by impact testing. Authors estimated it was the result of reducing the internal stresses among layer-on-layer overlap during printing and increasing degree of crystallization of polymer [1]. In the paper by K. Guduru and co-authors [2], the effect of a PLA material that was reinforced with carbon fibre at a level of 15 per cent and then subjected to two different post-treatment methods was investigated. One was a heat treatment and the other a chemical treatment. Both of methods affected on increase of strength. Chemical treatment gave results better about 12 % in comparison to heat treatment.

Application of fillers

One of the newest method of reinforcing PLA material is use different concentrations of marble-alumina and alumina coatings, as described in paper by Harun Kocak [3]. Printed samples (50 % fill) were placed in a metal mold to evenly apply a 0.5 mm coating on all surfaces. The samples were left for 48 hours to allow the polymer resin contained marble hardened.

The tensile strength for the composite-coated sample was 34.4 MPa. However, the compression test showed a lower strength compared to the uncoated sample, due to the brittleness and lower tensile strength of the PLA. The bending strength was 79.8 MPa for the uncoated sample, while the coated samples oscillated between 54.15 and 64.4 MPa. The adhesion test for the marble coating was 8.2 MPa, and for the alumina it was 5.5 MPa.

*Corresponding author: Marcin Głowacki, e-mail: marcin.glowacki@pbs.edu.pl

For the best results in terms of strength, adhesion and abrasion resistance, it is recommended to modify the surface with an initial coating of marble followed by alumina.

Reproduction of atmospheric conditions

In the article by J. Sedlak and co-authors [4], the effect of degrading factors on 3D printed materials. Samples from PLA were subjected to humidity, temperature cycles, UV radiation, which were simulated atmospheric conditions occurring outside. Samples left in a condensation chamber at 100 % humidity and 55 °C for 100 hours showed an increase in weight and a decrease in tensile strength after exposure. Samples that were exposed to alternating frost of -18 °C and room temperature of 21 °C for a total of 130 cycles behaved similarly. A slight increase in strength was observed in samples exposed to UV light for 20 and 100 hours. No significant changes were observed for the samples placed in the oven for 100 hours at 60 °C. Exposure of the samples to the outdoors for 98 days showed no clear effect also [4].

3. Summary

Summarizing, exist a wide range of methods of improving the mechanical properties a of printed elements from PLA. Studies presented in this paper only briefly demonstrate the potential for improving the properties of PLA prints through various methods. More complexity information about these problems can be find in papers by Głowacki et al. [5], Shirazi et al. [6], Afshar et al. [7], Reza Khosravani et al. [8].

With very high probability a progress in enhancing strength of PLA printed parts will expand the range of applications for 3D printing technology in various industries in future.

References

- [1] JAYANTH K. ET AL., *Effect of heat treatment on mechanical properties of 3D printed PLA*. J Mech Behav Biomed Mater. 2021, 123:104764
- [2] GUDURU K., SRINIVASU G. *Effect of post treatment on tensile properties of carbon reinforced PLA composite by 3D printing*. Material Today: Proc, 2020. 33(8): 5403 – 5407
- [3] KOCAK H. *Surface Modification of a Model Part Produced with 3D Printing from PLA, Material by Means of Composite Coating*. J Mater Eng Perform, 2021, 30(5): 3903 – 3910
- [4] SEDLAK J., ET AL., *Analysis of the Mechanical Properties of 3D-Printed Plastic Samples Subjected to Selected Degradation Effects*. Materials 2023.
- [5] SEDLAK J, JOSKA Z, JANSKY J, ZOUHAR J, KOLOMY S, SLANY M, SVASTA A, JIROUSEK J. *Analysis of the Mechanical Properties of 3D-Printed Plastic Samples Subjected to Selected Degradation Effects*. Materials (Basel). 2023 Apr 21;16(8):3268
- [6] GŁOWACKI M., ET AL., *Resistance of 3D-Printed Components. Test Specimens and Products to Work under Environmental Conditions—Review*. Materials (Basel). 2022 Sep 5;15(17):6162
- [7] SHIRAZI S.F.S., ET AL., *A review on powder-based additive manufacturing for tissue engineering: Selective laser sintering and inkjet 3D printing*. Sci Technol Adv Mater. 2015.16: 033502
- [8] AFSHAR A., MIHUT D. *Enhancing durability of 3D printed polimer structures by metalization*. J Mater Sci Technol, 2020, 50: 185 – 191
- [9] KHOSRAVANI R.M., ET AL., *Structural performance of 3D-printed composites under various loads and environmental conditions*. Sci Polym Test. 2020, 91: 106770

The possibility of using the OrthoNail hybrid intramedullary nail in the human body without risk of decohesion

D. GRYGIER^{1*}, P. KOWALEWSKI², M. DZIUBEK¹, R. JASTRZĄBEK³, M. OPAŁKA², J. SŁOWIŃSKI⁴

¹Automotive Engineering Department, Faculty of Mechanical Engineering,
Wrocław University of Science and Technology, Wrocław, Poland

²Department of Fundamentals of Machine Design and Mechatronic Systems, Faculty of Mechanical Engineering
Wrocław University of Science and Technology, Wrocław, Poland

³Orthoget sp. z o. o., ul. Muchoborska 18, 54-424, Wrocław, Poland

⁴Department of Mechanics, Materials and Biomedical Engineering, Faculty of Mechanical Engineering,
Wrocław University of Science and Technology, Wrocław, Poland

Key words: *intramedullary nail, hybrid drive, dynamic implant, lengthening of long bones*

1. Introduction

OrthoNail intramedullary nail is an implant with a unique hybrid magneto-mechanical mechanism that allows for highly precise human lower limb bone lengthening [1]. The implant is a solution that is to help patients with congenital, developmental, post-traumatic or iatrogenic defects, and in whom the asymmetry of the lower limbs is greater than 3 cm, and patients with short stature [2],[3]. The scale of patients in the area of medical indications for lower limb lengthening or reconstruction all over the world currently concerns > 120 million people, and nearly 200,000 people join the group of potential patients every year [1].

An extremely important aspect that had to be taken into account in the study was the structural strength of the implant, which, unlike the current competitive solutions, was supposed to allow it to be fully loaded. According to the design assumptions, the driving part of the implant is characterized by a simple and compact construction of the repeater, and the mechanical part has been developed in such a way as to enable the transfer of physiological load up to 80% of the patient's body weight to both legs of the patient, while maintaining the design life in fatigue cycles of min. 500,000 load cycles.

2. Materials and Methods

As part of the study, a model of the OrthoNail target implant with centrally placed bone screws was prepared and the effect of a force of 80% of the total load on the distribution of displacement, stress and strain in the implant volume was tested (Fig.1). The subject of the study was a dynamic nail design, and the model was additionally supplemented with a fragment imitating a fragment of bone fusion that occurs as a result of bone formation.

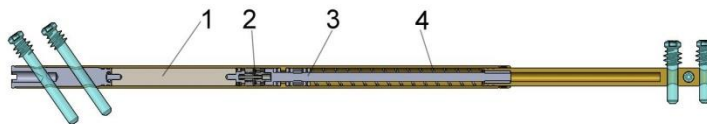


Fig. 1. OrthoNail intramedullary nail: 1-magnet, 2-mechanical gear, 3-screw, 4-spring

As part of the analysis, calculations were carried out to show what displacement would occur in the bone model at the interface between the fragments, assuming a load of 80% of the nominal load.

A nail protrusion of 50 mm was assumed to represent the largest displacements that could occur between the fragments. A single-leg standing case was chosen for the analysis (Fig.2). The force and

*Corresponding author: Dominika Grygier, e-mail: dominika.grygier@pwr.edu.pl

Finite element analysis of the influence of porosity and pore geometry on mechanical properties of orthopaedic scaffolds

A. GRYKO*, P. PROCHOR

Institute of Biomedical Engineering, Białystok University of Technology, Białystok, Poland

Key words: scaffold, porosity, pore, geometry, Young's modulus, yield strength

1. Introduction

Scaffolds play a key role in regenerative medicine in the repair of injuries, defects and cancerous changes in long bones [1]. For this reason, scaffolds should meet certain mechanobiological requirements, such as adequate porosity and pore geometry to ensure appropriate osteointegration as well as load transfer [2]. Taking into account the most frequently used cell units, this study attempted to evaluate the porous structures of orthopaedic scaffolds in terms of their strength parameters [3],[4].

2. Materials and Methods

2.1. CAD and FE models

Four pore geometries were selected for analyses: sphere, octagonal prism, cube and triangular prism, all with porosities of 10% up to 60% (Fig. 1a). Three different material properties were considered: Ti6Al4V alloy, CoCr alloy, 316L steel. Strength compression simulations were carried out on 144 models, 72 structures of cell units with dimensions of 4 x 4 x 4 mm and 72 structures of scaffolds with a diameter of 16 mm and a height of 15 mm. Cell units and cylindrical scaffolds were loaded with a rectangular block (Fig. 1b and 1c). The intention was to simulate compression tests in a testing machine in order to evaluate strength parameters.

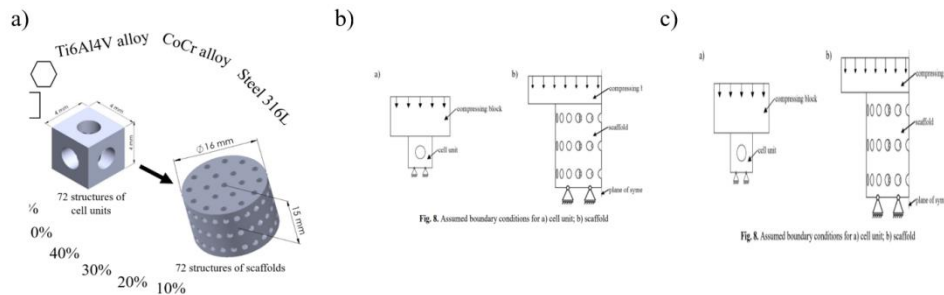


Fig. 1. CAD and FE models prepared for analyses: a) model variants, b) assumed boundary conditions for cell unit, c) assumed boundary conditions for scaffold

Averaged Huber-Mises-Hencky stresses were analysed as results. Based on stress-strain curves two parameters were calculated: effective Young's modulus (EYM) and 0.2% offset effective yield strength (0.2% OEYS). EYM of analysed structures was estimated by finding an elastic region in the stress-strain curve and linear slope equation. In the case of 0.2% OEYS, it was obtained by finding an intersection between the stress-strain curve and abscissa with a 0.2% offset that is parallel to the initial slope of the obtained curve. For comparison reasons, two more parameters were defined, which are

*Corresponding author: Anita Gryko, e-mail: anita.gryko@sd.pb.edu.pl

Young's modulus percentage decrease (EYM%) and yield strength percentage decrease (0.2% OEYS%) of cell unit or scaffold structures about solid material properties.

3. Results

Based on the conducted research, it can be concluded that some of the analysed structures are suitable for practical applications in orthopaedics. It is achieved if structure mechanical properties allow for appropriate load transfer (similar YM to bone's), while maintaining high strength. Therefore, to properly present the influence of pore geometry on selected mechanical parameters, the authors implement two parameters: Young's modulus percentage decrease (EYM%) and yield strength percentage decrease (0.2% OEYS%). These parameters allowed to estimate the influence of scaffolds geometry on their mechanical properties, giving an appropriate insight into differences between the use of selected pore types and porosities. Fig. 2 presents the influence of three considered variable on the previously described parameters.

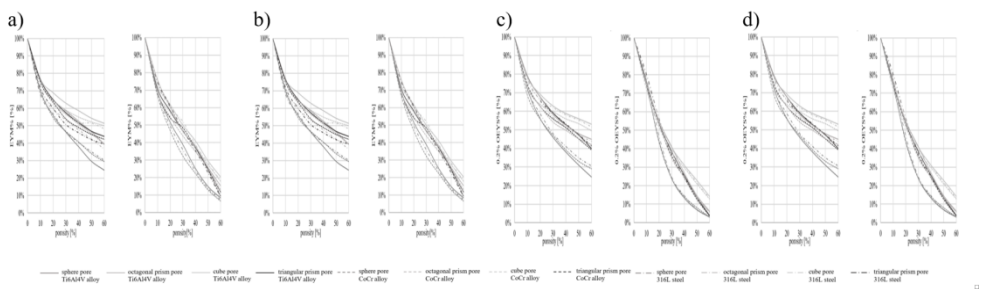


Fig. 2. The influence of porosity, pore geometry and material on the: a) EYM% parameter of cell unit, b) EYM% parameter of scaffold, c) 0.2% OEYS% parameter of cell unit, d) 0.2% OEYS% parameter of scaffold

Research has shown that scaffolds with bone like strength properties should be made of Ti6Al4V alloy. The value of 40% turned out to be of the best porosity. The remaining porosities showed much lower or much higher strength parameters and were significantly different from the properties of the bones.

4. Conclusions

The obtained data allow to indicate the most functional porous structure with Young's modulus similar to that possesses by core bone, while maintaining mechanical strength, allowing for its appropriate use in orthopaedic regenerative medicine.

Acknowledgments: The research was funded by Ministry of Education and Science as a part of projects WI/WM-IB/6/2023.

References

- [1] ZHU L., LUO D., LIU Y. *Effect of the nano/microscale structure of biomaterial scaffolds on bone regeneration.* Int J Oral Sci. 2020, 6,12(1):6, 1-15
- [2] POLO-CORRALES L., LATORRE-ESTEVES M., RAMIREZ-VICK J.E. *Scaffold Design for Bone Regeneration.* J Nanosci Nanotechnol, 2014, 14(1): 15-56
- [3] BANDYOPADHYAY A., ESPANA F., BALLA V.K., BOSE S., OHGAMI Y., DAVIES N.M. *Influence of porosity on mechanical properties and in vivo response of Ti6Al4V implants.* Acta Biomater. 2010, 6(4):1640-1648
- [4] ALMAHRI S., SANTIAGO R., LEE D.W., RAMOS H., ALABDOULI H., ALTENEJJI M., GUAN Z., CANTWELL W., ALVES M. *Evaluation of the dynamic response of triply periodic minimal surfaces subjected to high strain-rate compression.* Addit Manuf, 2021, 46, 1-15.

Influence of a single session of occlusion training on time parameters in isokinetic knee flexion-extension strength measurements

A. HADAMUS^{1*}, B. OSUCH², K. WIADERNA¹, T. JANKOWSKI⁴, A. FERENC¹, D. BIAŁOSZEWSKI¹

¹Department of Rehabilitation, Faculty of Dental Medicine, Medical University of Warsaw, Warsaw, Poland

²Students Scientific Society for Physiotherapy, Department of Rehabilitation, Faculty of Dental Medicine, Medical University of Warsaw, Poland

Key words: *occlusion training, knee muscle strength, time parameters*

1. Introduction

Blood-flow restriction training (BFRT) is used since the early 60-ties to improve muscle strength and stimulate muscle hypertrophy. Many publications showed that systematic training with low-pressure BFRT can improve different strength parameters [1]-[3]. Thus, there is no clear evidence of how occlusion influences muscle performance directly after the training and therefore if it can disturb the rest of the training or everyday activity.

This study is part of a wider project, concerning the influence of different types of occlusion on muscle strength and endurance. The aim of this analysis was to evaluate how a single session with occlusion bands influences time parameters in isokinetic strength measurements in the knee flexors and extensors.

2. Material and Methods

The study group included 17 women and 15 men (mean age 21.5 years, BMI 22.6 kg/m²), while the control group included 24 women and 6 men (mean age 21.8 years, BMI 22.6 kg/m²). Each participant performed an initial warm-up before the first measurement, which was done without BFRT bands. The bands were applied only in the study group and pumped to 175 mmHg. Then the second isokinetic measurement was performed and after that the band were removed, and the exercises continued for the next 5 minutes. Then the third measurement was performed. The control group maintained the same intervals between all three measurements, but without the BFRT bands.

Leg dominance was defined using the revised version of the Waterloo Footedness Questionnaire. Muscle strength in the dominant leg only was measured with the Humac Norm system under isokinetic conditions for knee flexion and extension (concentric/concentric) in an open kinetic chain at the following speeds: 60°/s (5 repetitions), 120°/s (7 repetitions) and 180°/s (10 repetitions). The following time parameters were analysed: Time to Peak Torque (TPT, the time from the beginning of torque development until the point where peak torque is first developed), Force Decay Time (FDT, the time from the end of peak torque production to the end of the motion), Reciprocal Delay (RD, the time required to reverse the limb direction), and Delay Time (DT, the time from the beginning of a motion until the beginning of torque development), separately for flexors and extensors muscle groups.

Statistical analysis was performed using PQStat 2021 software. Shapiro–Wilk test showed that the variables have non-normal distribution. Because of this and small group sizes, a non-parametric test (Friedmann’s ANOVA with post hoc Dunn–Bonferroni test) was used to analyse differences between the three measurements within the groups. The results were considered statistically significant for $p < 0.05$.

*Corresponding author: Anna Hadamus, e-mail: anna.hadamus@wum.edu.pl

3. Results

In the study group, significant differences were visible only between measurements 2 (with the band) and 3 (after removing the band). Delay time shortened significantly for the extensors group in the 60°/s trial ($p=0.0099$). In the high-speed trials (180°/s) FDT shortened significantly for the extensors ($p=0.0014$), while RD shortened both for extensors ($p=0.0035$) and the flexors ($p=0.0216$). Some minor changes were also visible in 120°/s trials in DT for flexors and extensors, RD for extensors and as well as in 180°/s trial in TPT for extensors ($p<0.05$ in ANOVA), but the post hoc test showed no clear results.

In the control group, some changes were visible in RD for extensors in 120°/s and 180°/s trials ($p<0.05$ in ANOVA), although the post hoc test showed no clear results.

4. Discussion and Conclusions

We found no studies concerning the influence of occlusion in any form on time parameters in isokinetic strength measurements. Better results (shorter time) obtained in the third measurement, especially in high-speed trials suggest that the application of the BFRT band is beneficial to muscle activation directly after the training. On the other hand, the improvement was not significant, when compared to the first measurement (before the application of the band). Therefore we concluded, that including BFRT in a training session can reduce the risk of muscle injury or, what is probably most important, it does not increase this risk. This study needs to be continued to analyse also strength and endurance parameters, as well as to compare the results with other groups.

References

- [1] NOYES F.R., BARBER-WESTIN S.D., SIPES L. *Blood Flow Restriction Training Can Improve Peak Torque Strength in Chronic Atrophic Postoperative Quadriceps and Hamstrings Muscles*. *Arthroscopy*, 2021,37(9):2860-2869
- [2] KE J., ZHOU X., YANG Y., SHEN H., LUO X., LIU H., GAO L., H.E., ZHANG X. *Blood flow restriction training promotes functional recovery of knee joint in patients after arthroscopic partial meniscectomy: A randomized clinical trial*. *Front Physiol*. 2022, 13:1015853
- [3] COUNTS B.R., DANKEL S.J., BARNETT B.E., KIM D., MOUSER J.G., ALLEN K.M., THIEBAUD R.S., ABE T., BEMBEN M.G., LOENNEKE J.P. *Influence of relative blood flow restriction pressure on muscle activation and muscle adaptation*. *Muscle Nerve*. 2016, 53(3):438-445

Simulation Research on Kinematic and Dynamic Requirements of Prosthetic Hand During Grasping

A. HANDKE, S. WUDARCZYK*

Department of Fundamentals of Machine Design and Mechatronics Systems, Faculty of Mechanical Engineering
Wrocław University of Science and Technology, Wrocław, Poland

Key words: control system, numerical model, contact force, force sensor, mechanism

1. Aim of the work

Before designing a prosthetic hand, it is necessary to obtain information on the kinematic and dynamic requirements for the prosthesis [1]. The main task carried out in this work was to develop a numerical model of the prosthetic hand in the computer system for dynamic analysis of multibody systems (ADAMS) and conduct simulation studies of the process of grasping selected objects. The simulation studies were aimed at: determining the sequence and range of angular displacements of the phalanges during the grasping process, evaluating the stability of the grasp, and determining the areas of contact between the phalanges and the object.

2. Building a computer model and simulation research

In the first stage of the design process of the anthropomorphic hand prosthesis, the kinematic scheme of the prosthesis (number of fingers, phalanges) was defined and the overall dimensions of the individual phalanges and metacarpals of the prosthesis were determined. In order to determine these dimensions when grasping an object, a dedicated numerical model was built in ADAMS. It was assumed that the movement of each phalanx could be realized independently. The solid model of the prosthetic hand is based on the developed kinematic scheme (Fig. 1), which reflects the basic movements of the fingers according to the anatomy of the human hand. The model assumes the following movements: bending at three joints for 4 fingers (index, middle, ring and pinky), bending at two joints of the thumb, adduction/reversal for each finger, opposing thumb, opposing little and ring finger (movement of metacarpal elements). On each phalanx, additional lumps of small thickness distributed along the phalangeal axis were introduced (Fig. 1). This approach allows easy identification of the contact point between the object and the phalanx.

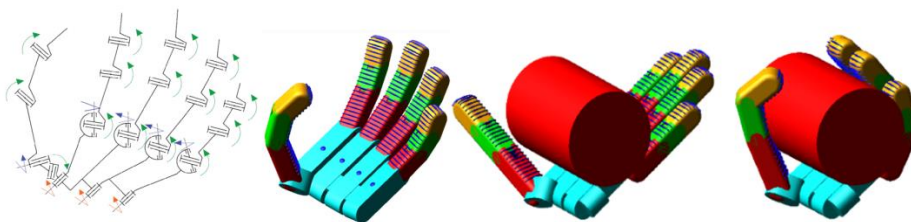


Fig 1 . Kinematic diagram and computer model view of the hand prosthesis

The aim of this procedure was to obtain the information needed to position the pressure sensors in the prosthesis. The contact forces between the object to be grasped and the phalanx, as well as between the phalanges (occurrence of collisions), formed the basis for developing an algorithm to control the

*Corresponding author: Sławomir Wudarczyk, e-mail: slawomir.wudarczyk@pwr.edu.pl

phalanges' drives during the grasping process. When modelling the contact forces, friction was taken into account and material parameters were assumed as for rubber-to-rubber contact.

Three types of solids (sphere, cylinder, cuboid), each in three sizes, were used for simulation studies of the grip stability of the objects of the developed hand prosthesis model [2]. The motion in the phalanx was forced directly in the kinematic pair and was subject to constraints due to the appearance of contact forces between the phalanges and the object to be grasped [3]. In the construction of the control system, sequential actuation of successive joints was assumed, according to a hierarchy: proximal joint (for the thumb, this is the opposing joint) - middle joint - distal joint. For each phalanx during the simulation, conditions were verified for stopping the movement of this phalanx when a given value of the phalanx force on the object appeared. The velocity of the kinematic excitation is adjusted according to the relation:

$$\omega = \omega_{max} \cdot \left(1 - \frac{\sum_i^2 F_{contact}}{F_{max\,pressing}}\right) \cdot \frac{1 + \operatorname{sgn}\left(1 - \frac{\sum_i^2 F_{contact}}{F_{max\,pressing}}\right)}{2} \quad \omega = \omega_{max} \cdot \left(1 - \frac{\sum_i^2 F_{contact}}{F_{max\,pressing}}\right) \cdot \frac{1 + \operatorname{sgn}\left(1 - \frac{\sum_i^2 F_{contact}}{F_{max\,pressing}}\right)}{2} \quad (1)$$

where: ω – angular velocity, i – Phalange No (1 – proximal, 2 – middle, 3 – distal), $F_{contact}$ – contact force, $F_{max\,pressing}$ – max pressing force

According to equation (1), the occurrence of contact on the distal phalanx implies that the whole finger (all 3 drives) stops working as soon as the minimum contact force of the finger on the object (total of all phalanges) is reached.

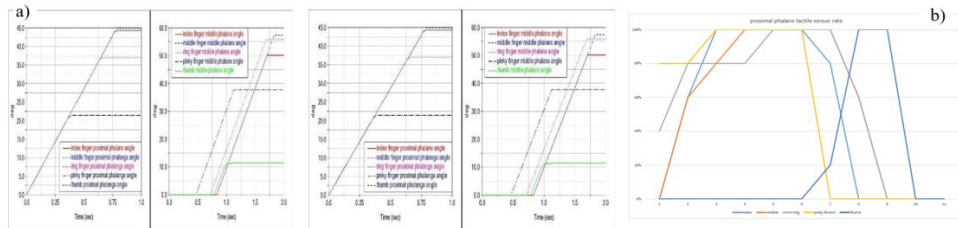


Fig. 2. Example runs for cylinder grasping ($\phi 100\text{mm}$): a) joint angles proximal and middle, b) contact incidence in proximal phalanges as a function of sensor position on the phalanx

The simulation research also included checking the reliability of object gripping. In order to do this, the prosthesis with the gripped object was moved and rotated according to an assumed acceleration run and taking gravity into account.

3. Summary

Analysis of the obtained results of simulated grasping of each object made it possible to determine the required angle ranges for individual joints, the nominal active moments necessary to generate the required finger force on the object, and the frequency and location of contact between the object and phalanges (and metacarpus). By comparing the results of the obtained angular displacements at the joints, kinematic coupling functions were obtained, which are the basis for the design of mechanisms coupling movements at subsequent joints. And thus to reduce the number of necessary actuators. The results obtained formed the basis for the design development of the hand prosthesis.

References

- [1] YAO K., BILLARD A. *Exploiting Kinematic Redundancy for Robotic Grasping of Multiple Objects*. IEEE Trans Robot. 2023, 39(3), 1982-2002
- [2] DENG Z., JONETZKO Y., ZHANG L., ZHANG J. *Grasping force control of multifingered robotic hands through tactile sensing for object stabilization*. Sensors (Basel). 2020, 14,20(4):1050
- [3] GONZALEZ F., GOSSELIN F., BACHTA W. *Analysis of hand contact areas and interaction capabilities during manipulation and exploration*. IEEE Trans Haptics, 2014, 7(4): 415-429

Numerical evaluation of the influence of selected parameters of orthopaedic scaffolds on load transfer within long bone

D. IWAN*, P. PROCHOR

Institute of Biomedical Engineering, Białystok University of Technology, Białystok, Poland

Key words: *scaffold, orthopaedic, long bone, Finite Element Method*

1. Introduction

One of the main purposes of tissue engineering is to create artificial structures, called scaffolds, to replace or to help regenerate damaged tissue or organs [1]. Currently, there are numerous manufacturing methods for scaffolds as well as experimental research, carried out in order to evaluate their mechanical parameters [2]. However, the detailed description of their influence on the load transfer through long bone is still missing. For this reason, the main goal of presented study was to carry out numerical evaluation of the influence of selected constructional and material parameters of orthopaedic scaffolds on the previously described load phenomenon.

2. Materials and Methods

2.1. CAD models and FE models

The model of the femur bone was made on the basis of CT scan. The bone was scanned from a 44-year-old man, whose weight was 85 kg and who was 1,85 m tall. The model of bone was built with the cortical and cancellous bone. The research analysed 3 different positions of the scaffold in the shaft of a long bone (200, 240 and 280 mm from the femoral head), which could have been a result from injury or disease factors. Scaffolds were located in the way that their flat surface was perpendicular to the bone axis.

The made pores were spherical in shape. The scaffold was made by creating holes, connected by cylindrical canals, to make a porosity of 20%, 40% and 60%. In the end, there were 9 scaffolds designed – each of three different porosity and three positions. Additionally each case in a different location. According to the literature, these porosities allow the greatest functionality of the scaffolds (among other things, in terms of the diffusion of mesenchymal cells in the scaffold) [3]. Example of designed scaffold and its positioning in bone are shown on Fig. 1a.

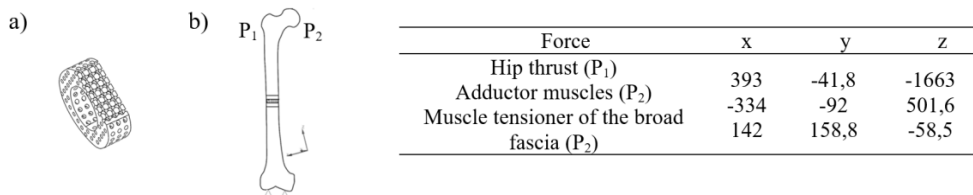


Fig. 1. a) Internal structure of the designed scaffolds (based on a scaffold with a porosity of 40%), b) the boundary conditions applied to the scaffold bone, the reference system and the values of the forces applied to the model [3]

The size and type of finite elements were therefore adjusted in order to obtain the best possible quality of results. Appropriate boundary conditions were established, that is, supports and forces acting on the bone, which correspond to the forces generated at 45% of the gait cycle. It drew on research

*Corresponding author: Dominika Iwan, e-mail: dominika.iwan@sd.pb.edu.pl

carried out by Behrens and colleagues [4]. Supports have been established, as well as the relevant directions on the coordinate system. It is shown on the Fig. 1b.

Cross-sections and paths were also produced to provide an accurate representation of the findings. Preparation of the study also required the use of appropriate material properties. The bone was divided into the cortical bone and cancellous bone. Scaffolds were assigned properties of titanium alloy (Ti6Al4V), PCL-HA (polycaprolactone with hydroxyapatite) and PLA (polylactide), respectively. Material properties such as Young's modulus, density and Poisson's ratio had to be set before the test could be performed. In order to simplify the study, the bone was assumed to have homogeneous and isotropic properties.

3. Results

Obtained values proved that all of analysed variables had an essential influence on analysed phenomenon, as we can see on figure (Fig.2).

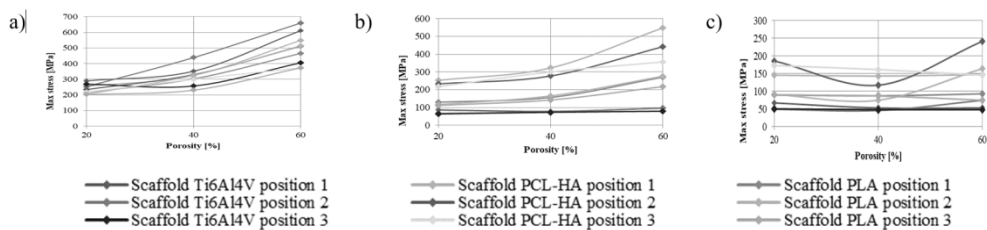


Fig. 2. Summary of Huber-Mises-Hencky maximum reduced stresses [MPa]: a) for scaffold bone models in each position, b) in areas of bone adjacent to the scaffold, c) for the cross-section of bone areas adjacent to the scaffold

4. Conclusions

The results obtained allow the selection of suitable material and design parameters for the manufacture of a scaffold for placement in the long bone. On their basis it can be stated that the most vulnerable position is the distal one, stresses generated within bone increase with the increase of scaffold's porosity as well as Ti6Al4V allows to obtain appropriate stress distribution. Obtained results can be further used to estimate in-vivo functionality of scaffolds designated for the orthopaedic regenerative medicine.

Acknowledgments: The research was funded by Ministry of Education and Science as a part of projects WI/WM-IB/7/2023.

References

- [1] DZIADEK M., PAWLIK J., MENASZEK E., STODOLAK-ZYCH E., CHOLEWA-KOWALSKA K. *Effect of the preparation methods on architecture, crystallinity, hydrolytic degradation, bioactivity, and biocompatibility of PCL/bioglass composite scaffolds.* J Biomed Mater Res B Appl Biomater. 2015, 103(8):1580-93
- [2] CHOCHOLATA P., KULDA V., BABUSKA V. *Fabrication of scaffolds for bone tissue regeneration.* Materials (Basel). 2019, 14,12(4):568
- [3] PROCHOR P., GRYKO A. *Numerical Analysis of the Influence of Porosity and Pore Geometry on Functionality of Scaffolds Designated for Orthopedic Regenerative Medicine.* Materials (Basel). 2020, 29,14(1):109
- [4] BEHRENS B. A., NOLTE I., WEFSTAEDT P., STUKENBORG-COLSMAN C., BOUGUECHA A. *Numerical investigations on the strain-adaptive bone remodelling in the periprosthetic femur: influence of the boundary conditions.* Biomed Eng Online. 2009,16,8:7

Development of a simulator of surgical procedures supported by a vision system

B. JASIŃSKI*, P. KROWICKI

Department of Mechanical Engineering, Wrocław University of Science and Technology, Wrocław, Poland

Keywords: *hand-tracking, vision system, surgical procedure simulator*

1. Introduction

To improve surgical training, computer simulations using virtual reality techniques are being used to offer an effective alternative to training and introducing surgical techniques [1]. The use of vision systems based on an algorithm that tracks the movement of the user's hand makes it possible to achieve high accuracy in the simulations performed. In addition, practicing on a simulator, it is possible to avoid critical situations that most often occur during the first operations of young surgeons.

2. Hand-tracking algorithm

The tracking algorithm uses a machine learning model in the Mediapipe library, which was developed to detect the hand and its specific points in images. The camera image is analyzed to locate the hand. Hand detection is followed by the estimation of 21 hand feature points, which correspond to the fingertips, interphalangeal joint, and wrist [2]. Then, using OpenCV, a library for image processing, a kinematic model of the hand is visualized, consisting of connected lines and circles. In addition, OpenCV was also used to calibrate the camera. An algorithm was created to detect the corners of the checkerboard, which made it possible to determine the geometric parameters of the camera, mainly the focal length. The data collected in the appropriate format was then sent to the Unity graphics engine, where visualization of the hand took place. Fig. 1 shows the hand detected by the real-time tracking algorithm along with the hand model generated in Unity and the checkerboard used for camera calibration. The result of the calibration process was a matrix with the included geometric parameters used, which could be used for the geometric correction of the camera.

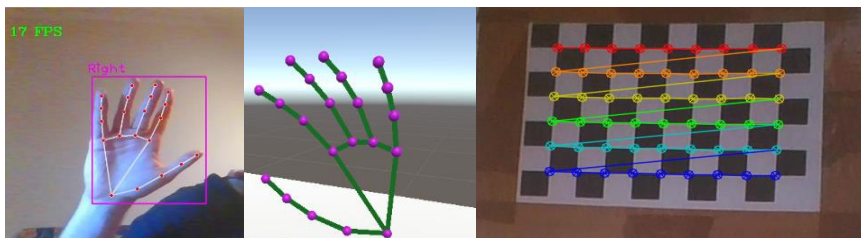


Fig. 1. The result of the tracking algorithm and the checkerboard detected by the camera calibration algorithm

3. Methods

The research was divided into two parts. The first part involved examining the impact of lighting intensity on the performance of the vision system. The effectiveness of the hand-tracking system was evaluated for different lighting intensity values. The study was conducted in a room equipped with a potentiometer for controlling the light intensity. The TES 1336A Light Meter (Fig. 3) was used for measurements. Initially, the maximum and minimum lighting intensities in the room were measured.

*Corresponding author: Bartosz Jasiński, e-mail: 249614@student.pwr.edu.pl

The first measurements were taken for the maximum value of 740 lx, then values were reduced by 50 lx increments until reaching the minimum value.

In the second stage, sample incisions (Fig. 3) were performed in the surgical simulator in Unity [3]. Control was done using the hand model depicted in Fig. 2.



Fig. 2. Tool for measuring light intensity and soft tissue cutting simulator

4. Results

The study results demonstrated that the system operates efficiently within the 740 lx to 150 lx range. Cutting experiments (Fig. 3) showcased the accuracy of the developed tracking algorithm. The black line represents the ideal cut, while the red line represents the result of the vision system control.

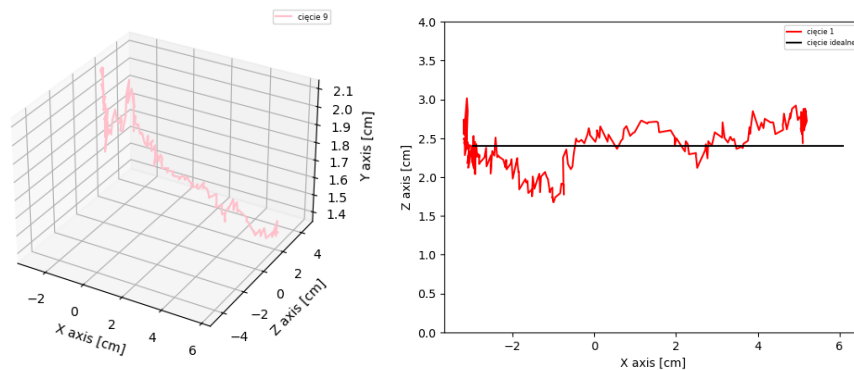


Fig. 3. Graphs visualizing the cutting path

5. Conclusions

The visible errors on the graphs are due to the algorithm's inaccurate calculation of the distance between the hand and the camera. This aspect requires improvement to ensure that the cutting characteristics performed by the vision system are as close as possible to the reference cuts that reflect the perfectly executed surgical maneuver.

References

- [1] ZIEGLER R., FISCHER G., MÜLLER W., GÖBEL M. *Virtual reality arthroscopy training simulator*. *Comput Biol Med.* 1995, 25(2):193-203
- [2] WANG X, GARG S, TRAN SN, BAI Q, ALTY J. *Hand tremor detection in videos with cluttered background using neural network based approaches*. *Health Inf Sci Syst.* 2021, 12:9(1):30
- [3] *Soft tissue simulator*, <https://aune-connie.itch.io/soft-tissue-simulator>, accessed: June 10, 2023

Mathematical modelling of coupled thermal and chemical effects in biological tissue during laser irradiation

M. JASIŃSKI*, M. ZADOŃ

Silesian University of Technology, Gliwice, Poland

Key words: bioheat transfer, optical diffusion equation, photodynamic therapy

1. Introduction

One of the primary cancer therapies is photodynamic therapy (PDT). During treatment, the photosensitiser microparticles (S_0) in the biological tissue react with the basic form of oxygen, the triplet form (3O_2), causing its transition to the singlet form (1O_2). It is the latter form that is cytotoxic to cancer cells. The trigger for triplet oxygen and photosensitiser reactions is light, such as a laser beam, whose interaction with biological tissue can also lead to a local increase in tissue temperature. Although increases in tissue temperature during PDT treatment are generally not large, they can affect the thermophysical parameters of the tissue, such as the perfusion coefficient, and this in turn can affect oxygen delivery to the treatment area [1].

The purpose of the work is the numerical analysis of phenomena that occur in tissue during PDT. The task includes steps related to the modelling of laser energy deposition, photochemical reactions in tissue, and temperature distribution. The proposed model uses the optical diffusion equation, the Pennes bioheat transfer equation, and reactions equations for PDT. The connection between bioheat transfer and PDT models was taken into account using the respective relationships between perfusion rate, capillary blood velocity, and maximum oxygen supply rate. Furthermore, a method was proposed to model abnormal vascular patterns in the tumour subdomain.

2. Governing equations

The reactions occurring during PDT are described by a set of coupled differential equations related to the concentration of triplet oxygen, singlet oxygen and photosensitiser [2],[3]:

$$\mathbf{x} \in \Omega : \begin{cases} \frac{dc_{3O_2}}{dt} + \gamma c_{S_0} = \psi_{sup}, & \gamma = \frac{\xi \phi c_{3O_2}}{c_{3O_2} + \beta} \\ \frac{dc_{S_0}}{dt} + \gamma \sigma c_{S_0} (c_{S_0} + \delta) = 0, & \psi_{sup} = \psi_{sup,max} \left(1 - \frac{c_{3O_2}}{c_{3O_2,init}} \right) \\ \frac{dc_{1O_2}}{dt} - \gamma c_{S_0} = 0 \end{cases}$$

$$t = 0 : \quad c_{3O_2} = c_{3O_2,init}, \quad c_{S_0} = c_{S_0,init}, \quad c_{1O_2} = 0 \quad (1)$$

where c_{3O_2} , c_{S_0} , c_{1O_2} [mol cm⁻³] are the concentrations of triplet-state oxygen, photosensitiser, and singlet-state oxygen, respectively, parameters β [mol cm⁻³], σ [cm³ mol⁻¹], ξ [cm² mW⁻¹ s⁻¹] and δ [mol cm⁻³] are the PDT photochemical parameters defined as oxygen quenching threshold concentration, specific photobleaching ratio, specific oxygen consumption rate, and the low concentration correction term, respectively, ψ_{sup} [mol cm⁻³ s⁻¹] is the oxygen supply rate and $\psi_{sup,max}$ [mol cm⁻³ s⁻¹] is the maximum oxygen supply rate while ϕ [W m⁻²] is total fluence rate which is the

*Corresponding author: Marek Jasiński, e-mail: marek.jasinski@polsl.pl

sum of collimated and diffused parts. The collimated part is described by using the Beer-Lambert law of absorption, while the estimation of the diffused part is based on the optical diffusion equation. The value of the maximum oxygen supply rate $\psi_{sup,max}$, is estimated on the basis of [2]:

$$\psi_{sup,max} = \frac{1200u_b R_c \left(R_c + \frac{a^2 + M_0^2}{2500 - M_0^2} \right)}{L_t (R_t + b)^2}, \quad \begin{array}{l} P_b = 100 \text{ mmHg: } a = 100, \quad b = 4.2 \\ P_b = 50 \text{ mmHg: } a = 50, \quad b = -4.2 \end{array} \quad (2)$$

where R_c [μm] is the capillary radius, R_t [μm] is the tissue cylinder around capillary radius [μm], L_t [μm] is the capillary length [μm], while Q_b [$\text{cm}^3 \text{s}^{-1}$] and u_b [cm s^{-1}] denote the blood flow rate in the capillary and the blood velocity in the capillary, respectively, M_0 [$\text{mol cm}^{-3} \text{s}^{-1}$] is the oxygen consumption rate and P_b [mmHg] is the partial pressure of $^3\text{O}_2$ in the blood vessel. The value $P_b = 100$ [mmHg] is typical for healthy tissue, while cancer tissue is often hypoxic, so the coefficient values for $P_b = 50$ [mmHg] refer only to this type of tissue.

The connection between bioheat transfer and PDT models uses, among other things, a variable perfusion coefficient w [s^{-1}]. This means that the velocity of blood in the capillaries, responsible for the delivery of oxygen to the tissues, must also be variable. Such a relationship may be written as follows [4]:

$$w = \frac{\pi R_c^2 u_b}{\pi R_t^2 L_t} \rightarrow u_b = w L_t \frac{R_t^2}{R_c^2} \quad (3)$$

It should be added that the paper assumes the perfusion coefficient w to be dependent on the degree of thermal tissue damage, i.e. indirectly on temperature (calculated based on the bioheat transfer equation). This means that during PDT treatment, blood velocity u_b and maximum oxygen supply rate $\psi_{sup,max}$, are varied.

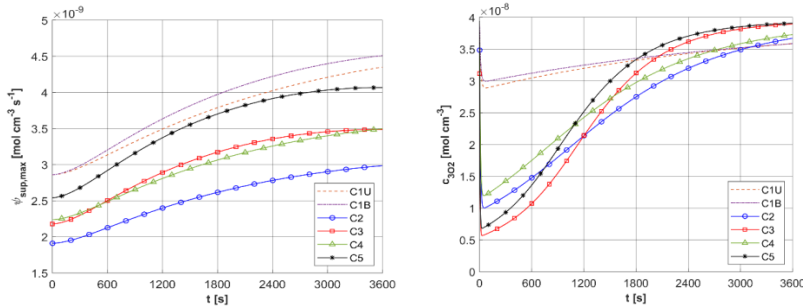


Fig. 1. Histories of oxygen maximum supply rate and $^3\text{O}_2$ concentration at selected points of the domain

Acknowledgments: The research is funded from the projects Silesian University of Technology, Faculty of Mechanical Engineering.

References

- [1] ABDEL-KADER M.H. *Photodynamic therapy: from theory to application*. Springer-Verlag, Berlin, Heidelberg, 2016
- [2] ZHU T.C., LIU B., PENJWEINI R. *Study of tissue oxygen supply rate in a macroscopic photodynamic therapy singlet oxygen model*. J Biomed Opt, 2015, 20(3):038001
- [3] JASIŃSKI M., ZADON M. *Mathematical modeling of the phenomena that occur in a biological tissue containing a photosensitizer*. Phys Med Biol. 1997, 42(9):1701-16
- [4] MCGUIRE B.J., SECOMB T.W. *A theoretical model for oxygen transport in skeletal muscle under conditions of high oxygen demand*. J Appl Physiol, (1985). 2001, 91(5):2255-65

Analysis of the influence of the bone fracture stabilization system on the biomechanics of the bone healing process

K. JASIURKOWSKA*, J. FILIPIAK

Department of Mechanics, Materials and Biomedical Engineering, Faculty of Mechanical Engineering,
Wrocław University of Science and Technology, Wrocław, Poland

Key words: bone, dog, FEM, implant

1. Introduction

Fractures of long bones are caused by exceeding the strength of the bone material. They result in tissue damage, disruption of blood flow, and haemorrhaging, among other things. Restoration of the proper structure of the bone occurs through self-repair, but the quality of the bone healing depends on the conditions in the fracture gap [1]. The research covers issues related to the influence of the bone fragment stabilization system on the biomechanical conditions occurring in the fracture gap.

2. Material and Method

In order to analyze the state of deformation in the bone callus, geometric models of the bone fragment-callus system were developed, as shown in the figure (Fig. 1. A). The model was fixed at the base of the lower fragment and loaded in two ways. The first caused axial displacement of the model, while the second caused rotation of the fragments.

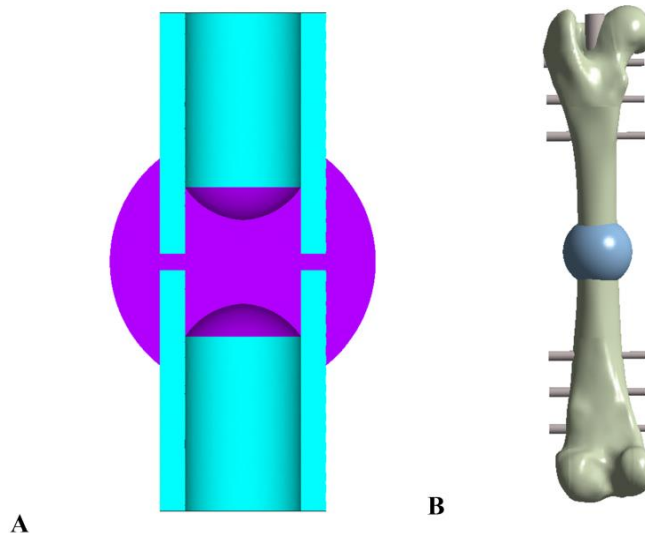


Fig. 1. Geometric model of the bone fragment-callus system (A) and geometric model of the bone-implant system (B)

A geometric model of the bone-implant system was then developed using CT scan data of the canine femur. A solid was created in the fracture gap to represent the callus. Bone fragments were stabilized with an intramedullary nail locked with bolts (Fig. 1. B). The design of the implant is based on

*Corresponding author: Karolina Jasiurkowska, e-mail: karolina.jasiurkowska@pwr.edu.pl

a prototype created in cooperation with Micromed [2]. Six geometrical models of bone-implant systems with different configuration and type of locking bolts (monocortical and bicortical) were analyzed.

3. Results

The geometric model of the bone fragment-callus system allowed a detailed analysis of the influence of the fracture gap size and loading conditions on the callus. Comparing the two loading variants, it was found that higher values of the analyzed parameters, such as strain, occurred with the rotation of the bone fragments.

Analysis of the values of selected mechanical parameters occurring in the callus allowed the assessment of the influence of the configuration and arrangement of locking bolts on the processes of callus formation. In the models in which bicortical bolts were used, the smallest displacement values were observed in the configuration with 6 bolts, while the largest values were observed in the model with 2 bolts. Comparing the models with monocortical and bicortical bolts, it was observed that the maximum displacement values occurring in the callus were lower in the models with monocortical bolts.

4. Conclusion

Numerical modelling of the changes occurring in the bone callus under the influence of variable boundary conditions (different distance between bone fragments, loading variants of the model) allowed us to determine the values of mechanical parameters relevant to the formation of callus.

Analysis of the bone model stabilized with an implant allowed us to conclude that the implants with monocortical bolts stabilize bone fragments in a similar way as implants with bicortical bolts. An additional advantage is that they increase the variety of implant options and allow different strain values to be achieved. In the future, numerical simulations may be a tool that will assist in the process of planning fracture treatment in veterinary patients.

Acknowledgments: The presented research, realized as a part of the research task "Numerical analysis of the process of canine femoral bone healing", was funded by the pro-quality subsidy for the development of research potential of Faculty of Mechanical Engineering of the Wrocław University of Science and Technology in 2022.

References

- [1] CLAES L. E., HEIGELE C. A. *Magnitudes of local stress and strain along bony surfaces predict the course and type of fracture healing.* J Biomech. 1999, 32(3):255-66
- [2] JASIURKOWSKA K., BIEŻYŃSKI J., NIKODEM A., FILIPIAK J. *Influence of the intramedullary nail locking method on the stiffness of the bone-implant system.* Acta Bioeng. Biomech, 2022, 24(1): 167-178

Developing a Literature-informed Intervention Protocol to Address post-COVID-19 Balance Disorders, Weakness and Muscle Fatigue in Individuals Aged 65+

K. KACZMARCZYK^{1*}, P. BOBOWIK¹, I. WISZOMIRSKA¹, J. GAJEWSKI¹, M. BŁAŻKIEWICZ¹,
M. CZUBA¹, A. MACIEJEWSKA- SKRENDO², Y. MATHARU³, K. KULIG³

¹Józef Piłsudski University of Physical Education in Warsaw, Warsaw, Poland

²Gdansk University of Physical Education and Sport, Gdańsk, Poland

³University of Southern California, USA

Key words: *post-COVID syndrome, fall risk, elderly, seniors, stabilography*

1. Introduction

The WHO declared COVID-19 a global pandemic [1], and the long-term consequences and aftermath of the disease remain unclear. Although the SARS-CoV-2 virus infects the respiratory system symptoms were also reported in the musculoskeletal system [2]-[3]. Recovering post COVID-19 elderly patients report prolonged general weakness and muscle fatigue. Falls, for instance, are a well-known consequence of reduced muscle strength [4]. There is also a need for greater clarity and tailoring of exercise related advice for people with post COVID-19 condition and improved support to resume activities important to individual well-being. To the best of our knowledge there are no studies describing exercise programs for seniors with post COVID-19 condition.

2. Objective of the study

The objective of this study is twofold, to characterize muscle strength, postural stability, body composition in older adults with history of COVID-19, and to develop and describe a subject-specific intervention protocol. Additional objectives of the Project are diagnosis of the health state of post-COVID-19 elderly patients, especially muscle strength, postural stability, body composition and analysis of quality of life of elderly with post-COVID-19 condition.

3. Material and Methods

The project will involve 50 Seniors, both sexes, age 65+ yrs old, positive RT-PCR test and/or positive result in test for antibodies against the SARS-CoV-2 coronavirus 3-12 months prior to the study start, from the 0-1-2 group based on the questionnaire to assess daily functioning after COVID-19 [5]. People with active cardiac disease, oxygen desaturation below 95%, dysfunction of the autonomic nervous system (orthostatic intolerance) will be excluded from the tests. Participants will be randomized to one of 2 groups: RT and control (no exercise). Training in study group aimed at improving balance and strengthening muscle strength (RT) will be held twice a week, 45 min per session in sub-maximal intensity for 8 weeks according to the recommendations of World Physiotherapy (World Physiotherapy, 2021 and NICE, 2020). Before starting the rehabilitation program, participants will be qualified by GP, exacerbation of post-exercise symptoms will be assessed based on a questionnaire [6] and an orthostatic test [7]). Muscle strength will be measured under dynamic (for the knee muscles) and static conditions (for the elbow, knee, hip and ankle muscles). Isokinetic knee strength will be examined using the Biodex System 3 PRO dynamometer (Biodex Medical Systems, NY,USA). Maximum muscle torques will be measured for the knee flexors (KF),

*Corresponding author: Katarzyna Kaczmarczyk, e-mail: katarzyna.kaczmarczyk@awf.edu.pl

knee extensors (KE), trunk flexors (TF), trunk extensors (TE), and elbow flexors (EF) under isometric conditions using a JBA Staniak® isometric torquemeter, by the Maximum Voluntary Contraction method. Balance will be assessed using a Biodex Balance System SD (BBS) platform. Postural Stability Test (PST) is performed on a stationary platform with eyes open (EO) and closed (EC) to determine: an OSI (overall stability index), APSI (anterior-posterior stability index) and MLSI (medial-lateral stability index). The Fall Risk Test is also carried out with EO on an unstable platform at levels ranging from 12 to 8, and 6 to 2. On this basis, the fall risk index (FRI) will be determined. Moreover, body composition assessment by DEXA and Quality of life tests (WHOQOL-Bref) will be conducted. All statistical calculations will be conducted using the Statistica 14.0.0.15 program (TIBCO Software Inc., Palo Alto, CA, USA, 2020). Normality of the distributions of the quantitative variables under study will be tested using the Shapiro-Wilk test. The mixed design ANOVA will be used to compare means. The interaction of fixed and repeated factors will be analyzed. Tukey's post-hoc test will be used for detailed comparisons.

4. Discussion

The purpose of the study is to develop a protocol of intervention that match the needs of the elderly affected by COVID-19 in order to maintain/improve the health, balance, muscle strength, cognitive function and, consequently, quality of life. Our results indicated that resistance exercise can contribute to better health by preventing musculoskeletal disorders, helping to maintain desirable body composition and improving self-efficacy. Improvements are seen in physical fitness and quality of life. In addition, the aging musculoskeletal system retains its responsiveness to resistance training, and most importantly, the correction of disuse is accompanied by a significant improvement in the level of functional mobility and the overall ability to conduct activities safely. To our knowledge, this is the first report to examine the effects of resistance exercise on improving quality of life and eliminating the adverse symptoms of post COVID-19 condition in seniors. Our main research outcome – a safe exercise protocol and intervention will address social and health needs for a particular social group: the elderly. Research outcomes will build the evidence-based practice for health professionals.

Acknowledgments: This research has been supported by the Polish National Agency for Academic Exchange under the NAWA Urgency Grants program (BPN/GIN/2022/1/00056/U/00001) and ZDROFIT.

References

- [1] LANDI F., BARILLARO C., BELLINI A., BRANDI V., CARFÌ A., ET AL., *The new challenge of geriatrics: saving frail older people from the Sars-Cov-2 pandemic infection.* J Nutr Health Aging. 2020, 24: 466–470
- [2] HASAN L., DEADWILER B., HARATIAN A., BOLIA I., WEBER A., PETRIGLIANO F. *Effects of Covid-19 on the musculoskeletal system: clinician's guide.* Orthop Res Rev. 2021, 13: 141–150
- [3] DISSER N., DE MICHELI A., SCHONK M., KONNARIS M., PIACENTINI A., EDON D., TORESDAHL B.G., ET AL., *musculoskeletal consequences of Covid-19.* J Bone Joint Surg Am. 2020, 102: 1197-204
- [4] BOBOWIK P., WISZOMIRSKA I., LEŚ A., KACZMARCZYK K. *Selected tools for assessing the risk of falls in older women.* Biomed Res Internat. 2020, 2020:2065201
- [5] KLOK F.A., BOON G.J.A.M., BARCO S., ENDRES M., GEELHOED J.J.M., ET AL., *The post-COVID-19 functional Status scale: a tool to measure functional status over time after COVID-19.* Eur Respir J. 2020, 56(1): 2001494
- [6] COTLER J., HOLTZMAN C., DUDUN C., JASON L.A. *A brief questionnaire to assess post-exertional Malaise.* Diagnostics (Basel). 2018, 11,8(3): 66
- [7] FREEMAN R., WIELING W., ET AL., *Consensus statement on the definition of orthostatic hypotension, neurally mediated syncope and the postural tachycardia syndrome.* Clin Auton Res. 2011, 21: 69–72

Optimisation of thickness of surgical implant used in abdominal hernia repair

S. KALINOWSKI^{1*}, K. SZEPIETOWSKA¹, E. FLORENTIN², I. LUBOWIECKA¹

¹Department of Structural Mechanics, Gdańsk University of Technology, Gdańsk, Poland

²INSA Centre-Val de Loire. Mechanical Laboratory Gabriel Lamé, France

Key words: *Topology optimization, Biomechanics, Implant, FEM, Surgical mesh*

1. Introduction

The study refers to topology optimization of surgical implant used in the treatment of abdominal hernia. Hernia is a frequently occurring medical problem that has high recurrence rate reported as 12-54% [1]. It is believed that mechanical compatibility between implant and the substituted tissue can help to avoid the recurrences [2]. This research aims to create an optimised surgical mesh compatible with human abdominal wall by changing thickness of different zones of the implant. Since the recurrence often appears on the tissue and implant interface, we assume that the uniform distribution of forces in the connections between native tissue and the implant may help to avoid a pick of those forces and thus the connection failure. Combination of commercial finite element software (Marc Hexagon) with in-house code in Python for optimization and control is applied in the analysis.

2. Materials and Methods

The implant was modelled as a decagonal membrane by means of finite element method (FEM) with the use of commercial software. A symmetry was applied to speed up calculations. The model consists of 784 4-node membrane finite elements with 3 degrees of freedom in each node. The loading conditions referred to physiological movements of human torso analysed in [3] and used in implant model in the form of its supports displacements according to [4]. The displacements were applied to support nodes (P1 to P5) as shown in (Fig. 1a). The material model is assumed as linear elastic and isotropic with Poisson's ratio 0.3 and Young's Modulus of 16.155 MPa [4]. The diameter of the membrane model is 13 cm.

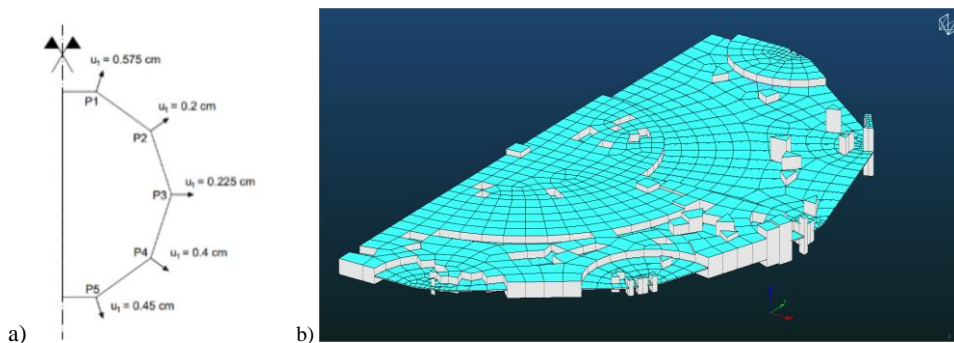


Fig. 1 Implant model: a) scheme with applied forced displacements u_1 - u_5 of the supports P1-P5, b) model after optimisation (thickness scaled up 10 times)

*Corresponding author: Szymon Kalinowski, e-mail: szykalin@student.pg.edu.pl

The thickness was optimised to the load conditions applied to the implant model. The objective function was defined by the formula (1),

$$F = \sum_{1 \leq i < j \leq n} |R_i - R_j|^2 \quad (1)$$

where R represent the resultant reaction forces magnitude and n refers to the number of the model supports. The optimisation is implemented in Python programming language while the FEM results are obtained from the commercial code in every optimisation run. The model thickness changes in each element, starting from initial thickness of 0.6 mm and varying between 0.3 and 0.9 mm. Resultant reaction force in each support node (P1 to P5) (Fig. 1a) are then passed to objective function (1). Sequential Least Squares are used to minimize the objective function (1) from SciPy libraries [5].

3. Results

Results of the optimisation can be seen on scaled up model in Fig. 1b. Table 1 shows initial and final (after optimisation) reaction forces and weighted average (based on the element size) thickness of the elements around supports. The difference between reaction forces in the optimised model have been reduced comparing with the initial one. Average thickness of model changed from 0.6mm to 0.47 mm. This was achieved in 11 iterations, 5498 function evaluations and 7 gradient evaluations.

Table 1. Reaction forces in supports P1 to P5 before and after optimization

| | Support 1 | Support 2 | Support 3 | Support 4 | Support 5 |
|---|-----------|-----------|-----------|-----------|-----------|
| Reaction force in initial model | 19.17 N | 4.92 N | 12.31 N | 14.61 N | 17.43 N |
| Reaction force in model after optimisation | 14.02 N | 4.38 N | 9.29 N | 11.38 N | 12.27 N |
| Optimised average thickness around supports | 0.60 mm | 0.44 mm | 0.64 mm | 0.36 mm | 0.30 mm |

4. Conclusions

Optimised reaction forces are reflecting the displacements forced in each support. The elements of higher thickness are concentrated mostly in regions around P1 and P3. Near the supports of smallest displacement some high thickness jumps are observed. This study shows preliminary research towards implants mechanically compatible with human abdominal wall.

Acknowledgments: This work was supported by the National Science Centre (Poland) [grant No. UMO-2017/27/B/ST8/02518].

References

- [1] VAN RAMSHORST G.H., EKER H.H., HOP W.C.J., JEEKEL J., LANGE J.F. *Impact of incisional hernia on health-related quality of life and body image: a prospective cohort study.* Am J Surg, 2012, 204:144e150.
- [2] LUBOWIECKA I., TOMASZEWSKA A., SZEPIETOWSKA K., SZYMCAK C., ŚMIETAŃSKI M. *In vivo performance of intraperitoneal onlay mesh after ventral hernia repair.* Clin Biomech (Bristol, Avon). 2020, 78:105076
- [3] SZYMCAK C., LUBOWIECKA I., TOMASZEWSKA A., ŚMIETAŃSKI M. *Investigation of abdomen surface deformation due to life excitation: Implications for implant selection and orientation in laparoscopic ventral hernia repair.* Clin Biomech (Bristol, Avon). 2012, 27(2):105-10
- [4] SZEPIETOWSKA K., MAGNAIN B., LUBOWIECKA I., FLORENTIN E. *Sensitivity analysis based on non-intrusive regression-based polynomial chaos expansion for surgical mesh modelling.* Struct Multidisc Optim, 2018, 57, 1391–1409
- [5] VIRTANEN P., GOMMERS R., OLIPHANT T. E., HABERLAND M., REDDY T., COURNAPEAU D., BUROVSKI E., PETERSON P., WECKESSER W., BRIGHT J., VAN DER WALT S.J., BRETT M., WILSON J., MILLMAN K.J., MAYOROV N., NELSON A. R. J., JONES E., KERN R., ET AL., *SciPy 1.0: fundamental algorithms for scientific computing in Python.* Nature Methods, 2020, 17(3), 261–272

Quantitative evaluation of the surgical treatment of cleft palate in infants

E. KAWLEWSKA^{1*}, P. CZARNECKI¹, A. MOL², T. KOSZUTSKI², M. GZIK¹, W. WOLAŃSKI¹

¹Department of Biomechanics, Faculty of Biomedical Engineering, Silesian University of Technology, Gliwice, Poland

²Department of Paediatric Surgery and Urology, Uppersilesian Child Health Center, Katowice, Poland

Keywords: *morphometry, 3D scanning, statistical analysis, unilateral and bilateral cleft palate*

1. Introduction

Cleft palate, a congenital condition characterized by a split or opening in the roof of the mouth, poses significant challenges for affected infants and their families [1]. Surgical interventions play a crucial role in addressing this condition, aiming to restore normal oral function, improve speech development, and enhance the overall quality of life for these young patients.

In recent years, advancements in medical imaging technologies have paved the way for more accurate and comprehensive assessments of surgical interventions. By capturing detailed three-dimensional representations of the anatomical structures involved, these techniques offer unprecedented insights into the effectiveness of surgical treatment and help guide further refinements in surgical approaches [2].

2. Materials and Methods

In this research it was performed the analysis of measurements of unilateral and bilateral cleft lips and palates in infants up to 6 months of age. The main aim was to evaluate the presurgical process of treatment with the use of personalized plates. In the study, a statistical analysis of geometrical measurements of cleft palates was carried out in 72 patients - 19 with bilateral clefts and 63 with unilateral clefts. For each patient, 3 dental impressions were made at several key moments of pre-surgical treatment: on the day of the first diagnosis, on the day of lip surgery and on the day of palate surgery. Between these moments, the children were treated with a size-matched plate, which is intended to reduce the size of the cleft fissure. All dental impressions were subsequently scanned with the use of laser scanner KScan Magic (*Scantech, China*), to obtain 3-dimensional virtual models. On the models there were marked 12 or 13 characteristic points (depend on the cleft type) [3], based on which it was possible to calculate some specific dimensions of cleft gap. All data were then analysed, to find some main determinants of cleft palate geometry.

3. Exemplary Results

To evaluate the changes in cleft gap geometry it was compared the values of specific dimensions and checked the percentage differences between them. Individual lengths were analysed, but due to individual factors, mainly percentage and dimensionless indicators were considered. Exemplary results are shown in the Fig. 1 and Fig. 2.

*Corresponding author: Edyta Kawlewska, e-mail: edyta.kawlewska@polsl.pl

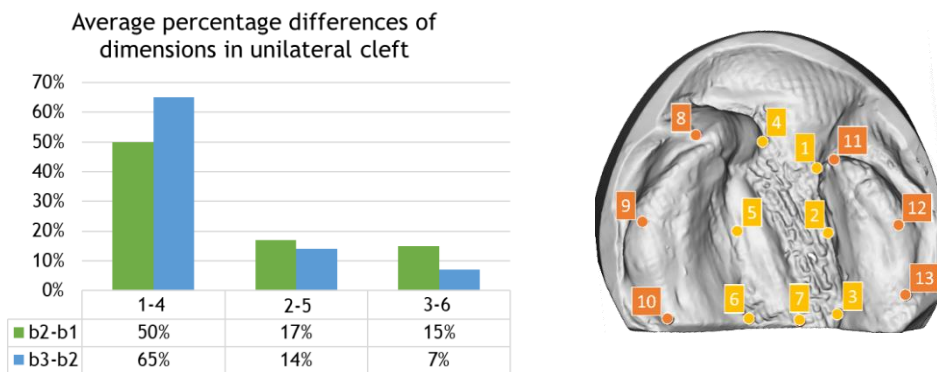


Fig. 1. Marked points in unilateral cleft palate and percentage difference of the dimensions in each stage of treatment

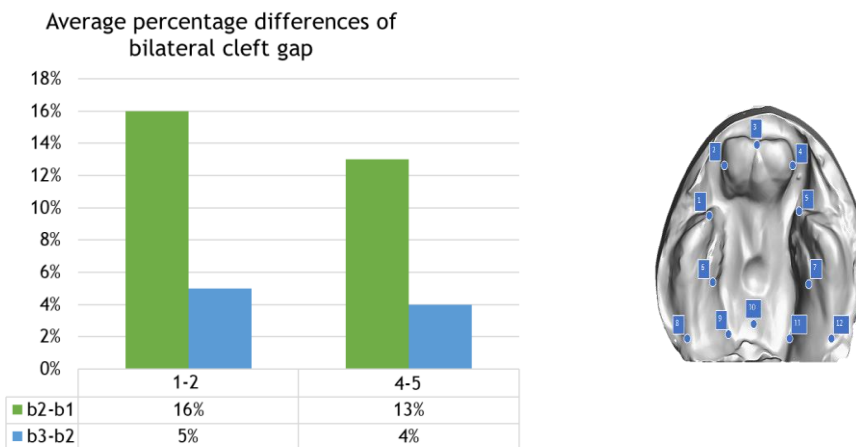


Fig. 2. Marked points in bilateral cleft palate and percentage difference of the dimensions in each stage of treatment

4. Conclusion

Based on obtained results it was stated that presurgical preparation significantly improves the surgical procedure and allows to reduce the complications during the surgery and the rehabilitation process.

References

- [1] BEJDOVÁ Š., KRAJÍČEK V., PETERKA M., TREFNÝ P., VELEMÍNSKÁ J. *Variability in palatal shape and size in patients with bilateral complete cleft lip and palate assessed using dense surface model construction and 3D geometric morphometrics.* J Craniomaxillofac Surg. 2012, 40(3):201-8
- [2] JAKLOVÁ L., BORSKÝ J., JUROVČÍK M., HOFFMANNOVÁ E., ČERNÝ M., DUPEJ J., VELEMÍNSKÁ J. *Three-dimensional development of the palate in bilateral orofacial cleft newborns 1 year after early neonatal cheiloplasty: Classic and geometric morphometric evaluation.* J Craniomaxillofac Surg. 2020, 48(4):383-390
- [3] JOOS U., MARKUS A. F., SCHUON R. *Functional cleft palate surgery.* J Oral Biol Craniofac Res. 2023, 13(2): 290-298

Electromyographic-based hand prosthesis movements control in Virtual Reality application for patient adaptation

M. KAZALSKI, E. ŚWIĄTEK-NAJWER*

Department of Mechanics, Materials and Biomedical Engineering, Faculty of Mechanical Engineering,
Wrocław University of Science and Technology, Wrocław, Poland

Key words: *electromyography, virtual reality, hand prosthesis*

1. Introduction

Adapting a hand amputation patient to EMG-controlled prosthesis is a well know issue among the producers [1]. Most often in the preliminary phase the patient applies basic standing prosthesis model and learn to generate the appropriate signals to move it motivated by observation. Virtual Reality can improve that approach, helping the patients to participate in such workshop shortly after the injury. Additionally, using VR glasses the patient observes the prosthesis as attached part of his body without any additional costs.

2. Material and Methods

The aim of this work was to develop the software for prosthetic rehabilitation and adapting patient to the prosthesis using a virtual reality (VR) environment visualizing Ada Hand V1.1 prosthesis model [2]. The software applies myosignals to control in the real time the virtual prosthesis movements according to designed control rules. The signals were recorded by an electromyograph (EMG) mini DTS from NORAXON with Ag/AgCl electrodes and processed in MR3 software. The myosignals were intercepted by a self-developed application created in Matlab, which decodes the data, checks and compares the amplitudes to the thresholds defined in rules and finally sends order to the Unity VR environment to move the virtual prosthesis model. For controlling the movements we have used 4 muscles: (1) brachioradialis muscle, (2) biceps brachii muscle, (3) extensor carpi radialis muscle, (4) triceps brachii. For each subject the system is calibrated in order to check the Maximal Voluntary Contraction (MVC) value for each muscle. The controlling rules are adapted for each subject using an interactive menu.

We developed three applications.

- In the learning of prosthesis control the scene presents visualization of 6 grips of prosthesis and videos of 6 upper limb movements associated with them in the context of control (Fig. 1A). Types of grips and applied activating muscles are bulleted in Table 1.

Table 1. Muscles activating the prosthesis grips (training A)

| Activating muscles | Grip |
|--------------------|-------------|
| 1,2 | Hook |
| 2,3 | Cylindrical |
| 1,4 | Pincer |
| 3,4 | Lateral |
| 1 | Palm |
| 4 | Spherical |

*Corresponding author: Ewelina Świątek-Najwer, e-mail: ewelina.swiatek-najwer@pwr.edu.pl

- (B) In the training of prosthesis control with a great variety of movements (Fig 1B) we applied a direct control. With the exception of the wrist rotation action, where continuous muscle tension is required, the algorithm only checks for the occurrence of muscle activity that breaks the state change threshold. After registering it, the prosthesis maintains the position it is in, unlike the first concept, where after relaxing the muscles, the prosthesis returns to the open form of the hand. The pose is changed by biceps brachii tension, changing mode to rotation by triceps brachii tension and, closing/opening/rotating movement by flexion of wrist.
- (C) In the three-difficulty-levels memory-and-skill game the user performs an appropriate upper limb movement to achieve presented grasp (without hints) and gets point for a proper result. The number of grasps to perform, speed of grasps change and variety of alternately activated muscles defines the difficulty level of game. (3)

The Unity application supports VR goggles visualization of prosthesis in the designed environment displaying commands to the user. The application cooperates with VR Meta Quest 2 goggles and Meta Quest 2 Touch controller on which it was tested, but it also should work on other VR devices. We performed tests of application on a group of 7 healthy volunteers. The research was carried out with the permission of the ethics committee.



Fig. 1. Unity application scenes (training A, training B, game C)

3. Results

The tests proved successful adaptation of subjects to control the prosthesis model in a short time. The rules created during the learning phase for the subject were efficient in controlling the prosthesis. Time of adaptation for 7 users in the second in training B option equalled 50 s to 550 s ($200 \text{ s} \pm 174 \text{ s}$, median 140 s). Results of the users in game C in three levels were as following: easy: 76%, medium: 70%, difficult: 51%.

4. Discussion

Obtained results are promising in aspect of aiding prosthetic rehabilitation. Proposed way to develop the project is to apply more sophisticated algorithms of prosthesis EMG control, such as neural networks, machine learning and deep learning. An interesting option would be to apply more muscles in controlling, since the EMG system was limited to 4 channels of simultaneous recording.

References

- [1] MAO L., LU C., YU C., YIN K. *Physiological and Neural Changes with Rehabilitation Training in a 53-Year Amputee: A Case Study*. Brain Sci. 2022 Jun 26,12(7):832
- [2] “ADA V1.1 ASSEMBLY INSTRUCTIONS — OPEN BIONICS” <https://openbionicslabs.com/obtutorials/ada-v1-assembly>

Comparative analysis of rheological models for human blood

N. KIZILOVA^{1*}, L. BATYUK²

¹Institute of Aeronautics and Applied Mechanics, Warsaw University of Technology, Warsaw, Poland

²Kharkiv National Medical University, Department of Medical and Biological Physics and Medical Informatics, Kharkiv, Ukraine

Key words: blood rheology, mathematical modelling, viscoelasticity, shear-thinning, blood flow

1. Introduction

Significant progress in numerical methods, computation fluid dynamics (CFD) and high performance computing methods allowed detailed blood flow simulations in the complex systems of blood vessels as patient specific models for individual planning of treatment, surgery and rehabilitation based on the in vivo pressure and blood flow measurements [1,2]. Since blood as a concentrated suspension of soft particles (blood cells) exhibit a set of complex rheological properties, the problem of a proper choice of the rheological model for CFD simulations in the large, medium and small blood vessels is of great importance in biomechanics of blood circulation including the neural networks [3] and digital twin [4] technologies.

2. Rheological properties of blood

As it was shown in numerous detailed experimental studies of the blood viscosity m_b , this value depends on the shear rate $\dot{\gamma}$, blood plasma viscosity m_p , concentration of plasma proteins C_p , red blood cell (RBC) concentration C_{RBC} , shape parameters c_j and rigidity k_j

$$m_b = m_b(\dot{\gamma}, m_p, C_{RBC}, C_p, c_j, k_j). \quad (1)$$

Besides, m_p depends also on the blood vessel diameter d (Fahraeus-Lindqvist effect), electric charge of the RBC, and some other specific parameters. A general rheological model (1) accounting for all the parameters is absent. The following rheological properties and mathematical relationships are mostly considered.

- 1) Shear-thinning $d\mu_{\text{eff}}/d\dot{\gamma} < 0$ properties of blood are described by the power Ostwald model
- $$\mu_b(\dot{\gamma}) = k(\dot{\gamma})^{n-1} \quad (2)$$

with $0 < n < 1$, $k = \text{const}$,

Viscoplastic behavior (tixotropy) when the blood flow starts when the shear stress applied $\tau > \tau_0$ exceeds the yield stress τ_0 needed to destroy the network of RBC aggregates in the form of the linear Bingham model

$$\dot{\gamma} = \frac{\tau - \tau_0}{\mu_b}, \quad \tau > \tau_0, \quad \dot{\gamma} = 0, \quad \tau < \tau_0 \quad (3)$$

or non-linear Casson model

$$\sqrt{\tau} = \sqrt{\tau_0} + \sqrt{\mu_b \dot{\gamma}}, \quad \text{when } \tau > \tau_0 \quad (4)$$

Dependence on the RBC concentration

*Corresponding author: Natalia Kizilova, e-mail: n.kizilova@gmail.com

$$\mu_b(C_{RBC}) = \frac{\mu_{bp}}{(1 - C_{RBC})^\alpha}, \quad \mu_{bp} = \frac{\mu_0}{1 - k_p C_p}, \quad (5)$$

where $k_p = \text{const}$, $\alpha = 2.5$ for spherical cells and $\alpha = \chi_1$ for the non-spherical ones.

Scale effects with the vessel diameter dependent viscosity due to presence of the cell-free boundary layer with thickness δ

$$\mu_b(d) = \frac{\mu_{bc}}{1 - (1 - \mu_{bc} / \mu_{bp})(1 - 2\delta / d)^4}, \quad (6)$$

where μ_{bc} is the viscosity of the blood core.

Viscoelastic properties of blood determined by elasticity of the RBC

$$k_1 \frac{\partial \tau}{\partial t} + \tau = \mu_{bp} \frac{\partial \dot{\gamma}}{\partial t} + k_2 \frac{\partial^2 \dot{\gamma}}{\partial t^2}, \quad (7)$$

where $k_1 = (\mu_{Hb} + \mu_{bp}) / E_m$, $k_2 = \mu_{Hb} \mu_{bp} / E_m$, E_m is the Young modulus of the membrane, μ_{Hb} is the viscosity of the hemoglobin solutions inside the RBC.

It is easy to show, the rheological properties 1)-5) can mask each other and the most common rheological models of human blood like Quemada model

$$\mu_b = \frac{\mu_{bp}}{(1 - k \cdot Ht / 2)^2}, \quad k = \frac{k_0 + k_1 \sqrt{\dot{\gamma} / \dot{\gamma}_{cr}}}{1 + \sqrt{\dot{\gamma} / \dot{\gamma}_{cr}}}, \quad k_{0,1}(Ht, k_{agg}, k_{def}) \quad (8)$$

where k_{agg} and k_{def} are the RBC aggregation and rigidity coefficients, Ht is the hematocrit, $\dot{\gamma}_{cr}$ is the critical shear rate value, Carreau-Yasuda model

$$\mu = \mu_\infty + (\mu_0 - \mu_\infty) \left(1 + (\lambda \dot{\gamma})^2\right)^{\frac{n-1}{2}}, \quad (9)$$

where $\mu_0 = 0.056 \text{ Pa} \cdot \text{s}$, $\mu_\infty = 0.00345 \text{ Pa} \cdot \text{s}$, $\lambda = 3.313 \text{ s}$, $n = 0.3568$, and Leonov model

$$\tau = 2\mu \dot{\gamma} + T, \quad \lambda \frac{\partial T}{\partial t} + T + \frac{\lambda}{2\mu} \dot{\gamma}^2 = 2\tilde{\mu} \dot{\gamma} \quad (10)$$

do not describe the set of rheological properties 1)-5).

In this study a generalized model in the form of (1) is discussed based on the (i) experimental measurements on the blood samples, (ii) dimension analysis of the dependence (1), and (iii) theoretical modeling of steady blood flow in circular rigid and soft tubes.

3. Conclusions

Based on the detailed experimental data on efficient viscosity of the blood of healthy and diseased patients, it is shown the existing rheological models do not describe the most important blood properties like shear-thinning, concentration dependence, viscoplastic and viscoelastic properties, and Fahraeus-Lindqvist effect and a more general approach is proposed.

References

- [1] HOFFMANN K., CAZEMIER K., BALDOW CH., ET AL., *Integration of mathematical model predictions into routine workflows to support clinical decision making in haematology*. BMC Med Inform Decis Mak. 2020, 10,20(1):28
- [2] KIZILOVA N., MIZERSKI J., SOLOVYOVA H. *Pulse wave propagation along human aorta: a model study*. J Theor Appl Mech. 2020, 58(1), 17-34
- [3] MOSER P., FENZ W., THUMFART S., ET AL., *Modeling of 3D Blood Flows with Physics-Informed Neural Networks: Comparison of Network Architectures*. Fluids, 2023, 8(2), 46.
- [4] CHAKSHU N.K., SAZONOV I., NITHIARASU P. *Towards enabling a cardiovascular digital twin for human systemic circulation using inverse analysis*. Biomech Model Mechanobiol. 2021, 20(2): 449-465

An in-vitro evaluation of mechanical properties and thermographic investigation of selected dental materials used in primary dentition - glass-ionomer cement (Fuji IX) and composite (Charisma)

S. KLIMAS^{1*}, A. NIKODEM², M. DOBRZYŃSKI¹

¹Department of Paediatric Dentistry and Preclinical Dentistry Wrocław, Wrocław Medical University, Wrocław, Poland

²Department of Mechanics, Materials and Biomedical Engineering, Faculty of Mechanical Engineering,

Wrocław University of Science and Technology, Wrocław, Poland

Key words: *thermographic investigation, mechanical properties, dental materials, glass - ionomers, composites*

1. Aim of the study

The aim of this study was to measure and compare mechanical parameters and temperatures generated during the polymerization of selected dental materials (Fuji IX, Charisma) used to reconstruct cavities in deciduous teeth. Scope of work included: measurement of physical properties (density), measurement of mechanical properties (Vickers hardness HV, Young's modulus E for dental tissues (enamel, dentine) and dental restorations, measurement of the maximum temperatures created during the polymerization of materials (20 s).

2. Materials and Methods

2.1. Materials

The tests were carried out for dental materials from 2 separate groups: glass - ionomer cement -Fuji IX and composite - Charisma. The samples were prepared using a special form: sample diameter (d) - 6mm, sample height (h) - 2,5 mm. The composite material was polymerized according to manufacturer's instructions for 20 s using a Bluephase Style 20i polymerization lamp (Ivoclar Vivadent, Schaan, Liechtenstein). Fuji IX is a chemo-binding material in the form of capsules. Before use, each capsule should be shaken and then placed in a shaker (3M ESPE CapMix) for 10 seconds. After this time, the capsule is placed on a special feeder-gun and the material is placed to the form. Net setting time is 2 minutes. For the thermographic investigation both materials were polymerized for 20 seconds.

2.2. Methods

The measurement of the density of dental fillings was determined on the basis of the weight to volume ratio. The samples were weighed using a RADWAG® PS 1000/C/2 laboratory analytical balance with an accuracy of 0.001 g. Then, using a Mitutoyo micrometer, the geometric parameters of each sample were measured. Mechanical tests (measurement of microhardness and Young's modulus) were carried out for both dental filling samples and tissues of deciduous and permanent teeth. Each of the tested samples was embedded in acrylic with self-polymerizing properties - Duracryl® Plus (SpofaDent, Czech Republic), previously placed in silicone molds. The samples prepared in this way were cut using the STRUERS® Accutom-5 metallographic cutter. The samples were wet polished using 1000 grit sandpaper. The tests were carried out using a CSM MicroCombi Tester™ microhardness tester where the Vickers microhardness and Young's modulus values were determined. The maximum

*Corresponding author: Sylwia Klimas, e-mail: sylwia.klimas@umw.edu.pl

temperatures resulting from the irradiation of samples from both groups were measured using a thermal imaging camera (FLIR ThermaCAM P640). Fig. 1 presents prepared samples of dental restorations and hard dental tissues after incorporation in Duracryl™ Plus SPOFA Dental).

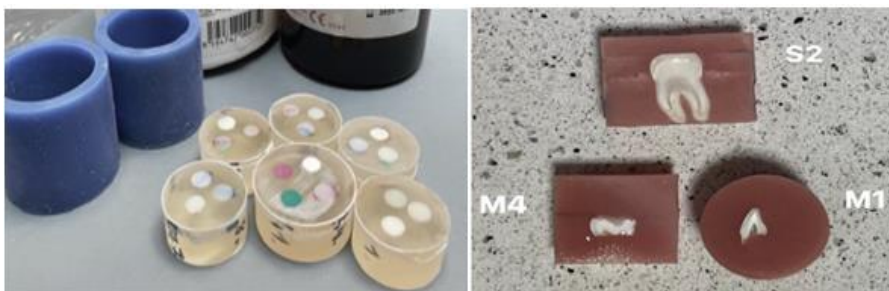


Fig. 1. Dental material samples and dental samples incorporated in Duracryl™ Plus SPOFA Dental), S2 - permanent molar, M4 - deciduous molar, M1 - deciduous incisor

2.3. Results

The average density with standard deviation [g/cm³], Young's modulus E [GPa] and Vickers hardness values HV were presented in the Table 1.

Table 1. Mechanical and physical properties of tested dental materials

| | Average density $\rho \pm SD$ [g/cm ³] | Young's modulus E [GPa] | Vickers microhardness [HV] |
|----------|---|----------------------------|-------------------------------|
| Charisma | 1,78 ±0,08 | 16,63 | 74,72 |
| Fuji IX | 1,65±0,15 | 24,02 | 62 |

The highest temperature during the polymerization of Fuji IX was 38,4 °C. In turn, the highest temperature obtained during the polymerization of Charisma was 52,1°C. However, it should be noted that critical temperature for the dental pulp is 42°C.

2.4. Conclusions

The results of the examined dental fillings indicate that different filling materials have different Young's modulus and microhardness values relative to each other. The obtained values for the fillings differ significantly from the results of microhardness and Young's modulus of enamel. The values obtained for the fillings oscillate in the values of microhardness and Young's modulus for dentin, which is desirable because it minimizes the risk of "abrasion" of the dental tissue due to too high strength parameters. The maximum temperature generated by the Charisma filling during polymerization of the material is significantly higher than the critical temperature for the pulp (52,1°C vs. 42°C) and may cause pulp damage.

References

- [1] GÜDER H.S., ŞAHİN E., ŞAHİN O., GÖÇMEZ H., DURAN C. *Vickers and Knoop Indentation Microhardness Study of β -SiAlON Ceramic*. ActaPhysicaPolonica, 2011, 120(6):1025-1033
- [2] HALGAS R., DUSZA J., KALIFEROVA J., KOVACSOVA L., MARKOVSKA N. *Nanoindentation testing of human enamel and dentin*. Ceramics-Silikaty, 2013, 57(2): 92-99
- [3] KHODADADI E., KHAFRI S., AZIZNEZHAD M. *Comparison of Surface Hardness of Various Shades of Twinky Star Colored Compomer Light-cured with QTH and LED Units*. Electron Physician, 2016, 8(5): 2355-2360
- [4] BAHSI E., SAGMAK S., DAYI B., CELLIK O., AKKUS Z. *The evaluation of microleakage and fluoride release of different types of glass ionomer cements*. Niger J Clin Pract. 2019, 22(7):961-970

Hyperelastic models comparison for abdominal aortic aneurysms

M. KOBIELARZ^{1*}, A. CHWILKOWSKA²

¹Department of Mechanics, Material and Biomedical Engineering,
Wroclaw University of Science and Technology, Wroclaw, Poland

²Department of Molecular and Cellular Biology, Wroclaw Medical University, Wroclaw, Poland

Keywords: *abdominal aortic aneurysm, material properties, constitutive model, tensile test*

1. Introductions

An abdominal aortic aneurysm (AAA) is a pathological enlargement of aortic diameters measured in perpendicular directions compared to the standard size of at least 50% [1]. The incidence of AAAs reaches even 10% of the global population, growing rapidly with age above 50 [2]. Most AAAs remain clinically silent and may rupture if not detected, with catastrophic clinical consequences. AAA rupture can be considered a classic case of material destruction resulting from excessive loading on the vessel wall, insufficient material strength, or both of these factors simultaneously. From the mechanical point of view, patient-specific FEM modelling of AAAs is considered the rational and factual method for progression and risk of rupture evaluation. However, patient-specific modelling requires crucial elements, i.e. materials properties determined by the constitutive models specifically for each patient's tissues. Hence, the main study's goal was to determine the difference between the behaviour of AAA specimens using different models.

2. Materials and Methods

2.1. Mechanical behaviour study

Uniaxial tensile tests for cut specimens off abdominal aortic walls into two perpendicular directions, i.e. circumferential and longitudinal, were performed on a testing machine (Synergie 100, MTS) with a constant rate of 2 mm/min at room temperature (22±1°C) and with continuous moisturisation. Before the test, the specimens were pre-loaded to 0.01 N and then pre-stretched for five loading-unloading cycles to 10% of strain. The Cauchy stress-stretch ratio relationships were determined for all the specimens.

2.2. Hyperelastic models

One of the most often used hyperelastic anisotropic material models for aortic and aneurysmal tissues' mechanical behaviour description is the model proposed by Holzapfel et al. [3]. The strain-energy functions of the fibrous composite models additively decompose into an isotropic contribution of the ground matrix, an anisotropic contribution of two symmetrical and mechanically equivalent collagen fibres families, and a contribution of the purely volumetric part represented by the Jacobian due to the incompressibility assumption:

$$\Psi = \frac{\mu}{2}(I_1 - 3) + \frac{k_1}{2k_2} \sum_{i=4,6} (e^{k_2(I_i-1)^2} - 1) \Psi = \frac{\mu}{2}(I_1 - 3) + \frac{k_1}{2k_2} \sum_{i=4,6} (e^{k_2(I_i-1)^2} - 1) \quad (1)$$

where: k_1 is a stress-like parameter related to the stiffness of the fibres, k_2 is a dimensionless material parameter related to the degree of nonlinearity, and invariants of the right Cauchy–Green deformation tensor I_4 and I_6 are related to the mechanical response of the family fibres aligned in preferred directions.

*Corresponding author: Magdalena Kobielarz, e-mail: magdalena.kobielarz@pwr.edu.pl

On the other hand, the most popular in solid mechanics AAA modelling is the isotropic polynomial model of Raghavan and Vorp [6]:

$$\Psi = c_1(I_1 - 3) + c_2(I_1 - 3)^2 \quad \psi = c_1(I_1 - 3) + c_2(I_1 - 3)^2 \quad (2)$$

where: c_1 and c_2 are stress-like parameters, and I_1 is the first invariant equal trace of the right Cauchy–Green deformation tensor.

Polzer et al. [7] proposed Yeoh's incompressible fifth-order hyper-elastic material model for AAA:

$$\Psi = \sum_{i=1}^5 c_i (I_1 - 3)^i \quad \psi = \sum_{i=1}^5 c_i (I_1 - 3)^i \quad (3)$$

where: c_i are stress-like material constants.

Models were used for fitting experimental data (Fig.1). The constitutive parameters were determined using a nonlinear least-squares *lsqnonlin* function in the Matlab software (ver. 2017b). The standard nonlinear Levenberg–Marquardt algorithm was used during the curve fitting. The coefficient of determination (R^2) evaluated the goodness of fit.

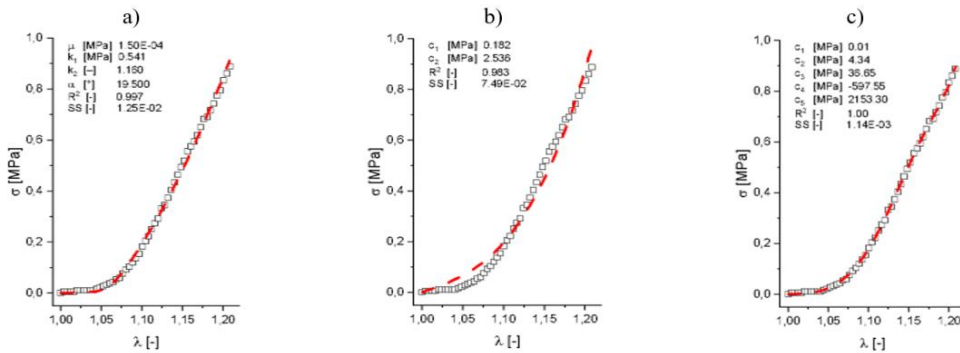


Fig. 1. AAA sample cut out in circumferential direction behaviour under uniaxial stress fitted by models by a) Holzapfel et al., 2000 [3], b) Raghavan and Vorp, 2000 [4], c) Polzer et al., 2013 [5]

The AAA wall is less anisotropic, and, at the same time, the nonlinearity of stress-strain relation is more pronounced. The wall stress computations are not particularly sensitive to constitutive descriptions as long as the wall's low initial stiffness, followed by its substantial stiffening at higher strains, is respected.

Acknowledgements: Grateful acknowledgements to the Polish National Agency for Academic Exchange. The researches were under a project within the Bekker Programme under grant no. BPN/BEK/2021/1/00166.

References

- [1] JOHNSTON K., RUTHERFORD R., TILSON M., SHAH D., HOLLIER L., STANLEY J. *Suggested standards for reporting on arterial aneurysms*. J Vasc Surg. 1991, 13(3):452-8
- [2] DIMARTINO E., BOHRA A., GEEST J., GUPTA N., MAKAROUN M., VORP D. *Biomechanical properties of ruptured versus electively repaired abdominal aortic aneurysm wall tissue*. J Vasc Sur, 2006, 43, 570-676
- [3] HOLZAPFEL G., GASSER T., OGDEN R. *A new constitutive framework for arterial wall mechanics and a comparative study of material models*, J Elast, 2000, 61, 1-48
- [4] RAGHAVAN M., VORP D. *Toward a biomechanical tool to evaluate rupture potential of abdominal aortic aneurysm: identification of a finite strain constitutive model and evaluation of its applicability*. J Biomech, 2000, 33, 475-482
- [5] POLZER S., GASSER T., BURSA J., STAFFA R., VLACHOVSKY R., MAN V., SKACEL P. *Importance of material model in wall stress prediction in abdominal aortic aneurysms*. Med Eng Phys, 2013, 35, 1282-1289

Evaluation of the possibility of using a hybrid magneto-mechanical drive in dynamic implants for lengthening long bones

P. KOWALEWSKI^{1*}, D. GRYGIER², P. KROWICKI³, R. JASTRZĄBEK⁴, M. OPALKA¹, M. KIEŁB¹

¹Department of Fundamentals of Machine Design and Mechatronic Systems,
Faculty of Mechanical Engineering, Wrocław University of Science and Technology, Wrocław, Poland

²Automotive Engineering Department, Faculty of Mechanical Engineering,
Wrocław University of Science and Technology, Wrocław, Poland

³Department of Laser Technologies, Automation and Production Management,
Faculty of Mechanical Engineering, Wrocław University of Science and Technology, Wrocław, Poland

⁴Orthoget sp. z o. o., ul. Muchoborska 18, 54-424, Wrocław, Poland

Key words: *intramedullary nail, hybrid drive, dynamic implant, lengthening of long bones*

1. Introduction

One of the ways to solve problems related to limb inequalities is to lengthen them surgically. Lengthening the limbs with external stabilizers, due to their size and high risk of infection and other complications, is burdensome and dangerous for the patient. The use of an internal fixator, which is an intramedullary nail, makes the healing process painless, and the internal implant does not hinder the patient's daily functioning [1]. In addition, there is a much lower risk of wound infection.

2. Hybrid magneto-mechanical drive

Existing dynamic intramedullary nailing solutions are characterized by a single energy source driving the implant components [2]. The dynamic intramedullary nail with a hybrid magneto-mechanical drive uses in a synchronized way the mechanical energy accumulated in the elastic element inside (spring) the implant and the magnetic energy coming from the outside.

The combination of two types of drives allows both to control the stretching process during treatment and minimizes the amount of energy generated outside and passing through the patient's body [3]. It also minimizes the size of the magnetic drive inside the implant, improving the compactness and mechanical strength of the structure. The intensity of the magnetic field generated by the external element driving the nail mechanism is limited to the necessary minimum. Fig. 1 shows a cross-section of the assembly drawing of the Orthoget hybrid drive intramedullary nail that was the subject of the study.

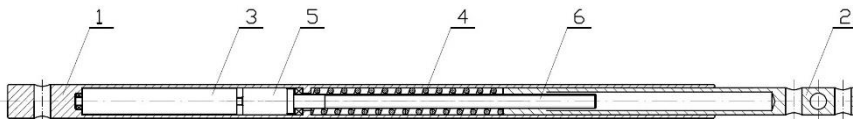


Fig. 1. Cross-section of an intramedullary nail with a hybrid drive. 1 - nail body, 2 - retractable element, 3 - magnetic rotor, 4 - drive spring, 5 - mechanical transmission, 6 - drive screw [2]

3. Materials and Methods

The measurement consisted of e.g. on the measurement of the nail extension force with a hybrid drive depending on the position relative to the external activator. This activator generated a pulsating and alternating magnetic field causing the rotation of the magnetic rotor inside the nail. The implant

*Corresponding author: Piotr Kowalewski, e-mail: piotr.kowalewski@pwr.edu.pl

was placed in five different locations simulating possible positions during the treatment process. The maximum extension force was recorded for each position. The tests for each item were repeated 3 times, and the average value was taken for analysis. The diagram and photo of the measurements are shown in Fig. 2.

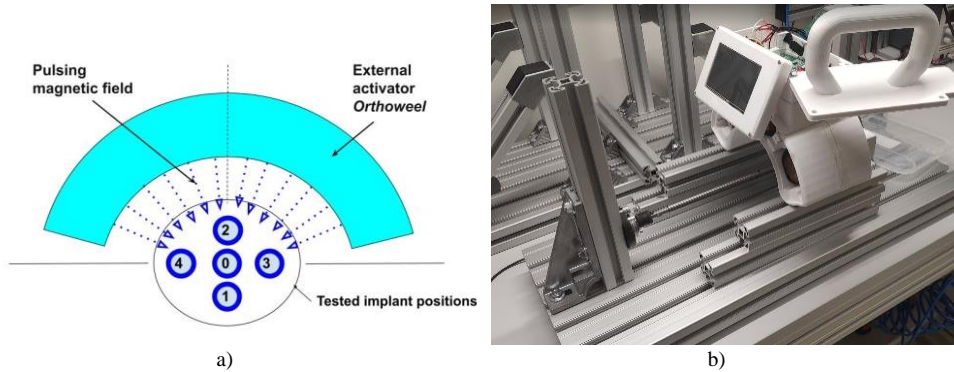


Fig. 2. Scheme (a) and photo (b) of the test of the propulsion force of the tested implant

4. Results

A clear difference can be noticed in the obtained force of the nail extension depending on its position in relation to the external exciter. The measured values with the range are presented in table 1.

Table 1. Measured values of the implant extension force depending on the location relative to the external activator

| Position | Average Extension Force [N] | Extension force range [N] |
|----------|-----------------------------|---------------------------|
| 0 | 128 | 5 |
| 1 | 97 | 7 |
| 2 | 163 | 10 |
| 3 | 105 | 7 |
| 4 | 97 | 9 |

5. Conclusions

The conducted research shows a high dependence between the location of the implant with a hybrid drive and the maximum extension force obtained. It can be seen that the extension force is the greater the closer the implant is to the geometrical center of the outer activator.

The applied spring generating mechanical force influences the load on the thrust bearings in the initial phase of extension, which increases the resistance to movement and reduces the maximum extension force. As the implant lengthens, the force generated by the internal mechanical accumulator decreases.

References

- [1] BAUMGART R., THALLER P., HINTERWIMMER S., KRAMMER M., HIERL T., MUTSCHLER W. *A Fully Implantable, Programmable Distraction Nail (Fitbone) – New Perspectives for Corrective and Reconstructive Limb Surgery, Practice of Intramedullary Locked Nails*. Berlin/Heidelberg: Springer-Verlag, 2006, 189-198
- [2] KOWLEWSKI P., GRYGIER D. *Dynamic Intramedullary Nail With Hybrid Drive, Dynamic Intramedullary Nail Kit With Magnetic Drive*. Zgłoszenie patentowe nr P.441270 (in polish)
- [3] GRYGIER D., SŁOWIŃSKI J., KOWALEWSKI P. *Wydłużanie kości długich – metody i zastosowanie (in polish)*. Inżynier i Fizyk Medyczny. 2020, 9(6): 458-460.

The effect of atherosclerosis on the susceptibility of the human aorta to delamination

M. KOZUŃ*, M. KOBIELARZ

Department of Mechanics, Materials and Biomedical Engineering,
Wrocław University of Science and Technology, Wrocław, Poland

Key words: *delamination, atherosclerosis, mechanical properties, human aorta, peeling test*

1. Introduction

Spontaneous aortic dissection is a result of negative remodelling of aortic wall structure and occurs in 5-30 cases per million people/year. This kind of dissection may be associated with development of atherosclerosis [2]. This disease changes the mechanical properties of the blood vessel wall, its individual layer [3] and affects the adhesion between them [1]. This leads to a loss of integrity of the vessel wall, and consequently to its delamination. Despite the mechanism of the aortic dissection process is still unknown and the subject of previous performed research are mainly healthy vessels [4][5]. There is still no answer how development of atherosclerosis affects the resistance to dissection of human artery. This is why the aim of this research is a determination of the mechanical properties of the interface between the individual layers of human thoracic aorta with different stages of atherosclerotic lesion.

2. Material and Method

The subject of the research was human aorta (n=91) removed “post mortem”. In the first step the histological examination was conducted and based on it the material was divided into six groups according to the histological scale proposed by Stary. The group of healthy, pathological unchanged vessel was classified as stage I (n=17) based on Stary’s scale and 74 arteries were classified to the group of atherosclerotic vessels (from II to VI according to Stary’s scale).

In the next step arteries were punched out in two directions: longitudinal and circumferential and 124 specimens were obtained for mechanical tests. Before them, each specimen was initially dissected about 5 mm and the peeling test with a T - configuration of (1) the adventitia and the media – intima complex (A-MIC) and (2) the intima and the media-adventitia complex (I-MAC) were performed with a constant speed rate of 2mm/min. During test, propagation of the previously initiated dissection was forced and the changes in value of force and displacement were recorded.

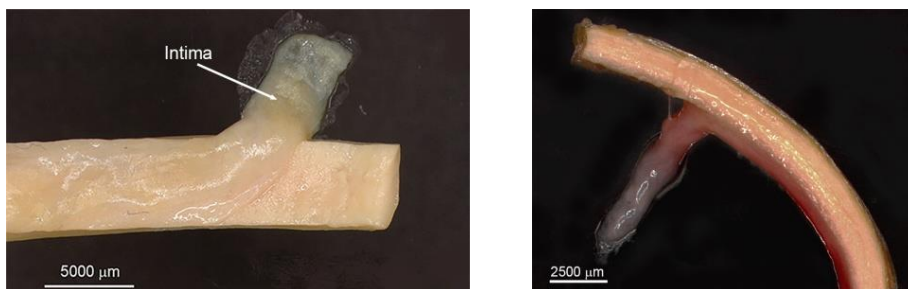


Fig.1. The method of initial dissection of specimens for the peeling test. The interfaces between the intima and the media-adventitia complex (I-MAC)

*Corresponding author: Marta Kozuń, e-mail: marta.kozun@pwr.edu.pl

3. Results

Based on the mechanical tests the mechanical properties: stiffness coefficient (k), energy dissipated during delamination (W), the maximum value of force (F_{MAX}) and average value of force during delamination (F_{AVER}) were calculated. The results indicate the values of mechanical parameter undergo significant changes in parallel with the development of atherosclerosis. The statistical analysis was performed by using Statistica 13.1 software (StatSoft) with level of statistical significance $\alpha = 0.05$. Significant differences were tested using the Kruskal-Wallis tests (one-way ANOVA on ranks) and the Dunn's post-hoc test.

The results show the mechanical properties undergo significant in parallel with the development of atherosclerosis. For the A-MIC interface the highest values of mechanical parameters: energy and average force were obtained for healthy tissue ($W=7.7$ mJ/cm² for circumferential and $W=9.3$ mJ/cm² for longitudinal specimens). This group is also characterized by the lowest values of stiffness coefficient. The values of energy and mean force decrease from healthy vessel until stage IV ($W=4.8$ mJ/cm² for circumferential and $W=5.6$ mJ/cm² for longitudinal specimens) and then they increase for V to VI group. In the case of both interface (A-MIC and I-MAC) higher values of the mechanical parameters were obtained for longitudinal specimens.

4. Discussion

The result indicate that development of atherosclerosis decreases resistance of the aortal wall to delamination. Due to the lowest value of energy the greatest risk of dissection is related to stage IV. The I-MAC interface is most susceptible to dissection due the fact that lesions develop within the intima. Regardless to the stage of atherosclerosis the mechanical properties of A-MIC and I-MAC are directional, indicating that atherosclerosis doesn't lead to the disappearance of the anisotropy. The lower value of energy for the circumferential direction indicate the delamination of the human aorta may propagate in this direction.

Acknowledgments: This work is part of the 'WROVASC – Integrated Cardiovascular Centre' project, co-financed by the European Regional Development Fund within the Innovative Economy Operational Programme, 2007-2013.

References

- [1] KARIMI A., ET AL., *Measurement of the uniaxial mechanical properties of healthy and atherosclerotic human carotid arteries*. Mater Sci Eng C, 2013, 33(5), 2550-2554
- [2] KOZUŃ M., ET AL., *The Impact of Development of Atherosclerosis on Delamination Resistance of the Thoracic Aortic Wall*. J Mech Behav Biomed Mater, 2018, 79, 292-300
- [3] TENG M., ET AL., *An experimental study on the ultimate strength of the adventitia and media of human carotid arteries in circumferential and axial directions*. J Biomech, 2013, 42(15), 2535-2539
- [4] TONG J., ET AL., *Dissection properties and mechanical strength of tissue components*. Ann Biomed Eng, 2011, 39(6): 1703-1719
- [5] SOMMER G. *Dissection properties of the human aortic media: an experimental study*. J Biomech Eng, 2008, 130(2), 1-12

Experimental and numerical tests of piercing the head of a pig subjected to a shock load

K. H. KRAWIEC^{1*}, D. PYKA¹, K. JAMROZIAK¹, A. NOSZCZYK-NOWAK²

¹Department of Mechanics, Materials and Biomedical Engineering, Faculty of Mechanical Engineering, Wrocław University of Science and Technology, Wrocław, Poland

²Department of Internal Medicine and Clinic of Diseases of Horses, Dogs and Cats, Wrocław University of Environmental and Life Sciences, Wrocław, Poland

Key words: skull injuries, bone piercing, numerical analysis, hybrid methods, energy intensity

1. Introduction

The growing demand for systems that absorb the energy caused by impulse load poses more and more a challenge to designers [1]. The available material systems dissipating the impact energy of the 9x19 mm FMJ Parabellum bullet used in the shells of the combat helmet meet the requirements of specific standards. As the experience of military missions in Iraq and Afghanistan showed [2], an important issue in testing modern combat helmets is the issue of head trauma [3],[4]. In this study, the authors focused their attention on testing the resistance to puncture of the animal skull bone. The determined strength parameters will be used for further work on the impact of blunt trauma on selected elements of a soldier's head protected by a combat helmet.

2. Materials and Methods

2.1. Research material

The head of a domestic pig cut through the middle of the nasal bone was used to carry out the research, creating two symmetrical halves. The total length of half of the head was 28 cm, width 17 cm. For this purpose, preliminary tests were carried out to determine the energy needed to punch the head along with tissue structures by two penetrators. The first spherical penetrator with a radius of $r = 4.5$ mm and the second conical penetrator $\alpha = 45^\circ$ were used, both on a shaft with a diameter of $d = 9$ mm and a length of 90 mm. Two halves of a pig's head, taken from the same animal, were selected as a reference point.

2.2. Quasi-static studies

Quasi-static piercing tests were carried out for 17 places in order to obtain the specified force values. Piercing were carried out at a constant speed $v = 5$ mm/s until a displacement of 50 mm was obtained. Fig. 1 shows the puncture points for external and internal sections. In this way, the maximum punching force for bone structures and anatomical tissues was determined.

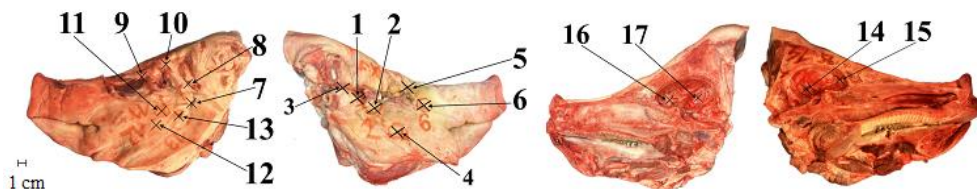


Fig. 1. Places of piercing the pig's head

*Corresponding author: Dariusz Pyka, e-mail: dariusz.pyka@pwr.edu.pl

2.3. Numerical analysis

Numerical analysis was performed in the Abaqus/Explicit program. For this purpose, the bone structure was modeled in a hybrid way, combining the classic FEM method to describe the compact part and SPH to the spongy part. The Johnson-Cook (JC) rheological model was used to describe the bones, while the Yeoh model was used to describe the soft tissues such as skin, muscles and fat. The system was modeled for selected examples of puncture with a given constant velocity of the penetrator.

3. Results and Discussion

Examples of piercing results in the quasi-static test and in FEM numerical analyzes are shown in Table 1. The test was performed for a sectional outer left half. As can be seen, the average force necessary to pierce the bone was approx. 1.8 kN and the anatomical tissue was approx. 0.5 kN. Numerical modeling results show slightly lower values. The relative error was estimated at 12.7% for the analyzed hard tissues and 11% for soft tissues.

Table 1. Comparison of the results of the maximum force for example experiments and numerical analysis.

| Measurement No. | Bone | | | Anatomic tissues | | | |
|-------------------|------|------|------|------------------|------|------|------|
| | 8 | 11 | 13 | 7 | 9 | 10 | 12 |
| Max. Force [N] | 5366 | 2143 | 1552 | 568 | 497 | 533 | 455 |
| Displacement [mm] | 21.5 | 19.4 | 19.3 | 40.0 | 26.8 | 14.4 | 20.5 |
| Medium force [N] | | 1847 | | | 513 | | |
| FEM | | 1612 | | | 456 | | |

4. Conclusion

The adopted hybrid numerical methods with the use of standard FEM and SPH to describe the bone tissue, together with the use of non-linear rheological models, approximately correspond to the maximum forces recorded in the experiment. This is due to the inaccuracy of the geometric models and the obtained material constants.

Acknowledgments: Calculations have been carried out in Wrocław Centre for Networking and Supercomputing (<http://www.wcss.pl>), grant No. 452

References

- [1] JAMROZIAK K., BAJKOWSKI M., BOCIAN M., ET AL., *Ballistic Head Protection in the Light of Injury Criteria in the Case of the Wz.93 Combat Helmet*. Appl Sci, 2019, 9(13), 2702
- [2] WOJCIK B.E., STEIN C.R., BAGG K., HUMPHREY R.J., OROSCO J. *Traumatic brain injury hospitalizations of U.S. army soldiers deployed to Afghanistan and Iraq*. Am J Prev Med. 2010, 38(1 Suppl): S108-16
- [3] WALLACE D., RAYNER S.P.S. *Combat helmets and blast traumatic brain injury*. J Mil Veteran Fam Health, 2012, 20(10)
- [4] RATAJCZAK M., KLEKIEL T., SŁAWIŃSKI G., BĘDZIŃSKI R. *Investigation of Helmet-Head Interaction in the Aspect of Craniocerebral Tissue Protection BT - Current Trends in Biomedical Engineering and Bioimages Analysis*, in: Korbicz J., Maniewski R., Patan K., Kowal M. (Eds.), Springer International Publishing, Cham, 2020, 308–315

Kinematic analysis of sway motions of elite dance sport competitors

S. KULIŚ*, J. GAJEWSKI

Józef Piłsudski Academy of Physical Education Warsaw, Warsaw, Poland

Key words: *dance sport, kinematic, sway, technique*

1. Introduction

Kinematic characterisation of top-level couples could help develop a movement model for a champion and, over a longer time horizon, may support the jurors in effectively and objectively assessing dance couples [1]-[2]. Literature references on movement technique in standard dance suggest that sway motions are regarded as one of the most important motions that are executed while dancing. The present available knowledge demonstrates that no research has yet been executed by other authors on the relationship existing between the technical execution of individual dance elements and the assessment awarded by the judges. The purpose of this paper was to identify a possible relationship between scores given by the jurors and variables that describe the sway movement in the Viennese waltz as performed by dance sport athletes.

2. Material and Methods

The study involved six world-class and six intermediate dance couples. The pairs were asked to perform three identical series of three natural spins of the figure in a Viennese waltz and were all recorded by camera as they danced to music. Six international adjudicators have evaluated all trials of each couple from the viewpoint of the technical quality component based on the Absolute Judging System. Triaxial rotational angular velocity measurement device was placed on the dorsal part of the pelvic girdle and on the posterior part of the thorax of every athlete [3].

3. Results

The analysis of covariance showed that maximum angular rotation velocities of the thoracic spine in forward sway movements in male dancers were strongly associated with the judging score obtained ($F_{1,9} = 11.5$, $p = 0.0240$, $\eta_p^2 = 0.449$) regardless of the assignment to the given group. Significant correlations of the mean angular rotation velocities in the forward leaning movement were noted in the champion group and the intermediate group. A stronger correlation in the angular rotation velocities of the pelvic girdle (ω_{z1}) were observed in the execution of the sway motion of women and men from the intermediate group ($R = 0.809$). For the champion group dancers, it amounted to ($R = 0.470$). As regards the characteristic description of changes in angular rotation velocity of the thoracic spine (ω_{z2}) of women and men from the champion group a high correlation was observed ($R = 0.851$). The Fig. 1 shows example of the mean angular velocity waveforms ω_{z1} during the execution of the forward sway motion of the female dancer (F) and male dancer (M) from champion and intermediate groups.

*Corresponding author: Szymon Kuliś, e-mail: szymon.kulis@awf.edu.pl

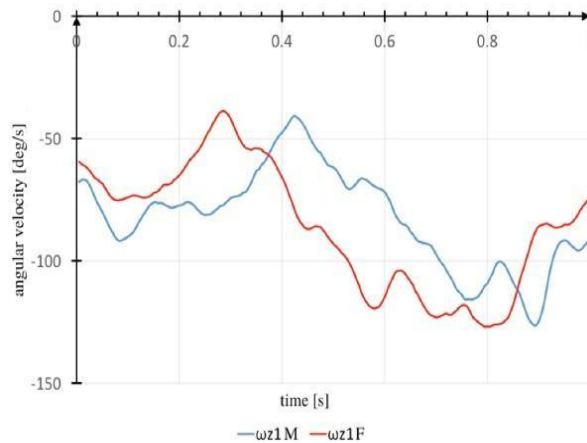


Fig. 1. Average angular velocity waveforms ω_{z1} during the performance by a female (F) and a male (M) dancer from the champion group of the forward sway movement, ω_{z1} – Angular velocity of rotation in relation to the sagittal axis of the pelvic girdle

4. Conclusion

The results of the conducted research indicate that the scores awarded by judges for the quality of movement technique are to a large extent convergent. Top category judges were unanimous in their judgement of dance couples from the champion and intermediate groups. The group of champion dancers differs from the group of intermediate dancers in terms of component criteria related to technical quality expressed quantitatively and qualitatively in terms of the courses of angular velocities performed during sway movements. It is worth noting that the exchange of movements during the dance between men and women observed in the champion group does not result in an obvious simultaneous different sway of women to the left and men to the right and vice versa, as should happen according to the rules laid down in dance manuals. It should be noted that the pelvic girdle is positioned in a rightward tilt most of the time and the thoracic spine is positioned in a leftward tilt. This is a very interesting phenomenon that indicates a greater complexity of body sway changes between men and women in the championship group than the one described in the dance literature.

Acknowledgments: The study was supported by university research project No. 3 'Postural assessment and accelerometric characterisation of movement technique in selected sports'.

References

- [1] CHANG M., HALAKI M., ADAMS R., COBLEY S., LEE K.Y., O'DWYER N. *An Exploration of the Perception of Dance and Its Relation to Biomechanical Motion: A Systematic Review and Narrative Synthesis*. J Dance Med Sci. 2016, 20(3):127-136. doi:10.12678/1089-313X.20.3.127
- [2] JEONG J.O., KIM E.J. *The Judges' Organization and Objectivity of a Dance Sport Competition*. J Sport Leisure Stud. 2006, 26:483-495. doi:10.51979/KSSLS.2006.05.26.483
- [3] STANIAK Z., BUŠKO K., GÓRSKI M., PASTUSZAK A. *Accelerometer profile of motion of the pelvic girdle in breaststroke swimming*. J Hum Kinet. 2016,52(1). doi:10.1515/hukin-2016-0002

Analysis of material and mechanical properties of stents to increase the effectiveness of urethral stenosis treatment

J. KUROWIAK*

Department of Biomedical Engineering, Faculty of Mechanical Engineering, University of Zielona Góra, Poland

Key words: biomaterials, polymers, regenerative medicine, tissue engineering

1. Introduction

Stenosis of the male urethra is a serious urological condition. The incidence increases with age. Urethral stenosis can have a variety of origins and causes. It is most often diagnosed in men after 65 years of age. Still no single effective treatment has been developed [1]. Urethral stenosis results in impaired urine flow and, if severe, can prevent urine from draining from the body. Symptoms of stenosis include e.g.: frequent urination, pain and discomfort, and even hematuria. Treatment of stenosis is difficult due to the specific conditions of the urethral tissues [2]. These conditions depend on the flow of urine, pressure and the influence of the adjacent muscles around the urethra. A promising method of treatment may be the use of stents, whose main purpose is to restore the free flow of urine [3]. Stents dedicated to the treatment of urethral stenosis should have certain characteristics. In order to determine the parameters of these properties, it is necessary to have a thorough understanding of the structure of the male urogenital system and the anatomy of the urethra. The next step is the search for a suitable material for stent and the development of its geometry.

2. Materials and Methods

In order to increase the effectiveness of the treatment of urethral stenosis, studies have been carried out to determine the conditions inside the urethra to learn about the mechanical characteristics of the urethral tissues, to select a suitable material for the stent and to develop its construction.

As part of the dissertation, urodynamic studies were performed under in vivo conditions on New Zealand White rabbits. These studies made it possible to determine the actual load conditions prevailing in the urethra. Mechanical characterization of the urethral tissues was performed on the collected material from the animals (New Zealand White rabbits) for two segments from the side of the bladder (P) and from the side of the urethral outlet (U), with a division into a physiologically healthy urethra „K” and with induced inflammation „F” [4]. The next stage of the study was the selection of polymer material for the construction of the urological stent. The study focused on two materials. It was sodium alginate (SA) and polydioxanone (PDO). A number of mechanical and material tests were performed for the proposed materials [5]-[7].

The final step was to develop a stent construction for the treatment of urethral stenosis, which will be able to function properly under the specific conditions of the male urethra, both during micturition and ejaculation [7].

3. Results

Urodynamic studies performed for the urethra of the New Zealand White rabbit at rest showed that the prevailing constant pressure is about 1,5 kPa, while during micturition it is about 5,5 kPa.

The determined parameters were important and provide criteria for further analysis [4].

*Corresponding author: Jagoda Kurowiak, e-mail: j.kurowiak@iimb.uz.zgora.pl

The mechanical characteristics of the urethral tissues made in the radial direction for the different groups was as follows: Young's modulus for the group of healthy New Zealand White rabbits „K” for the section of the urethra from the bladder side (P) is 0.015 MPa, for the same group „K”, but from the urethral outlet (U) is 0.020 MPa; for the irritated group „F”, from the bladder side (P) the value oscillates around 0.010 MPa, while from the urethral outlet (U) is 0.018 MPa. The mechanical properties of the urethral tissues change depending on the depending on the segment examined. The tissues in the segment from the side of the bladder are characterized by a lower Young's modulus (E) than tissues taken from the mouth of the urethra. It was observed that the mechanical characteristics of these tissues also changed when inflammation was present. Inflammatory changes cause a reduction in the deformability of the tissues, which become more rigid, affecting the on the stresses present in them. The research to select a stent material showed that polydioxanone (PDO) is a better material than sodium alginate (SA). SA shows good mechanical properties, but it degrades quickly when in contact with urine solution [6]. However, PDO shows promise for dedicated use in urology. Experimental studies have shown that PDO has a mechanical strength of 451 MPa (± 44 MPa), a tensile strength of 43 MPa (± 2 MPa), and a yield strength of 10 MPa (± 2 MPa) [7]. Based on the degradation studies, it is estimated that under real conditions, a stent made of PDO can perform its function for about 6 weeks. The developed stent design and the performed FEM numerical analysis confirmed the correct interaction of the proposed stent with the urethral wall. The obtained deformation results showed that the developed design and the selected PDO material will maintain proper urethral kinetics, which will counteract secondary tissue fibrosis.

4. Conclusions

In conclusion, the results obtained are promising and allow to increase the effectiveness of stents in the treatment of male urethral stenosis. During the development of the stent construction, it is important to establish its correct interaction with the urethral tissues. It is necessary to take into account the changing contact conditions, which are related to changes in tissues loading, the degradation time of the stent material and the process of tissues remodelling.

Acknowledgments: The work has been accomplished under the research project No. DEC-2016/21/B/ST8/01972, funded by National Science Center, Poland. *In vivo* tests was performed on the basis and in accordance with the decision of the 2nd Local Ethics Committee for Animal Experiments in Wroclaw (decision No. 1/2017 based on resolution No. 95/2015 of July 15, 2015).

References

- [1] SMITH T.G. *Current management of urethral stricture disease*. Indian J Urol, 2016, 32, 27-33
- [2] KUROWIAK J., KLEKIEL T., BĘDZIŃSKI R. *Requirements analysis for the design of stents designed for the treatment of urethral dysfunction*. In *Human Health-Prevention, Recognition and Treatment of Diseases*, Maciąg K., Maciąg M., Eds., Scientific Publisher TYGIEL, 2021, 181-189
- [3] KLEKIEL T., MACKIEWICZ A., KACZMAREK-PAWELSKA A., ET AL., *Novel design of sodium alginate based absorbable stent for the use in urethral stricture disease*. J Mater Res Technol, 2020, 9(4): 9004-9015
- [4] MACKIEWICZ A., KLEKIEL T., KUROWIAK J., PIASECKI T., BĘDZIŃSKI R., *Determination of Stent Load Conditions in New Zealand White Rabbit Urethra*. J Funct Biomater, 2020, 11(4), 1-9
- [5] KUROWIAK J., MACKIEWICZ A., ET AL., *Evaluation of Selected Properties of Sodium Alginate-Based Hydrogel Material-Mechanical Strength, μ DIC Analysis and Degradation*. Materials, 2022, 15(3), 1-15.
- [6] KUROWIAK J., ET AL., *Changes in the Mechanical Properties of Alginate-Gelatin Hydrogels with the Addition of Pygeum africanum with Potential Application in Urology*. Int J Mol Sci, 2022, 23(19), 1-16
- [7] KUROWIAK J., MACKIEWICZ A., KLEKIEL T., BĘDZIŃSKI R., *Material Characteristic of an Innovative Stent for the Treatment of Urethral Stenosis*. Acta Mech et Automat, 2023, 17(3), 477-484

Numerical analysis of damages chordae tendineae caused by myxomatous mitral valve disease in dogs

A. MACKIEWICZ^{1*}, W. DYLEWICZ¹, J. GACH², I. JANUS², T. KLEKIEL¹, A. NOSZCZYK-NOWAK²

¹Department of Biomedical Engineering, Faculty of Mechanical Engineering,
University of Zielona Góra, Zielona Góra, Poland

²Department of Internal Medicine and Clinic of Diseases of Horses, Dogs and Cats,
Wrocław University of Environmental and Life Sciences, Wrocław, Poland

Key words: *Myxomatous Mitral Valve Disease, Chordea Tendineae, Strain, Finite Element Method*

1. Introduction

Myxomatous Mitral Valve Disease (MMVD) is the most common acquired cardiovascular disease in dogs and accounts for about 75% of cases of chronic heart failure disease [1,2]. This disease is characterized by changes in the histological structure of the valve leaflets and tendon cords (accumulation of collagen fibers and glycosaminoglycans) which causes a significant reduction in the elastic properties of the chordae tendineae in particular and thus affects the pathology of the mechanism of opening and closing of the valve, causing regurgitation of the valve). In many cases, dogs develop a number of complications, such as chordae tendineae rupture, the development of pulmonary hypertension and rupture of the left atrium [3]. Chordae tendineae rupture in degenerative mitral valve disease leads to acute pulmonary edema and worsens the prognosis and general condition of canine patients.

The purpose of this experiment was to determine the mechanical properties of the chordae tendineae of normal and those taken from dogs with MMVD, and to perform a numerical analysis of mitral valve function in both conditions.

2. Material and Methods

The study was divided into 3 stages. In the first stage, observational studies involving the collection of clinical protocols with symptoms and imaging of mitral valve sinus functionality were performed. The next stage involved biomechanical testing of the dissected chordae tendineae from the hearts of died canine patients of the Wrocław University's of Environmental and Life Sciences veterinary clinic. During the study, a static tensile test of the tendon strings was performed on a Zwick/Roell EPZ 005 testing machine at 5 mm/min. Approximately 8 chordae tendineae were cut from one patient, of which 2 were submitted for histological examination (staining with hematoxylin-eosin, Masson-Goldner trichrome and Sirius red methods) to verify the condition of the tissue - with MMVD or intact. In the last step, a numerical model of the mitral valve was made by introducing boundary conditions obtained from echocardiography of the heart and material conditions from biomechanical studies. The geometric model was made in SolidWorks software based on digital images of mitral valve components and custom measurements. The model consisted of with integrated valve leaflets and ring, chordae tendineae and papillary muscles. The model was performed in Ansys Workbench 16.2 software in the Static Structural Module.

*Corresponding author: Agnieszka Mackiewicz, e-mail: a.mackiewicz@iimb.uz.zgora.pl

3. Results

Based on their biomechanical studies, a Young's modulus of 233 MPa was calculated for normal chordae tendineae, while for degenerated chordae tendineae the value was 43 MPa. The deformation characteristics were found to be different for the chordae tendineae coming off the anterior and posterior leaflets. There are maximum longitudinal deformations of 0.53 to 2.60 mm on chordae tendineae from healthy dogs, while for chordae tendineae from dogs with MMVD they range from 0.36 to 2.64 mm. Deformation values were found to be higher for degenerated specimens compared to corresponding healthy specimens. The deformation characteristics on the chordae tendineae coming off the posterior leaflet are similar between analyses.

4. Discussion and Conclusion

The literature describes several studies on chordae tendineae and their structural and biomechanical characteristics, but studies on dogs, especially in genetically stressed breeds, are still lacking. As a result of the study, it has been noted that any change in the geometry and topology of chordae tendineae distribution in the valvular apparatus affects the mechanics of mitral valve function. Studies have shown that changes in the mechanical durability of chordae tendineae are linked to changes in their structure. Chordae tendineae affected by the degenerative process showed lower strength in the tensile test. It is observed that there is a difference in mechanical response between basal and marginal chordae tendineae, in further work it would be worthwhile to use different parameters for them in the numerical model. It was observed that lower mechanical properties for chordae tendineae with apparent degenerative disease affect the phenomenon of mitral valve regurgitation in the numerical model.

Acknowledgments: A project funded by: the National Science Center MINIATURE 6 (DEC-2022/06/X/ST8/01465): *Numerical analysis of effort chordae tendineae caused by myxomatous mitral valve disease in dogs of large and small breeds* – 2022/2023, head of project Agnieszka Mackiewicz,

References

- [1] BORGARELLI M., HAGGSTRÖM J. *Canine degenerative myxomatous mitral valve disease: Natural history, clinical presentation and therapy.* Vet Clin N Am Small Anim Pract. 2010, 40, 651–663
- [2] GACH J., JANUS I., MACKIEWICZ A., KLEKIEL T., NOSZCZYK-NOWAK A. *Biomechanical-Structural Correlation of Chordae tendineae in Animal Models: A Pilot Study,* Animals (Basel). 2021, 4,11(6):1678
- [3] KEENE B.W., ATKINS C.E., BONAGURA J.D., FOX P.R., HÄGGSTRÖM J., FUENTES V.L., OYAMA M.A., RUSH J.E., STEPIEN R., UECHI M. *ACVIM consensus guidelines for the diagnosis and treatment of myxomatous mitral valve disease in dogs.* J Vet Intern Med. 2019, 33, 1127–1140

Sensitivity of biological tissue heating process described by Cattaneo-Vernotte equation with respect to perturbation of lag time

E. MAJCHRZAK^{1*}, B. MOCHNACKI²

¹Silesian University of Technology, Gliwice, Poland

²University of Occupational Safety Management in Katowice, Katowice, Poland

Key words: bioheat transfer, hyperthermia, Cattaneo-Vernotte equation, sensitivity analysis, finite difference method

1. Introduction

The specific internal structure of the tissue causes that the Cattaneo-Vernotte (C-V) equation, e.g. [1], which takes into account the delay time of the heat flux in relation to the temperature gradient (relaxation time), is a more accurate description of thermal processes in the tissue than the classical Pennes equation. So far, this equation has been used with the assumption that the thermophysical parameters of the tissue are constant. In recent years, the several publications appeared, in which (on the basis of experimental studies), the conclusions concerning the significant changes of these parameters with increase the tissue temperature, e.g. [2] were formulated. In the presented work, the C-V equation, which takes into account that the specific thermal capacity of the tissue, its thermal conductivity, metabolic heat source and blood perfusion rate are temperature-dependent is derived. This assumption significantly complicates the basic C-V equation and consequently also the sensitivity model.

The process of intensive heating of biological tissue using a laser beam (hyperthermia treatment) is analyzed. Such treatment is applied, among others, to the destruction of tumor-infected tissue. Due to the laser beam geometry, we consider a cylindrical tissue sub-domain. The dimensions of the cylinder were chosen in such a way that adiabatic conditions could be assumed on its boundary, while the laser action is taken into account by introducing the internal source function to the energy equation (which is a frequently applied approach).

The key parameter in the C-V equation is the relaxation time, which is determined experimentally and the basic aim of this research is the analysis of the connections between the perturbations of lag time and distribution of temperature. Therefore, it seems advisable to conduct a sensitivity analysis methods. The direct approach is used to formulate the sensitivity model. At the stage of numerical calculations, the implicit scheme of the finite difference method was used to solve the task considered. An authorial program realizing the numerical calculations was also developed.

2. Governing equations

The Cattaneo-Venotte equation for temperature-dependent thermophysical parameters derived in this work has the following form

$$C(T) \left(\frac{\partial T}{\partial t} + \tau_q \frac{\partial^2 T}{\partial t^2} \right) + \tau_q \frac{dC(T)}{dT} \left(\frac{\partial T}{\partial t} \right)^2 = \text{div} [\lambda(T) \text{grad} T] + Q + \tau_q \frac{\partial Q}{\partial t} \quad (1)$$

where $C(T)$ is the volumetric specific heat of tissue, $\lambda(T)$ is the thermal conductivity, τ_q is the relaxation time, $T=T(r, z, t)$ is the temperature, $Q=Q(r, z, t)$ is the source function, r, z are the geometric coordinates in the radial and axial directions, t is the time.

*Corresponding author: Ewa Majchrzak, e-mail: ewa.majchrzak@polsl.pl

The source function $Q=Q(r, z, t)$ is the sum of the component related to the blood perfusion, metabolism and laser action $Q_{ex}(r, z, t)$

$$Q(r, z, t) = w(T)c_b [T_a - T(r, z, t)] + Q_{met}(T) + Q_{ex}(r, z, t) \quad (2)$$

where $w(T)$ is the blood perfusion rate, c_b is the specific heat of blood, T_a is the arterial blood temperature, $Q_{met}(T)$ is the metabolic heat source. The mathematical model should be supplemented by appropriate boundary and initial conditions.

3. Sensitivity analysis

Using the direct approach of sensitivity analysis [3] the governing equations should be differentiated with respect to the parameter considered, and then (c.f. equation (1))

$$C(T) \left(\frac{\partial U}{\partial t} + \tau_q \frac{\partial^2 U}{\partial t^2} \right) + \frac{dC(T)}{dT} U \left(\frac{\partial T}{\partial t} + \tau_q \frac{\partial^2 T}{\partial t^2} \right) + C(T) \frac{\partial^2 T}{\partial t^2} + \left(\frac{dC(T)}{dT} + \tau_q \frac{d^2 C(T)}{dT^2} U \right) \left(\frac{\partial T}{\partial t} \right)^2 + \quad (3)$$

$$2\tau_q \frac{dC(T)}{dT} \frac{\partial U}{\partial t} \frac{\partial T}{\partial t} = \text{div}[\lambda(T)\text{grad}U] + \frac{d\lambda(T)}{dT} \text{div}(U\text{grad}T) + \frac{\partial Q}{\partial t}$$

where $U=\partial T/\partial \tau_q$ is the sensitivity function. The boundary and initial conditions should be also differentiated with respect to the relaxation time τ_q .

4. The results and final remark

One of the simulations concerned the tissue heating for $\tau_q = 10$ s, laser intensity $2.6 \cdot 10^5$ W/m² and exposure time 120 s (Fig. 1).

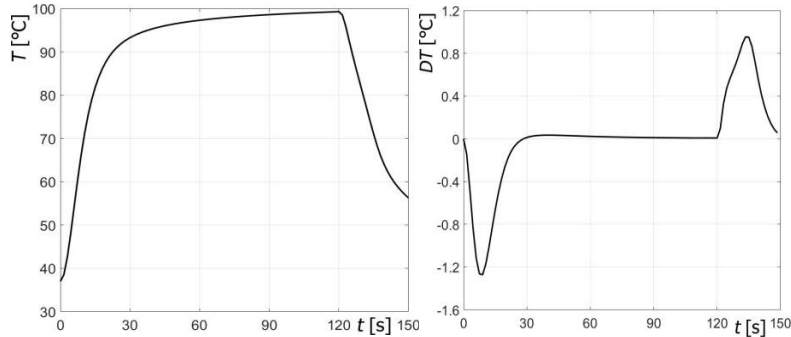


Fig. 1. Temperature history (left) and change of temperature due to the perturbation of 10% of relaxation time at the most heated point (right)

Summing up the research, it should be emphasized that changes in the temperature field caused by perturbations of the relaxation time are visible, but not very large.

Acknowledgements: The research was funded from financial resources from the statutory subsidy of the Faculty of Mechanical Engineering, Silesian University of Technology.

References

- [1] CATTANEO M.C. *A form of heat conduction equation which eliminates the paradox of instantaneous propagation.* Comptes Rendus, 1958, 247: 431-433
- [2] LOPRESTO V. ET AL., *Temperature dependence of thermal properties of ex vivo liver tissue up to ablative temperatures.* Phys Med Biol. 2019, 16,64(10):105016
- [3] KLEIBER M., *Parameter sensitivity in non-linear mechanics.* Willey, London, 1997

Determination of bone stiffness using multi-model optimisation

J. MAŁACHOWSKI*, Ł. MAZURKIEWICZ, K. PIETROŃ, K. SYBILSKI

Faculty of Mechanical Engineering, Institute of Mechanics and Computational Engineering,
Military University of Technology, Warsaw, Poland

Key words: optimization, FEA, bone, mechanical properties, correlation

1. Introduction

The bone structure forms during development and growth, adapting to the level of load carried, hence the variety of its structure. Bone has a hierarchical structure which, at a macroscopic level, is anisotropic. But by analyzing fragments of bone with a very small volume (Voxel), it can be assumed that it is isotropic in this volume. Upon determining the stiffness of each volume, the stiffness of the whole bone should be obtained. The smaller the Voxel volume, the more accurate the representation of the stiffness.

In this paper, the authors proposed a methodology for determining the stiffness of Voxels [1]. In the first step, a simple three-point bending strength test is performed. In the second, using optimization algorithms [3],[4], the stiffness of the Voxels is determined as a function of bone density.

2. Materials and Methods

Beef femurs were used in the study. The bones were cut into small fragments which were then polished. The finished samples (length 80.0 mm, height 12.0 mm and thickness 8.0 mm) were scanned using a high-fidelity CT scanner. Each sample had a distinctive chamfer at one of the corners to help with correct specimen positioning and identification. The samples were subjected to a three-point bending test (Fig. 1). A total of five specimens were prepared and tested from a single bone.

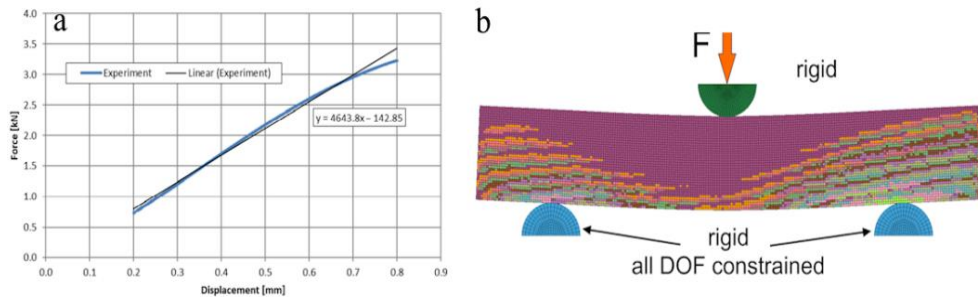


Fig. 1. Three-point bending test - initial set-up (a), scheme loading of the FE model (b)

Based on the experimental results and CT imaging, a numerical model was prepared for each sample. The volume of the models was divided into groups characterized by similar gray scale. It was assumed that in each sample, a specific gray scale level is characterised by the same stiffness value. Optimization analyzes were then carried out with the aim of selecting a stiffness value for each gray scale level, representing each of the experimental tests (Fig. 1), and determining the difference in sample strength (experiment vs. analysis). Optimization was carried out until the smallest difference was summed.

*Corresponding author: Jerzy Małachowski, e-mail: jerzy.malachowski@wat.edu.pl

3. Results

The optimization analyses carried out allowed stiffness values to be determined for each of the 11 gray scale levels. To verify the results obtained, it was decided to perform a three-point bending test for a sixth specimen from the same bone. It was also visualized using CT and a numerical model was prepared analogously to the previous specimens. As a final step, a numerical analysis that reproduces the experimental test was carried out, and the course of force as a function of displacement was compared for both cases (F). The result was found to be satisfactory.

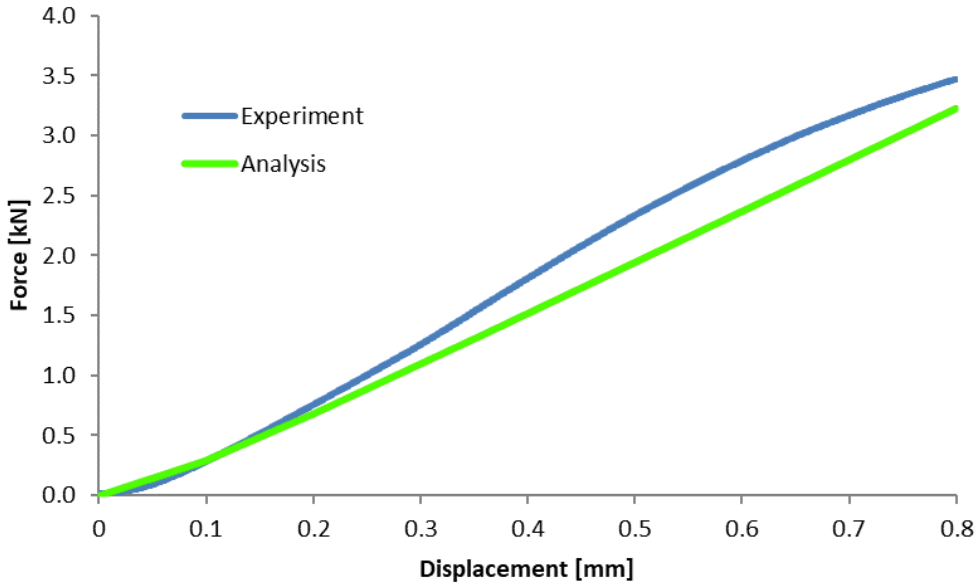


Fig. 2. Comparison of the stiffness of the real specimen and the numerical model for the parameters obtained in the optimisation

References

- [1] PIETROŃ K., MAZURKIEWICZ Ł., SYBILSKI K., MAŁACHOWSKI J. *Correlation of bone material model using voxel mesh and parametric optimization*, *Materials*, 2022, 15: 1-20
- [2] MAZURKIEWICZ Ł., BUKAŁA J., MAŁACHOWSKI J., TOMASZEWSKI M., BUSZMAN P.P. *BVS stent optimisation based on a parametric model with a multistage validation process*. *Mater Des.* 2021, 198, 109363. <https://doi.org/10.1016/j.matdes.2020.109363>
- [3] MAZURKIEWICZ Ł., MAŁACHOWSKI J., DAMAZIAK K., TOMASZEWSKI M. *Evaluation of the response of fibre reinforced composite repair of steel pipeline subjected to puncture from excavator tooth*. *Compos Struct.* 2018, 202, 1126–1135. <https://doi.org/10.1016/j.compstruct.2018.05.065>.

Mechanical characteristics determination of elastomer elements intended for the long gap esophageal atresia treatment

K. MARCULA*, M. KOZUŃ, J. FILIPIAK

Department of Mechanics, Materials and Biomedical Engineering, Faculty of Mechanical Engineering, Wrocław University of Science and Technology, Wrocław, Poland

Key words: *esophageal atresia, uniaxial stretching, elastomers, mechanical properties, soft tissue*

1. Introduction

Esophageal atresia in infants is one of the congenital defects which consists in underdevelopment of a fragment of an esophagus. A problem with proper swallowing, which results in additional symptoms, is caused by this condition. The treatment of atresia consists in surgical reconstruction of the continuity of the esophagus by stretching the undeveloped tissue [1][2].

Current methods of surgical treatment have positive and negative effects. Microdamages in the structure may be caused by an uncontrolled elongation of the tissue, which may lead to the forms of fibrosis and scars, which can negatively affect the biomechanics of the esophageal wall in the further development of the child. The aim of this study was to characterise the mechanical properties of the esophageal tissue in order to enable the search for new methods of treatment. Furthermore, the mechanical properties of the elastomer were characterised, which could be used in the future in alternative methods of surgical treatment.

2. Mechanical properties of soft tissue

The tests were taken on fragments of white Pekin ducks. An uniaxial tensile test was performed at a rate of 10 mm/min until a tissue rupture. By virtue of the test, it was possible to determine the force-displacement characteristics for the stretched samples and to set the tissue stiffness. The tests were carried out on the MTS Tytron 250 testing machine. The research group consisted of 15 fragments of the 50 mm long esophagus. Fig. 1 show exemplary tests results.

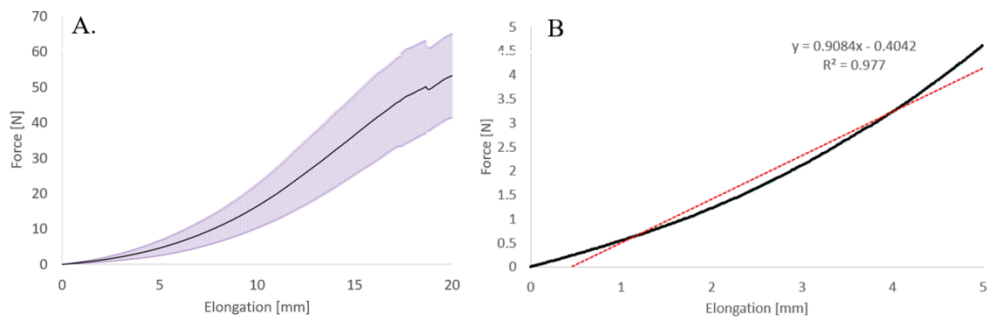


Fig 1. A. Average force-elongation characteristics with standard deviation and B. Low deformation area for averaged force-elongation characteristics, obtained for esophageal tissue

*Corresponding author: Karol Marcula, e-mail: karol.marcula@pwr.edu.pl

3. Force-elongation characteristics of elastomers

The elastomers were subjected to a tensile test of successively: 20, 30 and 40 mm. The return to the initial position took place after reaching the set elongation. The measurement started after reaching the preload with a force of 100 mN, the loading speed was 10 mm/min. 10 samples from each type of elastomers analysed were tested. Based on measurements, the force-elongation characteristics for individual samples were determined (Fig.3). The tests were carried out on the MTS Tytron 250 testing machine, the diagram of the measurement stand is shown in Fig. 2.

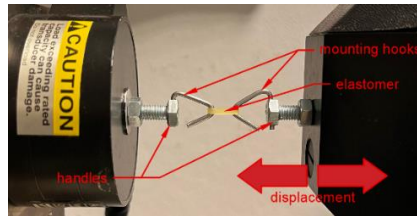


Fig. 2. Scheme of measurement stand for elastomers testing

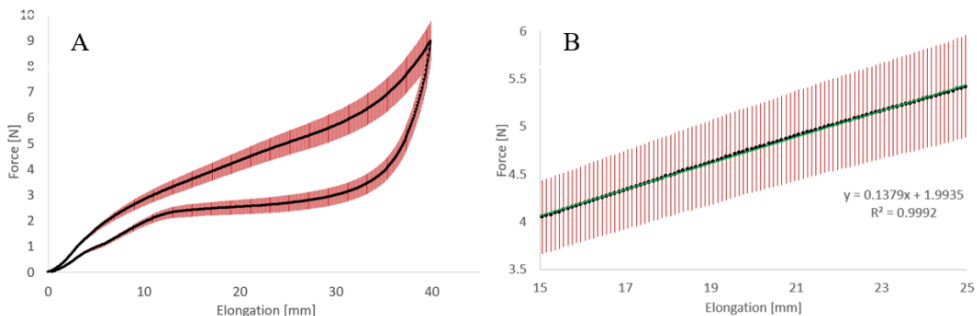


Fig. 3. A. Average force-elongation characteristics and B. Linear force-elongation characteristic fragment, obtained for elastomer during stretching. For both curves the standard deviation is marked

4. Results

As a result of the obtained measurements regarding to the stretching test of fragments of the esophagus, the stiffness of the tissue in the area of low and high deformations was determined. In the case of the low deformation area, the average stiffness was $CN = 0.91 \text{ N/mm} \pm 0.029 \text{ N/mm}$, while in the high deformation area it was $CW = 4.21 \text{ N/mm} \pm 0.22 \text{ N/mm}$. The stiffness of the material in the linear stretching area was determined in the matter of the analysis of elastomers tests (fig. 5). It was $C = 0.14 \text{ N/mm} \pm 0.015 \text{ N/mm}$. It was also observed that the tested elastomer tends to generate a force of similar value in the area of 15 to 25 mm elongation.

5. Conclusion

Taking into account the outcome of stiffness and the ability of the elastomer to generate a force of similar value over a certain area, it appeared that elastomers can be used in alternative methods of surgical treatment of esophageal atresia in infants. At a later stage of the research, an attempt to determine the method of treatment based on susceptible materials will be made.

References

- [1] KOZERA K. ET AL., *Esophageal atresia*. Post N Med, 2017, 11, 625-628
- [2] TOCZEWSKI K. ET AL., *Biomechanics of esophageal elongation with traction sutures on experimental animal model*. Sci Rep, 2022, 12, 3420

Investigation of 24-month biodegradation of PCL scaffolds with the addition of bioglass and Zn using computer microtomography

A. NIKODEM*

Department of Mechanics, Materials and Biomedical Engineering, Faculty of Mechanical Engineering,
Wroclaw University of Science and Technology, Poland

Key words: *dynamic analysis, computer microtomography, time, biodegradation, scaffold, PCL*

1. Introduction

Implantation of a medical device made of biomaterials into the human body is inevitably associated with its degradation, the rate of which determines the nature of tissue healing. This degradation is related to the breakdown of the material into smaller fragments, which are then released from the body. The rate of this decomposition depends on many factors [1] related to both the sample itself (hydrophobicity, type of material, surface) and the environment in which it is implanted (pH, chemical composition). Biomaterials degradation tests are carried out in accordance with the ISO 10993 standard and are related to the measurement of fluids in which samples are incubated and the weight of the scaffold itself. The material itself is also examined by many authors due to the change in the surface of the incubated sample using microscopy methods, e.g. SEM. Tests using computer microtomography, which examine the material in a non-invasive way, give information about changes not so much in surface but in total volume of the tested sample. This type of research, conducted for individual stages of degradation, makes it possible to observe and describe the mechanisms of sample destruction and their dynamics at individual stages of the research. The main objective of the study was the qualitative and quantitative analysis of scaffolds incubated for 24 months in PBS solution.

2. Materials and Methods

The tests were carried out on scaffolds made of PCL with additives such as bioglass and Zn. The main purpose of introducing such additives is to improve the bioactive properties of the tested devices. The scaffolds were prepared by 3D printing using the Oryginal Prusa® i3 MK3 printer, working in the FDM technique. Filaments made by injection molding were used for printing using a hydraulic Babyplast® 6/10P Rambaldi Group injection molding machine. Due to the chemical composition, the samples were divided into 3 measurement groups: the PCL group, the PCL group with bioglass and the PCL group with bioglass and zinc (Zn).

The evaluation of degradation was carried out in several stages: measurement of the physicochemical properties of the incubation fluid (pH, conductivity, concentration of Na⁺, K⁺, Ca²⁺ ions) and the analysis of changes and parameters of scaffolds (mass, sample morphology and volume changes). The analysis of changes in sample volume was performed using a 1172 SkyScan, Bruker® computer microtomograph. Measurements were carried out every 30 days. Samples were selected from each group and registered using the 1172 SkyScan, Bruker® microtomograph with a spatial resolution of 10 μm, with the lamp parameters 40kV/250 mA. The exposure time of a single recording is 315ms, the unit rotation angle is 0.4°. At each stage, the samples were recorded under the same conditions, which then allowed for comparative tests using the Data Viewer® software.

3. Results

*Corresponding author: Anna Nikodem, e-mail: anna.nikodem@pwr.edu.pl

Figure (Fig. 1) shows the volume changes of PCL and PCL samples with bioglass and Zn, comparing steps 6, 12, 18 and 24 to the reference step.

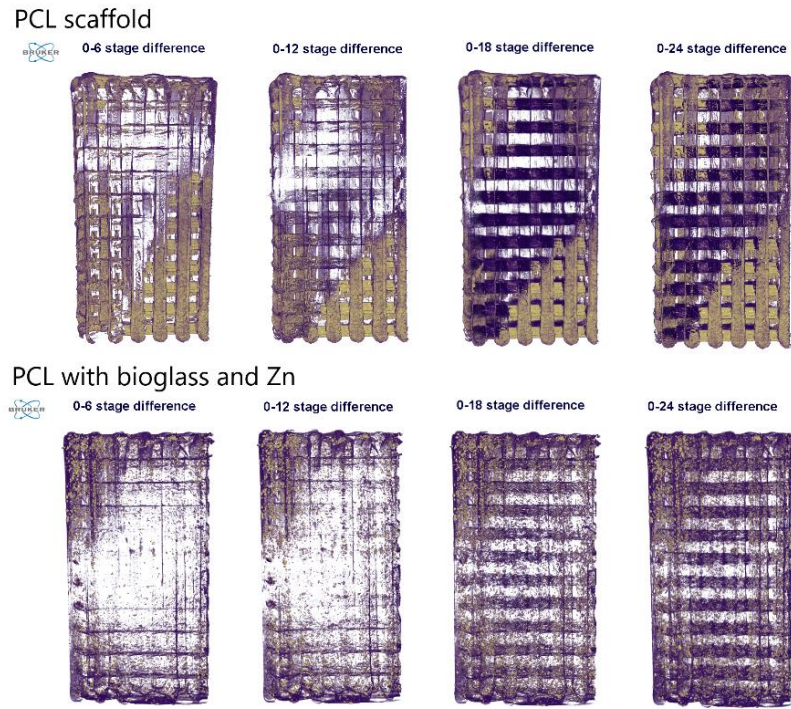


Fig. 1 Comparisons of changes between the reference stage (0) and the next scaffold degradation stage (6, 12, 18 and 24 months) in the PBS solution between the reference measurement. Results for an example sample of pure PCL and PCL with the addition of bioglass and Zn

4. Conclusion

The tests of PCL scaffolds carried out during 24 months indicate a weight loss of about 2%, which is associated with a decrease in volume to 1.8% for pure PCL, 2% for PCL scaffold with the addition of bioglass and as much as 9% decrease in volume after adding Zn. Comparing the research groups with each other, it can be said that the introduction of bioactive additives, the main purpose of which is to stimulate the growth of the peri-implant tissue, and from the point of view of the scaffold itself, accelerates the rate of its bioresorption (Fig.1). In addition, changes in conformation related to the twisting of the incubated samples can be observed.

Acknowledgment: I would like to sincerely thank prof. Izabella Rajzer and PhD Anna Kurowska from the University of Technology and Humanities in Bielsko Biala for preparing and providing samples for the research presented in the work.

References

- [1] HUTMACHER D., *Scaffold design and fabrication technologies for engineering tissues-state of the art and future perspectives*. J Biomater Sci, Polymer Edition, 2001, 12(1): 107-124
- [2] KUROWSKA A., NIKODEM A., ET AL., *Layered PCL scaffolds modified with bioactive additives fabricated by electrospinning and 3D-printing for the nasal bone and cartilage defects*. Mater Des, 2023, 233: 112255

The influence of cyclic loads on the structural properties of the femur bone tissue with osteoarthritis

A.NIKODEM*, M.KOZUŃ

Department of Mechanics, Materials and Biomedical Engineering, Faculty of Mechanical Engineering,
Wroclaw University of Science and Technology, Poland

Key words: *femur, osteoarthritis, cyclic load, dynamic changes, microtomography*

1. Introduction

In osteoarthritis, there are chronic processes of destruction of joint cartilage and formation of defects in it, and hypertrophy of bone tissue in the periarticular area. The disease causes both changes in the structural and mechanical properties of the tissues around the entire joint. The causes of OA are not well understood. There are still only hypotheses about the etiology of this disease, which point to its multifactorial basis and emphasize the importance of such elements as changes in the chemical composition and physical properties of the joint fluid, impaired nutrition of the articular cartilage, increased friction of the articular surfaces, disruption of the blood supply to the joint and accumulation of microcracks especially in the region of subchondral bone tissue [3]. The microcracks formed in the bone are the result of physiological loads resulting from daily activities that affect the human skeleton.

These loads are cyclic in nature, and even though their amplitude is much smaller than the yield stress of bone tissue, they lead to the accumulation of microcracks, cracks and consequently weaken the skeleton, contributing to fatigue damage to bone [1]. The effect of cyclic loading on bone tissue varies depending on the type of this tissue. For spongy tissue, relations between a single loading event and the amount of resulting microdamage have been described [2], but the effect of the number of loading cycles on the accumulation of fatigue-like microdamage is still not described for this tissue.

The problem is also the selection of the load value so that the tested value of simulated loads replicates physiological working conditions. How, then, to select this value so that it does not lead to too rapid and violent destruction of the sample in a high-cycle measurement.

The purpose of this work is to analyze the structural changes of spongy tissue specimens derived from femoral heads, in different stages of cyclic testing.

2. Materials and Methods

The study material consisted of 10x10x10 [mm] cubic specimens from 4 femoral heads obtained from osteoarthritis patients scheduled for hip alloplasty.

Four samples were prepared from each femoral head, of which 1 was the reference sample. The reference specimens were subjected to a destructive uniaxial compression test, and based on this, the amplitude of the loads was determined as (25%-50%) F_{max} , which was used in cyclic tests for specimens from the same preparation. Cyclic tests were conducted using an 858 MTS MiniBionix machine, in compression, at a frequency of 1 Hz.

To determine the changes in specimen geometry and structural properties of specimens subjected to cyclic loading, the specimens were registered using a 1172 SkyScan microtomograph, Bruker. The registration of the samples was carried out in 6 stages: after 100, 500, 1k, 5k, 10k and 50k cycles. All samples were registered with a spatial resolution of 10 μm , with source parameters of 89kV/112 mA, the use of Al+Cu filters, with an exposure time of 1400 ms, and a unit rotation angle of 0.4° to 360°

*Corresponding author: Anna Nikodem, e-mail: anna.nikodem@pwr.edu.pl

rotations. Then, using NRecon® software, the samples were reconstructed and analyzed for changes occurring in DataViewer®, Bruker.

3. Results

The use of computed microtomography allowed us to obtain both qualitative results, presenting them as changes in the geometry of the test specimen during successive stages of cyclic loading (Fig. 1A, B), and quantitative results. Example values of BV [%] and BS/BV [1/mm] parameters are shown in Fig. 1C.

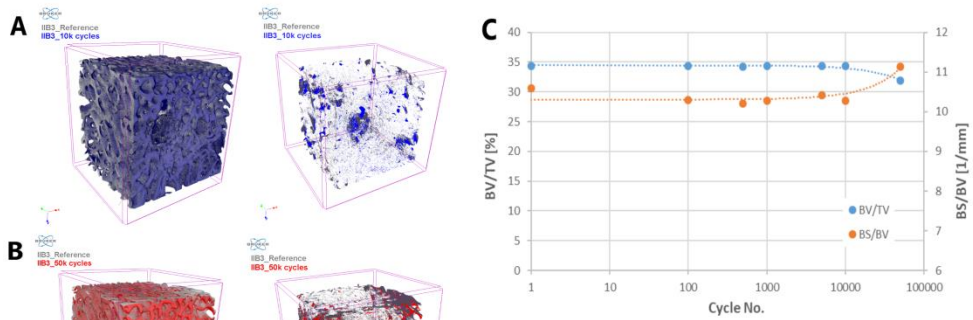


Fig. 1 Comparisons of changes in the geometry of exemplary trabecular bone tissue subjected to cyclic testing: A. after 10k cycles; B. after 50k cycles; C. Comparison of BV/TV [%] and BS/BV [1/mm] parameter values

4. Conclusion

The research conducted shows how important a parameter in cyclic testing is the selection of an appropriate load value. In the study, 2 specimens failed in successive loading steps, even though we selected the loading values based on a reference specimen from an adjacent site of the same femoral head. However, after analyzing the results, we found that these samples had lower density values. Therefore, in this type of study, it is very important to take into account the individual physical (density), structural and mechanical properties of each patient and even the sites from which we prepare samples when selecting load values. In our study, differences in density values within the head alone were as high as 20%. For the other samples, the load value was so well chosen that even at 10k cycles, the greatest changes in the geometry and structure of the test sample were observed at the points of load application.

Acknowledgment: The study material came from patients undergoing hip alloplasty at the Clinical Department of Orthopaedic and Traumatologic Surgery, Wrocław Medical University, and was part of project No. N N518 505139 funded by the National Science Centre.

References

- [1] RAPILLARD L., CHARLEBOIS M., ZYSSET P.K. *Compressive fatigue behaviour of human vertebral trabecular bone*, J Biomech, 2006, 39: 2133-2139.
- [2] ACEVEDO C., STADELMANN V.A., PIOLETTI D.P., ALLISTON T., RITCHIE R.O. *Fatigue as the missing link between bone fragility and fracture*. Nat Biomed Eng. 2018, 2(2):62-71
- [3] NIKODEM A. *Correlations between structural and mechanical properties of human trabecular femur bone*. Acta Bioeng Biomech. 2012;14(2):37-46

Application of Transformer-Based Neural Networks in the Cells Segmentation Task in Fluorescent Microscopic Images

G. OSTROWSKI*, M. PAWLKOWSKI, P. GARBACZ

Warsaw University of Technology, Warsaw, Poland

Key words: *computer vision, cell segmentation, biological analysis, neural networks*

1. Introduction

Image segmentation is a process of recognizing objects in the picture and highlighting region of the array containing objects of interest. Along with the progress in the machine learning methods the computer vision field have adopted multiple algorithms. For many years, application of convolutional deep neural networks had been the most widely adopted solution, until the new method has arrived. The rise of long attention models, one of which is transformer algorithm, was the dawn of modern large language models, which have also greatly impacted the field of the computer vision and image segmentation. [4]

One of the key challenges in the analysis of a cell culture or a tissue specimen is recognizing and selecting boundary of the desired objects. That information can be utilised to analyse the state of the cells, to perform statistical analysis on the culture or to isolate the desired item from the image for further analysis. For example, segmentation analysis can be performed on fluorescent microscopy images to derive information about ongoing processes inside the cell. With the utilisation of the image segmentation techniques the analysis can be performed automatically or semi-automatically with precision reaching the human level but with far smaller time cost. Information gathered during this process can be later used in the statistical analysis of the colony, anomaly detection in the cells behaviour or for the inference and parametrization of predictive mathematical models of the biological processes. [3]

2. Materials

The aim of the study was to perform cell segmentation on fluorescent microscopic images of cells. The model was able to discern the cells from the background, noise and other cells. On top of that the algorithm was supposed to perform the analysis on different channels of the fluorescent images with minimal training data.

The program uses pretrained and finetuned *Segment Anything Model* (SAM) [2] for proposing cell masks. The segmented masks are then postprocessed and validated. The training dataset used for training the model to recognize the nuclei was *An annotated fluorescence image dataset for training nuclear segmentation methods* [1]. Dataset contains 79 images of cell nuclei with annotations. The inference dataset used for testing the capabilities of the program was the *Human Protein Atlas - Single Cell Classification* released during the classification challenge [5]. The dataset holds over eighty thousand images containing information about the cell nuclei, microtubule, protein and endoplasmic reticulum. Example of the image from the test dataset is presented in the Fig. 1A.

*Corresponding author: Gustaw Ostrowski, e-mail: gustaw.ostrowski.dokt@pw.edu.pl

3. Results and Discussion

Prepared program creates masks for each cell. Generated output recognise cells on each image channel, as can be seen in the Fig. 1B.

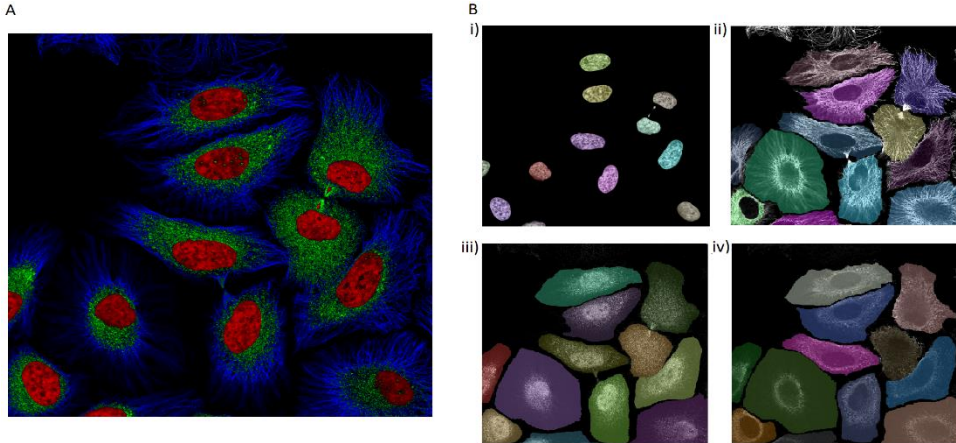


Fig. 1. A – original fluorescence microscopy image. B - segmentation masks overlaid with the original image channels: i) nuclei, ii) microtubules, iii) protein, iv) endoplasmic reticulum

Proposed segmentation pipeline is capable of recognizing and separating cells and their body parts from fluorescence microscopic images with minimal training as presented above. Program have been tested on multiple images with satisfactory results. As for the future development it might be advisable to finetune model weights for better prediction and separation objects on the microtubule, protein and endoplasmic reticulum channels.

References

- [1] KROMP F., BOZSAKY E., RIFATBEGOVIC F., ET AL. *An annotated fluorescence image dataset for training nuclear segmentation methods*. Sci Data2020, 7, 262. <https://doi.org/10.1038/s41597-020-00608-w>
- [2] KIRILLOV A., ET AL., *Segment Anything*, arXiv:2304.02643, 2023, <https://doi.org/10.48550/arXiv.2304.02643>
- [3] WEN T., TONG, B., LIU Y., ET AL., *A review of research on the instance segmentation of cell images*, Comput Methods Programs Biomed. 2022, 227:107211
- [4] YU Y., WANG C., FU Q., ET AL, *Techniques and Challenges of Image Segmentation: A Review.*, Electronics 2023, 12, 1199. <https://doi.org/10.3390/electronics12051199>
- [5] *Human Protein Atlas - Single Cell Classification 2021*, accessed: 20 may 2023, <https://www.kaggle.com/c/hpa-single-cell-image-classification>

Investigating Pediatric Head Trauma in Unmanned Aerial Vehicle Accidents

R. PERZ*

Faculty of Power and Aeronautical Engineering, Institute of Aeronautics and Applied Mechanics, Warsaw
University of Technology, Warsaw, Poland

Key words: *Unmanned Aerial Vehicle, UAV accidents, Head Trauma Injuries*

1. Introduction

Unmanned aerial vehicles (UAVs) are devices widely used in various areas of human activity. The main advantage of UAVs is their ability to wirelessly record video, audio and also other types of data. An additional advantage of the widespread use of drones is the extensive range of manufacturers providing UAVs with a variety of parameters (dimensions, weight, speed, range, etc.), equipped with various accessories (cameras, microphones, sensors, etc.). The ever-increasing use of UAVs generates a number of safety risks, including human health and life, posed by the right to impact. The degree of human injury during a collision with a UAV depends on the circumstances of the incident (speed, mass of the UAV) and the physical conditions of the person hit. Among those at risk of the most severe impact are children, due to their early stage of development of body systems, such as the skeletal system. Particular risks are posed by blows to the head, which can cause concussion and, in extreme cases, even death [1],[2].

The objective of this paper was to experimental estimate the head injuries occurring in a 3-year-old child during an hit of an unmanned aircraft from different directions. The severity of injuries during impact was determined by determining the Head Injury Criterion (HIC) and correlating the results obtained with the Abbreviated Injury Scale (AIS). The research was carried out using the author's research methodology, including the use of an auto test rig and the author's UAV model.

2. Materials and Methods

The investigation of head injuries of a 3-year-old following a UAV impact was carried out based on the author's research methodology of determining negative health consequences based on the HIC value compiled with the AIS scale. HIC is commonly used in the estimation of head injuries during crashes and requires the recording of acceleration values and duration, according to formula (1). The AIS is a 6-point health consequence scale determined by formula (2) where 0 means no injury and 6 means certain death. The AIS scale assumes that the higher the HIC value, the more severe the health consequences [1],[2].

$$HIC = \left(\frac{1}{t_2 - t_1} \int_{t_1}^{t_2} a dt \right)^{2.5} (t_2 - t_1) \quad (1)$$

$$AIS = \begin{cases} C_{HIC}^{AIS1} HIC & (HIC \leq 25) \\ C_{HIC}^{AIS1} HIC + Offset_{HIC}^{AIS2} & (HIC > 25) \end{cases} \quad (2)$$

In order to collect the data necessary to determine the HIC, a test stand was prepared, which was a launcher with which the UAV was shot towards the head. The stand consisted of a trolley mounted on profiles to which elastic bands were attached to pull the trolley with the UAV on it. The trolley's impact forces were recorded with an EMS70 force sensor, allowing the UAV's velocity during impact to be calculated based on the principle of conservation of momentum. A mannequin head of a 3-year-old

*Corresponding author: Rafał Perz, e-mail: rafal.perz@pw.edu.pl

child, manufactured by Humanetics Innovative Solutions, Inc, model Q3, equipped with an Endevco 7264C accelerometer set, was used for the tests. Each impact was recorded with a high-speed NAC HX-3 camera, with a 35mm lens. The UAV used for the tests was an infused T300 carbon fibre and epoxy resin UAV, measuring 30cm x 30cm and weighing 260g. The geometry reference was a Phantom 2, from manufacturer DJI, mapped on a smaller scale. Measurements were carried out for impacts to the head from four directions: front, back, left and right. For each variant, 10 impacts were carried out, from which the HIC and drone velocities at impact were determined. The results of the HIC values were compared with the AIS scale, from which the effects of injury were determined for each impact variant.

3. Results

The results of the tests are presented in Fig. 1, where the UAV speeds at each impact are indicated, and in Fig. 2, where the HIC results are compared with the AIS scale.

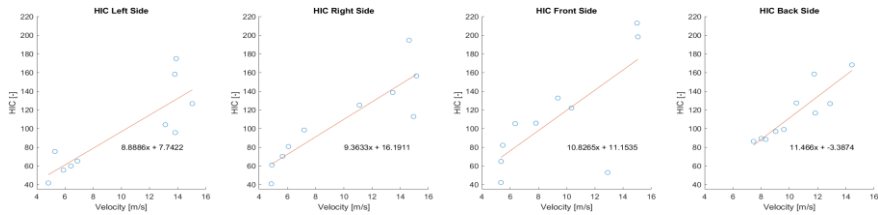


Fig. 1. HIC and velocity results

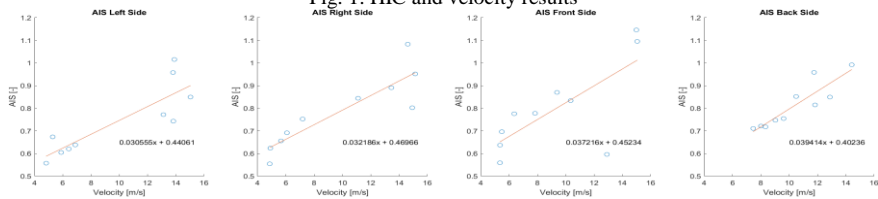


Fig. 2. HIC and velocity results

4. Discussion and Conclusions

The collected results demonstrate, head accelerations during UAV impacts increased with increasing drone speed. HIC values for UAV speeds below 10 m/s reached a maximum of about 140. Impacts at about 14 m/s generated a HIC value of 180. It was observed that impacts to the head from all sides translated into similar HIC values. The juxtaposition of the HIC results with the AIS scale indicates that, for the adopted test scenario, the UAV impact did not lead to significant head injuries to the 3-year-old child. The age of the victim was taken into account when analysing the HIC scores and their mapping with the AIS scale. Simulation and experimental results [1] indicated that a drone falling from a height of 30 - 50 ft can induce a HIC value of approximately 16 - 56. An impact to the head of a DJI Phantom III [2] at a velocity of 8 - 10 m/s translates into a HIC value of 150 - 250. The results of the study remain consistent with the results of other post-measurements presented in [1],[2]. Further testing is required with heavier weight vessels on an upgraded stand, providing the ability to adjust the speed of the UAV. This will enable full recognition of head injuries to a 3-year-old child associated with drone impact.

References

- [1] KOH C.H., LOW K.H., ET AL., *Estimation of weight threshold of falling UAVs (Unmanned Aerial Vehicles) based on impact energy*. Transp Res Part C Emerg. 2018, 93, 228-255
- [2] RATTANAGRAIKANAKORN B., GRANSDEN D.I., ET AL., *Multibody system modelling of unmanned aircraft system collisions with the human head*. Int J Crashworthiness, 2020, 25:6, 689-707

Fluoride release and selected chemo mechanical characteristics of three different commercially available dental materials for sealing

A. PISZKO^{1*}, A. NIKODEM², P. PISZKO³, M. DOBRZYŃSKI¹

¹Department of Paediatric Dentistry and Preclinical Dentistry Wrocław, Wrocław Medical University, Wrocław, Poland

²Department of Mechanics, Materials and Biomedical Engineering, Faculty of Mechanical Engineering, Wrocław University of Science and Technology, Wrocław, Poland

³Department of Polymer Engineering and Technology, Faculty of Chemistry, Wrocław University of Science and Technology, Wrocław, Poland

Key words: biomaterials, dentistry, fluoride, sealant, mechanical properties

1. Introduction

One of the most effective ways to prevent the formation of caries, especially in cavities, fissures, cracks or microdamages of the enamel, are fissure sealants developed in the 1960s. Caries has become a civilization disease, which, due to lifestyle, develops more and more often in younger and younger patients. [1]. Lacquers are polymer composites based on resins, which additionally contain many chemical substances, such as: solid fillers, i.e. barium-aluminum-silicon glass, fire silica and titanium dioxide, as well as additional photoinitiators, catalysts, pigments or inhibitors that delay the rate of various reactions. The effectiveness of sealants depends on their chemical formula and chemo mechanical characteristics, such as hydrophilic/hydrophobic character, microstructure and homogeneity of the layers or marginal tightness. The aim of the work was a comparative analysis of the physicochemical properties of selected fissure sealants.

2. Material and Methods

The material for the study consisted of 3 different materials commercially introduced to the market and used in dental surgeries in terms of chemical composition (Table 1). Cylindrical samples with dimensions of 6x2.5 [mm] (diameter x height) were prepared in a special form from each material.

Table 1. Materials for sealing evaluated in the study

| Material | Manufacturer | Composition |
|-----------------|--------------|--|
| Flow-Color | Arkona | dimethacrylate resins: Bis-GMA, TEGDMA, UDMA, Bis-EMA, Mineral fillers, Al-Ba-B-Si glass, Ba-Al-B-F-Si glass, pyrogenic silica, pigments |
| Fissure Sealant | Arkona | Bisphenol A diglycide ether dimethacrylate, urethane dimethacrylate, triethylene glycol dimethacrylate, barium-aluminum-silicon glass, barium-aluminum-boron-fluorine glass, fire silica, titanium dioxide), photoinitiators, inhibitors, catalysts, stabilizers, pigments |
| Flow-It | Pentron | Filler, 2,2'-ethylenedioxy dimethanol dimethacrylate, ethoxylated bisphenol A-dimethacrylate, Bis (1,2,2,6,6-pentamethyl-4-piperidyl) sebacate |

2.1. Water contact angle (WCA)

Surfaces with increased hydrophobicity are assumed to be more resistant against attack by water or water-soluble species [2]. The cell surface of bacterial strain *S. Mutans* which is a pathogen causing caries, was classified as hydrophobic. Values of WCA are depicted at the Fig 1A.

*Corresponding author: Aleksandra Piszko, e-mail: . aleksandra.piszko@student.umed.wroc.pl

2.2. Fluoride release

Fluorine release studies were performed with a use of an ORION 9609 ion-selective electrode (Thermo Fisher Scientific Co., Waltham, MA, USA) connected to a pH/ion meter CPI-551 Elmetron microcomputer. Measurements of fluoride ions ($\mu\text{g}/\text{mm}^2/\text{h}$) performed at intervals of 3, 24, 24, 48, 72 and 96h, and 1, 2, 3, 4, 5, 6 and 7 weeks in artificial saliva at 4 pH values (4.5; 5.5; 7; 7.5).

2.3. Mechanical tests

Microhardness tests were carried out using the CSM MicroCombi Tester using a Vickers (HV) indenter. During the measurement, the indenter was introduced perpendicularly to the surface of the samples with a force of 400 mN, deforming them for a period of 10s [3].

2.4 FT-IR analysis

All of the evaluated sealants contain various methacrylate derivatives as a matrix. The major difference in their composition is in the filler and additions, hence their difference in clinical properties. FT-IR analysis is shown at the Fig. 1B.

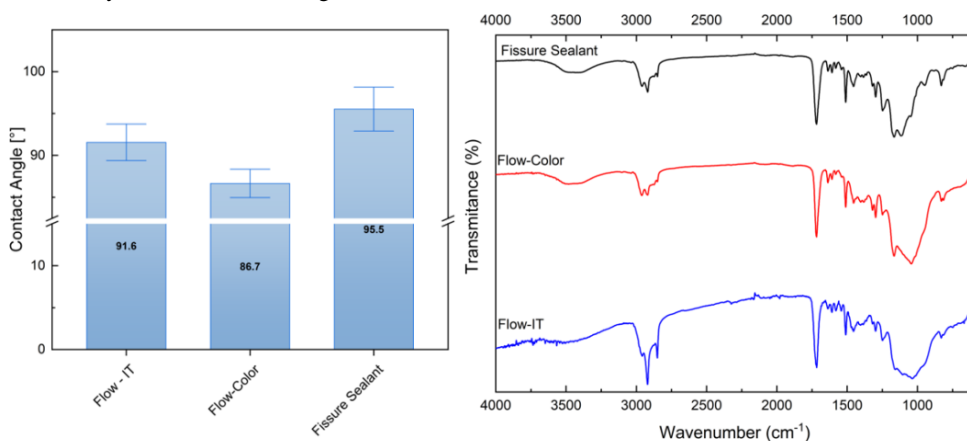


Fig 1. A. Water contact angle of analysed materials; B. FT-IR spectra of evaluated sealants measured in the range of 4000-400 cm^{-1}

3. Conclusions

The conducted research showed that each of these materials is characterized by different values of operational parameters. The highest Young's modulus values were obtained for the Fissure Sealant material (12.6 MPa). It is particularly visible in the case of mechanical tests, here the variances reach even 300%. Also this material was characterized by the highest average hardness value HV 51.9 and the value of the contact angle. The lowest values were obtained for Flow-IT sealant.

References

- [1] AHOVUO-SALORANTA A., FORSS H., WALSH T., NORDBLAD A., ET AL., *Pit and Fissure Sealants for Preventing Dental Decay in Permanent Teeth*. Cochrane Database Syst Rev. 2017, 31;7(7):CD001830
- [2] RUERMANN S., BERGMANN N., BEIKLER T., RAAB W.H., JANDA R. *Bacterial viability on surface-modified resin- based dental restorative materials*. Arch Oral Biol. 2012, 57(11):1512-21
- [3] KOSIOR P., KLIMAS S., NIKODEM A., ET AL., *An in vitro examination of fluoride ions release from selected materials - resin-modified glass-ionomer cement (Vitremer) and nanohybrid composite material (TetricEvoCeram)*. Acta Bioeng Biomech, doi: 10.37190/ABB-02251-2023-01

Concept of mechatronic device for supporting balance during locomotion with the function of recording kinematic parameters

P. PROCHOR*, A. SZCZERBA, S. PISZCZATOWSKI

Institute of Biomedical Engineering, Białystok University of Technology, Białystok, Poland

Key words: balance disorders, elderly, locomotion, mechatronics

1. Introduction

Elderly, due to limitations typical for their age, such as chronic diseases or social isolation, are an important group among people with special needs. It is a group present in society regardless of the development of medicine or social changes, thus causing the occurrence of constant and necessary needs to be fulfilled. One of these needs is independent locomotion, which directly affects their quality of everyday life. Balance disorders occurring in the elderly are one of the most common obstacles in their independent locomotion [1]. Symptoms of balance disorders, perceived by the patient as subjective dizziness, are one of the three most commonly reported complaints. For people aged 65 years, their frequency is about 30%, while for elderly aged 80 and above, about half of the population struggles with this problem. In addition to social impairment, which causes i.a. a number of mental disorders, the impossibility of independent locomotion also causes physical changes in the body (reduced bone density, disorders in the digestive and respiratory systems, reduced efficiency of the heart muscle). In the absence of taking physical activities these changes deepen over time, contributing to the emergence of new dysfunctions and diseases of all body systems [2]. Ultimately, this process often results in the premature death, which can be prevented by the use of appropriate assistive devices independent locomotion.

2. Design assumptions

The device planned for development will be able to support balance during locomotion, in five ways, by:

Method I – ensuring the possibility of developing an individual and effective treatment and rehabilitation process, based on the information provided by the device, collected during the user's daily activities (habits, incorrect posture, dysfunctions of the musculoskeletal system),

Method II – active stimulation of postural correction and behaviour to assist in maintaining balance during locomotion,

Method III – monitoring the rehabilitation process by analysing the improvement in the efficiency of performing specific exercises,

Method IV – developing appropriate habits in terms of maintaining balance by the user,

Method V – comparison of the results from the device with subjective scales, such as e.g. DHI (Dizziness Handicap Inventory scale), for the purpose of psychological therapy making the patient aware of the actual objective degree of his disability.

In order to implement the assumed functionalities, it is important to provide the device with features such as:

Recording spatial kinematic parameter, during the performance of normal everyday duties, responsible for maintaining proper balance during locomotion. These parameters will be analysed with

*Corresponding author: Piotr Prochor, e-mail: p.prochor@pb.edu.pl

the use of artificial intelligence algorithms and used to: a) diagnose the causes of balance disorders and plan the treatment and rehabilitation process, b) control operation of the compensating mechanism,

1. The use of compensatory mechanisms, which, depending on the analysis of kinematic parameters during imbalances, will actively assist in maintaining balance during locomotion,
2. Ensuring small dimensions and weight of the device by using miniature sensors and placing the recording system and compensating mechanisms in wearable textile vest, possible to be used under the outer clothing. This will allow for long-term use of the device and will give the possibility of a realistic assessment of factors contributing to the loss of balance in everyday life conditions and the possibility of developing appropriate habits in correction of posture and behaviours, minimising the risk of losing balance.

3. Prototype

Appropriate placement of sensors is crucial for obtaining viable kinematic parameters. In Fig. 1a, we have suggested positioning of sensors to monitor human body pose, that is visualised in Fig. 1b. Simplified version of the system in the form of flexible vest, allowing to monitor body falls, was presented in Fig. 1c. All suggestions and designs are a matter of future studies.

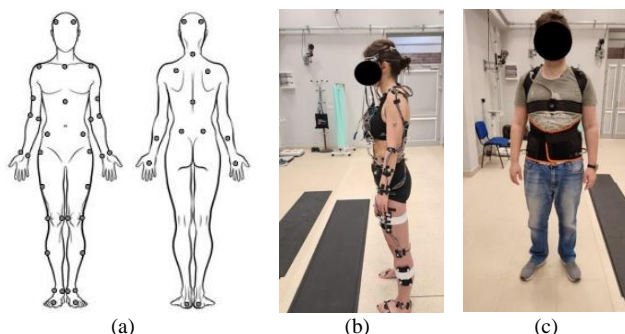


Fig. 1. Suggested sensors setup on human body: a) sensors positioning, b) direct placement of sensors on human body, c) a prototype of the flexible vest for recording kinematic parameters – sensors on limbs were neglected for simplification purposes in initial version of the system (more sensors can be added in future studies)

4. Predicted effect

The device in the form of a vest, will increase not only the range of movement of the user, but also increase his sense of safety while performing everyday activities. Moreover, awareness of the independence of the performed activities will also increase a person's self-esteem, contributing to the increase in the number of undertaken activities. The use of the feedback aspect between the patient and the device will make it possible to help him to trust the therapy he is undergoing to a greater extent, which will significantly increase the likelihood of the rehabilitation process being effective.

Acknowledgments: This research was funded by the National Center for Research and Development, as a part of the governmental 'Accessibility Plus' program competition entitled 'Things are for people'. Project: 'Mechatronic device to assist in maintaining balance during locomotion with function of recording gait kinematic parameters', contract no. Rzeczy są dla ludzi/0009/2020.

References

- [1] EIBLING D. *Balance Disorders in Older Adults*. Clin Geriatr Med, 2018, 34(2), 175-181
- [2] CUEVAS-TRISAN R. *Balance Problems and Fall Risks in the Elderly*. Phys Med Rehabil Clin N Am, 2017, 28(4), 727-737

Analysis of tribological properties of prosthetic materials under different conditions of use

A. PTAK*, A. TOMCZAK

Department of Fundamentals of Machine Design and Mechatronic Systems, Faculty of Mechanical Engineering
Wrocław University of Science and Technology, Wrocław, Poland

Keywords: prosthetic materials, tribology, wear, coefficient of friction

1. Introduction

Oral diseases are common for many people worldwide, causing pain and discomfort. It is estimated that about 3.5 billion people suffer from it. According to a 2022 WHO report, the estimated global average incidence of total tooth loss is almost 7% among people aged 20 years and over, accounting for approximately 350 million cases. For people aged 60 and older, the prevalence is already 23%. According to research conducted in 2018, 43.9% of toothless people aged 65-74 in Poland. Knowledge of the properties of dental materials is of great importance in dental prosthetics. For this reason, selecting appropriate dental materials is crucial to obtain durable, aesthetic and functional prosthetic solutions. Therefore, the primary purpose of this work was to determine the tribological characteristics of materials used in dental prosthetics, which will be the basis for their qualitative analysis.

2. Tribological investigations

2.1. Methodology

Three materials used for prosthetic components were selected for this study: zirconium oxide, PMMA and composite material. Tribological tests were carried out using reciprocating motion, where the cooperating element was a stainless steel ball. The tests were carried out for three loads in different friction conditions. To simulate different working environments, the tests were carried out in conditions of technically dry friction, in the presence of artificial saliva, and with the addition of nuts and carrots.

2.2. Results

Tribological tests allowed us to obtain primary data enabling the description of the tribological properties of the tested materials. In the experiment, static and kinetic friction coefficients were determined (Fig. 1), and the wear was qualitatively described (Fig. 2).

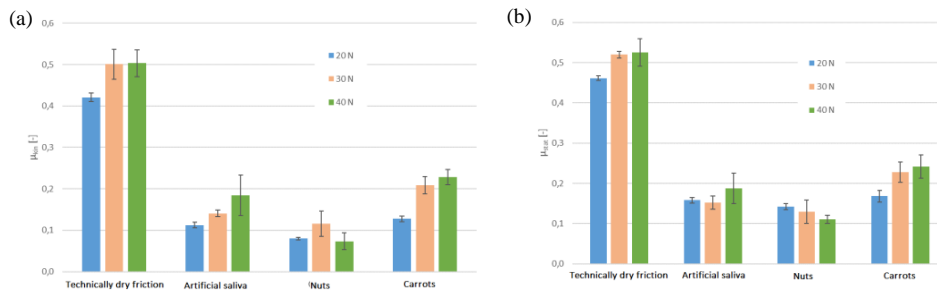


Fig. 1. Examples of graphs of the average values of the coefficient of friction
(a) static and (b) kinetic for a sliding pair with PMMA

*Corresponding author: Anita Ptak, e-mail: anita.ptak@pwr.edu.pl

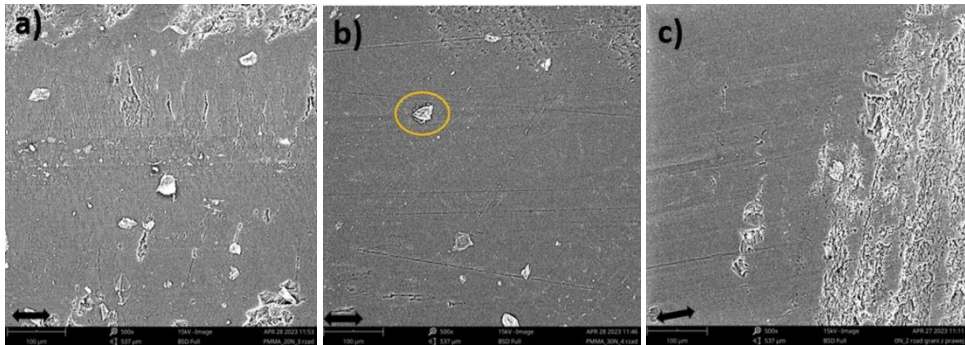


Fig. 2. Examples of PMMA friction surfaces after the experiment (a) in conditions of technically dry friction (b) with artificial saliva (c) with nuts

3. Summary

The research conducted in this paper shows the effect of food intake and the presence of lubricant on frictional resistance and wear of prosthetic materials. The highest wear resistance characterizes zirconium oxide. However, attention should also be paid to the high friction coefficients achieved by this material. In the conditions of technically dry friction, much greater surface wear of all tested materials was observed than during the use of lubricants in the form of artificial saliva or food. This confirms the important role of saliva and oral lubrication.

References

- [1] FOULY A., IBRAHIM A.M.M., SHERIF E.S.M., FATHEL-BAB A.M.R., BADRAN A.H. *Effect of low hydroxyapatite loading fraction on the mechanical and tribological characteristics of poly(Methyl methacrylate) nanocomposites for dentures*. Polymers (Basel). 2021,11,13(6):857
- [3] ZHANG H., SUN Y., GUO J., MENG M., HE L., TAY F.R., ZHANG S. *The effect of food medium on the wear behaviour of veneering porcelain: An in vitro study using the three-body abrasion mode*. J Dent. 2019, 83:87-94
- [4] <https://www.who.int/news-room/fact-sheets/detail/oral-health> (download date: 20.03.2023).
- [2] ZAFAR M.S. *Prosthetic applications of polymethyl methacrylate (PMMA): An update*. Polymers (Basel). 2020, 8,12(10):2299
- [3] WIŚNIEWSKA G., ORCZYKOWSKA M. *Biomechaniczne warunki okluzyjne narządu żucia w warunkach normy fizjologicznej i po całkowitej utracie uzębienia - W świetle piśmiennictwa oraz na podstawie badań własnych (in polish)*. Protet Stomatol. 67 (2017) 277–286.
- [4] EL-TAMIMI K.M., BAYOUMI D.A., AHMED M.M.Z., ALBAIJAN I., EL-SAYED M.E. *The Effect of Salinized Nano ZrO2 Particles on the Microstructure, Hardness, and Wear Behavior of Acrylic Denture Tooth Nanocomposite*, Polymers (Basel). 2022,12,14(2):302

Analysis of implant-bone junction fracture induced by force impulse in traffic collision

D. PYKA^{1*}, A. NOWICKI², Ł. PAŁKA³, A. KURZAWA⁴, K. H. KRAWIEC¹, K. JAMROZIAK¹

¹Department of Mechanics, Materials and Biomedical Engineering, Faculty of Mechanical Engineering, Wrocław University of Science and Technology, Wrocław, Poland

²NZOZ Reg-Med Sp. z o.o., Żary, Poland

³Diamante Dental Clinic, Lubin, Poland

⁴Department of Lightweight Elements Engineering, Foundry and Automation, Wrocław University of Science and Technology, Wrocław, Poland

Key words: dental implants, airbags, traffic accident, numerical analysis

1. Introduction

Data analyses have shown that 1.2 million people die and 50 million are injured every year as a result of traffic accidents [1]. Developments in technology and engineering are contributing to ever more effective safety systems. In passenger cars, airbags are one such system. While prosthetics and engineering may seem like two separate disciplines, by interweaving the two it is possible to conduct advanced strength and optimisation studies of implant-tissue associations in a variety of use and loading situations including airbag deployment [2],[3]. In this paper, the authors show how different types of implants and their placement affect the jaw after loading it with an impulse impact induced by an airbag explosion.

2. Materials and Methods

2.1. Research material

Four types of screw implants made of Ti6Al4V titanium alloy, complying with EN 868-3.5 and ISO 11607-2 by SterileRight, were used in the study. Fig 1 shows the selected three conical screw implants and one cylindrical screw implant. The implants were inserted into jaw models made by the manufacturer Promedicus, which are made from materials with parameters identical to those of human bone. Table 1 shows the properties of the four samples prepared. The implant for sample S1 was placed in the location of the canine, and for the other specimens symmetrically in the jaw model.



Fig. 1. Implants used in the study

*Corresponding author: Dariusz Pyka, e-mail: dariusz.pyka@pwr.edu.pl

Table 1. Summary of tested samples.

| Sample no. | S1 | S2 | S3 | S4 |
|---------------------|---------|---------|---------|-------------|
| Number of implants | 1 | 6 | 6 | 6 |
| Shape | conical | conical | conical | cylindrical |
| Implant diameter | M4 | M3.5 | M3 | M4 |
| Implant length [mm] | 20 | 10 | 12 | 8 |
| Jaw model | 10-1020 | 10-1040 | 10-1040 | 10-1040 |

2.2. Experimental studies and numerical analysis

Four airbag bursts were initiated, one for each sample. Using a high-speed camera, the process was recorded at 0.02 ms, according to cushion inflation time standards. Strength calculations of the screw-bone contact were carried out in ABAQUS. The Johnson-Cook (J-C) constitutive model for elastic-plastic materials of titanium alloy including the plastic part was used. Tetra elements were used for discretisation and the system itself was modeled as symmetrical with respect to the sagittal plane of the human figure. Example results are presented in Fig. 2.

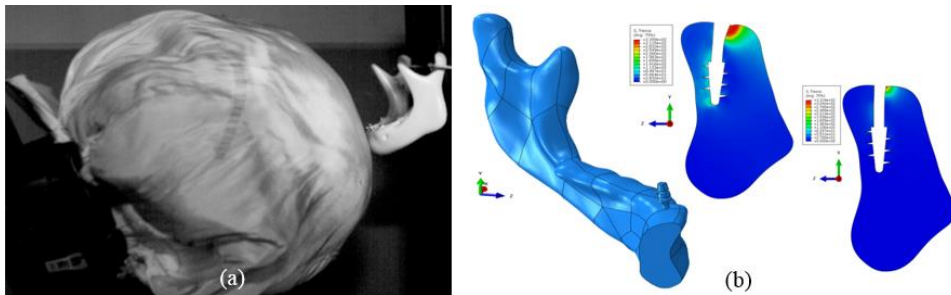


Fig. 2. Results for sample S2: (a) airbag detonation, (b) numerical model of the screw-bone of the mandible

3. Results and Discussion

The impulse impact of the airbag on samples S3 and S4 caused it to fracture at the insertion point of one of the six implant screws. By using a high-speed camera, it was possible to record the moment of fracture of the mandible after the airbag impact. Implant insertion into bone has a debilitating effect on its dynamic strength. The thread shapes and geometric dimensions of the implants (length, diameter) influence the stress concentration at the mandibular-implant interface. Implants that form a larger active surface area with the bone are less likely to fracture. Numerical analysis of the impact event caused by the airbag impact confirms the results obtained experimentally.

Acknowledgments: Calculations have been carried out in Wrocław Centre for Networking and Supercomputing (<http://www.wcss.pl>), grant No. 452

References

- [1] PRENTKOVSKIS O., SOKOLOVSKIJ E., BARTULIS V. *Investigating traffic accidents: A collision of two motor vehicles*. *Transport*, 2010, 25(2), 105-115. doi.org/10.3846/transport.2010.14
- [2] HAMSON D. *Facial injury: A review of biomechanical studies and tests procedures for facial injury assessment*. *J Biomech*, 1995, 28(1), 1-7. doi: 10.1016/0021-9290(95)80001-8
- [3] MALARA P., MALARA B., DRUGACZ J. *Characteristics of maxillofacial injuries resulting from road traffic accidents – a 5-year review of the case records from Department of Maxillofacial Surgery in Katowice, Poland*. *Head Face Med*, 2006, 2(27). doi: 10.1186/1746-160X-2-27

Analytical and numerical analysis of soft tissue penetration on the example of a pistol ammunition shot

M. ROSZAK, M. MAMYS, D. PYKA, M. BOCIAN, K. JAMROZIAK*

Department of Mechanics, Materials and Biomedical Engineering, Faculty of Mechanical Engineering,
Wroclaw University of Science and Technology, Wroclaw, Poland

Key words: *ballistics, gunshot injuries, tissue damage, pistol ammunition, numerical analysis*

1. Introduction

Numerical methods are a very important and useful tool in search of approximate solutions and often complicated observations and complex cases. This is particularly important from the point of view of biomedical engineering, where research can be carried out on living beings, where experimental analyses carry the risk of mutilation test subject or its death, so minimization is mandatory the possibility of unwanted effects (e.g. resulting from failure of the tested structure). The aim of this paper is to carry out a numerical analysis of the penetration of the soft tissues of the human body as a result of penetration with a pistol bullet. For this purpose, a literature analysis was carried out on the mechanisms of this type of injury depending on the type of projectile, initial velocity, and thus energy, as well as the shape of the projectile [1],[2],[3]. It should be emphasized that the analytical solutions describing the penetration of soft tissues are in fact the resulting form. It is difficult or practically impossible to present the physical phenomena occurring during soft tissue cavitation as a result of the impact of the impulse wave generated in forefront of the bullet head when the bullet penetrates into individual layers of the human tissue system. Numerical analysis using the FE method are helpful here. A geometric model of the 9x19 mm FMJ Parabellum projectile was performed for this purpose and then imported into the Abaqus/Explicit dynamic simulation software. The metallic components of the projectile are described by the Johnson-Cook constitutive equation [4],[5]. The behavior of the tissues was described using the Ogden hyperelastic constitutive model [6] and compared with modelling soft tissues as an elastoplastic material with EOS hydrodynamics [7]. Conversion of SPH particles at the limit strain ϵ_{gr} was adopted as the failure model. The final result of the research is a comparative analysis of tissue penetration obtained as a result of numerical simulations with real gunshot wounds resulting from a pistol ammunition shot, as well as checking the adequacy of mathematical relationships (1,2) in estimating the scale of injuries in the literature on the subject.

2. Approach to the analysis issues

2.1. Phenomena occurring during tissue penetration with a projectile

Gunshot wounds caused by bullets have long been the subject of medical research. As a result of research on the mechanism of this type of injury, two main hypotheses have been put forward:

- the first involves the mechanism of gunshot damage, the generation of transverse and longitudinal vibrations in the hollow tissue, transferring energy in the directions of the projectile's motion and perpendicular to it,
- the next one concerns the side impact, which is experienced by particles located in the vicinity of the projectile's path, which causes their perpendicular displacement and pulsations of the so-called temporary gunshot cavity (Fig. 1).

*Corresponding author: Krzysztof Jamrozak, e-mail: krzysztof.jamrozak@pwr.edu.pl

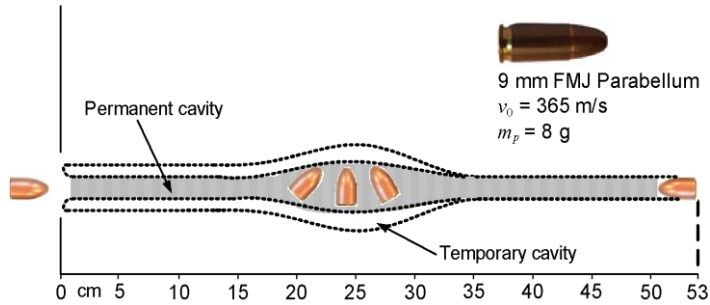


Fig.1. Wound profile a gunshot in a gelatin block of a non-deformable pistol bullet with a characteristic tumbling [2]

2.2. Gunshot wound analysis

It is possible to mathematically estimate the size of the gunshot wound and the time taken to reach the maximum diameter of the temporary gunshot cavity [1]. The maximum radius of the gunshot cavity after the first expansion is determined with a good approximation by equation (1), if the initial collision velocity is greater than 100 m/s.

$$r_1 = \sqrt[3]{\frac{3\rho v_0^2}{2p_0}} r_0 \quad (1)$$

Where: r_1 – wound maximum radius, ρ – density of tissues, p_0 – initial pressure, v_0 – initial collision velocity, r_0 – projectile caliber.

The time after which the greatest expansion of the gunshot wound occurs is described by the following relationship (2).

$$t_1 = \frac{3}{5} \cdot \frac{r_0}{v_0} \left[\left(\frac{r_1}{r_0} \right)^{\frac{5}{2}} - 1 \right] \quad (2)$$

Where: t_1 - the time after which the maximum expansion of the wound occurs.

References

- [1] WŁODARCZYK E. *Balistyka końcowa pocisków amunicji strzeleckiej (in polish). Tom 1*, Warszawa, 2006
- [2] JAMROZIAK K. *Ocena obrażeń od broni palnej w świetle kryterium urazowości (in polish)*. Aktualne Problemy Biomechaniki, 2016, 11, 33-46
- [3] JAMROZIAK K. *Nieśmiercionośna broń o działaniu kinetycznym w odniesieniu do przepisów prawa. [w] Użycie broni palnej jako środka przymusu bezpośredniego (in polish)*. Aspekty prawne. Robert Netczuk (red.) Uniwersytet Śląski 2015, 247-264
- [4] WISNIEWSKI A., GMITRZUK M. *Validation of numerical model of the Twaron CT709 Ballistic fabric. proc. 27th Int Symp Ballist, Ballist, 2013, 2(16): 1535-1544*
- [5] PYKA D., PACH J., JAMROZIAK K. *Numerical modeling of ballistic resistance of thermoplastic laminate under 9 mm Parabellum ammunition*. Eng Mech. 2019, 307-310.
- [6] ODDES Z., SOLAV D. *Identifiability of soft tissue constitutive parameter from in-vivo macro-indentation* J Mech Behav Biomed Mater. 2023,140:105708
- [7] BRACQ A., DELILLE R., BOURCEL B., MARECHAL C., HAUGOU G., LAURO F., ROTH S., MAUZAC O. *Numerical recreation of field cases on a biofidelic human FE model involving deformable less-lethal projectiles*. Mech Eng Def Saf, 2019, 3, 5

Preliminary 3D simulations of osteoarthritis in the knee joint

Key words: *knee osteoarthritis, Finite Element Method, is silico simulations, computational methods*

1. Introduction

The osteoarthritis (OA) is joint degeneration disease affecting bones and articular cartilage. The OA cause immobility in joints, which leads to limited joint motion. Moreover, it can cause pain correlated with motion of joint. It's most common in older age, an estimated 85% of people over the age of 65 suffer from this disease. OA is often not detected until serious symptoms occur, and when treatment is difficult or even impossible. However, the disease can develop regardless of age. The main non-age-related causes are obesity, trauma, or cyclic overloading. The rate of developing of OA is still not well known and that's why it should be studied not only in vitro and in vivo but also in silico.

Development of OA depends on angiogenesis in knee joint and bone growth into cartilage. The bone growing into articular cartilage applies pressure and load and leads to microcracks and destruction of cartilage. In response to this articular cartilage sends intercellular signals in the form of vascular endothelial growth factor (VEGF) which stimulates new vessels to grow in direction of signal. Expression of VEGF begin angiogenesis in articular cartilage, the healthy tissue of which is avascular. New blood vessels deliver more nutrients to affected area which intensify bone grow. All these stages loop and drive each other as shown in [1].

2. Methods

2.1. Geometrical model

In these studies, we decided to build 3D model of bones and articular cartilage out of computer tomography images. The subject was a healthy person with diagnosed OA. Using 3D Slicer, we extracted from CT images trabecular and cortical bone tissues of femur and tibia, and articular cartilage between these two bones (Fig.1). For simulations we cropped the model only to the close surrounding of the joint. This simplification allowed us to save time needed for simulation and calculations. Model was then uploaded to Space Claim in Ansys and converted into bodies which were next meshed in Mechanical Ansys module.

2.2. Computational environment

The boundary conditions were set as fixed support at tibia, and we fixed femur displacement in transverse plane, to imitate support in knee joint and the loading has been applied to femur (Fig.1.) in order to simulate physiological loads during standing, force was approximation of 107% body weight of average human, 675N [2], and overloads. The simulations were carried out in Ansys using Finite Element Method (FEM) in subsystem called Static Structural. Simulations allowed us to designate stress and strain distribution across the cartilage and subchondral bone, which then was applied to OA model. The material properties were set as in Table 1.

*Corresponding author: Szymon Sikora, e-mail: szymon.sikora.dokt@pw.edu.pl

Table 2 - Material properties

| Material | Young's Modulus | Poisson Ratio |
|---------------------|-----------------|---------------|
| Cortical bone | 17000MPa | 0.3 |
| Trabecular bone | 500MPa | 0.25 |
| Articular cartilage | 10MPa | 0.46 |

2.3. OA model

To simulate development of OA we chose model proposed in [1], which is based on von Mises stress (so called effective stress) and elastic strain energy distribution in subchondral bone. The model was chosen because not only because it includes development of bone into articular cartilage but also it takes into consideration angiogenesis, delivery of nutrients and microcrack occurring during bone ingrown. We adopted this model to a 3D case.

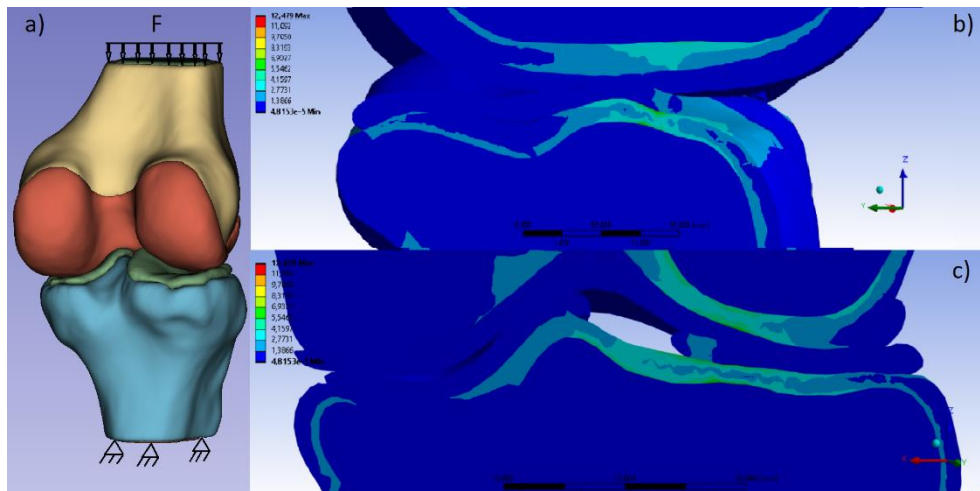


Fig. 1a). 3D model of knee with boundary conditions, b) Von Mises stress distribution in sagittal plane through medial condyle, c) stress distribution in frontal plane

3. Results and Discussion

The stress distributions show possible regions of OA occurrence, i.e., areas of higher stress values for a 3-dimensional case, not only for one specific plane in 2 dimensions. The results indicate that physiological loads should not induce OA in healthy knee in a person with average body weight, unless other factors occur, such as older age, trauma, or injury in knee. Stress in bone causes bone remodeling phenomenon to occurs at the first place, and next angiogenesis might be triggered [3].

References

- [1] BEDNARCZYK E.I., LEKSYCZKI T., GLINKOWSKI I.W. *Effect of micro-cracks on the angiogenesis and osteophyte development during degenerative joint disease*. Comput Assist Methods Eng. Sci, 2018, 24(3): 149 - 156
- [2] KUTZNER I., ET AL., *Loading of the knee joint during activities of daily living measured in vivo in five subjects*”, J Biomech. 2010, 10, 43(11): 2164-73
- [3] SHOKRANI A., SHOKRANI H., MUNIR M. T., KUCINSKA-LIPKA J., KHODADADI YAZDI M., SAEB I M.R. *Monitoring osteoarthritis: A simple mathematical model*. Biomedical Engineering Advances, 2022, 4: 100050, doi: 10.1016/j.bea.2022.100050

Mechanistic evaluation of the sodium alginate/chitosan hydrogel matrices for the release of a photosensitizing substance

M. SKRODZKA*, M. NOWICKA, M. ŁABOWSKA, J. DETYNA, K. MATCZYSZYN

Department of Mechanics, Materials and Biomedical Engineering, Faculty of Mechanical Engineering,
Wrocław University of Science and Technology, Wrocław, Poland

Keywords: hydrogels, drug delivery systems, adhesive materials, photodynamic therapy

1. Introduction

Photodynamic therapy is a minimally invasive form of effective treatment for cancerous and skin lesions and also finds its application in antibacterial therapy [1],[2]. In addition to the appropriate irradiation parameters or the presence of oxygen in the treated tissue, the key aspect is the amount of photosensitizer absorbed by the exposed lesion. One method of delivering therapeutic substances is the use of mucoadhesive hydrogel matrices, which are designed to ensure a sufficiently long residence time of the active substance in the tissue or protect it from factors that can lead to degradation [3]. In addition, such matrices may reduce pain symptoms by providing a moist environment that promotes wound healing or the release of additional analgesic substances.

2. Materials and Methods

The study aimed to adapt a 9% sodium alginate-based hydrogel using a different polymer to achieve appropriate adhesive properties and simultaneously improve methylene blue's controlled release, exhibiting photosensitizing properties [4]. The hydrogel would find application as a system for delivering a photosensitizing substance to lesions formed in the oral mucosa as a result of chemotherapeutic treatments. Chitosan in various concentrations (1% and 3%) was proposed as a material additive. Different ways of crosslinking the hydrogel were investigated to determine their effect on the mechanical properties of the matrix. Two different concentrations of calcium chloride solution, 0.1M and 0.5M were utilized in the experiment. The hydrogel fabrication scheme is shown in Fig. 1.

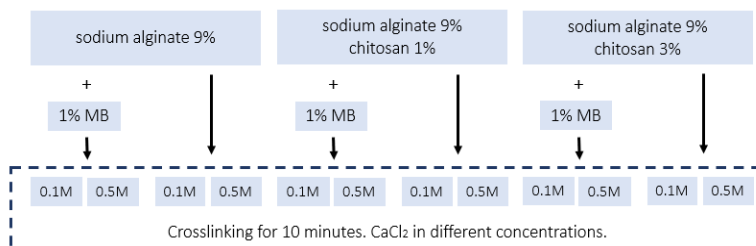


Fig. 1 Sample preparation scheme

The tests carried out are *in vitro* using animal tissues (pig cheeks). In order to determine the strength of adhesion between the material and the tissue, a T-peel test was performed (Fig. 2b). The residence time of the hydrogel in the tissue was determined using the small cup slurry test (Fig. 2a). For a more complete mechanical description of the fabricated structures, a uniaxial tensile test was also carried out, using which the material's Young's modulus (Table 1, Fig. 1) and tensile strength of the material was determined. The kinetics of methylene blue release from individual matrices were also determined.

*Corresponding author: Maria Skrodzka, e-mail: maria.skrodzka@pwr.edu.pl

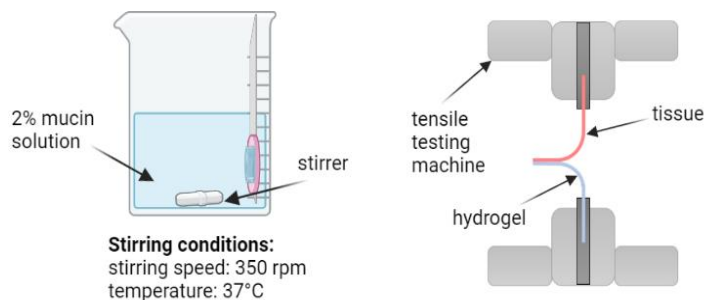


Fig. 2 Adhesion testing schemes a) small cup slurry test b) T-peel test

Table 1. Young's Modulus of investigated hydrogels (N=5)

| | SA | SA-MB | SA-CH1 | SA-CH3 | SA-CH1-MB | SA-CH3-MB |
|-------------------------------|-------------------------------|--------------------------------|----------------------------|-----------------------------|----------------------------|-----------------------------|
| Young's Modulus [MPa]* | 1347.6 ± 534.2 ^{abc} | 1656.0 ± 195.1 ^{defg} | 945.6 ± 203.3 ^d | 735.8 ± 251.1 ^{ae} | 544.2 ± 57.7 ^{bf} | 573.7 ± 214.9 ^{cg} |

a,b,c... - statistically significant differences for $p < 0.05$.

* Tukey test (result presented as mean ± standard deviation).

3. Results and Conclusions

The study concluded that the addition of chitosan significantly improved the residence time of the hydrogel matrices on the tissue. The residence time on the tissue lengthened with increasing the amount of chitosan in the matrix. At the same time, additives improving the mucoadhesiveness of alginate are necessary due to its poor adhesive properties.

The addition of methylene blue reduces both the mechanical strength of the material (by 46% in the case of pure alginate samples), lowers Young's modulus (by 43% in the case of alginate/chitosan samples), and significantly reduces the residence time of the hydrogel dressing on the tissue. Crosslinking parameters were also shown to affect the mechanical properties of hydrogel samples and the degradation time of the structures. The kinetics of methylene blue release from alginate/chitosan hydrogel matrices indicate that the addition of this material does not negatively affect the release of the active substance.

In conclusion, the study indicates that sodium alginate-based hydrogel matrices can be used for the release of methylene blue. At the same time, it is necessary to use additives to improve the mucoadhesiveness of alginate due to its low adhesive properties. The proposed alginate/chitosan/methylene blue material will be tested for rheological properties and adapted for processing by additive methods. Fabrication the matrices using additive manufacturing technology will allow their personalization in terms of both geometry and concentration of the active substance.

References

- [1] AGOSTINIS P., BERG K., CENGEL K. A., FOSTER T. H., GIROTTI A. W., GOLLNICK S. O., ET. AL., *Photodynamic therapy of cancer: an update*. CA Cancer J Clin. 2011,61(4):250-81
- [2] PIKSA M., LIAN C., SAMUEL I. C., PAWLI, K. J., SAMUEL I. D., MATCZYŹYŹYŹN K. *The role of the light source in antimicrobial photodynamic therapy*. Chem Soc Rev. 2023, 6,52(5):1697-1722
- [3] VASHIST A., VASHIST A., GUPTA, Y K., AHMAD S. *Recent advances in hydrogel based drug delivery systems for the human body*. J Mater Chem B. 2014, 14, 2(2):147-166
- [4] MALISZEWSKA I., WANARSKA E., THOMPSON A. C., SAMUEL I. D., MATCZYŹYŹYŹN K. *Biogenic gold nanoparticles decrease methylene blue photobleaching and enhance antimicrobial photodynamic therapy*. Molecules. 2021, 25, 26(3):623

Trunk rotation and posture control asymmetry in children and young adults

M. SOBERA*, P. PROSKURA

Wroclaw University of Health and Sport Sciences, Wroclaw, Poland

Key words: *body scanning, posture control, asymmetry*

1. Introduction

Deformations in the trunk area in three planes: sagittal, frontal and transverse are characteristic for incorrect posture and scoliosis also at the initial stage of development of these body posture deficiencies [1]. Abnormalities in the trunk position correlate with the quality of keeping body balance in the vertical bipedal position [2] and therefore on the functioning of postural control. The development of a habit of asymmetrical posture control at an early age contributes to postural abnormalities. Children undergoing early sports specialization are often exposed to this effect. The purpose of this study is to determine the relationship between the occurrence of postural asymmetry and the symmetry/asymmetry of right and left lower limb function during standing balance control in children and young adults.

2. Material and Methods

A total of 89 subjects were included in the study, including: 13 girls and 17 boys aged 7-8 years, a group of 12 artistic gymnasts: 10 girls and 2 boys aged 7-12 years, and a group of young adults - students of the University of Physical Education in Wroclaw: 20 women and 27 men aged 21-25 years. The children's parents gave their written consent to the research. Each subject first underwent a laser scan of the body and then performed a body balance control test on force platforms. A system of four SkanWorks by Human Solution 3D laser scanners was used to scan the body. The subjects were scanned in a natural standing position in a darkened booth, bounded by four tripods (3.5 m high, placed at the four corners of the 2/2 m base) for the four scanners moving from top to bottom. The laser beams made it possible to obtain a precise 3D image of the subject's body. The scanning time was approximately 12 seconds.



Fig. 1. Scan of the trunk from the dorsal side (left) and a photo of the same figure from above (right). Example result of a trunk rotation of 7.4° to the right (-7.4°).

The result of the body scan was the determination of the degree of trunk rotation (TR), which was automatically marked with a minus sign on the right and a plus sign on the left (Fig. 1). Before the body scan, was made the feet print to reproduce the same foot distance during the posture control test on the force platforms. The subject stood on two AccuSway (AMTI) platforms placed side-by-side, left foot on one, right foot on the other.

*Corresponding author: Małgorzata Sobera, e-mail: malgorzata.sobera@awf.wroc.pl

Recording of center of pressure (COP) displacements from both synchronized platforms took 20 s, sampling frequency 100 Hz. Stability indices were calculated from the course of COP changes as a function of time: medial-lateral (COPX) and anterior-posterior (COPY) COP amplitude, COP ellipse area and velocity (V COP [cm/s]) separately for the left and right lower limbs. Rank ANOVA Kruskal-Wallis test was used to assess the significance of intergroup differences in TR angle. The intragroup differences between the left and right COP indices were assessed by Wilcoxon's rang test. The correlations between TR and the posture control indicators were determined by Spearman's correlation coefficient (r_s).

3. Results

The TR angle in the students group was significantly lower than in the children and gymnasts groups (Fig. 2). The latter two groups did not differ, but the range of results (min-max) is significantly greater in the children's group than in the gymnasts' group.

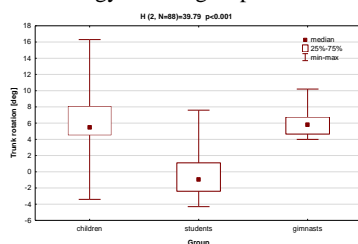


Fig. 2. Results of intergroup differences in trunk rotation angle (TR)

In the group of gymnasts, no TR to the right was recorded, in the group of children only 2 showed TR to the right, the majority - to the left. Students showed TR both to the right ($n=33$) and to the left ($n=14$). There were no significant differences in COP indices between the left and right lower limbs in all three groups ($p>0.05$). A significant intragroup correlation between TR and posture control indices of left and right lower limb were found only in the student group (TR and COPY amplitude of left foot, $r_s = -0.32$) and in the gymnast group (TR and COPX amplitude of left foot, $r_s = -0.59$). In the group of children, no such correlation was found.

4. Discussion and Conclusions

TR results in the gymnasts show that specialized training in childhood "stabilizes" the asymmetry in the alignment of the trunk in the right torsion position (from 4 to 10°). This may be an effect of training with many exercises performed on one side, due to the functional dominance of the right side [3]. The above average inverse significant correlation of TR with COPX of the left lower limb in this group confirms the relationship between asymmetry of support function and asymmetry of trunk alignment. Similar correlation results were found in the student group, although these subjects showed TR direction both to the right and to the left.

The results of this study provide the basis for the claim that asymmetry of lower limb function in posture control in natural posture may be a symptom of trunk rotation, and this means that studies of postural asymmetry can be diagnosed by studying symmetry/asymmetry of posture control.

References

- [1] NEGRINI S., DONZELLI S., AULISA A.G., CZAPROWSKI D., ET AL. 2016 *SOSORT guidelines: orthopaedic and rehabilitation treatment of idiopathic scoliosis during growth*. *Scoliosis Spinal Disord.* 2018, 10,13:3
- [2] WILCZYŃSKI J., BIENIEK K. *Correlations of somatic traits and postural defects in girls and boys aged 10-12*. *Acta Bioeng Biomech.* 2019,21(1):79-86
- [3] BOURELLE S., ET AL., *Computerized static posturography and laterality in children. Influence of age*. *Acta Bioeng Biomech.* 2017, 19(2):129-139

Determination of intrinsic strength for the mandibular elevator muscles during unilateral mastication of different foodstuffs

P. STRÓŻYK*

Department of Mechanics, Materials and Biomedical Engineering, Faculty of Mechanical Engineering,
Wrocław University of Science and Technology, Wrocław, Poland

Key words: human masticatory system, chewing, foods

1. Introduction

Intrinsic strength (k) is one of many parameters used to describe masticatory muscle function. An analysis of the available literature indicates few publications on the parameter k value concerning masticatory muscles and physiological loads. One of the oldest papers relating to intrinsic strength values is that of Fick [1], in which the author reports $k=1\times 10^6$ N/m². In the 1940s and 1960s, papers [2],[3] were published in which intrinsic strength values of 0.9×10^6 N/m² and 0.7×10^6 N/m² were given, respectively. On the other hand, analysing works from the turn of the 20th and 21st centuries [4],[5],[6],[7],[8], it can be concluded that the value of the k parameter is in the range of $0.35\times 10^6\div 0.40\times 10^6$ N/m². A common feature of the abovementioned publications is using a single intrinsic strength value for all masticatory muscles.

This study aimed to determine intrinsic strength values for the masseter, medial pterygoid, and temporalis muscle during unilateral chewing of selected foods. Due to the complexity of chewing, intrinsic strength values were determined for the first bite.

2. Methods

In order to determine the intrinsic strength (k) of the masseter (M), medial pterygoid (MP) and temporalis (T) muscles, five foods (i) differing in structure (texture) and mode of manufacture (natural and artificial) were selected, i.e. carrot (c), apple (a), dark chocolate (d), chocolate bar (b) and sausage (s). Based on publications [9],[10], intrinsic strength (k), is determined from knowledge of maximum muscle force (F_H) and physiological cross-sectional area ($PCSA$) - equation 1. Calculations were performed for the working (W) and non-working (N) sides.

$$k = F_H / PCSA \quad (1)$$

3. Results

Equation (1) was used to calculate intrinsic strength, which was adjusted to the selected muscles according to the selected foods for the working (k_{Wi}) and non-working (k_{Ni}) sides, respectively-Table 1. The data given in the paper [11] were used to determine intrinsic strength and the $PCSA$ values on the working and non-working sides were assumed to be the same [6].

4. Discussion

The results in Table 1 indicate that, during unilateral chewing, the intrinsic strength value (k) should be analysed in the context of the food, the muscle and the side of the mandible (the working and the non-working sides). An analysis of the work [11],[12] indicates that food imposes individual patterns of muscle activity that must adapt to different functional requirements depending on the input. [13].

*Corresponding author: Przemysław Stróżyk, e-mail: przemyslaw.strozyk@pwr.edu.pl

Table 1. Values of intrinsic strength (k_{W} , k_{N}) for selected muscles (the masseter (M), medial pterygoid (MP) and temporalis (T) muscles) in relation to food (i) and to the side of the mandible, i.e. the working side (W) and the non-working side (N)

| Muscle | $PCSA$ [$\times 10^{-4} \text{ m}^2$] | Chocolate (d) | Chocolate bar (b) | Apple (a) | Carrots (c) | Sausage (s) |
|---|--|-------------------|-----------------------|---------------|-----------------|-----------------|
| k_{W} [$\times 10^6 \text{ N/m}^2$] | | | | | | |
| M | 6.80 | 0.34 | 0.22 | 0.16 | 0.40 | 0.19 |
| MP | 4.37 | 0.47 | 0.31 | 0.23 | 0.56 | 0.26 |
| T | 8.23 | 0.06 | 0.05 | 0.03 | 0.06 | 0.03 |
| k_{N} [$\times 10^6 \text{ N/m}^2$] | | | | | | |
| M | 6.80 | 0.29 | 0.19 | 0.14 | 0.35 | 0.16 |
| MP | 4.37 | 0.41 | 0.26 | 0.20 | 0.48 | 0.22 |
| T | 8.23 | 0.05 | 0.03 | 0.02 | 0.06 | 0.02 |

In other words, food (texture, mechanical parameters) is an overriding parameter concerning muscle strength, among other things. The analysis of intrinsic strength values concerning muscles shows that the highest values of the k parameter are obtained for the pterygoid muscle and the lowest for the temporalis muscle. In contrast, the values obtained for the masseter muscle are 28% lower than those calculated for the medial pterygoid muscle - irrespective of food and side.

Equation 1 indicates that attention should also be paid to the $PCSA$ value to determine intrinsic strength, as using different $PCSA$ values (for $F_H = \text{const}$) leads to different k values for the same muscle.

References

- [1] FICK H. *Handbuch der Anatomie und Mechanik der Gelenke*, G. Fischer, Jena. 1904, (Classic Reprint–Forgotten Books 2018). <https://www.forgottenbooks.com/en>
- [2] MORRIS C.B. *The measurement of the strength of muscle relative to the cross-section*. Res Q Am Assoc Hlth Phys Educ. 1904, 19, 295–303
- [3] IKAI M., FUKUNAGA T. *Calculation of muscle strength per unit cross-sectional area of human muscle by means of ultrasonic measurement*. Int Z Angew Physiol. 1968, 26, 26–32
- [4] WEIS W.A., HILLEN B. *Cross-sectional areas and estimated intrinsic strength of the human jaw muscles*. Acta Morphol Neerl Scand. 1985, 23, 267–274
- [5] KOOLSTRA J.H., VAN EIJDEN T.M.G.J. *Application and validation of a three-dimensional mathematical model of the human masticatory system in vivo*. J Biomechanics. 1992, 25, 175–187
- [6] LANGENBACH G.E.J., HANNAM A.G. *The role of passive muscle tensions in a three-dimensional dynamic model of the human jaw*. Arch. Oral Biol. 1999, 44, 557–573
- [7] ZHENG K., LIAO Z., YODA N., FANG J., CHEN J., ZHANG Z., ZHONG J., PECK C.H., SASAKI K., SWAIN M.V., LI Q. *Investigation on masticatory muscular functionality following oral reconstruction—An inverse identification approach*. J Biomech. 2019, 90, 1–8
- [8] SLAGER G.E.C., OTTEN E., VAN EIJDEN T.M.G.J., VAN WILLIGEN J.D. *Mathematical model of the human jaw system simulating static biting and movements after unloading*. J. Neurophysiol. 1997, 78, 3222–3233
- [9] MAY B., SAHA S., SALTZMAN M. *A three-dimensional mathematical model of temporomandibular joint loading*. Clin. Biomech. 2001, 16, 489–495
- [10] PRUIM G.J., DE JONGH H.J., TEN BOSCH J.J. *Forces acting on the mandible during bilateral static bite at different bite force levels*. J. Biomech. 1980, 13, 755–763
- [11] STRÓZYK P., BALCHANOWSKI J. *Application of numerical simulation studies to determine dynamic loads acting on the human masticatory system during unilateral chewing of selected foods*. Front Bioeng Biotechnol. 2023, 11, 1-18
- [12] MIOCHE L., BOURDIOL P., MARTIN J.F., NOËL Y. *Variations in human masseter and temporalis muscle activity related to food texture during free and side imposed mastication*. Arch Oral Biol. 1999, 44, 1005–1012
- [13] FITTS R.H., McDONALD K.S., SCHLUTER J.M. *The determinants of skeletal muscle force and power: their adaptability with changes in activity pattern*. J Biomech. 1991, 24, 111–122

Relationships between leg stiffness and displacement of centre of mass during countermovement jumps to specific and various height

A. STRUZIŁ*

Department of Biomechanics, Wrocław University of Health and Sport Sciences, Wrocław, Poland

Key words: *potential elastic energy, quasi-stiffness, submaximal jump, vertical jump*

1. Introduction

Leg stiffness is a variable that has been mainly used in locomotion analyses. Stiffness is a quantitative measure of the elastic properties that determine the ability to accumulate potential elastic energy in a compliant tissues. For vertical jumps, the potential elastic energy accumulated during the countermovement phase increases the energy supplied by active contraction of the muscles used in the take-off phase. Consequently, the potential elastic energy will impact the jump height [1]. The occurrence of this phenomenon is considered to be one of the reasons for reaching mostly greater heights during a vertical jump preceded by lower limb countermovement than during a vertical jump from a specific static position, i.e., a squat [2]. Despite the clarity of the above phenomenon, the practice of sports training reveals some questions regarding the role of potential elastic energy as a key factor responsible for determining performance. The reason for this obscurity is the lack of concrete recommendations that would allow for the improve speed-strength abilities of motion system. The speculations concerning a desirable value of leg stiffness that is the most advantageous for the accumulation of potential elastic energy and most favours reaching maximal sport performance have already been addressed [1]. However, no studies have provided unequivocal evidence for the presence of a desired value of leg stiffness.

A review of the literature on leg stiffness reveals a number of unexplained issues. For example, the studies failed to analyse the problem of leg stiffness during jumps to heights different than maximal [1]. Therefore, the aim of this study is to identify the relationships between leg stiffness and displacement of centre of mass during countermovement jumps (CMJs) to specific and various height (from minimal to maximal). Leg stiffness is understood as a ratio of changes in ground reaction forces to respective changes in "spring length" that represents both lower limbs. This virtual spring is responsible for accumulation of potential elastic energy during countermovement phase of the jump.

2. Material and Methods

The study was carried out on a group of 10 male basketball players (age: 21.0 ± 0.8 years, body height: 1.87 ± 0.07 m, body mass: 78.0 ± 9.3 kg, training experience: 5.5 ± 2.0 years). Each participant performed 20 single vertical CMJs with arm swing to specific and various height. Measurements were performed using Kistler force plate and BTS SMART motion analysis system.

Before measurements, the reflective markers were located at the height of the greater trochanters of the femur (conventional upper end of the lower limb). It was adopted that the change in the height of the greater trochanter represents a measure of the change in the "length" of virtual spring Δl (which represents both lower limbs). The participants performed 20 CMJs to the specific and various height so that every jump was to a different height (from minimal to maximal with random order). The participant was only slightly guided, receiving feedback on the relative height of the jump without giving the exact value of the height obtained. The main aim of the experiment was to make CMJs as natural and as

*Corresponding author: Artur Struzik, e-mail: artur.struzik@awf.wroc.pl

undisturbed by the instructions as possible. Leg stiffness was determined as a ratio of changes in ground reaction forces (ΔF) to the respective change in the height of the greater trochanter of the femur (Δl) [3]. Computations were made separately for the countermovement and take-off phases. Displacement of centre of mass during CMJ (jump height) was determined indirectly based on flight time method. The r-Pearson's correlation coefficient was used to evaluate the relationships between leg stiffness and CMJ height in each participant separately. Furthermore, the analysis of covariance ANCOVA was also performed to assess the above relationship for the entire study group [4]. In all tests used, the level of significance was set at $\alpha = 0.05$.

3. Results

Negative, significant relationships between the CMJs height and leg stiffness in the countermovement ($r \in <-0.86, -0.47>$) and take-off ($r \in <-0.90, -0.57>$) phases were observed in each study participants. The analysis of covariance with PERSON as a constant factor and HEIGHT as an accompanying variable confirmed these relationships for the entire study group. The HEIGHT quantitative predictor was significant, which indicated that leg stiffness in the countermovement ($F = 131.7, p < 0.001, \eta^2 = 0.41$) and take-off ($F = 116.2, p < 0.001, \eta^2 = 0.38$) phases is related to the height of the CMJs. Furthermore, the significance of the PERSON qualitative predictor indicated different leg stiffness values of the study participants in the countermovement ($F = 16.4, p < 0.001, \eta^2 = 0.44$) and take-off ($F = 5.3, p < 0.001, \eta^2 = 0.2$) phases.

4. Discussion and Conclusions

Vertical jump performed to a part of maximal height has a slightly different movement pattern compared to a maximal jump. Changes are observed in the contributions of individual muscles and joints [5]. Vertical jumps to the maximal height are characterized by greater ranges of motion in the joints of the lower limbs to achieve higher value of kinetic energy in the countermovement phase. Furthermore, lower amounts of energy are needed to perform vertical jump to a specific height. To reduce energy waste, countermovement and arm swing are performed to a lesser extent. When jumping to a specific height, the benefits from accumulation of potential elastic energy are negligible.

In this study increases in CMJs height (from minimal to maximal) were accompanied by reduced values of leg stiffness in the countermovement and take-off phases. These results suggest that relatively low values of leg stiffness are beneficial to CMJ height. Therefore, smaller values of leg stiffness cause that changes in the "length of the spring" (representing the lower limbs) can be made using lower forces. Consequently, the countermovement can be greater, which positively affects the value of the accumulated potential elastic energy and jump height.

References

- [1] STRUZIK A. *Measuring leg stiffness during vertical jumps: theory and methods*. Springer Nature Switzerland AG, Cham, 2019
- [2] BOBBERT M.F., GERRITSEN K.G.M., LITJENS M.C.A., VAN SOEST A.J. *Why is countermovement jump height greater than squat jump height?* Med Sci Sports Exerc. 1996, 28(11):1402-12
- [3] STRUZIK A., ZAWADZKI J. *Application of force-length curve for determination of leg stiffness during a vertical jump*. Acta Bioeng Biomech. 2016,18(2):163-71
- [4] BAKDASH J.Z., MARUSICH L.R. *Repeated measures correlation*. Front Psychol, 2017, 8, 456
- [5] VANRENTERGHEN J., LEES A., LENOIR M., AERTS P., DE CLERCQ D. *Performing the vertical jump: movement adaptations for submaximal jumping*. Hum Mov Sci. 2004, 22(6):713-27

Proper identification of body mass distribution modifies the outcome of the simulation. Preliminary results

M. SYCZEWSKA^{1*}, J.MICHOŃSKI², M.KALINOWSKA¹, E.SZCZERBIK¹, R. SITNIK³

¹Department of Paediatric Rehabilitation, The Children's Memorial Health Institute, Warsaw, Poland

²PhiLab SA, Plochocińska 111/115, 03-044 Warszawa

³Faculty of Mechatronics, Warsaw University of Technology, Warsaw, Poland

Key words: *body mass distribution, inertial properties, simulation*

1. Introduction

Body models in musculoskeletal analyses predominately use body mass distribution among segments based on anatomy specific for young, healthy men [1] or based on regression equations and anthropometric measurements [2]. Patients' body proportions and anatomy often differ substantially from that of the young men. Therefore the aim of this study was to assess the impact of the more personalized body mass distribution among segments on the results of the simulations.

2. Methods

Four subjects participated in this study: one healthy young man, one middle-aged woman, one young male adult with CP, and one young female teenager with extreme obesity. All subjects underwent objective gait analysis (VICON MX system) with full body Plug-In-Model marker set and model. They walked at their natural, self-selected speed. Kinematic data and ground reaction data (Kistler force plates) were later used for simulations. At the time of the gait analysis, they also underwent detailed body shape measurements with the use of a structured light-based system [3]. From this data, segment volumes were estimated and used to prepare a personalised body mass distribution.

The simulations were performed in OpenSim using the Hamner [4] full body with upper limbs model. The simulations were performed twice. First, the model was scaled (static trial data) while preserving the mass distribution during scaling, according to the generic model. In the second, the masses of the pelvis, torso, and upper and lower limbs were adjusted (after scaling) according to the data from body shape measurements. The data of one, the same in both cases, gait trial per subject was used, with one left and one right step with ground reaction force data. In both cases, the following steps were done in OpenSim: inverse kinematics, inverse dynamics, static optimization and calculation of joint reaction forces. In the last step, both forces and moments were calculated, and from them, the hip, knee and ankle forces and moments were analysed.

3. Results

No differences were found for the young man, in case of other subjects the biggest differences were found for ankle joints. The examples showing the most pronounced differences are presented on the graphs, presented on Fig.1.

*Corresponding author: Małgorzata Syczewska, e-mail: m.syczewska@ipczd.pl

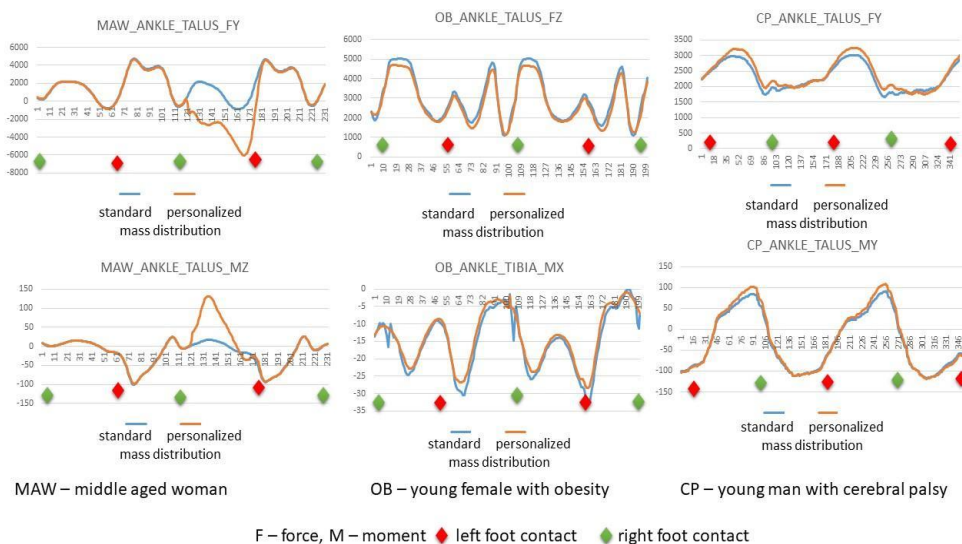


Fig. 1. Comparisons of the simulation results for the ankle joint, for the three subjects for generic and personalized mass distribution models. F – joint force, M – joint moment. X – sagittal axis, Y – frontal axis, Z – transverse axis, SI units were applied: force in Newtons, moment in Newton-meters.

4. Discussion

From our results it can be seen that the body mass distribution can influence the simulation outcome, but the nature of the force and moments changes is preserved. No changes were found for the young man, whose body shape, proportions and mass distribution among segments matched the standard model. Personalization of the body mass distribution can improve the accuracy of the musculoskeletal modelling. The presented results were chosen as those which differ depending on the type of the mass distribution, other components were not sensitive to the mass distribution.

The main shortcomings of this study are: limited number of subjects, artefacts in the 3D scans, inconsistencies in segment extraction between subjects, adjusting only the mass distribution among segments, calculation of the segment mass assuming homogeneous density, and limited optimization of the model. In the next steps we plan to personalise the inertial properties and density of the body. Another limitation of the study is the choice of the dynamic activity with low accelerations: gait. This was caused by the fact that patient with cerebral palsy was not able to perform more dynamic activity.

Acknowledgments: This study was performed within INERTBODY research project financed by CMHI.

References

- [1] DEMPSTER W.T. *Space requirements of the seated operator. Geometrical, kinematic, and mechanical aspects of the body with special reference to the limbs.* Univ. Michigan, Ohio, July 1955
- [2] HATZE H. *Parameter identification for human body segment models.* Theor Issues Ergon Sci. 2005, 6: 331-334
- [3] LIBERADZKI P., ADAMCZYK M., WITKOWSKI M., SITNIK R. *Structured-Light-Based System for Shape Measurement of the Human Body in Motion.* Sensors. 2018, 18(9):2827
- [4] HAMNER S.R., SETH A., DELP S.L. *Muscle contributions to propulsion and support during running.* J Biomech 2010, 43: 2709-2716

Personalised finite element models of the human abdominal wall under material model uncertainties

K. SZEPIETOWSKA^{1*}, M. STAAT², M. RYKACZEWSKI³, I. LUBOWIECKA¹

¹Gdańsk University of Technology, Gdańsk, Poland

²FH Aachen University of Applied Sciences, Aachen, Germany

³University Clinical Centre, Gdańsk, Poland

Key words: *finite element modelling, global sensitivity analysis, Sobol indices, probabilistic method polynomial chaos, abdominal wall mechanics*

1. Introduction

The study concerns computational modelling of the human abdominal wall. Understanding the behaviour of the abdominal wall is important in the ventral hernia medical context. Models with good predictive capacity can be used in *in silico* testing of new implant design. However, it should be taken into account that the natural variability of mechanical properties and geometry is relatively high in case of biological tissues [1]. A detailed personalised geometrical model can be constructed based on CT or MRI images to decrease the uncertainty related to the variability of the geometry. The aim of this paper is to compare two personalised models in terms of the geometry models under material model uncertainties.

2. Methods

2.1. Finite Element Models

Two Finite Elements (FE) solid models of the abdominal wall have been created. Mimics and 3-matic (Materialise) software have been used to segment images, reconstruct 3D geometry and generate tetrahedral mesh models based on medical images. Fig. 1a shows a model constructed based on MRI images of a man and Fig 1b shows a model created based on CT images of a woman. The models are composed of the main components of the abdominal wall: rectus abdominis, external oblique, internal oblique and transverse abdominis muscles as well as *linea alba* tissue with aponeurosis. Marc (Msc. Software/Hexagon) – FE software has been used to perform static analysis. Boundary conditions reflect origin and insertion of the muscles (pelvis, ribs, xiphoid processes). Abdominal wall is subjected to intraabdominal pressure. Linear elastic isotropic material model is assumed for all the tissues.

2.2. Uncertainty quantification and global sensitivity analysis

Regression-based polynomial chaos (PC) method is used to propagate uncertainties and calculate Sobol indices (measures of global sensitivity analysis) [2]. This method is based on constructing a meta-model, is non-intrusive and allows to propagate uncertainties with relatively low computational cost. The Young's modulus of each muscle is assumed to be a uniform random variable. There are 5 independent random variables. Based on the previous examples [3], Sobol sequence points are chosen as regression points to construct the PC meta-model. The displacement of the node in the middle of the rectus muscle is assumed to be the quantity of interest.

*Corresponding author: Katarzyna Szepietowska, e-mail: katszepi@pg.edu.pl



Fig. 1. Models of the abdominal wall a) male model based on MRI images b) female model based on CT images

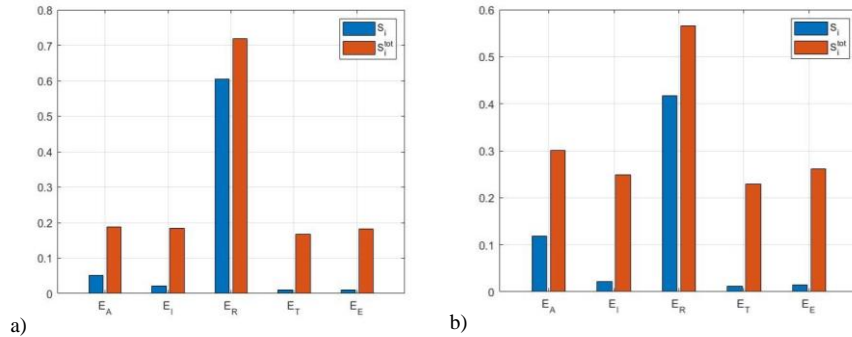


Fig. 2. Sobol and total Sobol indices for a) male model b) female model, E_R refers to Young's modulus of rectus abdominis, E_E – external oblique, E_I – internal oblique and E_T – transverse abdominis muscles, E_A - *linea alba* tissue with aponeurosis

3. Results

The ranking of the variables obtained for both models is very similar, but the values of the Sobol indices are different (Fig 2). As expected, the Young's modulus of the rectus abdominis muscle is the most important variable in both models. However, in case of the model based on female CT images, the value of total Sobol index is lower. In both cases, interactions between parameters play a crucial role and total indices are much higher than first order Sobol indices.

4. Conclusions

In the studied example, the differences in geometry did not have a large impact on the distribution of the investigated quantity of interest. However, the contribution of each variable to the total variance has changed and consequently conclusions of importance of variables have changed. In the next step, other quantities of interest will be considered.

Acknowledgments: This work was supported by the National Science Centre (Poland) [grant No. UMO-2017/27/B/ST8/02518]. Calculations were carried out partially at the Academic Computer Centre in Gdansk

References

- [1] COOK D., JULIAS, M., NAUMAN E. *Biological variability in biomechanical engineering research: Significance and meta-analysis of current modeling practices*. J. Biomech.2014, 47(6), 1241-1250
- [2] SUDRET B. *Global sensitivity analysis using polynomial chaos expansions*. Reliab Eng Syst Saf. 2008, 93(7), 964–979
- [3] SZEPIETOWSKA K., MAGNAIN B., LUBOWIECKA I., FLORENTIN E. *Sensitivity analysis based on non-intrusive regression-based polynomial chaos expansion for surgical mesh modelling*. Struct Multidiscip Optim. 2018, 57, 1391-1409

Analysis of the degree of mechanical wear in the transpedicular stabilization of the spine

K. SZKODA-POLISZUK^{1*}, M. ŻAK¹, A. BROŃCZYK², C. PEZOWICZ¹

¹Department of Mechanics, Materials and Biomedical Engineering, Faculty of Mechanical Engineering,
Wrocław University of Science and Technology, Wrocław, Poland

²Department of Fundamentals of Machine Design and Mechatronic Systems, Faculty of Mechanical Engineering,
Wrocław University of Science and Technology, Wrocław, Poland

Key words: *sliding pedicle screws, biomechanics, friction, wear*

1. Introduction

One of the innovative solutions for treating scoliosis in children is stabilization systems that allow spinal modelling without the need for revision surgery while allowing uninhibited growth. Designs of such stabilizers use kinematic pairs, allowing the screw to slide along the rod. Unfortunately, friction between the sliding elements of the stabilizer causes wear and tear, resulting in the deposition of titanium alloy particles in the surrounding tissues [1],[2]. Currently, solutions are being sought to eliminate friction products through coatings. The study aimed to assess the mechanical properties and evaluate the frictional wear of a sliding screw-rod connection used in spinal stabilization.

2. Material and Methods

The tests were carried out for two groups of single sliding kinematic screw-rod pairs made of Ti6Al4V titanium alloy and with diamond-like carbon (DLC) coating, in which the head of the polyaxial bolt was aligned with the axis of the bolt (the angle of inclination is 0°). The established research goal was realized by achieved conducting mechanical tests microscopic tests and topographic studies of the mating surfaces of the elements of the stabilizer kinematic pair (Fig. 1).

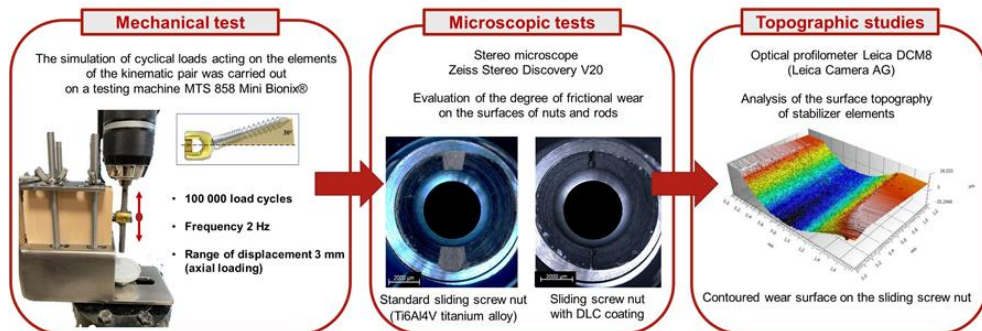


Fig. 1. The research methods used: mechanical tests, microscopic tests and topographic studies

The cyclic loads acting on the components of the kinematic pair were simulated on an MTS 858 Mini Bionix® testing machine. The tests were performed for 100,000 load cycles at a frequency of 2 Hz, so as to approximate as closely as possible the frequency of human walking. A displacement range of 3 mm was assumed for axial loading.

*Corresponding author: Klaudia Szkoda-Poliszuk, e-mail: klaudia.szkoda-poliszuk@pwr.edu.pl

Mechanical tests made it possible to determine the average value of the friction force over successive cycles. Analysis of the surface topography made it possible to decide on an isometric map of the surface of the nuts (using an optical profilometer Leica DCM8, Leica Camera AG). The amount of tribological wear was determined by measuring the depth of the cavity conducted along profiles at different rubbing heights.

3. Results and Discussion

The average value of the friction force determined from the mechanical tests, together with the standard deviation over successive load cycles, was presented every 10,000 cycles. It was shown that, for both test groups, the frictional force increases with successive cycles (Fig. 2). The friction force was shown to increase (from 0N to 14N) with successive cycles for standard implants. For implants with DLC coating, the friction force was smaller and practically constant (from 0N to 4N).

As a result of the titanium rod's friction against the nuts' surface, there was surface wear in the contact areas of these elements. It was observed that the amount of wear on the area located above the nut hole (upper friction area) was noticeably less compared to the lower area (bottom friction area).

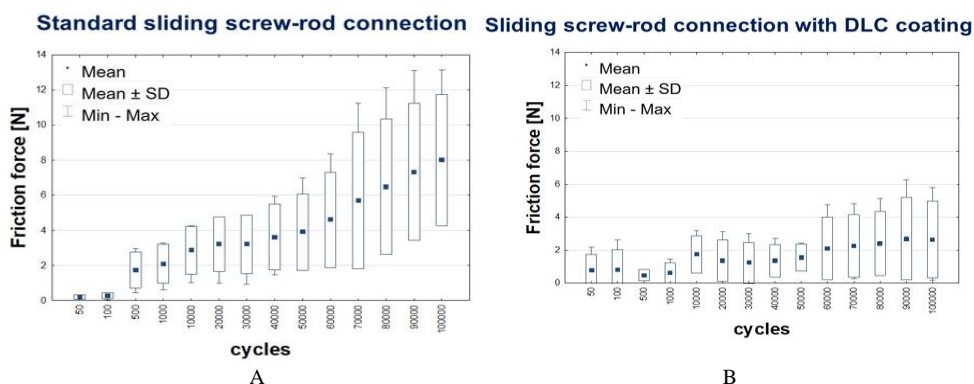


Fig. 2. Average value of the friction force over successive cycles: a) standard sliding screw-rod connection, b) sliding screw-rod connection with DLC coating

Acknowledgments: The presented research results realised within the research task "Evaluation of the frictional wear of a sliding screw-rod connection used in spinal stabilization", financed from the pro-quality subsidy for the development of research potential of the Faculty of Mechanical Engineering of Wrocław University of Science and Technology in the year 2022.

References

- [1] LIU P.Y., LAI P.L., LIN C.L. *A biomechanical investigation of the retentive force of pedicle screw structures for different screw tulip designs*. Clin Biomech (Bristol, Avon). 2019, 70:23-30
- [2] ÇETIN E., ÖZKAYA M., GÜLER Ü. Ö., ACAROĞLU E., DEMİR T. *Evaluation of the effect of fixation angle between polyaxial pedicle screw head and rod on the failure of screw-rod connection*. Appl Bionics Biomech. 2015, 2015:150649

Mechanical properties and microscopic characterization of human fascia lata

S. SZOTEK^{1*}, J. DAWIDOWICZ², A. CZOGALLA³, K. MAKSYMOWICZ⁴

¹Department of Mechanics, Materials and Biomedical Engineering, Faculty of Mechanical Engineering, Wrocław University of Science and Technology, Wrocław, Poland

²Veterinary Clinic Brynów, Brynowska 25c, 40-585 Katowice, Poland

³Faculty of Biotechnology, University of Wrocław, Wrocław, Poland

⁴Department of Forensic Medicine, Wrocław Medical University, Wrocław, Poland

Key words: *fascia lata, mechanical properties, uniaxial tensile test, collagen and elastic fibres*

1. Introduction

Basically, fascia can be defined as a widespread network of fibrous tissue infiltrating the entire body. It surrounds, supports, suspends, protects, connects and divides muscular, skeletal and visceral tissues of an organism. The *fascia lata* (FL) envelops deep structures of the thigh, constitute a very important part of musculoskeletal system. That is way its dysfunction and inflammation may lead to the widespread pain and substantial motion restriction. Histologically, FL consists mainly of fibrous structural proteins (collagens, elastin) and contains much less amounts of ground substance and cells. [1],[2]. Collagen and elastin are known to be key elements for the biomechanical properties of the fascial structures. Collagen fibres can be easily visualize by means of light and confocal microscopy (autofluorescence), but visualisation of elastic fibres, particularly accessing their three-dimensional arrangement is much more demanding [3].

The aim of the study was to clarify the comprehensive mechanical properties and microscopic structure of human *fascia lata* for a better understanding of its behavior.

2. Material and Methods

The samples, of pathologically unchanged human *fascia lata*, used in this study were collected *post-mortem* from 36 adult males in different age groups (I group – age up to 21 years old, II group –age range 40-51 years old, III group – age over 60 years old). The material had not been frozen prior to examination. Specimens were excised in two directions: longitudinal and transvers to the collagen fibres alignment.

Uniaxial tensile tests were performed at room temperature at a constant crosshead speed of 5 mm/min using an MTS® Synergie 100 testing machine. The initial specimen length was always 15 mm, the correct tensile test were preceded by 3 loading-unloading cycles. Additionally part of the material were fixed in 10% buffered formalin, paraffin-embedded, sectioned to 5 µm sections, stained with haematoxylin and eosin (H&E). The observations of the collagen fibres were carried out using a light microscope (Zeiss Axio Imager M1m). Use of confocal microscopy (Zeiss LSM 510 META) combined with selective fluorochrome sulforhodamine (SRB) assay helped to visualize elastic elements more efficiently [4]. The laser at 561 nm was used to excite SRB and the corresponding signal from elastic was collected within the range 575-615 nm.

*Corresponding author: Sylwia Szotek, e-mail: sylwia.szotek@pwr.edu.pl

3. Results and Discussion

The completed mechanical tests have shown, above all, the anisotropic properties of the examined tissue. Nonlinear stress-strain curves were obtained from each tested specimen. The conducted tests determined the values of the particular mechanical parameters, e.g., stiffness coefficient (k), ultimate tensile strength (σ_{UTS}), and Young's modulus (E) (Fig.1A).

In case of the stiffness coefficient, the direction of excision of the samples was important, as much higher values (even more than 10 times) were obtained for the longitudinal direction in all age groups. Tensile strength values obtained for longitudinal samples were higher than for transverse samples and their average values were in the range of 6-12 MPa. In case of Young's modulus, the obtained values were even 10 times higher for longitudinal than transverse samples, the average values of this parameter ranged from about 8-83 MPa.

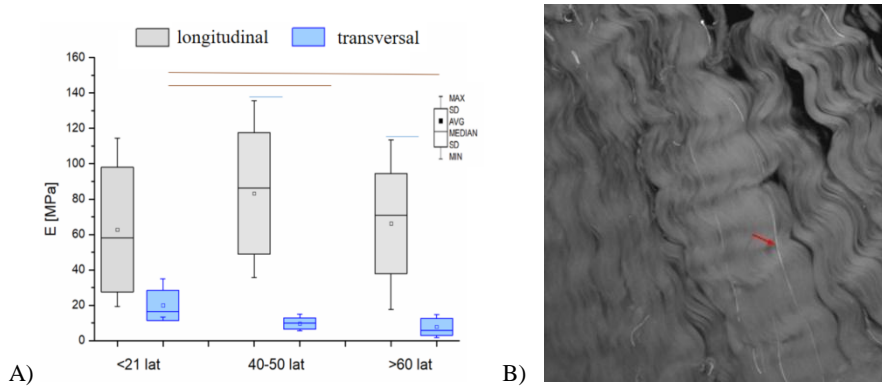


Fig. 1. A) Median Young's modulus (E) for specimens of human FL tested longitudinally (grey) and transversally (blue) to collagen bundles arrangement. B) Elastic fibres (arrow) within the human FL selectively stained with SRB in confocal microscopy (scale bar: 40 mm)

Confocal microscopy and sulforhodamine B (SRB) assay enabled us to visualise collagen and elastin elements more efficiently without a need for sample fixation (Fig. 1B). The collagen bundles were much more numerous and they were organised regularly and tightly. Elastin fibres, comparing to collagen fibres were less numerous and in general, they were organised parallel to the main directions of collagen bundles arrangement. They exhibited different thickness and length.

Knowledge of the mechanical behaviour and microscopic characteristic of human FL is a key feature in many clinical and tissue engineering applications as well as numeric fascial modelling.

Acknowledgments: This research project is supported by grant NCN no. N N518 286540.

References

- [1] PEABODY T., BORDONI B. *Anatomy, Bony Pelvis and Lower Limb: Fascia Lata*. StatPearls Publishing, 2023
- [2] BONALDI L., BERARDO A., PIRRI C., STECCO C., CARNIEL E.L., FONTANELLA C.G. *Mechanical Characterization of Human Fascia Lata: Uniaxial Tensile Tests from Fresh-Frozen Cadaver Samples and Constitutive Modelling*. *Bioengineering* (Basel). 2023, 7,10(2):226
- [3] SZOTEK S., DAWIDOWICZ J., EYDEN B., MATYSIAK N., CZOGALLA A., DUDZIK G., LEŚNIEWICZ A., MAKSYMOWICZ K. *Morphological features of fascia lata in relation to fascia diseases*. *Ultrastruct Pathol*. 2016, 40(6):297-310
- [4] SZOTEK S., DAWIDOWICZ J., GENIUSZ M., KOZAK M., ŁUKOMSKI R., CZOGALLA A., *The biomechanical characteristics of spinal dura mater in the context of its basic morphology*. *Acta Bioeng Biomech*. 2021,23(4):149-159

Electromyographic activity of selected muscles of the lower limbs and the type of lunge in badminton

A. SZPALA*, M. KOŁODZIEJ, M. KAŻMIERCZAK, Z. BAŃKOSZ

Department of Biomechanics, Wrocław University of Health and Sport Sciences, Wrocław, Poland

Key words: *badminton, surface electromyography, lower limb muscles, movement phase*

1. Introduction

Lunge in badminton is the most common movement during the game. Lunge is the last step of the approach shuttlecocks in badminton, the exception being the shots in front of you from the back of the court. It also consists for the first step of returning to the center of the court. The movement structure of the lunge depends on the situation on court, but usually it is a long stride with bent lower limbs, with the rear limb (in right-handers, the left) has mainly a stabilizing function, while the front one (forelimb) fills movement function.

The aim of the study was to assess the selected lower limb muscles activity during three types of badminton lunges (forward vs. sideways vs. backward).

It was assumed that changing the side of the court (forehand vs. backhand), the type of lunge (forward vs. sideways vs. backward) and the phase of movement (approach vs. return) would differentiate the EMG activity of the examined muscles on the right and left side of the body [1]-[5].

2. Material and Methods

A 23-year-old man with a body weight of 70 kg and a body height of 175 cm participated in the study. The examined person had 12 years of competitive experience and was characterized by an advanced level of technical skills.

The study used the method of surface electromyography (EMG) and goniometry (the electrogoniometer was placed in the axis of the knee joint in order to differentiate muscle activity depending on the phase of movement - approach vs. return). A 16-channel electromyographic device (TeleMyo 2400T G2, Noraxon, Inc., Scottsdale, Arizona, USA) was used to acquire EMG signals. The EMG signal was recorded and analyzed with the MyoResearch XP software (Master Edition 1.07.05, Noraxon, USA). The sampling frequency of the EMG signal was 3 kHz. The EMG activity of the following muscles of the right (R) and left (L) lower limbs was measured: vastus lateralis (VL), vastus medialis (VM), rectus femoris (RF), biceps femoris (BF) and gluteus maximus (GM) [6]. At the beginning of the experiment, the EMG signal of the tested muscles was measured under maximal voluntary contraction (MVC) conditions in standardized positions. The MVC measurement accounted for 100% of muscle activity, enabled the normalization of the EMG signal in the further stages of the research and its statistical analysis carried out on percentage data. The main task of the tested person was to perform three types of lunges (forward, sideways and backward) from the starting position (so-called neutral) to both sides of the court (forehand, backhand) and return as soon as possible. The examined person was right-handed, hence the muscles of the right lower limb had a motor function, and the left one – a stabilizing function. The subject performed 8 repetitions of each type of exercise with a badminton racket. During the measurements, the subject simulated the shuttlecock shots.

*Corresponding author: Agnieszka Szpala, e-mail: agnieszka.szpala@awf.wroc.pl

Statistical analysis was performed in Statistica v.13.3. (StatSoft, Inc., Tulsa, Oklahoma, USA). The differentiation of variables was assessed by multivariate analysis of variance. The significance level was set at $p < 0.05$.

3. Results

Based on the multivariate analysis, a significant effect of the side of the court, the direction of the lunge and the phase of movement on the differentiation of lower limb muscle activity was found. The direction of the lunge differentiated the activity of the following muscles VM_L, RF_L and BF_P only at the forehand, while VL_R, RF_R and GM_L at the backhand, GM_R activity was differentiated at both sides of the court. The highest activity for these muscles was recorded in the back lunge, with the exception of GM_R, whose activity was the highest during the forward lunge for the forehand and the side lunge for the backhand. Muscle activity in VM_L, VL_L was higher during the return than in the backhand side lunge approach, while for BF_L and GM_L the activity was higher during the forward lunge approach and the forehand lunge backward approach.

4. Conclusions

The relationship between the activity of the lower limb muscles during the player's movement in badminton with the side of the court, the direction and the phase of the lunge may be important in creating training plans to strengthen these muscle groups that play the greatest role during motor tasks in badminton. They can also be useful in creating the concept of strength training that eliminates too large differences in the level of activity of the muscles of the lower and right lower limbs [7], [8], [9].

References

- [1] NADZALAN A.M., MOHAMAD N.I., LEE J.L.F., TAN K., JANEP M., HAMZAH S., CHINNASEE C. *Muscle activation analysis of step and jump forward lunge among badminton players*. J Sci Eng Res. 2017, 1(2): 60-65
- [2] STURGESS S., NEWTON R. U. *Design and implementation of a specific strength program for badminton*. Strength Cond J. 2008, 30(3), 33-41
- [3] KUNTZE G., MANSFIELD N., SELLERS W. *A biomechanical analysis of common lunge tasks in badminton*. J Sports Sci, 2010, 28(2), 183-191
- [4] FARROKHI S., POLLARD C. D., SOUZA R. B., CHEN Y. J., REISCHL S., POWERS C. M. *Trunk position influences the kinematics, kinetics, and muscle activity of the lead lower extremity during the forward lunge exercise*. J Orthop Sports Phys Ther, 2008, 38(7), 403-409.
- [5] HUSSAIN I., ARSHAD BARI M. *Kinematical analysis of forehand and backhand smash in badminton*. Innov Syst Des Eng. 2011, 2(7):20-6
- [6] HERMENS H.J., FRERIKS B., DISSSELHORST-KLUG C., RAU G. *Development of recommendations for SEMG sensors and sensor placement procedures*. J Electromyogr Kinesiol, 2000, 10:361-374
- [7] TSAI C.L., YANG C.C., LIN M.S., ET AL., *The surface EMG activity of the upper limb muscles of badminton forehand and backhand smashes*. In: Schwameder H, Strutzenberger G, Fastenbauer, et al., editors. 24th International conference of biomechanics in sports. Salzburg: 2006. pp. 3-6.
- [8] TSAI C.L., YANG C.C., LIN M.S., ET AL., *The surface EMG activity analysis between badminton smash and jump smash*. In: Wang Q, editor. 23th International Symposium on Biomechanics in Sports. Beijing: 2005. pp. 483-486
- [9] GOWITZKE B.A., WADDELL D.B. *Biomechanical studies of badminton underarm power strokes, court movement, and flexibility - a review*. In: Morrison WE, editor. 7th International Conference on Biomechanics in Sports. Victoria: 1989. p. 1-24

Analysis of ways to mount prosthetic dental bridge on implants

A. SZUST^{1*}, A. WYBRANIEC¹, D. NASULICZ², M. MAJ¹

¹Department of Mechanics, Materials and Biomedical Engineering, Faculty of Mechanical Engineering, Wrocław University of Science and Technology, Wrocław, Poland

²Nasulicz i Nosow LTD

Key words: dental prosthetic bridge, mandible implantation

The study presents results of preliminary experimental and analytical studies aiming to establish an optimal way to mount a prosthetic bridge on mandible implants.

Optimal mounting of prosthetic bridge will help to reduce a risk of previously observed complications. Such complications may appear immediately after implantation and are typical for single tooth implantation cases [2,3]. But there is another set of problems that can arise even after several months since mounting of prosthetic bridge. Previous observations show that fixed prosthetic bridges mounted on implants get less stable over time. Distal implants during loading gradually widen the canal in which they were implanted.

In this study three ways of mounting a prosthetic bridge are shown:

- bridge mounted on 4 implants (front and middle)
- bridge mounted on 4 implants (front and back)
- bridge mounted on 6 implants (Fig. 1)



Fig. 1. X-ray of patient's mandible several months after implantation. Showing dental prosthetic bridge, mounting implants, and conspicuous bone loss in area of distal implants

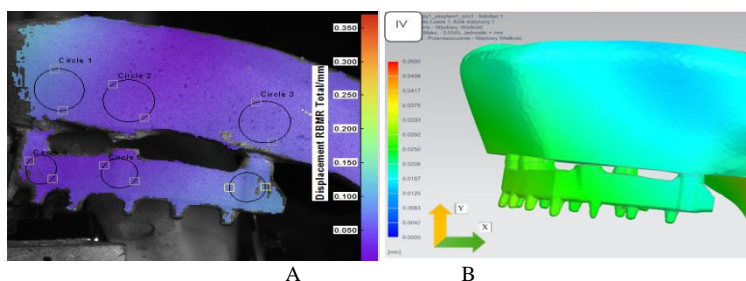


Fig. 2. A. Image of displacements obtained during experiment (DIC) B. Image of displacements obtained using analytical method – FEM

*Corresponding author: Agnieszka Szust, e-mail: agnieszka.szust@pwr.edu.pl

Measurements of displacements on the mandible surface and prosthetic bridge were done using Digital Image Correlation (DIC) method. Fig. 2 A shows marked areas analysed during the experiment. Same areas were evaluated using analytical method – FEM.

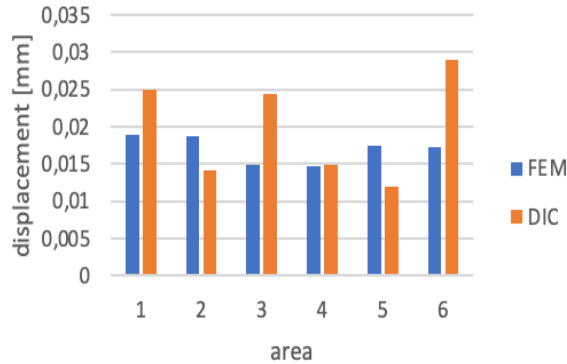


Fig. 3. Comparison of total displacement values in analysed (Fig. 2) mandible (1,2,3) and bridge (4,5,6) areas in case of 6 implant mounting method.

In this study polyurethane mandible models and actual prosthetic bridges and dedicated dental implants were used. The study is advanced phase but many mounting combinations were not analyzed yet. For the final conclusions we need to wait until the project is finished.

References

- [1] ZHONG J., GUAZZATO M., CHEN J., ZHANG Z., SUN G., HUO X., LIU X., AHMAD R., LI Q. *Effect of different implant configurations on biomechanical behavior of full-arch implant-supported mandibular monolithic zirconia fixed prostheses*. J Mech Behav Biomed Mater. 2020, 102:103490
- [2] ZOR Z., KILINÇ Y., ERKMEN E., KURT A. *Evaluation of biomechanical effects of different implant thread designs and diameters on all-on-four concept*. J Osseointegration, 2021, 13(3), 101–108
- [3] AHMADI A., DÖRSAM I., STARK H., HERSEY S., BOURAUUEL C., KEILIG L. *The all-on-4 concept in the maxilla-A biomechanical analysis involving high performance polymers*. J Biomed Mater Res B Appl Biomater. 2021, 109(11):1698-1705

Advancements in Maxillofacial Reconstruction: Design and Manufacturing of Patient-Specific Implants

P. SZYMCZYK-ZIÓLKOWSKA*, G. ZIÓLKOWSKI, D. KĘSZYCKI, K. KOBIELA, M. RUSIŃSKA, K. SEKUŁA

Faculty of Mechanical Engineering, Wrocław University of Science and Technology, Wrocław, Poland

Key words: *Maxillofacial Reconstruction, Patient-Specific Implants (PSI), Electron Beam Powder Bed Fusion (PBF-EB/M), Mandible Injury, Finite Element Analysis (FEA)*

1. Introduction

Craniofacial reconstruction requires proper attention to aesthetics and matching the patient's anatomy. Autologous bone grafts and generic implants used in this type of surgery allow only partial restoration of the patient's appearance, mainly focusing on restoring mechanical and protective functions. While this physical features are of the highest importance, it is crucial to also take into consideration the patients mental well-being, that can be strongly influenced with after-reconstruction appearance. Especially when the reconstructed body part is exposed in everyday life and might be surrendered to public reactions. Commercially available implants for craniofacial restoration come in standard shapes that require manual adjustments and sculpting to achieve a perfect fit for each patient [1]. Unfortunately, this process is time-consuming and imprecise [2], moreover the bending and adjusting of the implants during surgical procedures not only lead to fatigue and stress but also increase the risk of implant failure in general. Regarding the bone grafts may not be well-matched to the geometry of the face, leading to potential issues with facial symmetry and appearance. This lack of precise fit could result in complications and suboptimal aesthetic outcomes for the patient. The patient specific implants used in mandibular deformity surgeries allow for a significant reduction in pain, improved speech, appearance, and well-being of the patient. Facial symmetry and occlusion are also restored, with correct movements in all planes [3]

The patient, for whom implant was designed was 32 years old male who suffered from mandible injury caused by a gunshot in the chin area of craniofacial region. Immediately after the accident, the patient was treated in clinic, and fragments of shattered mandible were removed from the surrounding soft tissues. Bone loss was replaced by two plates and there were no drastic loss in soft tissues after the medical procedure. Resulting bone loss is located in the 33-41 area. As a result of surgery the whole thickness of mandible was not restored, which qualified the patient for the secondary reconstruction.

2. Materials and Methods

2.1. Material and Technology

The Ti-6Al-4V ELI powder was used to manufacture implants. The chemical composition (in wt%) of powder was determined by the spectroscopy method to be: 6% Al, 4% V, 0.25% Fe, and Ti as the remainder is per the ASTM F136-13 Standard. Process parameters were selected for the production of test samples and demonstrators in the form of personalized jaw implant.

2.2. PSI Design method

Fig. 1 presents stages of designing revised PSI. In a) the state right after the first surgery is shown, when bone loss is treated with two plates.

*Corresponding author: Patrycja Szymczyk - Ziółkowska, e-mail: patrycja.e.szymczyk@pwr.edu.pl

In b) is the proposed geometry of an implant overlapping with the model of a mandible after plates were removed is presented. In c), the implant is selected over the bone tissue to subtract one from another, and finally, in d) is the model of an implant with trimmed bone tissue is shown.

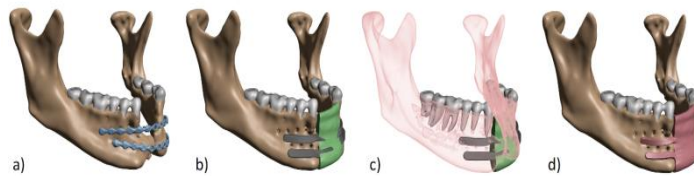


Fig.1. Flow chain of personalised jaw implant designing

2.3. Numerical Analysis

Most of the loads in the mandible are related to the mastication process. Muscles in the craniofacial area of human body allows to perform clamping of the teeth. Numerical analysis were performed to determine behaviour of the implant's model in that mechanical condition.

2.4. Post Processing

Use of additive manufacturing technology required the application of a multistage post-processing treatment. The first stage involved machining, which could be limited to only the finishing process of mounting sockets of the implant, thanks to the use of AM. In terms of manufacturing the implant, the most crucial aspects was to make the mounting points between the implant and the patient's bone tissue. Since the implant is designed to function in the human body for a long period of time, the dimensional and geometrical accuracy of a non-permanent fastening connection was an important issue.

3. Results

Presented process for designing and manufacturing PSI includes processing CT scans to acquire volumetric models of bone tissue, which were used to propose geometry of the implant. FEA allowed to determine if the implant would fulfil the mechanical criteria for its proper behaviour after implantation. The obtained results demonstrated that the geometry of an implant would not exceed mechanical strength of the material, which can be understood as the correct design of the geometry. Manufacturing the implant revealed technological aspects that also have to be considered throughout the process, such as creating mounting points, proper orientation of the element in the working chamber of PBF-EB/M and post-processing. As shown, the process of designing an implant is a complex issue, with many variables, which may affect the patient's final outcome, a crucial factor in medical applications. Nevertheless, future investigating into implant design need to be complemented with the influence of different manufacturing methods and mechanical tests, which will validate calculations obtained from the FEA and will determine if the manufacturing process is repeatable and consistently leads to a high-quality product.

References

- [1] MOIDUDDIN K., MIAN S.H., ELSEUFY S.M., ABDO BMA, ET AL., *Craniofacial Reconstruction with Personalized Lightweight Scaffold Fabricated Using Electron-Beam Additive Manufacturing*. Metals. 2022, 12(4):552
- [2] YANG W., CHOI W.S., WONG M.C.-M., POWCHAROEN W., ZHU W., ET AL., *Three-Dimensionally Printed Patient-Specific Surgical Plates Increase Accuracy of Oncologic Head and Neck Reconstruction Versus Conventional Surgical Plates: A Comparative Study*. Ann Surg Oncol. 2021, 28, 363–375
- [3] V U., MEHROTRA D., HOWLADER D., SINGH P.K., GUPTA S. *Patient Specific Three-Dimensional Implant for Reconstruction of Complex Mandibular Defect*. J Craniofac Surg. 2019, 30(4):e308-e311

Analysis of bone remodelling in the mandible with the implant reconstruction of bone defect

A. TOMASZEWSKA*, S. PISZCZATOWSKI

Institute of Biomedical Engineering, Białystok University of Technology, Białystok, Poland

Key words: *bone remodelling, bone tissue, mandibular, implant, numerical simulation*

1. Introduction

A mandibular bone defect is the most often caused by removal of a cancerous lesion. In order to restore the anatomical structure of the mandible, such defects are reconstructed with use of implants. The introduction of the implant into the native bone structure disrupts the biomechanical conditions of the mandibular bone functioning and thus triggers the bone remodelling process. At this point, the bone tissue adapts to the new biomechanical conditions.

The aim of the present study was to analyse the bone remodelling occurring around the implant used for mandibular bone defect reconstruction. Influence of the various loading conditions, resulting from chewing variations, on the bone remodelling process will be analysed also.

2. Methods

2.1. Geometrical model and Material properties

The geometrical model of the mandible was developed on the base of image data acquired using computed X-ray tomography, processed with use of MIMICS software (Materialise, Belgium). The entire bone volume was divided into two regions, basing on the occurrence of the trabecular or cortical tissue. Cortical layer with thickness in the range 1.6÷7.8 mm surrounded inner trabecular structure [1]. Bone defect was modelled by cutting bone fragment and an implant was introduced into this space. The discretisation of the model was performed in ANSYS software (Ansys Inc., Canonsburg, USA) using Solid187 10-node tetrahedral elements. The mesh was optimised globally and locally - in the region of implant-bone contact.

A simplified isotropic model was used, both for cortical and trabecular bone, assuming the following material parameters; for trabecular bone: $E=1.37$ GPa; $\nu=0.3$; $G=0.52$ GPa and for cortical bone: $E=13.7$ GPa; $\nu=0.3$; $G=5.26$ GPa. Two variants of implant material was analysed, taking implant material properties corresponding to technically pure titanium ($E=103$ GPa; $\nu=0.3$; $G=76.9$ GPa) and polyether ether ketone (PEEK) ($E=20$ GPa; $\nu=0.3$; $G=1.38$ GPa). [2]

2.2. Loading conditions

The mandibular model was supported in a way simulating conditions occurring in the temporomandibular joints, leaving only the possibility of rotation around the joint axes and fixing the other degrees of freedom. Forces developed by the particular muscles that are involved in the chewing mechanism [3] were applied also. Moreover, contact conditions occurring between the teeth of the mandible and maxilla during chewing were also modelled taking into account 4 variants of masticatory conditions: variant 1 - represented the way in which the lower incisors symmetrically contact with the upper incisors (Fig. 1a); variant 2 - represented the way in which the lower molars symmetrically contact with the upper molars (Fig. 1b); variant 3 - represented a way in which the lower molars on the implant side contact with the upper molars (Fig. 1c); variant 4 - represented a way in which the lower molars on the opposite side to the implant contact with the upper molars (Fig. 1d).

*Corresponding author: Anna Tomaszewska, e-mail: anna.tomaszewska@sd.pb.edu.pl

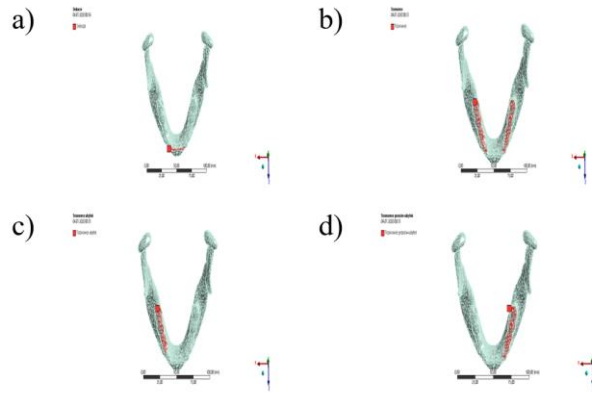


Fig. 1. Location of tooth contact during mastication: a) variant 1; b) variant 2; c) variant 3; d) variant 4

2.3. Remodelling of the bone tissue

Bone remodelling was simulated using the algorithm based on the procedure proposed by Huiskes [4] and further developed by Weinans [5]. The change in bone density (ρ) was related to the response to a mechanical stimulus (S), which was expressed as the ratio of strain energy to bone density. The change in density over time was described as (1).

$$\frac{d\rho}{dt} = B(S - k), \quad (1)$$

where: ρ – bone density, S – mechanical stimulus, k – threshold value for the stimulus, B – constant.

3. Results and Discussion

The main results of the simulations were the patterns of bone density distributions including changes resulting from functional adaptation. It is possible to observe, that:

- the most intensive bone remodelling has occurred around the corners of the implant,
- metallic implant (pure titanium) provided more intensive stimulation of bone remodelling comparing to PEEK implant,
- in the case of masticatory conditions where the contact between the lower and upper molars is asymmetrical, the distribution of bone density is also asymmetrical in regard to the sagittal plane with increased bone remodelling intensity to the side where the teeth meet.

Some weaknesses were noted in the simulation of bone remodelling using the Huiskes-Weinans procedure. Further development of the model, taking into account biological aspects of the bone remodelling process is necessary for further improvement of accuracy of bone adaptation prediction.

Acknowledgments: Research was performed as a part of projects WI/WM-IIB/7/2021 and WI/WM-IIB/5/2023 and financed with use of funds for science from Polish Ministry of Education and Science.

References

- [1] COX T., KOHN M. W. *Computerized Analysis of Resorbable Polymer Plates and Screws for the Rigid Fixation of Mandibular Angle Fractures*, J Oral Maxil Surg. 2003, 61(4): 481-487
- [1] FESTAS A.J, ET AL., *Medical devices biomaterials – A review*. J Mater Design Appl, 2020, 234(1), 218-228
- [2] GREGOLIN R.F, ZAVAGLIA C.A, ET A., *Biomechanical Stress and Strain Analysis of Mandibular Human Region from Computed Tomography to Custom Implant Development*, Adv Mater Sci Eng. 2017, 2017: 1-9
- [3] HUISKES R., ET A., *Adaptive Bone-Remodeling Theory Applied To Prosthetic-Design Analysis*, J Biomech, 1987, 20(11-12), 1135-1150
- [4] WEINANS H., ET A., *The Behavior Of Adaptive Bone-Remodeling Simulation-Models*, J Biomech1992, 25(12), 1425-1441

Research on the flow characteristics in artificial vessels: an experimental investigation using the PIV method

M. TOMASZEWSKI^{1*}, M. KUCEWICZ¹, R. RZEPLIŃSKI², J. MAŁACHOWSKI¹, B.M. CISZEK²

¹Faculty of Mechatronics, Armament and Aviation, Institute of Rocket Technology and Mechatronics, Military University of Technology, Warsaw, Poland

²Department of Descriptive and Clinical Anatomy, First Department of Anesthesiology and Intensive Care, Medical University of Warsaw, Warsaw, Poland

Key words: *PIV, artery, blood flow*

1. Introduction

It is estimated that one person dies of a stroke every 6 seconds worldwide [1]. Therefore, stroke prevention poses a significant scientific challenge, and understanding of precise stroke mechanisms is being made possible through experimental research and numerical methods. The blood vessels in the brain have considerably smaller dimensions compared to other arteries in our body, resulting in distinct blood flow characteristics [2]. This paper explores the potential of employing the particle image velocimetry (PIV) technique to study flow in small-diameter vessels and its potential application in investigating printed vessels within the circulatory system, which offer high transparency.

2. Conducting of experimental tests

2.1. PIV method description

The experimental flow study was conducted using the optical Particle Image Velocimetry (PIV) measurement technique [3,4]. This technique involves the use of a two-pulse laser source to create a measurement plane. The laser beam is directed into the measurement section through carefully positioned mirrors and lenses. A CCD camera is positioned perpendicular to the measurement plane to capture a series of double images, effectively freezing the exposure. On the basis of a sequence of images taken at predetermined intervals, calculations are performed to determine the displacement of particles within the flowing fluid. Small-diameter vessels and their potential application in investigating printed vessels within the brain circulatory system, which offer high transparency.

2.2. Experimental stand

A dedicated frame was used for measurements, simplifying precise positioning of the various components of the kit and ensuring that perpendicular angles are maintained. The frame used in this study is located at the WIM WAT facility. In the center of the frame is a tank made using additive manufacturing technology. Inside the tank, filled with water, a vessel was attached in which the flow will be analyzed (Fig. 1). Special connectors were used at the ends of the measuring sections, which it is possible to connect the silicone tubes that supply the fluid.

*Corresponding author: Michał Tomaszewski, e-mail: michal.tomaszewski@wat.edu.pl

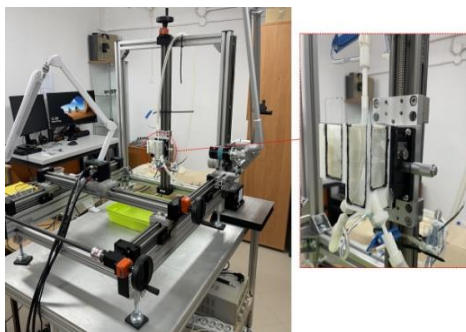


Fig. 1. View of the test stand and close-up of the measuring sample

3. Results

As a result, velocity distributions were obtained in selected vessel geometries. The measurement was analyzed for pulsatile flow. The pressure and flow rate curves for individual outlets were recorded. A selected qualitative map of the velocity distribution from PIV measurements for the vessel at the bifurcation location is presented below (Fig. 2). This presentation is part of ongoing research, and the described aspects will be further discussed during the conference.

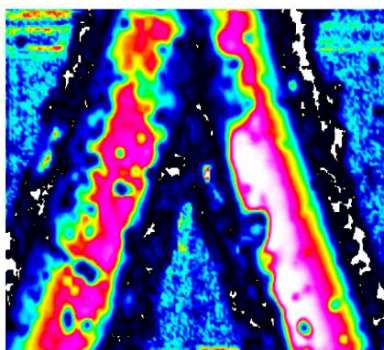


Fig. 2. Qualitative distribution of fluid flow velocity based on PIV measurement

Acknowledgments: The study was founded by the National Science Centre, Poland (award number 2020/37/B/ST8/03430, Recipient: Jerzy Małachowski, Prof., D.Sc., Ph.D., Eng.).

References

- [1] MENG H., TUTINO V.M., XIANG J., SIDDIQUI A. *High WSS or Low WSS? Complex Interactions of Hemodynamics with Intracranial Aneurysm Initiation, Growth, and Rupture: Toward a Unifying Hypothesis.* *AJNR Am J Neuroradiol.* 2014, 35(7):1254-62. DOI:10.3174/ajnr.A3558
- [2] RZEPLIŃSKI R., TOMASZEWSKI M., SŁUGOCKI M., KARCZEWSKI K., KRAJEWSKI K., SKADORWA T., MAŁACHOWSKI J., CISZEK B. *Method of creating 3D models of small caliber cerebral arteries basing on anatomical specimens.* *J Biomech.* 2021 Aug 26,125:110590. doi: 10.1016/j.jbiomech.2021.110590
- [3] TOMASZEWSKI M., SYBILSKI K., BARANOWSKI P., MAŁACHOWSKI J. *Experimental and numerical flow analysis through arteries with stent using particle image velocimetry and computational fluid dynamics method.* *J Appl Biomater Funct Mater.* 2015 Jul 4,13(2):e116-26. doi: 10.5301/jabfm.5000217
- [4] TOMASZEWSKI M., SYBILSKI K., MAŁACHOWSKI J., WOLAŃSKI W., BUSZMAN P.P. *Numerical and experimental analysis of balloon angioplasty impact on flow hemodynamics improvement.* *Acta Bioeng Biomech.* 2020, 22(3): 169-183

Clustering of Strains Datasets of Human Abdominal Wall with Self-Organising Maps

M. TROKA*, K. SZEPIETOWSKA, I. LUBOWIECKA

Department of Structural Mechanics, Gdańsk University of Technology, Gdańsk, Poland

Key words: *mechanics of abdominal wall, machine learning, in vivo measurements, strain field, clustering*

1. Introduction

The study aims to make a step towards mechanical identification of mechanically similar regions of human anterior abdominal wall. Motivation of the conducted studies are recurrences of the ventral hernia, which affect around 30% of operated patients [1]. Hernia is a medical condition characterised by a discontinuity of the abdominal wall (AW). It needs a common surgical reconstruction procedure which usually is done with the use of an implant [1].

To improve well-being of patients and decrease the number of recurrences there is a need for an implant which is mechanically compatible with the abdominal wall. To develop such an implant the knowledge of mechanical properties of AW is an imperative. To gather this knowledge, we collected information of mechanical behaviour of human AW under changing pressure load and analysed it using Self-Organising Maps (SOM), an unsupervised machine learning model, which is able to cluster experimental data based on their similarity. Hence, it can provide us with information about regions of AW which may have similar mechanical performance under pressure load.

2. Material and Methods

2.1. DIC

Experimental data were acquired during peritoneal dialysis (PD) of twelve patients with the use of Digital Image Correlation (DIC) system. All participants submitted a consent to participate in the study under a protocol approved by the local Ethics Committee (NKBBN 314/2018). PD is a medical procedure in which a dialysis fluid is introduced into the abdominal cavity. This causes a growth of intraperitoneal pressure and a deformation of AW. DIC is able to track and register movements of special patterns printed on the surface of abdomen [2]. Measured data were used to calculate 3D fields of displacements and strains, which later were applied as an input for SOM analysis. Half of the AW surface is considered due to the experiment limitations, i.e., patients had a catheter and a part of the abdominal wall covered by a bandage.

2.2. SOM

Self-Organising Maps is an unsupervised machine learning model, which is able to reduce dimensionality of large multivariate datasets, thus making it possible to visualise and analyse [3]. In this paper the feature of SOM that is utilised is clustering power. Clustering is done by algorithmic calculation of data samples and grouping similar data in said clusters. In this study SOM Toolbox for MATLAB was used [4]. Input for SOM analysis are principal strains \mathcal{E}_1 calculated for the tested human subject on the basis of experimental data for all time steps of PD, which takes around 10minutes. This way we can consider the change of \mathcal{E}_1 in time during loading, here 2048 time steps.–Therefore, the input

*Corresponding author: Mateusz Troka, e-mail: mateusz.troka@pg.edu.pl

vector for SOM contains \mathcal{E}_1 varying in time and in the space of the AW surface (2048 variables, 493 points on the AW surface).

3. Results

The results of SOM can be presented on U-matrix (unified distance matrix) map as clusters of data as presented in Fig. 1. Those clusters are groups of points of abdominal wall that are characterised by similar evolution of \mathcal{E}_1 in time. Then, the clusters can be reversely mapped onto the surface of the abdomen of the patient (Fig. 1c) showing the resultant areas of similar mechanical behaviour under pressure. The best clustering quality was found to come from two clusters. It was evaluated based on silhouette value, which is a common index for visual evaluation of clustering [5]. Apart from that, it is confirmed on the U-matrix and clusters map (Fig. 1a,b). Clusters borders divide different groupings, which can be visually identified by bright colours of distance nodes (Fig. 1a). In case of analysed subject, the clusters divide the abdominal wall into three horizontal zones, where top and bottom belong to the same cluster and the middle horizontal-like stripe behaves differently.

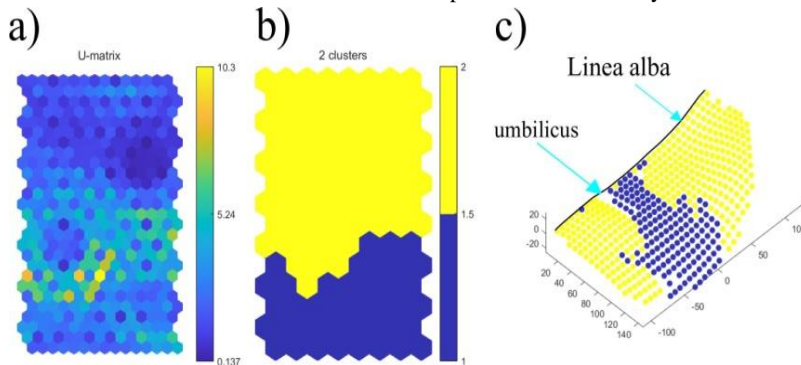


Fig. 1. a) U-matrix, b) clusters colour map, c) surface of the abdomen of examined patient with mapped clusters

4. Conclusions

The study based on SOM allowed us to consider a large range of deformation states of the whole abdominal wall surface during loading in one analysis. This type of analysis, gives us more information than observation of a single mechanical quantity in a single time moment. The analysis enables to reduce dimensionality of description of full-field deformation in time. The obtained clusters indicate two separate areas of the abdominal wall, which may differ from each other in terms of mechanical properties and performance. The presented methodology may help to adjust the design of implants used in hernia repairs to the specific regions of the human abdominal wall.

Acknowledgments: This work was supported by the National Science Centre (Poland) [grant No. UMO-2017/27/B/ST8/02518]. Calculations were carried out partially at the Academic Computer Centre in Gdansk.

References

- [1] DEEKEN C.R. LAKE S.P. *Mechanical properties of the abdominal wall and biomaterials utilized for hernia repair.* J Mech Behav Biomed Mater. 2017, 74:411-427
- [2] LUBOWIECKA I., ET AL., *A novel in vivo approach to assess strains of the human abdominal wall under known intraabdominal pressure.* J Mech Behav Biomed Mater. 2022 Jan,125:104902
- [3] KOHONEN T. *Essentials of the self-organizing map.* Neural Netw. 2013, 37:52-65
- [4] VESANTO H. J., JUHA. *SOM Toolbox for Matlab 5*, vol. 2, no. 0, 2000.
- [5] KAUFMAN L. ROUSSEEUW P. J., EDS., *Finding Groups in Data.* HOBOKEN, NJ, USA: JOHN WILEY & SONS, INC., 1990

The development process of the tissue's direct piezoelectric effect measurement device

I. WAŻYDRĄG*, S. ŁAGAN

Faculty of Mechanical Engineering, Cracow University of Technology, Cracow, Poland

Key words: *direct piezoelectric effect, bone tissue, compressive test*

Abstract

A piezoelectric material is considered to be any material that changes its polarity when external stresses are applied, and the application of an external electric field causes a change in its dimensions [1]. This effect also occurs in tissues, including bone tissue through type I collagen [2, 3]. Its physiological importance and potential applications in biomaterials and implant engineering [4] are the motivation for the development of a device that allows easy and universal measurement of the direct piezo effect in tissues. This work presents further development of the device for quantitative measurement of direct piezoelectric effect dedicated to tissues and biomaterials. It outlines the theoretical basis of the piezoelectric effect in human body using bone tissue as an example, an improved version of the measurement system, for which the device architecture and the test protocol were modified. To verify the device's performance, two bovine tibia bones were obtained. Specimens from both frozen and those from treated cortical bone were connected by electrodes to the device and galvanically separated from the mechanical test system, after which they were subjected to a compression test. Based on the data obtained during the tests, it is possible to determine the piezoelectric charge constants of the material.

References

- [1] Blicharski M., *Inżynieria materiałowa*. WNT, Warsaw, 2014.
- [2] Fukada E., Yasuda I. *On the piezoelectric effect of bone*. J Phys Soc Japan, 1957, 12 (10), 1158-1162
- [3] Minary-Jolandan M. *Shear piezoelectricity in bone at the nanoscale*. Appl Phys Lett, 2010, 97, 153127
- [4] Khare D., Basu B., Dubey A.K. *Electrical stimulation and piezoelectric biomaterials for bone tissue engineering applications*. Biomaterials. 2020, 258:120280

*Corresponding author: Igor Ważydrąg, e-mail: igor.wazydrag@gmail.com

Numerical simulations of mandible angle fracture stabilization by means of mini-plate stabilization

P. WĄDOŁOWSKI*

The Institute of Aeronautics and Applied Mechanics, Warsaw University of Technology, Warsaw, Poland

Key words: *osteosynthesis, mandible fracture, mini-plate connection, FEM analysis, contact mechanics*

1. Introduction

The aim of this study was to analyse the stabilization performance of five most common mini-plate fixation types. As a key performance indicators were used relative displacement of bone fragments, overall fixation stiffness, the elastic strain intensity within cortical bone, equivalent stress within metallic plates and temporomandibular joints forces variation. Numerical simulations were conducted for both, bearing and sharing load transfer types.

2. Materials and Methods

2.1. Modeling approach

The mandible bone geometry was mapped from a CT scan of a 24-year-old male hospitalized at the 1st Department of Craniofacial Surgery, Infant Jesus Clinical Hospital in Warsaw. The fracture occurred in the left mandible angle area. Based on the CT data, the three dimensional solid model of mandible bone has been restored, including the cortical and cancellous bone layers. Additionally, the temporomandibular joint model has been created to assure the physiological movement of the bone under applied loads. After the consultation with maxillo-facial surgeon, five connection models have been selected, varying in the number and location of the plates. The plate and screw geometry has been created based on the catalogue of the manufacturer KLS Martin, with the assumption of a simplified threaded connection.

2.2. Numerical model

The discrete models for every type of connection have been created with strong emphasis on the contact modelling and mesh resolution of connecting devices, since this problem is notoriously neglected in studies, but is crucial from the connection mechanics point of view.

Following the Arbeitsgemeinschaft für Osteosynthesefragen organization, the load bearing and load sharing types of connections have been analysed, including the manual forming before the installation. Orthotropy material properties has been assigned to the cortical bone due to the significant stiffness variation along the mandible, while the cancellous bone is described by the elasto-plastic isotropic material curve [1]. For the metallic parts, also the elasto-plastic material curves have been assigned due to the non-linearity phenomena. Considering the manual forming of plates, the prestress effects and residual stresses have been included.

*Corresponding author: Piotr Wądołowski, e-mail: piotr.wadolowski@pw.edu.pl

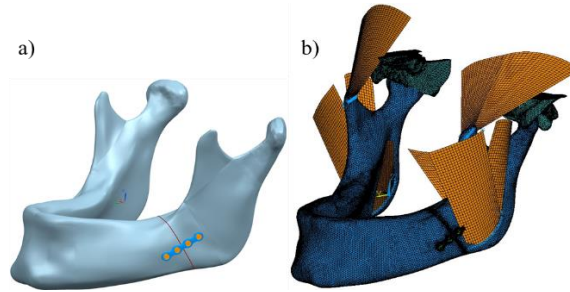


Fig. 1. An example of geometry (a), and FEM (b) of one of the analysed fracture stabilization model

A series of analysis have been calculated for both mentioned types of connection with maximum physiological loading and different types of fracture line clearance conditions. Presented material is a continuation of the works described in article [2].

3. Results

To compare assumed fixation approaches the five performance criterions have been introduced. These include the following:

- mutual displacement of fracture bone fragments, measured on the fracture plane,
- overall fixation's stiffness, measured as the vertical axis direction displacement,
- the elastic strain intensity observed at the cortical bone,
- equivalent stress within the connecting plates,
- temporomandibular reaction variation.

Below figure presents the performance ranking by the colour code, prepared based on the analysis results.

| | Best | Good | Satisfactory | Disappointing | Bad |
|--------------------------|--------|--------|--------------|---------------|-------|
| Model | | | | | |
| Mutual displacement | Yellow | Red | Blue | Green | Blue |
| Overall stiffness | Green | Orange | Blue | Yellow | Blue |
| Elastic strain intensity | Orange | Red | Blue | Yellow | Green |
| Equivalent stress | Yellow | Red | Blue | Yellow | Green |
| TMJ reaction variation | Green | Green | Blue | Orange | Blue |
| Total | 3 | 5 | 1 | 4 | 2 |

Fig. 2. Fixations performance comparison

Presented comparison clearly shows that connection model with two plates located at the angle of mandible provides overall best performance in each criterion. Also the approach with the plate on the oblique line presents acceptable conditions, while the efficiency of one-plate fixations is much worse. However, before the selection of connection type, some more consideration from the medical point of view, like soft tissues damage and blood flow assurance have to be taken.

References

- [1] SCHWARTZ-DABNEY C.L., DECHOW P.C. *Edentulation Alters Material Properties of Cortical Bone in the Human Mandible*. J Dent Res. 2002 Sep,81(9):613-7
- [2] WĄDOŁOWSKI P., KRZESIŃSKI G., GUTOWSKI P. *Finite Element Analysis of Mini-Plate Stabilization of Human Mandible Angle Fracture – A Comparative Study*. Acta Bioeng Biomech. 2020, 22(3):105-116

Multitechnique analysis of dynamics of numerical pedestrian model for forensic applications

D. WADOWICZ, M. PTAK*

Department of Machine Design and Research, Faculty of Mechanical Engineering,
Wroclaw University of Science and Technology, Wroclaw, Poland

Key words: *accident reconstruction, V-SIM, multibody, pedestrian, human body model*

1. Introduction

Forensic experts use various techniques of reconstruction of pedestrian accident. Motion of a human body after impact is often analysed analytically by assuming a point-mass projectile motion [1]. or by using regression formulas derived from results of dummy crash tests or in-depth accident studies [2]. While simple to use, these techniques have limitations, and for more detailed studies human body models (HBMs) are used [3]. HBMs are implemented in various commercial reconstruction packages [4], which allow to integrate police-collected evidence to recreate accident sites and use databases of models of vehicles for simulation. This allows modelling of various accident scenarios, from pedestrian impact to such out-of-the-box cases as falls from heights [5]. An HBM implemented in such a program needs to be easy-to-use, computationally effective and robustly validated to allow for a variety of possible applications.

This study presents how various techniques of analysis of numerical pedestrian model can be used to validate the response of a particular HBM: CYBID Multibody Pedestrian model [6]. The HBM was created using multibody techniques and has already found use in accident reconstruction. In this study, two approaches to analysing the response of an HBM will be presented: using results of a dummy crash test, and an analysis of response of the HBM for various pedestrian initial positions.

2. Methods

Dummy crash test

In the crash test study, a biofidelic PRIMUS dummy was used [7]. The dummy was suspended on an automatic release system. The impacting vehicle was a Toyota Corolla instrumented with an on-board VBOX device to measure velocity. At the moment of impact, the vehicle was fully braking and the collision velocity was recorded to be 46 km/h. The crash test was simulated in V-SIM. The vehicle model was taken from the programs' library and its motion was simulated to match the registered time-velocity curve from the test. Joints of the HBM were positioned using a point cloud of the test site that was registered with 3D scanners before the crash. The final position of the dummy was also recorded using 3D scanning techniques.

The throw distance of the dummy was 12,4 m, while the HBM result was 13.1 m. Joints of the HBM were positioned using a point cloud of the test site that was registered with 3D scanners before the crash. The final position of the dummy was also recorded using 3D scanning techniques. The throw distance of the dummy was 12.4 m, while the HBM result was 13.1 m.

To study the influence of the initial position of the pedestrian, a series of simulations was run. The simulation setup was as described by [8], i.e. Toyota Camry 2010 impacted the pedestrian in full braking; collision velocity was 60 km/h. For each simulation, initial position of the HBM was moved



Fig. 1. Initial posture of the HBM in relation to

*Corresponding author: Mariusz Ptak, e-mail: mariusz.ptak@pwr.edu.pl

in 2cm intervals against the front of the vehicle, resulting in 300 simulations. The setup and running of each simulation was automatized using a dedicated V-SIM scripting interface.

The results for the simulations were compared against a selection of available mathematical models that describe the relation between impact velocity and throw distance, derived for central impact [2], [9], [10].

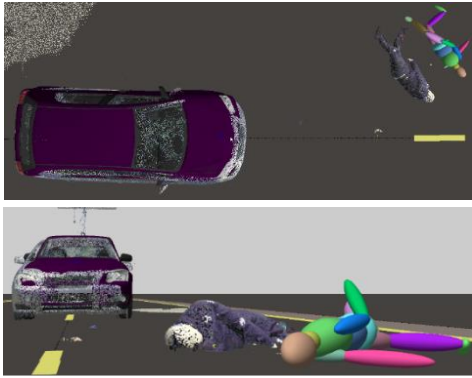


Fig. 2. Comparison between the test and the simulation. Visualization created in V-SIM software

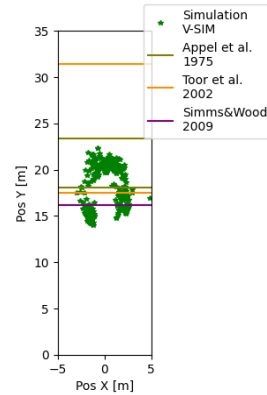


Fig. 3. Final positions of pedestrian body for various central collisions (N=300).

3. Conclusions

Pedestrian impact simulation displayed a higher value of throw distance when compared to dummy crash test, but lower than mathematical models. These difference showcase how diverse reference data for validation of pedestrian HBMs can be. Based on the results, the authors consider the response of the model to be acceptable. Future studies will involve further investigations of the model's sensitivity to initial conditions.

Acknowledgments: The research was partially conducted as a part of the “Implementation PhD” program. The authors acknowledge the support of CYBID sp. z o.o. sp.k. for providing the software and sharing the results of dummy experiments.

References

- [1] SEARLE J. A. *The Physics of Throw Distance in Accident Reconstruction*. 1993, SAE Technical Paper 930659
- [2] SIMMS C., WOOD D. *Pedestrian and cyclist impact: A biomechanical Perspective*, 2009, 166, Springer Science & Business Media
- [3] FERNANDES F.A.O., ALVES DE SOUSA R. J., PTAK M. *Head Injury Simulation in Road Traffic Accidents*. Cham: Springer International Publishing, 2018
- [4] WADOWICZ D., PTAK M. *Numerical Approaches to Pedestrian Impact Simulation with Human Body Models: A Review*. Arch Comput Methods Eng., 2023: 0123456789
- [5] WACH W. UNARSKI J. *Fall from height in a stairwell – mechanics and simulation analysis*. Forensic Sci Int. 2014, 244: 136–151
- [6] WADOWICZ D., BULKA D. *Model ciała człowieka CYBID Multibody Pieszy. Specyfikacja, generator modelu, prace badawcze nad rozwojem modelu (in polish)*. Paragraf na Drodze, 2022, 3(3): 41–56
- [7] SCHÄUBLE A., WEYDE M. *Biomechanical Validation of a New Biofidelic Dummy*, in 26th ESV Conference, 2019
- [8] RICHARDSON S., ET AL., *Pedestrian throw distance impact speed contour plots using PC-Crash*. SAE Tech Pap. 2015: 1–1418
- [9] APPEL H., STÜRTZ G., GOTZEN L. *Influence of impact speed and vehicle parameter on injuries of children and adults in pedestrian accidents*, in Proceedings of the International Research Council on the Biomechanics of Injury Conference, 1975, 3: 83–100
- [10] TOOR A., ARASZEWSKI M., JOHAL R., OVERGAARD R., HAPPER A. *Revision and validation of vehicle/pedestrian collision analysis method*, SAE Trans. 2002: 697–708

Mechanical properties of lattice structures fabricated using incremental technology

K. WILIŃSKA¹, A. NIKODEM, M. KOZUŃ^{2*}

¹BioAddMed, Faculty of Mechanical Engineering, Faculty of Mechanical Engineering, Wrocław University of Science and Technology, Wrocław, Poland

²Department of Mechanics, Materials and Biomedical Engineering, Faculty of Mechanical Engineering, Wrocław University of Science and Technology, Wrocław, Poland

Key words: lattice structures, 3D printing, cellular scaffolding, scaffolds

1. Introduction

In medicine, lattice structures are used in the design of personalized bone implants. The application of lattice structures in medicine is a relatively new area of research, however, many studies indicate that their use can provide many benefits in the treatment of various conditions. The purpose of this study was to characterize the mechanical properties of lattice structures fabricated using incremental technologies and to evaluate the effect of the geometry of the lattice structures on their mechanical properties.

2. Material and method

The material was lattice structures made of polylactide (3D GO Snow White PLA filament) using Fused Deposition Modeling (FDM) incremental technology (Original Prus I3 MK3S printer). Cube specimens (n=60) with an edge of 15 mm were prepared for testing—Six research groups were studied: gyroid, cross, X cell, Schwarz P cell, rings and star. Groups were different not only in geometry, but also in size of unit cells, and density of unit cells in the structure. The geometries of the samples are shown in Fig. 1.

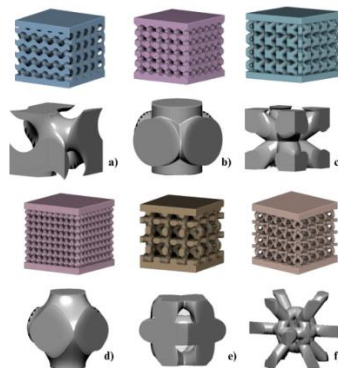


Fig.1 Specimens geometry and their unit cells for the group of a) gyroid b) cross c) X cell d) Schwarz_P cell e) rings f) star

To determine the mechanical properties of specimens, a uniaxial compression test was conducted at a loading rate of 1mm/min. The test was performed using an MTS 858 Mini Bionix testing machine. On the basis of this test, parameters such as Young's modulus (E), yield strength (Re) and conventional

*Corresponding author: Marta Kozuń, e-mail: marta.kozun@pwr.edu.pl

elastic limit were determined ($R_{0.05}$). One specimen from each group was subjected to 3D structural studies using computed microtomography before the mechanical test. For this studies, parameters such as percent object volume (Obj.V/TV), closed porosity (Po(cl)), open porosity (Po(op)), total porosity (Po(tot)), structure thickness (St.Th) were determined.

3. Results

The analysis of mechanical properties showed that the cross group had the highest value of all analysed mechanical parameters. The of these parameters (median) are: 26.4 MPa (R_e), 24.5 MPa ($R_{0.05}$) and 797.2 MPa (E). The lowest value of mechanical parameters is characterized the star group. The values of them obtained for this group are 5.9 MPa (R_e), 5.2 MPa ($R_{0.05}$) and 231.1 MPa (E). The differences obtained between the test groups are statistically significant ($p < 0.05$) and are, respectively: 78%, 79% and 71% (Table 1). The highest values of 3D structural parameters were respectively: Obj.V/TV: 98.53% (star), St.Th: 0.31 μm (star and gyroid), Po(cl): 3.29% (cross), Po(op): 2.04 (rings), Po(tot) 2.65% (rings). The smallest values of these parameters were: Obj.V/TV: 96.4% (cross), St.Th: 0.22 μm (rings), Po(cl): 0.63% (rings), Po(op): 0.32 % (cross), Po(tot) 1.47% (star).

Table 1 Mechanical parameters of lattice structures

| Research group | R_e [MPa] | $R_{0.05}$ [MPa] | E [MPa] |
|----------------|-------------|------------------|---------|
| Gyroid | 10.0 | 8.9 | 379.0 |
| Cross | 26.4 | 24.5 | 797.2 |
| X cell | 13.5 | 12.5 | 453.9 |
| Schwarz P cell | 6.8 | 5.7 | 481.6 |
| Rings | 6.5 | 6.0 | 328.7 |
| Star | 5.9 | 5.2 | 231.1 |

4. Conclusions

Comparing the obtained results with the literature [1], it was found that the course of stress-strain curves are typical for porous materials. The study also showed that the geometry of lattice structures (size and shape of the unit cell) affects the mechanical properties of the obtained samples. The highest values of mechanical parameters are characterized by samples from the cross group. This is also the group that had the highest value of total porosity in the morphometric analysis. Comparing the results obtained in the paper for lattice structures with the mechanical properties of bone tissue [2][3], it was shown that the cross group is not characterized by values of mechanical parameters similar to trabecular bone tissue. The most optimal structure for the application in trabecular bone tissue scaffolds is the star group. None of the groups show similar mechanical properties to cortical bone tissue.

Acknowledgment: The paper is part of the research task entitled. "*Optimization of mechanical properties of lattice structures produced using 3D printing technology*" funded under the pro-quality subvention for the development of research potential of the Mechanical Engineering Department in 2023.

References

- [1] GHOUSE S., BABU S., NAI K., HOOPER P.A., JEFFERS J.R.T. *The influence of laser parameters, scanning strategies and material on the fatigue strength of a stochastic porous structure.* Addit Manuf. 2018, 22: 290–301
- [2] HERMAN I.P. *Physics of the human body in Biological and Medical Physics.* Biomedical Engineering Springer Science & Business Media, 2007, ISBN: 3540296042
- [3] OFTADEH R., PEREZ-VILORIA M., VILLA-CAMACHO J.C., VAZIRI A., NAZARIAN A. *Biomechanics and mechanobiology of trabecular bone: a review.* J Biomech Eng. 2015, 137(1):0108021–01080215

Stock market indexes in assessing balance of patients with Parkinson's disease

P. WODARSKI*, J. JURKOJC¹, J. MICHALSKA², A. KAMIENIARZ², G. JURAS², M.GZIK¹

¹Department of Biomechanics, Faculty of Biomedical Engineering, Silesian University of Technology, Gliwice, Poland

²Department of Human Motor Behavior, Institute of Sport Sciences, Academy of Physical Education in Katowice, Poland

Key words: *Parkinson Disease, Trend Change Index, Posturography, Body Balance*

1. Introduction

Postural stability disorders are one of the basic human problems related to the degeneration of all functional and anatomical systems [1,2]. Problems with balance affect not only elderly people but also patients with neurological problems such as Parkinson's disease (PD) [3]. These disorders can be problematic during activities of daily living and can cause falls resulting in serious injuries [4]. Early diagnosis of PD can lead to earlier treatment, and thus minimize the effects of the disease and associated motor problems. The currently conducted tests use dynamic tests, because effective method of diagnosis and assessment of the severity of PD based on data from the static test on stabilographic platform with open eyes (QS) has not been developed [5],[6].

The conducted investigations aim to utilize stock exchange indices based on trend change analyses in the evaluation of the PD stages using COP displacement signals during the activity of QS.

2. Methods

The experimental groups consisted of 30 subjects with idiopathic PD, 40 age-matched, healthy control subjects, and 20 young, healthy control subjects. The demographic and clinical characteristics of the subjects are presented in Table 1.

Table 1. Characteristics of test groups

| Designation | CGy | CG | PDII | PDIII |
|-------------------------|--------------------------|---------------------------------------|---|--|
| Designation description | Healthy control subjects | Aged-matched healthy control subjects | A group of people with stage II Parkinson's disease | A group of people with stage III Parkinson's disease |
| Group size | 20 (8m and 12f) | 40 (8m and 32f) | 15 (11m and 3f) | 15 (11m and 3f) |
| Age [years] | 20±1.1 | 69±5.5 | 63±7.2 | 69±8.6 |
| Body mass [kg] | 63.9±11 | 71.6±13 | 82±11 | 83±20 |
| Body height [cm] | 171±7.2 | 163±8.4 | 172±8 | 170±8 |

Each of the test subjects performed the QS test three times with eyes open and eyes closed. Each trial lasted 30 s and was repeated three times. The AMTI platform (AccuGait) was used in the measurements. The platform sampling frequency was 100 Hz. A dual-pass 7 Hz low-pass Butterworth filter was used for forces (F_x, F_y, F_z) and moments (M_x, M_y, M_z), which were later used to calculate the COP. All calculations were performed using MATLAB software.

Data analysis was performed based on displacements of the center of pressure (COP) towards AP and ML. On the basis of the obtained COP displacement waveforms, a technical analysis of the signal was carried out and the following quantities were determined: indices related to the number of trend changes (TCI), indices defining a mean time (TCI_dT), and mean displacement (TCI_dS) and mean velocity (TCI_dV) between such changes [7],[8].

*Corresponding author: Piotr Wodarski, e-mail: piotr.wodarski@polsl.pl

3. Results

Statistical analysis was performed for all calculated indicators. The TCI results indicate a normal distribution and homogeneity of variance, hence the means were compared using parametric tests. The results of the other indicators do not show normal distributions, hence non-parametric tests were used and the medians and quartile range were compared.

In the next step the reliability was calculated by taking into consideration three measurements for each person. The obtained interclass correlation coefficient (ICC) values in the case of the TCI were within the range of 0.80-0.92, whereas other values were in the range of 0.74-0.88. The results of the calculations for the studied groups and samples are presented on Fig. 1.

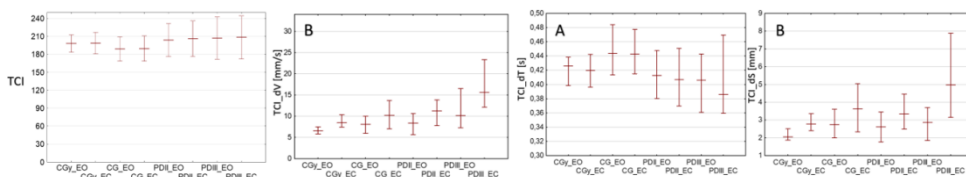


Fig. 1. Obtained values of TCI and TCI_dV, TCI_dS and TCI_dT coefficients. The results are presented for the eye open EO and EC closed tests

The results indicate a higher TCI value for PD than for CG ($p < 0.05$). In the case of PD patients, there was also an increase in the TCI_dS value by 2-5 mm, which mainly contributed to the increase in TCI_dV. Statistically significant differences for the TCI_dT values occurred between all groups in which differences in the average COP velocity were noted.

4. Discussion and Conclusions

The results obtained in the study indicate that the increase in TCI_dV in the PD group in the EC test is the result of an increase in TCI_dS. There was an extension of the movement between successive changes in the trend. The change in TCI_dS may be a new indicator in the assessment of the diagnosis of people with Parkinson's disease. The developed method of analysis provides new information on the strategies for maintaining balance in people with PD. The use of this method to differentiate the severity of PD requires further research.

References

- [1] BŁASZCZYK J.W., CZERWOSZ L. *Postural stability in the process of aging*, *Gerontol. Pol.* 2005, 13(1):25–36
- [2] SOTO-VARELA A., ROSSI-IZQUIERDO M., FARALDO-GARCÍA A., ET AL., *Balance Disorders in the Elderly: Does Instability Increase Over Time?* *Ann Otol Rhinol Laryngol.* 2016, 125(7):550-8
- [3] SCHONEBURG B., MANCINI M., HORAK F., NUTT J.G. *Framework for understanding balance dysfunction in Parkinson's disease.* *Mov Disord.* 2013, 28(11):1474-82
- [4] SOUZA C.O., VOOS M.C., BARBOSA A.F., CHEN J., FRANCATO D.C.V, MILOSEVIC M., POPOVIC M., FONOFF E.T., CHIEN H.F., BARBOSA E.R. *Relationship Between Posturography, CLINICAL Balance and Executive Function in Parkinson's Disease.* *J Mot Behav.* 2019, 51(2):212-221
- [5] REZVANIAN S., LOCKHART T., FRAMES C., SOANGRA R., ET AL., *Motor Subtypes of Parkinson's Disease Can Be Identified by Frequency Component of Postural Stability.* *Sensors (Basel).* 2018, 18(4):1102
- [6] FADIL R., HUETHER A., BRUNNEMER R., BLABER A.P., LOU J.S., TAVAKOLIAN K. *Early Detection of Parkinson's Disease Using Center of Pressure Data and Machine Learning.* *Annu Int Conf IEEE Eng Med Biol Soc.* 2021, 2021:2433-2436
- [7] WODARSKI P., CHMURA M., GZIK M., GRUSZKA G., JURKOJC J. *Technical Analysis of the Displacements of the Centre of Pressure in the Standing Posture Based on Data Obtained Using Selected Stock Market Indicators,* *International Conference BIOMDLORE, 2021*, pp. 1-6
- [8] WODARSKI P., CHMURA M., GRUSZKA G., ROMANEK J., JURKOJC J. *The stock market indexes in research on human balance.* *Acta Bioeng Biomech,* 2022, 24(2):163-176

Assessment of type of control in chosen ADL performances of wheelchair patient with DMD and healthy adolescent: case study

W. WOJNICZ^{1*}, B. ZAGRODNY², M. LUDWICKI², A. SOBIERAJSKA-REK³,
J. JABŁOŃSKA-BRUDŁO³, K. FORYSIAK¹

¹Gdansk University of Technology, Gdansk, Poland

²Lodz University of Technology, Lodz, Poland

³Medical University of Gdansk, Gdansk, Poland

Key words: DMD, EMG, kinematic data, upper limb, ADL, passive manipulator

1. Introduction

Duchenne muscular dystrophy (DMD) is a genetic neuromuscular disorder with progressive muscle weakness. A therapy of patients with DMD is mainly concentrated on rehabilitation of musculoskeletal system dealing with activities of daily living (ADL). This rehabilitation can be facilitated by using passive/active external devices (end-effectors, manipulators, exoskeletons).

The general aim of the study was to define the type of control that used wheelchair patients with DMD while performed ADL motions in given conditions. The scope of this study involved testing the patient chosen from the group of patients with DMD being at different stages of DMD progress (these patients are treated in the Rare Diseases Centre of Medical University of Gdansk) and the healthy adolescent (Control) chosen from the reference group composed of healthy adolescents. Testing of ADL motions had been performed in two different conditions: 1) in natural conditions (without any external device), 2) by using passive light-weight manipulator.

2. Method of testing

Detailed description of tested participants, protocol of testing, measurement technique and implementation of method of motion quantitative analysis are presented in [1]. With respect to the results published in [1], in this study we present new results referring to testing of horizontal motions by using 200g weight and 500g weight in two different conditions. In each tested motion and given condition a type of control used by tested subject was identified by assessing correlations between subject's muscle activity and the displacement of subject's wrist joint (kinematic type of control) and the displacement of centre of mass of subject's upper limb (dynamic type of control).

To define the type of control used by each tested subject the piecewise multi-regression analysis was performed between normalized kinematic data (referring to a displacement of wrist joint (WJ_x, WJ_y, WJ_z, ΔW) and centre of mass of upper limb (COM_x, COM_y, COM_z, ΔCOM)) and normalized muscle activity of four tested superficial muscles (upper trapezius (EMG₁), lateral head of triceps brachii (EMG₂), anterior deltoid (EMG₃) and biceps brachii (EMG₄)). Muscle activity was assessed on the base of Root Mean Square (RMS) data normalized with respect to the Relative Maximum Contraction (RMC) [1]. A piecewise multi-regression analysis was performed by treating muscle activations (EMG₁, EMG₂, EMG₃, EMG₄) as independent variables and kinematic data (WJ_x, WJ_y, WJ_z, ΔW , COM_x, COM_y, COM_z, ΔCOM) as dependent variables. To assess a type of control used by the tested subject to perform given ADL motion in a given condition, we only consider statistically significant results ($p \leq 0.05$) that met all the requirement referring to the normal distribution of residuals and had a coefficient of determination R² bigger than 0.75 ($R^2 \geq 0.75$).

*Corresponding author: Wiktoria Wojnicz, e-mail: wiktoria.wojnicz@pg.edu.pl

3. Results

In this study we assessed results in two different conditions by applying: 1) piecewise linear multi-regression, 2) piecewise nonlinear multi-regression (quadratic polynomial, cubic polynomial, exponential, power and logarithm functions). Chosen results of piecewise linear multi-regression of testing with 500g weight with passive light-weight manipulator are given on Fig.1: a) mean value of RMS normalized data over time motion (patient with DMD (Fig.1A) and Control (Fig.1D)), b) results of linear piecewise multi-regression analysis with respect to WJX coordinate over time motion (patient with DMD (Fig.1B) and Control (Fig.1E)), c) accumulated antagonistic part and synergistic part with respect to WJX coordinate (patient with DMD (Fig.1C) and Control (Fig.1F)).

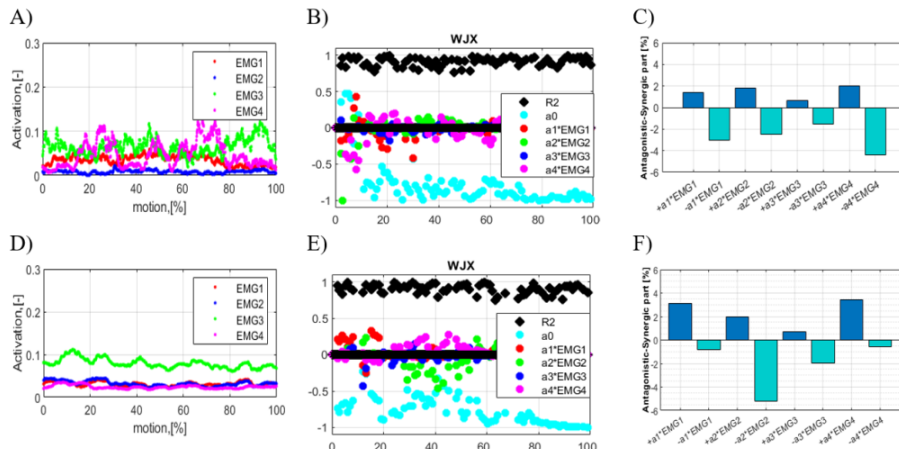


Fig. 1. Results of testing with 500g weight with passive light-weight manipulator: A) mean value of RMS normalized data of patient with DMD over time motion, B) results of linear piecewise multi-regression analysis of patient with DMD with respect to WJX coordinate over time motion, C) accumulated antagonistic and synergistic parts of patient with DMD with respect to WJX coordinate, D) mean value of RMS normalized data of Control over time motion, E) results of linear piecewise multi-regression analysis of Control with respect to WJX coordinate over time motion, F) accumulated antagonistic and synergistic parts of Control with respect to WJX coordinate

4. Conclusions

In this study we propose a new method of motion quantitative analysis that help clinicians: 1) to identify a type of control used by the tested subject to perform given ADL motion in given condition, 2) to deduce whether applied rehabilitation strategy and used external device (passive light-weight manipulator) evokes tested superficial muscles in a proper way. Results of piecewise multi-regression analysis visualize contributions of all tested muscles in motion performance. Results of Control are used as reference ones. It is worth emphasizing that kinematic type of control can be realized by using information from proprioception, visual and tactile senses, whereas dynamic type of control is mainly realized on the base of proprioception and tactile senses, i.e. without visual feedback.

Acknowledgments: Project "The 'e-Pionier - using tertiary education institutions' potential to boost ICT solutions in the public sector', No. WG-POPC.03.03.00-00-0008/16-00, "Custom-made device to assist the motor functions of the upper limb with muscular dystrophy", 2018-2020

References

[1] WOJNICZ, W., SOBIERAJSKA-REK, A., ZAGRODNY, B., LUDWICKI, M., ET AL., *A new approach to assess quality of motion in functional task of upper limb in Duchenne Muscular Dystrophy*. Appl Sci. 2022, 12, 12247

Long-term observation of porous structure PLGA scaffold degradation in an incubation environment

J. WOLICKA*, J. FILIPIAK, A. NIKODEM

Department of Mechanics, Materials and Biomedical Engineering, Faculty of Mechanical Engineering,
Wroclaw University of Science and Technology, Wroclaw, Poland

Key words: *PLGA, scaffolds, degradation, biomaterials, knee joint*

1. Introduction

Osteoarthritis is one of the most prevalent musculoskeletal conditions, affecting 303 million people worldwide in 2017 [1]. Among the joints, the knee joint is considered the most susceptible to osteoarthritis [2]. Repairing joint damage is challenging due to the slow regenerative nature of articular cartilage. Currently, the most effective approach involves removing the damaged tissue and replacing it with new tissue as soon as possible after injury [3].

A promising treatment method involves the use of biodegradable scaffolds, which are biomaterial-based frameworks. These implants bear the load in place of the removed tissue while acting as a scaffold for regenerating tissue. To ensure successful treatment, the scaffold should possess specific properties, such as mechanical characteristics that match the surrounding tissues and a degradation rate aligned with tissue growth [4]. Thus, this study aimed to observe the degradation process of polymer implants.

2. Material and Method

The study employed 30 scaffolds with dimensions of 5 mm in height and 10 mm in diameter, featuring a porosity of 65%, fabricated from poly(lactide-co-glycolide) (PLGA) at an 85:15 ratio. The degradation of the scaffolds was carried out under static conditions, where the specimens were immersed in phosphate-buffered saline (PBS) solution and maintained in an incubator at a constant temperature of 36°C for a duration of 51 weeks. Throughout the experimental period, the incubation medium was periodically renewed, and the scaffolds were subjected to systematic evaluation, encompassing measurements of weight, microscopic examinations (Discovery v20, Zeiss®), pH level assessments, conductivity analyses, and quantification of sodium (Na), potassium (K), and calcium (Ca) ions in the incubation milieu. Additionally, monthly samplings were performed to facilitate micro-computed tomography (1172 SkyScan, Bruker) and mechanical testing, encompassing uniaxial compression assessments (MTS 858 MiniBionix).

3. Results

The scaffolds exhibited a progressive degradation pattern, with notable changes observed in various structural and mechanical parameters. Surface characterization revealed slow changes, with the scaffolds' appearance evolving towards a matte texture after approximately 25 weeks, accompanied by the emergence of cracks. Furthermore, the pH of the incubation medium displayed a modest increase by week 28, followed by intermittent fluctuations thereafter. The concentration of ions (Na, K, Ca) in the incubation solution exhibited irregular changes over time, while the solution's conductivity gradually decreased.

Structural analysis of the scaffold's geometry captured in micro-computed tomography revealed that the implant experienced swelling up to the 14th week. After this period, a gradual reduction in the

*Corresponding author: Justyna Wolicka, e-mail: justyna.wolicka@pwr.edu.pl

strut thickness of the scaffold occurred. The scaffold volume demonstrated a corresponding change. From the initial stages of degradation until the 35th week, the scaffolds exhibited a relatively high stiffness, ranging from 94 to 130 N/mm. However, after this period, a noticeable decrease in the stiffness was observed, with values ranging between 25 and 44 N/mm by the 44th week. This progressive reduction in the stiffness indicated a loss of mechanical integrity in the scaffolds. As the degradation process advanced, the scaffolds displayed increased susceptibility to fracture during the compression tests. At week 35, only one of the samples experienced fracturing, while the remaining samples underwent significant deformation and buckling. By week 44, all samples were found to be highly susceptible to fracturing, resulting in fragmentation into smaller pieces during the compression test. This indicated a substantial decrease in the scaffold's load-bearing capacity and structural integrity.

Notably, the observed fracture pattern was characterized by the detachment of individual struts, which contributed to the overall reduction in scaffold dimensions. Despite this detachment phenomenon, the struts remained structurally intact, but they became increasingly brittle and susceptible to mechanical failure (Fig.1).

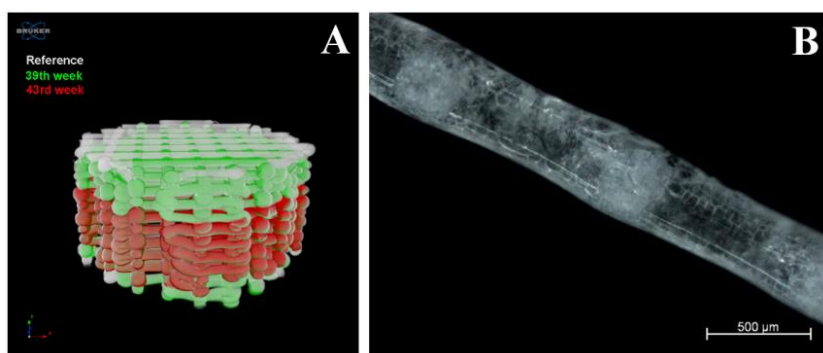


Fig 1. A: 3D reconstruction of scaffold geometry - difference between: reference (white), 39th week (green) and 43rd (red) week, B: mat and cracked surface of the scaffold struts after 51 weeks

4. Discussion

Overall, the results demonstrate that the degradation process of the PLGA scaffolds is complex and dynamic, affecting both their structural and mechanical properties. These findings have implications for the potential use of these scaffolds in tissue engineering applications, particularly in load-bearing tissue regeneration, where long-term mechanical stability is essential. However, further investigations are warranted to explore the underlying mechanisms driving the observed degradation patterns and to optimize the design and performance of PLGA-based scaffolds for regenerative medicine applications.

References

- [1] SPENCER J. L., ET AL., *Global, regional, and national incidence, prevalence, and years lived with disability for 354 diseases and injuries for 195 countries and territories, 1990–2017: a systematic analysis for the Global Burden of Disease Study 2017*. The Lancet, 2018, 392.10159, 1789-1858
- [2] ALEXANDROS A.A. ET AL., *Prevalence of symptomatic knee, hand, and hip osteoarthritis in Greece. The ESORDIG study*. J Rheumatol, 2006, 33.12, 2507-2513.
- [3] JOERN M. ET AL., *The epidemiology, etiology, diagnosis, and treatment of osteoarthritis of the knee*. Dtsch Arztebl Intl, 2010 107.9, 152
- [4] NUERNBERGER S. ET AL., *The influence of scaffold architecture on chondrocyte distribution and behavior in matrix-associated chondrocyte transplantation grafts*. Biomaterials 2011, 32.4. 1032-1040

A comparative study of mandibular bone implants using commercial reconstructive and a personalized implants

A. WYBRANIEC*, A. SZUST

Department of Mechanics, Materials and Biomedical Engineering, Faculty of Mechanical Engineering,
Wroclaw University of Science and Technology, Wroclaw, Poland

Key words: reconstruction implant, implant printed, DIC

1. Introduction

The main function of the stomatognathic system, which includes the upper jaw and mandible, is to bite and chew food. In oncology patients who have undergone partial or total resection of a fragment of the pathologically altered mandible, the main goal is to restore bone continuity. This task is accomplished by using a titanium plate shaped to the geometry of the removed bone fragment. Using commercial reconstruction plates, it is often difficult to replicate the geometry of the bone being replaced. Pre-operative or intra-operative over-bending of the plate can lead to plate fracture during patient use [1],[2].

2. Method and results

Bone Tissue Engineering can come to the help, allowing the best possible reproduction of the geometry of the patient's missing bone [3].

This paper presents the results of an experimental study showing the value of occurring displacements of the analysed areas with the use of different types of plates for reconstruction after total mandibular body bone resection Fig.1.



Fig. 1. Types of plates used: A-standard plate (Modus M-4566), B-openwork plate (Modus M2-4603), C-personalized implant

The study used two types of commercially available implants and one implant manufactured using incremental technologies.

The models were supported symmetrically, and loaded with a force of 180N. The DANTEC (DIC) system was used to analyze the displacement of the model. The results obtained are presented in Fig. 3.

*Corresponding author: Anna Wybraniec, e-mail: anna.wybraniec@pwr.edu.pl

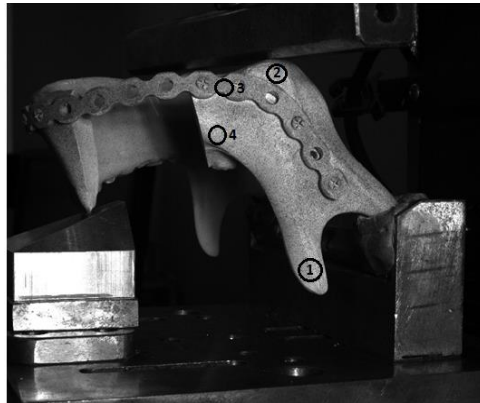


Fig. 2. The way the model is loaded and supported, with the analyzed areas marked

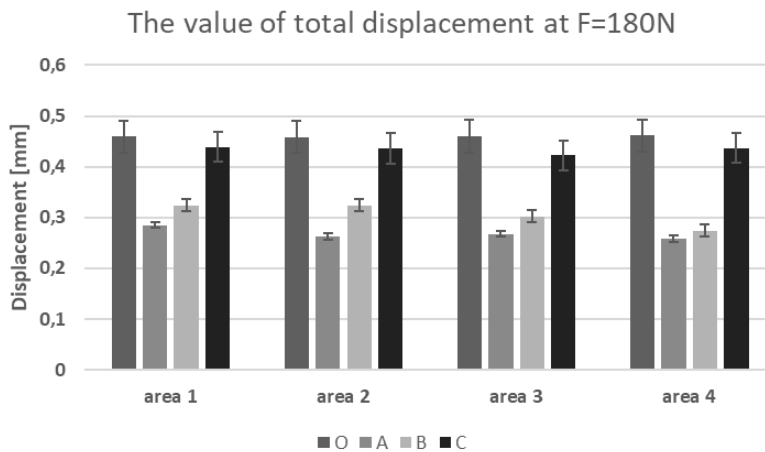


Fig. 3. Total displacement values for the analyzed models. O-reference model, A-standard plate, B-openwork plate, C-personalized implant

Studies have shown that a better mapped geometry allows to obtain results close to the geometrically unaltered model. The use of commercial implants (A,B) over-stiffens the model and it can cause pain in the muscles of the stomatognathic system. Stiffening of the bone-implant connection can cause implant fractures or the occurrence of necrotic lesions on the bone [1].

References

- [1] HABIB A., HASSAN S. *The feasibility of rib grafts in long span mandibular defects reconstruction: A long term follow up.* J Maxillofac Surg, 2019, 47(1), 15-22
- [2] KAWASAKI G., IMAYAMA N., YOSHITOMI I., FURUKAWA K. *Clinical Study of Reconstruction Plates Used in the Surgery for Mandibular Discontinuity Defect.* In vivo, 2019, 33, 191-194.
- [3] HOLZAPFEL B., RUDERT M., HUTMACHER D. *Gerüstträgerbasiertes Knochen-Tissue-Engineering [Scaffold-based Bone Tissue Engineering].* Orthopade, 2017, 46(8), 701-710

Influence of double excitation in Lumped Parameter Model of Implanted Human Middle Ear

R. ZABŁOTNI*, R. RUSINEK

Department of Applied Mechanics, Lublin University of Technology, Lublin, Poland

Key words: middle ear, ossicles, vibration, modelling

1. Introduction

Hearing is one of the most important human senses. It enables the ability to communicate through speech, which has been shaped over tens of thousands of years. In addition, thanks to the ability to hear, the man from the beginning of time received stimuli from the environment, thanks to which he was able to avoid situations that threaten health or life. Nowadays, a person is exposed to constant receiving of auditory stimuli both at work and at home. In large cities, a person is constantly exposed to noise caused, among other things, by traffic conditions. According to the WHO, by 2050, approximately 2.5 billion people will have some degree of hearing impairment, and the current number is approximately 1.1 billion [1].

The implantable middle ear hearing device (IMEHD) is a promising solution for patients with hearing loss, particularly those with conductive or mixed hearing loss. It is a surgically implanted device that directly stimulates the middle ear bones, allowing for improved sound transfer to the inner ear. The IMEHD bypasses the damaged parts of the middle ear and can provide significant hearing improvement for patients who are not candidates for traditional hearing aids [2].

This work focuses on a implanted human middle ear represented by the lumped parameter model with five degrees of freedom.

2. Lumped Parameter model of implanted human middle ear

The lumped parameter model of the implanted human middle ear with Kelvin-Voigt type of viscoelasticity consist of five masses. The three masses representing the three bones of the middle ear - malleus, incus, and stapes, and there are two masses connected to the incus that represents implant. The malleus is the first mass, and the stapes is the last mass. In this lumped parameter model exciting force is applied on the malleus and on the implant. All of the masses are connected to each other by spring and dampers (Fig.1).

Fig. 2 shows the resonance curves that were acquired from the lumped parameter model of implanted human middle ear. One can observe the system's response to various types of excitation, such as double excitation, excitation with an implant represented as mechanical force applied on the case of the implant, and excitation with the eardrum represented as the mechanical force applied to the first mass of the system which is malleus. The responses are compared to the experimental results of the intact ear at 90 dB SPL, which is a value reported in the literature. Furthermore, the analysis will entail examining the phase shift of the double excitation to determine whether changes in the resonance curves occur.

*Corresponding author: Robert Zablotni, e-mail: r.zablotni@pollub.pl

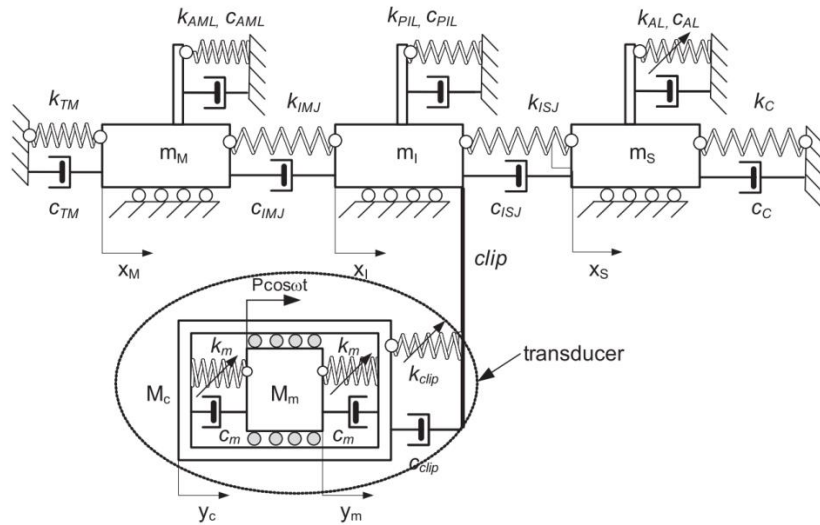


Fig. 1. 5 DOF Lumped Parameter Model with Floating Mass Transducer and mechanical excitation

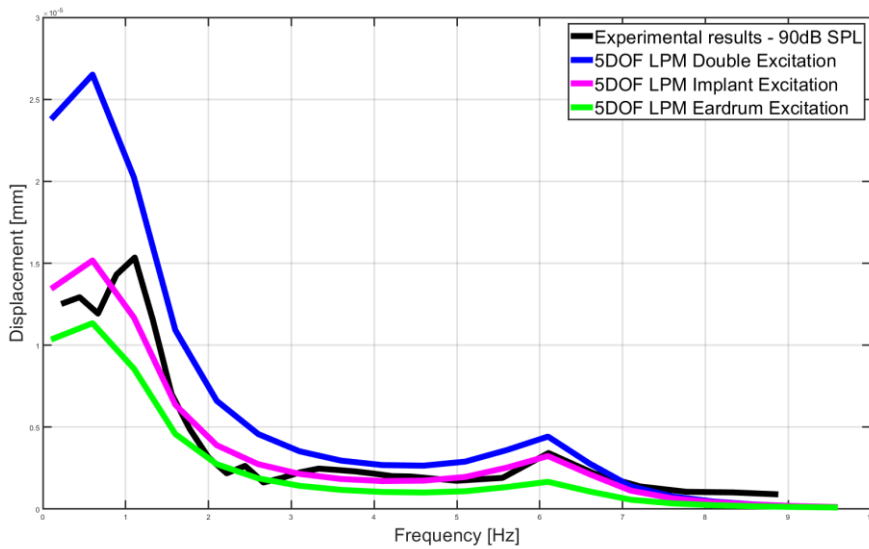


Fig. 2. Resonance curves obtained from the LPM model of implanted human middle ear and from experiment

Acknowledgments: The research was financed in the framework of the project Nonlinear effects in human ear stimulated with sound and implant simultaneously, no. 2022/45/N/ST8/02447, funded by the National Science Centre, Poland.

References

- [1] www.who.int/news-room/fact-sheets/detail/deafness-and-hearing-loss
- [2] CARLSON M., PELOSI S., HAYNES D. S. *Historical development of active middle ear implants*. *Otolaryngol Clin North Am.* 2014, 47(6):893-914

Comparison of the surface and mechanical properties of low viscosity acrylic bone cements

Z. ZAJĄC*, A. LIBER-KNEĆ, S. ŁAGAN

Faculty of Mechanical Engineering, Cracow University of Technology, Cracow, Poland

Key words: bone cement, compressive strength, wettability

1. Introduction

Bone cements are biomaterials used to bone support. Depending on their clinical, orthopedic and dental uses, they are formed on the basis of calcium phosphate or poly(methyl methacrylate) [1]. Bone cements are used in the treatment of periodontal diseases, and are used for bonding, filling and repairing bone defects of varying shape and volume resulting from trauma or cancer, also in the treatment of the spine or the setting of artificial joints [1]-[4]. Bone cements are characterized by good biocompatibility, osteoconductivity and moderate impermeability to X-rays. They can be used as drug delivery systems, growth factors or, when mixed with other biomaterials, as an additive to modulate the rate of degradation [3]-[5].

Acrylic bone cements are polymeric materials that are obtained by polymerization reactions. They provide a stable, non-absorbable material. Bone cements based on poly(methyl methacrylate) (PMMA) are two-component systems, consisting of a solid phase (polymer powder) and a liquid phase (liquid monomer). Bone cements can also be defined as a mixture of substances that, when mixed and homogenized, form a paste, which has the ability to harden and self-stabilize when applied to the body [3],[4].

As a bone defect filler and a stabilization system for bone implants, bone cement is exposed to complex states of physical, chemical and thermal loading. Therefore, it is important to determine the effects of both mechanical loading and the biological environment on the properties of bone cement.

Acrylic bone cements are recommended to be evaluated according to ISO 5833 [6], while guidelines for assessing wettability are formulated in ISO 19403-2 [7]. When designing polymer-based bone cements as bone tissue substitutes, it is important to know the compressive courses and mechanical strength parameters. These are essential for matching the nature of the bone defect filling response. Surfaces of the materials will interact with each other under the loading conditions of the body, so it is necessary to determine the interaction of the solid (bone cement) and liquid (simulation of the biological environment). Wettability (hydrophobicity and hydrophilicity) of surfaces affect surface protein adsorption and cell adhesion. Cells are more likely to adhere to hydrophilic surfaces [8].

Differences in the determined parameters of bone cements relative to tissues are due not only to the physiological state of the bone (healthy or osteoporotic bone, or bone with metastases), but also to the location in the skeletal system, the direction of the test sample, its shape, or the use of analytical models [10]. Therefore, mechanical studies of bone tissues are still being conducted and new formulations of bone cements are being developed to refine the convergence of the mechanical response of the bone-cement system.

The purpose of the present study was to compare the wettability, surface free energy and strength properties of two bone cements, taking into account the aging conditions of the materials.

*Corresponding author: Zuzanna Zajac, e-mail: zuzanna.zajac@student.pk.edu.pl

2. Materials and Methods

The aim of this study was to compare the surface free energy and mechanical properties of bone cements used in human orthopedics. Two acrylic bone cements were used in the study: Synicem (Synergie Ingenierie Medicale, France) and Cemex radiopaque shading cement with low viscosity polymerization temperature and low viscosity (TECRES S. p. A., Italy). The mechanical properties were determined by compression tests, a contact angle was observed with a goniometer and the surface free energy was calculated by Owens-Wendt model. Two states of material (dry initial and after incubation in saline solution) were considered.

References

- [1] FADA R., BABADI N.F., AZIMI R., KARIMIAN M., SHAHGHOLI M. *Mechanical properties improvement and bone regeneration of calcium phosphate bone cement, Polymethyl methacrylate and glass ionomer*. J Nanoanalysis. 2021. 8(1): 20
- [2] BISTOLFI A., FERRACINI R., ALBANESE C., VERNÈ E., MIOLA M. *PMMA-Based Bone Cements and the Problem of Joint Arthroplasty Infections: Status and New Perspectives*, Materials 2019, 12, 4002
- [3] ROBU A., ANTONIAC A., GROSU E., VASILE E., RAICIU A.D., IORDACHE F., ANTONIAC V.I., YANKOVA V.G., DITU L.M. ET AL., *Additives Imparting Antimicrobial Properties to Acrylic Bone Cements*. Materials 2021, 14, 7031
- [4] SOBCZYK-GUZENDA A., BONIECKA P., LASKA-LEŚNIEWICZ A., MAKOWKA M., SZYMANOWSKI H. *Additives MICRO- AND NANO OPARTICULATE PMMA-BASED BONE CEMENTS AND THE PROBLEM OF JOINT ARTHROPLASTY INFECTIONS: STATUS AND NEW PERSPECTIVES*. MATERIALS 2019, 12, 4002
- [5] SOBCZYK-GUZENDA A, BONIECKA P, LASKA-LESNIEWICZ A, MAKOWKA M, SZYMANOWSKI H. *Micro- and Nanoparticulate Hydroxyapatite Powders as Fillers in Polyacrylate Bone Cement-A Comparative Study*. Materials (Basel). 2020 Jun 17;13(12):2736
- [6] WEKWEJT M., MICHALSKA-SIONKOWSKA M., BARTMAŃSKI M., NADOLSKA M., ŁUKOWICZ K., PAŁUBICKA A., OSYCZKA A.M., ZIELIŃSKI A. *Influence of several biodegradable components added to pure and nanosilver-doped PMMA bone cements on its biological and mechanical properties*. Mater Sci Eng C Mater Biol Appl. 2020;117:111286
- [7] ISO 19403-2:20127 - *Determination of the surface free energy of solid surfaces by measuring the contact angle*
- [8] ISO 5833:2002 - *Implants for surgery — Acrylic resin cement*
- [9] CAI S., WU C., YANG W., LIANG W., YU H., LIU L. *Recent advance in surface modification for regulating cells adhesion and behaviors*. Nanotechnology Reviews, 2020, 9(1), 971-989
- [10] ŚWIECZKO-ŻUREK B., ZIELIŃSKI A., BOCIĄGA D., ROSIŃSKA K., GAJOWIEC G. *Influence of different nanometals implemented in PMMA bone cement on biological and mechanical properties*. Nanomaterials 2022, 12(5), 732

Comparison of knee joint kinematics in patients after ACL reconstruction and ACL repair using Internal Bracing method

P. ZALEWSKA^{1*}, T. GUSZCZYN², S. PISZCZATOWSKI¹

¹Institute of Biomedical Engineering, Bialystok University of Technology, Bialystok, Poland

²Medical University of Bialystok Children's Clinical Hospital, Bialystok, Poland

Key words: *knee joint, ACL reconstruction, ACL repair, knee kinematics, gait*

1. Introduction

Anterior cruciate ligament (ACL) rupture is one of the most common knee injuries [1,2] occurring most frequently for young people [2]. Currently, the gold standard in the treatment of ACL damages to restore knee stability and kinematics is still reconstruction [3], but studies show that it has variable success rates for revision and patient satisfaction [4]. Thus, there is growing interest in ACL repair method such as Internal Bracing [5]. In this method, the damaged ligament is not replaced using graft, but ruptured parts of ACL are connecting together using a lasso suture and high-strength tape [6,7]. Due to the preservation of native ligament, Internal Bracing is a promising method with potential advantages over reconstruction [6]. Hence, the aim of the study is to compare the knee kinematics in patients after ACL reconstruction with hamstrings autograft and ACL repair using Internal Bracing method.

2. Methods and Materials

The studies involved individuals after ACL reconstruction with hamstrings autograft (ACLR, 22 persons) and individuals after ACL repair using Internal Bracing method (IB, 14 persons) as well as 53 healthy subjects (Controls). Patients were qualified for the project on the basis of clinical assessment made by an orthopaedist. The research was approved by the bioethics committee.

The Qualisys motion capture system (Qualisys AB, Sweden) was used to determine knee kinematic parameters of gait. The motion capture system consisted of 10 infrared cameras (Oqus 500+) and 1 video camera (Oqus 210C). In addition, ground reaction forces were measured using two Kistler 9260AA dynamometer platforms (Kistler, Switzerland). The force platform data and the marker position were recorded at 1298 Hz and 118 Hz, respectively. This system allowed the determination of the markers position that were placed on the subject's body, according to the following protocol: anterior and posterior superior iliac spines, greater trochanters, in the middle of the thigh, medial and lateral femoral epicondyles, medial and lateral tibial condyles, tibial tuberosity, in the middle of the shank, medial and lateral ankles, 1st and 5th metatarsal heads and the most posterior point on the heel.

Each subject were instructed to walk barefoot along a 9-metre walkway at a preferred speed until at least five properly trials were recorded. Test were performed for both the operated limb and the non-operated limb (ACLR, IB), as well as both healthy limb (Controls).

Visual3D software (C-Motion, USA) was used to analyse the knee kinematics, in which the knee joint angles were determined.

* Corresponding author: Paulina Zalewska, e-mail: paulina.zalewska@sd.pb.edu.pl

3. Results

Figure (Fig.1) presents example results of knee joint angles for the operated limb (ACLR, IB) and also healthy subjects (Controls, averaged for both limbs).

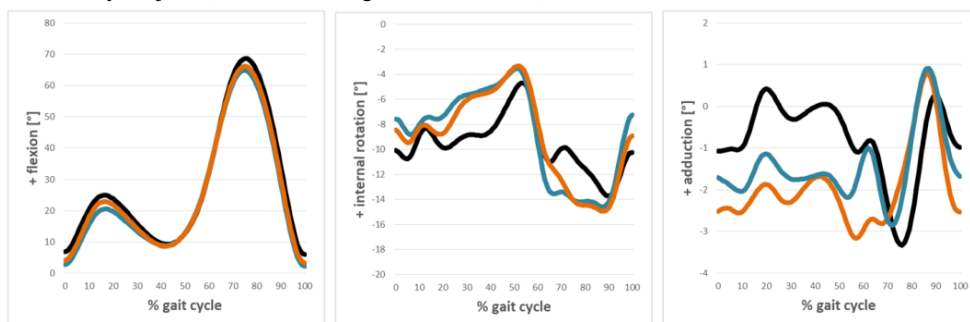


Fig. 1. Mean knee joint angles [°] during gait for operated limb (ACLR – blue line, IB – orange line) and healthy subjects (Controls – black line)

4. Discussion

When analysing the example results of knee joint angles (Fig.1) it can be seen differences between particular groups of patients and the Controls.

The greatest differences can be observed in adduction/abduction angle, where during the stance phase both IB and ACLR obtained greater abduction angle than Controls, but in parallel IB group obtained higher knee abduction angle than ACLR group. For the swing phase, both IB and ACLR achieved a maximum adduction angle slightly faster than Controls. For rotation, both IB and ACLR group obtained quite similar result, but they generally reached smaller knee external rotation during the stance phase, and greater knee external rotation during the swing phase comparing to Controls. In the case of flexion angle, the results in all groups are fairly comparable, with the greatest differences observed at the beginning of the gait (0-30%GC) and during the second knee flexion, where the ACLR group achieved the lowest flexion angle values.

Summarizing, it can be concluded that there is a visible effect of the damage and ACL reconstruction or ACL repair on knee kinematics. However, further studies is underway in order to gain a deeper understanding of the discussed phenomena.

Acknowledgments: Research was performed as a part of projects WI/WM-IIB/7/2020, WI/WM-IIB/5/2023 and financed with use of funds for science from Polish Ministry of Education and Science

References

- [1] BRAM J.T., MAGEE L.C., MEHTA N.N., ET AL., *Anterior cruciate ligament injury. Incidence in Adolescent Athletes: A Systematic Review and Meta-analysis*. Mater Sci Eng C Mater Biol Appl. 2020, 117:111286
- [2] MUSAHL V., KARLSSON J. *Anterior Cruciate Ligament Tear*. N Engl J Med. 2019, 380(24):2341-2348
- [3] VAISHYA R., OKWUCHUKWU M.C., AGARWAL A.K., VIJAY V. *Does Anterior Cruciate Ligament Reconstruction prevent or initiate Knee Osteoarthritis? -A critical review*. J Arthrosc Jt Surg 2019, 6(3), 133-136
- [4] PACHE S., DEL CASTILLO J., MOATSHE G., LAPRADE R.F. *Anterior cruciate ligament reconstruction failure and revision surgery: Current concepts*. J ISAKOS, 2020, 5(6), 351-358
- [5] WILSON W.T., HOPPER G.P., BANGER M.S., BLYTH M.J.G., RICHES P.E., MACKAY G.M. *Anterior cruciate ligament repair with internal brace augmentation: A systematic review*. The Knee, 2022, 35, 192-200
- [6] HEUSDENS C.H.W. *ACL repair: A game changer or will history repeat itself? A critical appraisal*. J Clin Med. 2021, 26,10(5):912
- [7] LU W., DENG Z., ET AL., *Clinical Research Progress of Internal Brace Ligament Augmentation Technique in Knee Ligament Injury Repair and Reconstruction: A Narrative Review*. J Clin Med. 2023, 2,12(5):1999

A three-link model of a fetal lower limb for simulating the fetal kicking movement

X. ZHAO^{1,2*}, J. AWREJCEWICZ¹, D. GRZELCZYK¹, Y. GU²

¹Department of Automation, Biomechanics and Mechatronics, Lodz University of Technology, Lodz, Poland

²Faculty of Sports Science, Ningbo University, Ningbo, China

Key words: fetal movement, kicking, fetal lower limb

Abstract

Fetal movement has long been of interest as an indicator of fetal well-being. Detection and description of fetal movement provide essential information of the integrity of in utero development and fetal wellbeing [1]. The observation of fetal movements by real time scanning machines in uterus has been widely performed for assessment of fetal well-being [2]. The uterus provides a special growth environment and mechanical stimulation for the fetus.

In this study, a three link model of a fetal lower limb was built for simulating the fetal kicking. The fetal foot and uterine wall contact during the kicking movement was simulated in Mathematica. The fetal lower limb was segmented into three rigid bodies: thigh, shank, and foot. The segmentations of the fetal lower limb was connected by the ankle and knee joints [3]. The 3D model of the fetal lower limb was obtained by the MRI scanning created in the Mimics and segmented in the 3-matic. The fetal kicking movement was recorded by the 2D cine ultrasound. The kinematics of the fetal lower limb during the kicking were analyzed by using the Kinovea software (Fig. 1).

This study provides a novel method to simulate the fetal kicking movement and shed light on the measurement of the mechanical simulation of the fetal kicking against the uterus wall. The obtained ground reaction force could can be used for the finite element analysis of the computational modelling the fetal lower limb.

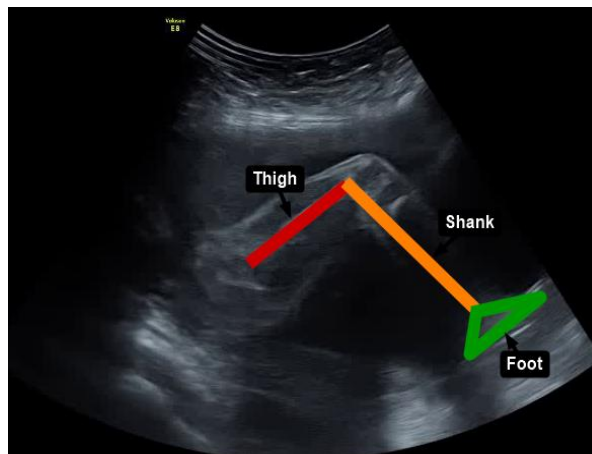


Fig. 1. Modelling of the fetal lower limb which the kicking movement in Kinovea

*Corresponding author: Xiaoxue Zhao, e-mail: xiaoxue.zhao@dokt.p.lodz.pl

Acknowledgments: This paper has been completed while Xiaoxue Zhao was the Doctoral Candidates in the Interdisciplinary Doctoral School at the Lodz University of Technology, Poland.

References

- [1] ZHAO X., AWREJCEWICZ J., LI J., HE Y., GU Y. *The Lower Limb Movements of the Fetus in Uterus: A Narrative Review*. Appl Bionics Biomech. 2023, 23,2023:4324889
- [2] LIU Y, XUAN R, HE Y, REN F, GU Y. *Computation of Fetal Kicking in Various Fetal Health Examinations: A Systematic Review*. Int J Environ Res Public Health. 2022, 5,19(7):4366
- [3] CHEN H., SONG Y., XUAN R., HU Q., BAKER J.S., GU Y. *KineOmatic Comparison on Lower Limb Kicking Action of Fetuses in Different Gestational Weeks: A Pilot Study*. Healthcare (Basel). 2021, 18,9(8):1057

Methods of evaluating mechanical parameters and the stability of the cervical interbody fusion cage

M. ŻAK*, A NIKODEM, C. PEZOWICZ

¹Department of Mechanics, Materials and Biomedical Engineering, Faculty of Mechanical Engineering, Wrocław University of Science and Technology, Wrocław, Poland

Key words: fusion cage, 3D printed, mechanical properties, osteointegration

1. Introduction

In the case of interbody fusion cages, it is required to achieve optimal conditions between the geometry and the mechanical parameters to achieve a stable connection at the border with the bone tissue. In our work, we present the research results of the cervical interbody fusion cage based on assessing mechanical properties and the conditions related to osseointegration resulting from the adopted geometry [1].

2. Material and Methods

The cage was designed as a titanium alloy Ti6Al4V implant obtained by the incremental method (SLA) strengthened with mesh lattice structures to obtain larger osseointegration between the implant and bone tissue – Fig.1. Based on the indentation test, the stiffness and the maximum force values of the modification of the geometrical dimensions of the mesh lattice structures were determined. Also, was performed adhesion test for Balb/3T3 fibroblasts and NHOst osteoblasts. The mechanical parameters and quality of the construction cervical interbody fusion cage were determined in: a uniaxial compression test to the failure of the implant (with ASTM F2077 standard), CT scan and microscopic analysis.

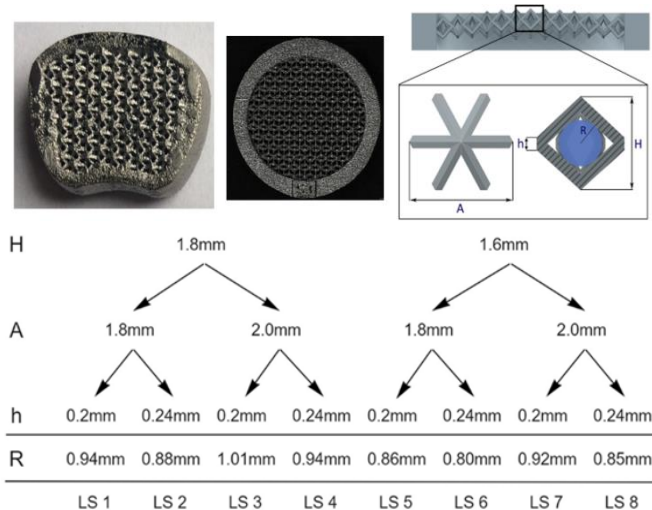


Fig. 1. Growth-guidance system (GGs) by NovaSpine with included a stabilization system in which the surface of the rod and the sliding nuts made of Ti-6Al-4V alloy was applied a 1000 nm thick DLC coatings (with the PVD method with 20 nm thick CrN interlayer)

*Corresponding author: Małgorzata Żak, e-mail: malgorzata.a.zak@pwr.edu.pl

3. Results and Discussion

Based on the indentation test, the stiffness values of the modification of the geometrical dimensions of the mesh lattice structures were determined. The research showed that an essential geometric parameter influencing the mesh strength is the height of the connection point between the arms of the mesh cells – fig.2. There was no significant influence of the mesh geometry on the number and survival of Balb/3T3 and NHOst cells. Fibroblast cells more readily formed colonies in the area where cells of the mesh meet, unlike osteoblasts, which were more numerous at their tips.

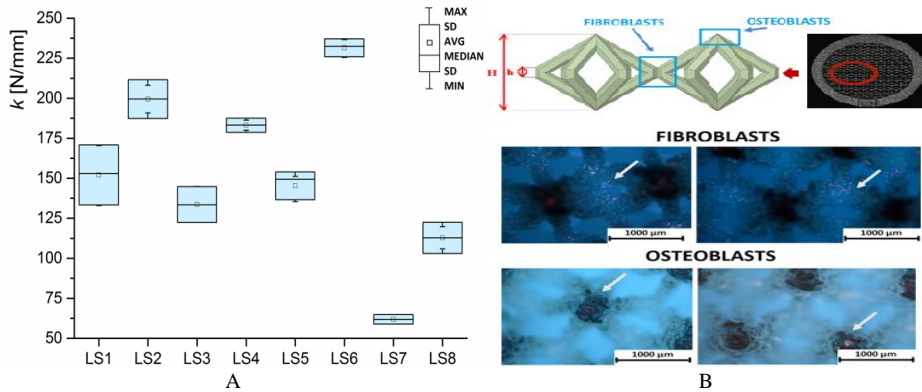


Fig. 2. Exemplary research results: A) the average value of the stiffness coefficient (k) in different mesh groups, B) example image of cell Balb/3T3 fibroblasts and NHOst osteoblasts adhesion on the surface of studied meshes made with a mixture of fluorescent dyes

With a non-destructive load in the force range up to 500N, the implant stiffness was from 14 to 17KN/mm. On the other hand, the value of the ultimate forces does not exceed 40kN and the stiffness 22kN/mm. The CT scan showed that the structure of the implant is continuous and that there are no closed pores in the implants printed. The average porosity calculated from CT scans of control volume was $0.15 \pm 0.3\%$.



Fig. 3. Exemplary research results: A) mechanical properties and microscopic analysis until rupture of the implants, B) cross-section through implants taking into account critical areas using the technical computed tomography system CT

References

- [1] WANG Q., ZHOU P., LIU S., ATTARILAR S., MA R. L., ZHONG Y., WANG, L. *Multi-Scale Surface Treatments of Titanium Implants for Rapid Osseointegration: A Review*. Nanomaterials (Basel, Switzerland). 2020, 10(6), 1244.

Effect of DLC coating of growth-guidance system implants on changes in mechanical and kinematic properties of the spine

M. ŻAK^{1*}, S. SZOTEK¹, K. SZKODA-POLISZUK¹, J. FILIPIAK¹, M. WRZOSEK², K. KOŁTOWSKI³,
P MENARTOWICZ⁴, C. PEZOWICZ¹

¹Department of Mechanics, Materials and Biomedical Engineering, Faculty of Mechanical Engineering,
Wrocław University of Science and Technology, Wrocław, Poland

²Dogs and Cats, Faculty of Veterinary Medicine,
Wrocław University of Environmental and Life Sciences, Wrocław, Poland

³Department of Pediatric Surgery and Urology, Wrocław Medical University, Wrocław, Poland

⁴St. Hedwig of Silesia Hospital, Trzebnica, Poland

Key words: *spine, scoliosis, growth-guidance system (GGS), mechanical properties*

1. Introduction

Early onset scoliosis (EOS) is a three-dimensional curvature of the spine and trunk that occurs in children nine years of age or younger. The EOS tend to develop progressively, requiring early surgical intervention with spine stabilization. Currently stepwise treatment method involving the displacement of the stabilizer by operating methods is being used. It is necessary to develop a solution that would allow scoliosis to be corrected as soon as possible while reducing the number of operations and the risk of complications [1].

2. Material and Methods

The research aimed to develop a modification of the internal spine stabilizer for the treating scoliosis in children by increasing its abrasion resistance and thus reducing the risk of tissue degradation and disorders in the kinematics of the spine column. The study used the scoliosis stabilisation system offered by Novaspine, which has kinetic pairs in its design to allow relative displacement of stabiliser components without external intervention. The stabilization system consisted of a four-segment stabilization with four central polyaxial screws. The use of kinetic pairs (screw-rod) in the stabilization system makes their relative displacement during the child's growth is possible. The friction between the sliding elements made of titanium alloys contributes to the wear of the material, the particles of which are deposited, among others, in the tissue surrounding the stabilizer and form the so-called "tissue tattoo". In our research, to eliminate frictional wear, an applied DLC (Diamond-Like Carbon) coatings in kinematic pairs, which, as the research shows, is used as a coatings for implants – Fig.1.

The first, performed cyclic compression test using a pig's spine model with included a stabilization system consisting of 100.000 long-term cycles loads with 1.5 Hz frequency in the range of loads between 150 – 650 N using an MTS Bionix 858 Mini testing machine. Then, performed restoration of spine stabilization conditions in vivo studies in an animal model. The research included microstructural analysis of bone tissue in the area of inserted transpedicular screws and analysis of the degree of wear and degradation of the nuts.

*Corresponding author: Małgorzata Żak, e-mail: malgorzata.a.zak@pwr.edu.pl

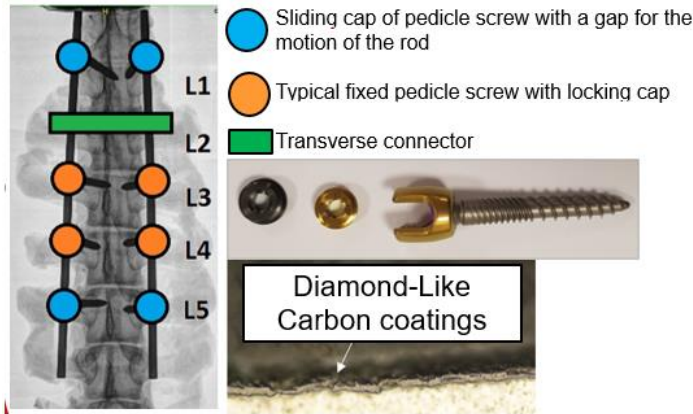


Fig. 1. Growth-guidance system (GGs) by NovaSpine with included a stabilization system in which the surface of the rod and the sliding nuts made of Ti-6Al-4V alloy was applied a 1000 nm thick DLC coatings (with the PVD method with 20 nm thick CrN interlayer)

3. Results and Discussion

Tests were carried out to assess the mechanical and kinematic properties of the spine-stabilizer system for selected modifications stabilization without coatings (NC), stabilization with DLC coatings and spine without stabilization (C). At this study stage, a more than 8% decrease in group WC stiffness was demonstrated for DLC-coated implants compared to implants without DLC (Fig.2.A). Then, in vivo study was carried out on domestic pigs, assessing the effect of the applied modification on the reduction of the mass of titanium alloy particles infiltrating into the tissues surrounding the implant and determining the effect of modified stabilizing systems on changes in the vertebra bone structure. As a consequence, the increased mobility of the stabilizer follower node led to excessive movement between the transpedicular screw and the bone tissue, leading to their loosening and inflammation (Fig.2.B).

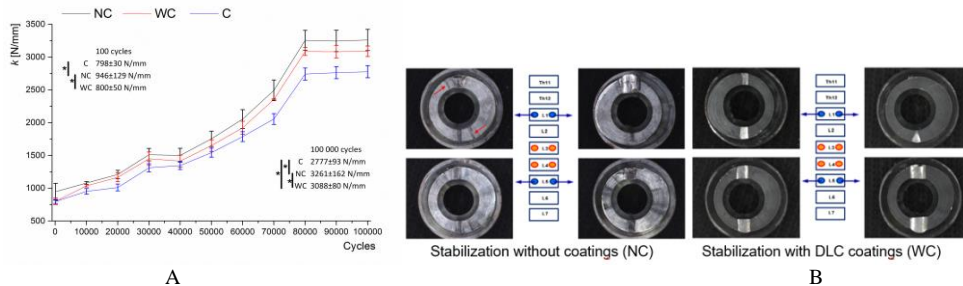


Fig. 2. Exemplary research results: A) the average value of the stiffness coefficient (k) in subsequent cycles for the studied groups, B) The degree of wear and degradation of the nuts. The research groups: Control (C) – spine without stabilization, stabilization without coatings (NC), stabilization with DLC coatings (WC)

Acknowledgments: Work to be implemented under the Intelligent Development Operational Program 2014-2020 - Project no. POIR.04.01.01-00-0020/19-00.

References

[1] DANIELEWICZ A., WÓJCIAK M., SAWICKI J., DRESLER S., SOWA I., LATALSKI M. *Comparison of Different Surgical Systems for Treatment of Early-onset Scoliosis in the Context of Release of Titanium Ions*. Spine (Phila Pa 1976), 2021, 46(10), E594-E601

Compressive properties of polyurethane foam mimicking trabecular tissue in femoral head of synthetic bones

K. ŻERDZICKI*, W. KORBUT, A. KONDRUSIK

Faculty of Civil and Environmental Engineering, Gdańsk University of Technology, Gdańsk, Poland

Key words: *synthetic bone, polyurethane foam, trabecular tissue, compressive properties, Synbone*

1. Introduction

A lot of orthopedic implants and devices are most commonly tested on the artificial bones of different producers, i.e. Synbone, Sawbone, Bonesim [1]. Their mechanical properties are usually evaluated based on experiments conducted on the specimens cut out of the blocks supplied by the manufacturers [1],[2]. However, the properties of the foams in the final ready-to-use bone analog product may be different. In the same time, more and more biomechanical simulations are performed by numerical calculations and advanced computing systems. These numerical models should be experimentally validated either on real human bones like was done in [3],[4],[5], or at least on artificial bone analogs to prove their correctness. Therefore, it is of the key importance to know the properties of the artificial bones that are used for experimental testing and numerical validation of orthopedic implants.

2. Materials and Methods

The Sawbones synthetic polyurethane left femur bones (Sawbones USA A Pacific Research Company, product number 1130-192 and 1130-21-8) were used for samples preparation. The femurs were firstly cut by mechanical saw into slices of 4 mm in coronal plane. Then, the slices were cut in strips of 10 mm width along horizontal plane (A), vertical plane (B), and the femoral neck slope (C). The specimens were cut out of the inner foam mimicking trabecular tissue. The cuboid samples of about 10 mm x 10 mm x 4 mm dimensions (according to ISO 604 standard requirements) were compressed till fracture with the crosshead rate of 1 mm/min according to the ISO 604 and ASTM D-695 standard recommendations.

The Young's modulus, Poisson's ratio and yield limit were identified with standard manner in the elastic domain for all the tested samples. The ANOVA test was used to analyze the differences between samples loaded in different directions. The Student's t-test was used for comparison between two types of bone analogs.

3. Results

The obtained parameter values of the trabecular analog material for the 1130-192 and 1130-21-8 synthetic femurs are presented in Table 1 and Table 2, respectively. There were no statistical important differences ($p > 0.05$) for Young's modulus, Poisson's ratio, and yield limit between loading directions A, B and C for both analyzed femur analogs. When comparing results between 1130-192 and 1130-21-8 synthetic femurs, there were statistically important differences for all the mechanical properties in question ($p < 0.05$).

* Corresponding author: Krzysztof Żerdzicki, e-mail: krzysztof.zerdzicki@pg.edu.pl

Table 1. Properties of Sawbones 1130-192 femur analog cancellous material

| Loading direction | Young's modulus [MPa] | Poisson's ratio [-] | Yield limit [MPa] |
|-------------------|-----------------------|---------------------|-------------------|
| A | 50.1±19.4 | 0.31±0.13 | 1.01±0.29 |
| B | 46.9±32.8 | 0.24±0.06 | 0.77±0.43 |
| C | 53.2±35.4 | 0.36±0.19 | 0.74±0.18 |

Table 2. Properties of Sawbones 1130-21-8 femur analog cancellous material

| Loading direction | Young's modulus [MPa] | Poisson's ratio [-] | Yield limit [MPa] |
|-------------------|-----------------------|---------------------|-------------------|
| A | 19.8±7.1 | 0.31±0.08 | 0.64±0.12 |
| B | 17.8±5.7 | 0.26±0.05 | 0.54±0.14 |
| C | 23.3±4.4 | 0.34±0.05 | 0.70±0.04 |

4. Discussion

The obtained results showed that the material has isotropic character, despite the fact that the polyurethane foams are believed to have different mechanical properties for foaming and transverse direction [2]. It probably depends on the foam type, as Sawbone producer uses cellular and open cells foams, as well as different manufacturing techniques for production femur analogs. The obtained mechanical parameters can be used for numerical calculations of biomechanical constructs made of synthetic femurs analyzed in this study.

Acknowledgments: Financial support of these studies from Gdansk University of Technology by the DEC-47/2020/IDUB/I.3.3 grant under the ARGENTUM TRIGGERING RESEARCH GRANTS 'Excellence Initiative - Research University' program is gratefully acknowledged.

References

- [1] BROWN A. D., WALTERS J. B., ZHANG Y. X., SAADATFAR M., ESCOBEDO-DIAZ J. P., HAZELL P. J. *The mechanical response of commercially available bone simulants for quasi-static and dynamic loading*. J Mech Behav Biomed Mater. 2018, 90: 404–416, 2019
- [2] MARTER A. D., DICKINSON A. S., PIERRON F., FONG (KIKI) Y. K., BROWNE M. *Characterising the compressive anisotropic properties of analogue bone using optical strain measurement*. Proc Inst Mech Eng. Part H J Eng Med. 2019, 233(9): 954–960
- [3] ENNS-BRAY W. S., ET AL., *Morphology based anisotropic finite element models of the proximal femur validated with experimental data*. Med Eng Phys. 2016, 38(11): 1339–1347
- [4] OP DEN BUIJS J., DRAGOMIR-DAESCU D. *Validated finite element models of the proximal femur using two-dimensional projected geometry and bone density*. Comput Methods Programs Biomed, 2011, 104(2): 168–174
- [5] TRABELSI N., YOSIBASH Z., WUTTE C., AUGAT P., EBERLE S. *Patient-specific finite element analysis of the human femur-A double-blinded biomechanical validation*. J Biomech. 2011, 44(9): 1666–1672

eMotion - system for computer aided rehabilitation - first usability tests on patients

M. ŻUK^{1*}, U. CZAJKOWSKA¹, K. BULIŃSKA², M. POPEK¹, M. ŁOPUSIEWICZ¹

¹Department of Mechanics, Materials and Biomedical Engineering,
Wrocław University of Science and Technology, Wrocław, Poland

²Wrocław University of Health and Sport Sciences, Department of Physiotherapy, Wrocław, Poland

Key words: *motion analysis, virtual reality, rehabilitation*

1. Introduction

The main objective of this study is to present the possibilities of using a proprietary eMotion system in rehabilitation, along with the results of the tests on patients. The use of VR technology in rehabilitation is a relatively new issue, however, previous studies have demonstrated the effectiveness of rehabilitation using this technology [1].

2. Material and Methods

The eMotion system enables exercise and rehabilitation in the form of interactive, immersive, motion-controlled games, together with quantitative motion analysis for an assessment of the correctness of exercises and progress. The eMotion system consists of: 1) commercially available hardware, including: virtual reality headset (HTC Vive Pro, HTC Taiwan) and low cost motion capture system (Vive Trackers 3.0, HTC Taiwan), 2) custom software, including: eMotion Game, Scenario Editor, and Motion Analysis Tool (presented in the paper [2]), 3) developed motion analysis protocols for a kinematic evaluation. The mechanics of the eMotion game are to hit or avoid incoming or static virtual objects using selected body parts. The eMotion system has been tested in the group of elderly people, neurological patients with hemiplegia, children, and young adults with spinal muscular atrophy (SMA). In this paper results are presented for a selected SMA patient, an eight-year-old girl. The following data were collected during gameplays: headset, controller and tracker positions, orientations and velocities, selected muscle activity using surface electromyography using mini DTS Noraxon (Noraxon, USA). In addition, satisfaction surveys were conducted for each group.

3. Results

The analysed part of the game, which consisted of catching incoming objects placed in a circle, was easily performed by the patient through alternating, repeatable, circular hand motions. High qualitative repeatability of the hand trajectories and symmetry can be observed (presented in fig.1), while mean ranges of motion for 5 repetitions were: for right hand 619 mm (std 25 mm) horizontally, 619 mm (std 30 mm) vertically, for left hand 590 mm (std 19 mm) horizontally, 620 mm (std 21 mm) vertically. The activity investigated involved both muscles with a predominance of the biceps.

*Corresponding author: Magdalena Żuk, e-mail: magdalena.zuk@pwr.edu.pl

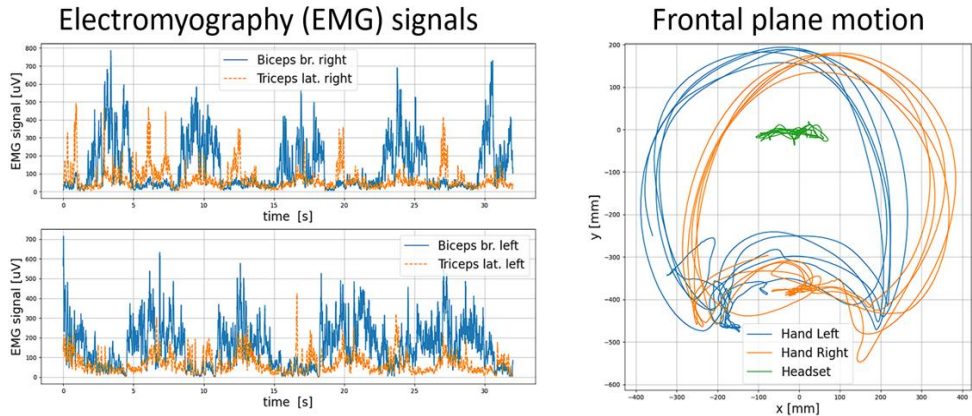


Fig. 1. Electromyography of biceps and triceps muscles (RMS on 50 ms window) and frontal plane trajectories during circular hand motion

4. Conclusions

The proposed eMotion game has versatile, simple, easily digestible, and intuitive mechanics, which is adapted to virtual reality technology and forcing various physical activities, which can be planned in Scenario Editor. The difficulty level can be smoothly increased by changing the arrangement of objects, their speed, numbers, mutual configuration, as well as individually adjusted to the patient's abilities. The positions of the objects were automatically determined relative to the height of the player and the arm span measured during the calibration step, which is extremely useful for patients with a very different range of motion. Motion analysis tool enables an advanced, additional assessment of exercise correctness, as well as quantitative assessment of patient outcome. The conducted tests confirmed the usefulness of the system in each group of analysed patients.

Acknowledgements: This work was supported by the The National Centre for Research and Development in Poland, in frames of the project: “eMotion-system for computer aided workout and rehabilitation using motion capture technology and virtual reality”, LIDER/37/0200/L-10/18/NCBR/2019.

References

- [1] PATSAKI I., DIMITRIADI N., DESPOTI A., TZOUMI D., LEVENTAKIS N., ROUSSOU G., PAPATHANASIOU A., NANAS S., KARATZANOS E. *The effectiveness of immersive virtual reality in physical recovery of stroke patients: A systematic review.* Front Syst Neurosci. 2022, 22,16:880447
- [2] ŽUK M., WOJTKÓW M., POPEK M., MAZUR J., BULIŃSKA K. *Three-dimensional gait analysis using a virtual reality tracking system.* Measurement, 2022, 188: 110627

Index of Authors

A

Alves de Sousa R.J. 28
 Andruszkiewicz F. 38
 Arkusz K. 12
 Aschenbrenner P. 14
 Awrejcewicz J. 173

B

Bacik B. 16, 26
 Bacik K.A. 16,
 Bańkosz Z. 140
 Batyuk L. 80
 Białoszewski D. 60
 Błażkiewicz M. 18, 72
 Bobowik P. 72
 Bobrowska M. 20
 Bocian M. 120
 Bonik A. 22
 Borkowski P. 24
 Borkowski R. 18
 Brachman A. 26
 Brończyc A. 136
 Bulińska K. 40, 181

C

Carmo G.P. 28
 Chmura M. 30
 Chwiłkowska A. 84
 Cichański A. 32
 Cieślak A. 34
 Ciszek B.M. 148
 Ciszewicz A. 36
 Ciupik L.F. 22, 38
 Czajkowska U. 40, 181
 Czaplicki A. 42
 Czarnecki P. 76
 Czogalla A. 138
 Czuba M. 72

D

Daniel N. 44
 Dawidowicz J. 138
 Denisov O. 46
 Detyna J. 34, 124
 Dobrzyński M. 82, 112
 Dylewicz W. 96
 Dymek M. 28
 Dziubek M. 56

E

Erdmann W. 14

F

Ferenc A. 60
 Fernandes F.A.O. 28
 Ferreira A. 48
 Filipiak J. 70, 102, 163, 177
 Filipiak-Kaczmarek A. 50

Florentin E. 74
 Forsyśkiak K. 161
 Fryc D. 52

G

Gach J. 96
 Gajewski J. 48, 72, 92
 Garbacz P. 108
 Głowacki M. 54
 Górski M. 48
 Gruszka G. 30
 Grygier D. 56, 86
 Gryko A. 58
 Grzelczyk D. 173
 Gu Y. 173
 Guszczyn T. 171
 Gzik M. 76, 159

H

Hadamus A. 60
 Haliński A. 12
 Handke A. 62

I

Iwan D 64

J

Jabłońska-Brudło J. 161
 Jamroziak K. 90, 118, 120
 Jankowski K. 122
 Jankowski T. 60
 Janus I. 96
 Jaročka M. 18, 42
 Jasiński B. 66
 Jasiński M. 68
 Jasiurkowska K. 70
 Jastrząbek R. 56, 86
 Juras G. 159
 Jurkojć J. 30

K

Kaczmarczyk K. 18, 72
 Kalinowska M. 132
 Kalinowski S. 74
 Kamieniarz A. 159
 Kawlewska E. 76
 Kazalski M. 78
 Kaźmierczak M. 140
 Kęszycki D. 144
 Kiełb M. 86
 Kierzkowska A. 22, 38
 Kizilova N. 46, 80
 Klekiel T. 96
 Klimas S. 82
 Kobiela K. 144
 Kobielarz M. 84, 88

| | | | |
|-------------------------|---|------------------------|-------------------|
| Kołodziej M. | 140 | Ostrowski G. | 108 |
| Kołtowski K. | 177 | Osuch B. | 60 |
| Kondrusik A. | 179 | | |
| Korbut W. | 179 | P | |
| Kosobucka Z. | 20 | Pająk G. | 38 |
| Koszutski T. | 76 | Pałka Ł. | 118 |
| Kowalewski P. | 56, 86 | Pasik K. | 12 |
| Kozuń M. | 88, 102, 106, 157 | Pawlikowski M. | 108, 122 |
| Krakos (Podwin) A. | 34 | Perz R. | 110 |
| Krawiec K.H. | 90, 118 | Pezowicz C. | 40, 136, 175, 177 |
| Krowicki P. | 66 | Pietroń K. | 100 |
| Kucewicz M. | 148 | Piszczatowski S. | 114, 146, 171 |
| Kulbacka J. | 34 | Piszko A. | 112 |
| Kulig K. | 72 | Piszko P. | 112 |
| Kuliś S. | 92 | Pniewski J. | 20 |
| Kurowiak J. | 94 | Popek M. | 40, 181 |
| Kurzawa A. | 118 | Powchowicz P. | 38 |
| | | Prochor P. | 58, 64, 114 |
| L | | Prosкура P. | 126 |
| Liber-Kneć A. | 169 | Ptak A. | 116 |
| Lubowiecka I. | 74, 134, 150 | Ptak M. | 28, 155 |
| Ludwicki M. | 161 | Pyka D. | 90, 118, 120 |
| | | | |
| Ł | | R | |
| Łabowska M. | 34, 124 | Rogers T. | 16 |
| Łagan S. | 152, 169 | Romanek J. | 30 |
| Łopusiewicz M. | 40, 181 | Rozsak M. | 120 |
| | | Rusinek R. | 167 |
| M | | Rusińska M. | 144 |
| Maciejewska- Skrendo A. | 72 | Rykaczewski M. | 134 |
| Mackiewicz A. | 96 | Rzepliński R. | 148 |
| Maj M. | 142 | | |
| Majchrzak E. | 98 | S | |
| Maksymowicz K. | 138 | Sacewicz T. | 42 |
| Małachowski J. | 44, 100, 148 | Sekula K. | 144 |
| Mamys M. | 120 | Sikora S. | 122 |
| Marcuła K. | 102 | Silva A. | 28 |
| Matczyszyn K. | 124 | Sitnik R. | 132 |
| Matharu Y. | 72 | Skrodzka M. | 124 |
| Mazurkiewicz A. | 54 | Słoiński E. | 22 |
| Mazurkiewicz Ł. | 100 | Słowiński J. | 56 |
| Menartowicz P. | 177 | Smerd K. | 40 |
| Michalska J. | 159 | Sobera M. | 126 |
| Michoński J. | 132 | Sobierajska-Rek A. | 161 |
| Mochnacki B. | 98 | Sobota G. | 16, 26 |
| Mol A. | 76 | Staat M. | 134 |
| | | Stróżyk P. | 128 |
| N | | Struzik A. | 130 |
| Naplocha K. | 50 | Sybilski K. | 44, 100 |
| Nasulicz D. | 142 | Syczewska M. | 132 |
| Nikodem A. | 50, 82, 104, 106, 112, 157, 163, 175 | Szczerba A. | 114 |
| Noszczyk- Nowak A. | 90, 96 | Szczerbik E. | 132 |
| Nowicka M. | 124 | Szepietowska K. | 74, 134, 150 |
| Nowicki A. | 118 | Szkoda-Poliszuk K. | 136, 177 |
| Nowicki K. | 32 | Szłęczak M. | 30 |
| | | Szotek S. | 138, 177 |
| O | | Szpała A. | 140 |
| Olszewska E. | 20 | Szust A. | 142, 165 |
| Opalka M. | 56, 86 | Szymczyk-Ziółkowska P. | 144 |

| | | | |
|-------------------|---------|------------------|---------------|
| Ś | | | |
| Świątek-Najwer E. | 78 | | |
| T | | | |
| Tabor P. | 20, 48 | | |
| Tomaszewska A. | 146 | | |
| Tomaszewski M. | 148 | | |
| Tomczak A. | 116 | | |
| Troka M. | 150 | | |
| U | | | |
| Urbański R. | 14 | | |
| W | | | |
| Walański J. | 42 | | |
| Ważydrąg I. | 152 | | |
| Wądołowski P. | 153 | | |
| Wdowicz D. | 155 | | |
| Wiaderna K. | 60 | | |
| Wilińska K. | 157 | | |
| Wiszomirska I. | 72 | | |
| Wodarski P. | 30, 159 | | |
| | | | |
| | | Wojciechowski K. | 52 |
| | | Wojnicz W. | 161 |
| | | Wolański W. | 76 |
| | | Wolicka J. | 163 |
| | | Wrzosek M. | 177 |
| | | Wudarczyk S. | 62 |
| | | Wybraniec A. | 142, 165 |
| | | Z | |
| | | Zabłotni R. | 167 |
| | | Zadoń M. | 68 |
| | | Zagrodny B. | 161 |
| | | Zajac Z. | 169 |
| | | Zalewska P. | 171 |
| | | Zdrodowska A. | 18 |
| | | Zhao X. | 173 |
| | | Ziółkowski G. | 144 |
| | | Ż | |
| | | Żak M. | 136, 175, 177 |
| | | Żerdzicki K. | 179 |
| | | Żuk M. | 40, 181 |